A UNITED STATES DEPARTMENT OF COMMERCE PUBLICATION

SECTION A

JOURNAL OF RESEARCH

of the NATIONAL BUREAU OF STANDARDS

JNBAAR 77A (2) 179–307 Mar.–Apr. 1973

Physics and Chemistry

U.S. DEPARTMENT OF COMMERCE
National Bureau of Standards

Journal of Research

of the

National Bureau of Standards

A. Physics and Chemistry

Mar.–Apr. • 1973

VOLUME • 77A

NUMBER • 2

Editor: C. W. Beckett

Associate Editor: D. D. Wagman

Publication dates:
Feb. 1, Apr. 1, June 1, Aug. 1, Oct. 1, Dec. 1, 1973

J. Res. Nat. Bur. Stand. (U.S.), A

JOURNAL OF RESEARCH

The National Bureau of Standards Journal of Research reports research and development in the fields of activity shown at right. Also included from time to time are survey articles on topics closely related to the Bureau's scientific and technical program.

The Journal is published in two separate sections as follows:

A. Physics and Chemistry

Contains papers of interest primarily to scientists working in these fields. Issued six times a year. Annual subscription: domestic, $17.00; foreign, $21.25. Single copy, varies.

B. Mathematical Sciences

Presents studies and compilations designed mainly for the mathematician and the theoretical physicist. Issued quarterly. Annual subscription: domestic, $9.00; foreign, $11.25. Single copy, $2.25.

The National Bureau of Standards[1] was established by an act of Congress March 3, 1901. The Bureau's overall goal is to strengthen and advance the Nation's science and technology and facilitate their effective application for public benefit. To this end, the Bureau conducts research and provides: (1) a basis for the Nation's physical measurement system, (2) scientific and technological services for industry and government, (3) a technical basis for equity in trade, and (4) technical services to promote public safety. The Bureau consists of the Institute for Basic Standards, the Institute for Materials Research, the Institute for Applied Technology, the Center for Computer Sciences and Technology, and the Office for Information Programs.

THE INSTITUTE FOR BASIC STANDARDS provides the central basis within the United States of a complete and consistent system of physical measurement; coordinates that system with measurement systems of other nations; and furnishes essential services leading to accurate and uniform physical measurements throughout the Nation's scientific community, industry, and commerce. The Institute consists of a Center for Radiation Research, an Office of Measurement Services and the following divisions:

Applied Mathematics — Electricity — Mechanics — Heat — Optical Physics — Linac Radiation[2] — Nuclear Radiation[2] — Applied Radiation[2] — Quantum Electronics[3] — Electromagnetics[3] — Time and Frequency[3] — Laboratory Astrophysics[3] — Cryogenics[3].

THE INSTITUTE FOR MATERIALS RESEARCH conducts materials research leading to improved methods of measurement, standards, and data on the properties of well-characterized materials needed by industry, commerce, educational institutions, and Government; provides advisory and research services to other Government agencies; and develops, produces, and distributes standard reference materials. The Institute consists of the Office of Standard Reference Materials and the following divisions:

Analytical Chemistry—Polymers—Metallurgy—Inorganic Materials—Reactor Radiation—Physical Chemistry.

THE INSTITUTE FOR APPLIED TECHNOLOGY provides technical services to promote the use of available technology and to facilitate technological innovation in industry and Government; cooperates with public and private organizations leading to the development of technological standards (including mandatory safety standards), codes and methods of test; and provides technical advice and services to Government agencies upon request. The Institute also monitors NBS engineering standards activities and provides liaison between NBS and national and international engineering standards bodies. The Institute consists of a Center for Building Technology and the following divisions and offices:

Engineering and Product Standards—Weights and Measures—Invention and Innovation—Product Evaluation Technology—Electronic Technology—Technical Analysis—Measurement Engineering—Building Standards and Code Services[4]—Housing Technology[4]—Federal Building Technology[4]—Structures, Materials and Life Safety[4]—Building Environment[4]—Technical Evaluation and Application[4]—Fire Technology.

THE INSTITUTE FOR COMPUTER SCIENCES AND TECHNOLOGY conducts research and provides technical services designed to aid Government agencies in improving cost effectiveness in the conduct of their programs through the selection, acquisition, and effective utilization of automatic data processing equipment; and serves as the principal focus within the executive branch for the development of Federal standards for automatic data processing equipment, techniques, and computer languages. The Center consists of the following offices and divisions:

Information Processing Standards—Computer Information—Computer Services—Systems Development—Information Processing Technology.

THE OFFICE FOR INFORMATION PROGRAMS promotes optimum dissemination and accessibility of scientific information generated within NBS and other agencies of the Federal Government; promotes the development of the National Standard Reference Data System and a system of information analysis centers dealing with the broader aspects of the National Measurement System; provides appropriate services to ensure that the NBS staff has optimum accessibility to the scientific information of the world, and directs the public information activities of the Bureau. The Office consists of the following organizational units:

Office of Standard Reference Data—Office of Technical Information and Publications—Library—Office of International Relations.

---

[1] Headquarters and Laboratories at Gaithersburg, Maryland, unless otherwise noted; mailing address Washington, D.C. 20234.
[2] Part of the Center for Radiation Research.
[3] Located at Boulder, Colorado 80302.
[4] Part of the Center for Building Technology.

U.S. DEPARTMENT OF COMMERCE
Frederick B. Dent, Secretary

NATIONAL BUREAU OF STANDARDS
Richard W. Roberts, Director

Order all publications from the Superintendent of Documents
U.S. Government Printing Office, Washington, D.C. 20402

The Secretary of Commerce has determined that the publication of this periodical is necessary in the transaction of the public business required by law of this Department. Use of funds for printing this periodical has been approved by the Director of the Office of Management and Budget through June 30, 1976.

JOURNAL OF RESEARCH of the National Bureau of Standards – A. Physics and Chemistry
Vol. 77A, No. 2, March–April 1973

An Adiabatic Solution Calorimeter and Measurements of a Standard Reaction for Solution Calorimetry

Edward J. Prosen and Marthada V. Kilday

Institute for Materials Research, National Bureau of Standards, Washington, D.C. 20234

(November 9, 1972)

This paper discusses in detail the design, construction, and performance of the vacuum jacketed, adiabatic solution calorimeter which was used for the work in the certification of two NBS Standard Reference Materials for solution calorimetry. As a test for the calorimetric precision the following enthalpies of reaction were measured (referred to the mass or moles of $H_2SO_4 \cdot 8\,H_2O$):

$$H_2SO_4 \cdot 8\ \ H_2O + 2.36\,(NaOH \cdot 2620\,H_2O) = (Na_2SO_4 \cdot 0.36\,NaOH \cdot 6193\,H_2O)_{soln}$$

$$\Delta H_r(298.15\,K) = -590.692 \pm 0.101\,J \cdot g^{-1}$$

$$= -34{,}194.1 \pm 5.9\,cal \cdot mol^{-1}$$

$$H_2SO_4 \cdot 8\,H_2O + 2.6\,(NaOH \cdot 714\,H_2O) = (Na_2SO_4 \cdot 0.6\,NaOH \cdot 1866\,H_2O)_{soln}$$

$$\Delta H_r(298.15\,K) = -590.828 \pm 0.193\,J \cdot g^{-1}$$

$$= -34{,}203.4 \pm 11.1\,cal \cdot mol^{-1}$$

Key words: Adiabatic solution calorimeter; enthalpy of reaction of H_2SO_4 in aqueous $NaOH$; H_2SO_4, enthalpy of reaction in $NaOH(aq)$; heat of reaction of H_2SO_4 in aqueous $NaOH$; heat of solution of H_2SO_4 in aqueous $NaOH$; solution calorimetry; thermochemistry.

Contents

	Page
1. Introduction	179
2. General description of the calorimeter and procedures	180
3. The calorimeter in detail	181
3.1. The vessel and its appendages	181
a. The stirrer assembly	185
b. The vent and the wells	186
c. The platinum sample holder	186
3.2. The adiabatic shield	188
3.3. The jacket	189
3.4. The vacuum system and the hydraulic lift	190
3.5. The calibrating heater and the control thermocouples	190
3.6. The electrical calibration and electronic control instruments	193
3.7. The thermometers	194
4. Procedures	195
4.1. Samples and solutions	195
4.2. Temperature measurements	195
4.3. Electrical calibrations	196
5. Measurements of a standard reaction	197
5.1. Sample and the solutions	198
5.2. Experimental results	198
a. Temperature profiles for the adiabatic shield	199
b. Enthalpy of reaction of $H_2SO_4 \cdot 8H_2O$ with excess NaOH(aq)	200
6. Other measurements	200
7. Conclusions	202
8. Prefixes, symbols, and abbreviations	202
9. References	202

1. Introduction

The construction of an adiabatic solution calorimeter began in 1962 in the Thermochemistry Section at the National Bureau of Standards. The calorimeter was to have the capability of measuring with high precision, enthalpies of solution of refactory materials in corrosive solutions, such as aqueous HF, at temperatures as high as 363 K. The first complete calorimetric experiments were done near the end of 1964, and since that time many improvements have been made which increased the precision and accuracy of the measurements, and the dependability of the calorimetric system.

This calorimeter was used for the work which led to the certification of two NBS Standard Reference Materials for solution calorimetry, and it seemed appropriate to provide a detailed description of the calorimeter as documentation for that work as well as

for other projects which will follow. Section 2 of this paper provides a general description of the calorimetric apparatus and procedures for those who are not interested in the great detail given in sections 3 and 4; these sections will interest those who are primarily concerned with details of construction and performance, and they have been written to benefit novices in calorimeter construction as well as teachers and students in calorimetry. Specific formulae and equations used for calculations have been given as an aid to other workers in this field. We have tried to answer many of the questions about the calorimeter posed by visitors to our laboratory and in some cases we have given the reasons for the choice of materials, instruments, or procedures.

Section 5 gives an example of measurements made with this calorimeter for a test reaction to indicate the precision of the calorimetric measurements.

2. General Description of the Calorimeter and Procedures

This adiabatic solution calorimeter operates in a 70-deg temperature range (293 to 363 K); the solution capacity is 300 ± 15 cm^3; the maximum volume for liquid or solid samples in the platinum sample holder is 2.7 cm^3; the electrical energy equivalent is approximately 1700 J $\cdot$ K^{-1} when the vessel contains 300 cm^3 of H_2O, or approximately 450 J $\cdot$ K^{-1} when empty; the stirring speed can be changed from 200 to 850 rpm in steps of 50 to 100 rpm; and a precision (2 sdm) of ± 0.02 percent has been achieved in measurements of the electrical energy equivalents and of some enthalpies of reaction. The calorimeter is capable of measuring the enthalpies of solution reactions which occur at atmospheric pressure between 293 and 363 K providing the chemicals involved do not attack platinum or react with the components of air. However, the calorimeter can be closed to allow gases other than air to be utilized.

A diagram of the calorimeter is shown in figure 1. The vessel is silver, lined with platinum, and all parts in contact with the solution and its vapor are of platinum including the wells for the thermometer and for the calibrating heater, the stirrer, the sample holder, and five tubes (two are not shown) leading up from the cover which carry leads, etc., out of the calorimeter. The level of the solution is normally 0.5 cm below the cover of the vessel. The adiabatic shield is gold-plated copper. Its temperature is controlled automatically by heaters on the external surface to follow the vessel temperature. The temperature difference between the cover of the vessel and the cover of the shield is sensed by a six-junction, copper-constantan thermocouple. During rating periods this temperature difference is less than 0.0001 K. The nickel-plated copper jacket confines the vacuum which surrounds the vessel. The pressure in the system during calorimetric measurements is usually between 3 and 11×10^{-2} Pa (2 and 8×10^{-4} mm Hg).

Heat transfer from the calorimeter through the five tubes above the cover of the vessel is minimized by

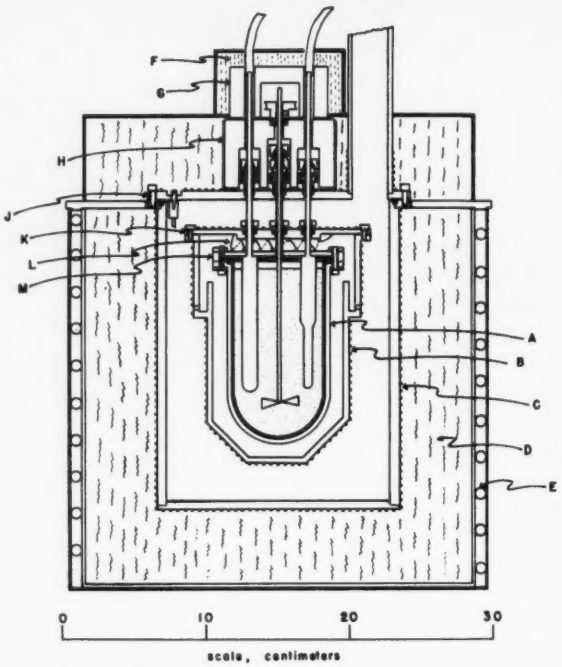

FIGURE 1. *Diagram of the adiabatic solution calorimeter.*

(A) The vessel (silver, lined with platinum), (B) the adiabatic shield, (C) the constant temperature jacket, (D) the Fiberglas insulation, (E) the coil for circulation of cold water in experiments below room temperature, (F) the Styrofoam insulation, (G) an aluminum block at ambient temperature, (H) an aluminum block at controlled temperature, (J) the jacket cover, (K) the shield cover, (L) the shield control thermocouples, and (M) the vessel cover.

by two additional heaters which are controlled automatically to follow the shield temperature: the first is on an aluminum block surrounding the fittings above the jacket cover, and the second is on the external surface of the jacket cover. Both of these areas as well as the cover of the adiabatic shield are in good thermal contact with the five platinum tubes, thus they are essentially at the shield temperature before entering the calorimeter.

Figure 2 is a photograph of the calorimeter showing (at center) the three covers for the jacket, the adiabatic shield, and the vessel, with the heater well and sample holder (front), the stirrer, and the thermometer well (rear), suspended from the cover of the vessel. The sample holder shown here is the earliest design; the improved design will be discussed in detail in section 3.1a. Also shown in figure 2 is the jacket well which is surrounded by the calorimeter insulation (Fiberglas). This unit is raised by a hydraulic lift to form a vacuum-tight seal with the jacket cover by means of the Buna-N rubber o-ring shown in the rim of the jacket well.

Approximately 3 h is the minimum time required for a single experiment from the time the calorimeter is assembled until the measurements are completed. The usual experiment involves measurements of four rating periods (20 to 30 min each); an initial electrical calibration occurs between the first and second rating periods, the chemical reaction occurs between the second and third rating periods, and a final elec-

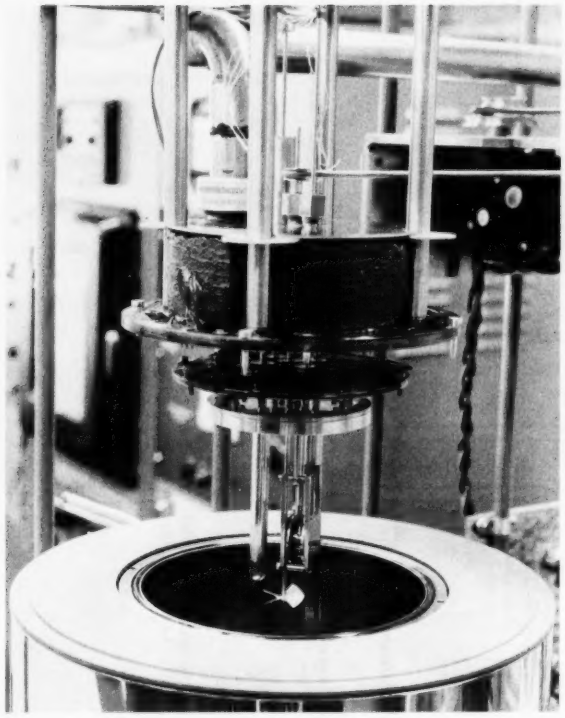

FIGURE 2. *The open calorimeter.*

The jacket well (at bottom) and above it the stirrer, the first sample holder, the wells for the heater and the thermometer. Near center, the covers for the vessel, the shield, and the jacket.

trical calibration occurs between the third and fourth rating periods.

Figures 3 and 4 are schematic diagrams of the systems for measuring the calorimeter temperature and the electrical energy, and for the temperature control of the adiabatic shield. Some of the equipment used in these measurement and control systems are shown in figure 5, and will be described in detail later in this paper. In the first rack (foreground) are the instruments for measuring and recording temperature changes in the calorimeter vessel. The resistance of the 25-Ω platinum resistance thermometer is measured with the G-3 Mueller-type thermometer bridge (on the table) using a microvolt amplifier or a nanovoltmeter as a null detector, and the output of the null detector is recorded on the strip chart recorder near the top of the rack. Recently the platinum resistance thermometer was replaced by a quartz-oscillator thermometer which was calibrated against the 25-Ω platinum resistance thermometer; the temperature changes were read directly in °C on the quartz thermometer.

In the second rack shown in figure 5 are the instruments for controlling the temperature of the adiabatic shield, the jacket cover, and the aluminum block above the jacket. Above the table top in this rack are the current-adjusting-type (C.A.T.) control unit and electronic null detector for controlling the temperature of the adiabatic shield. The output of the null detector (which indicates the temperature difference between the covers of the vessel and of the adiabatic shield) is recorded on the strip chart recorder. The two sets of C.A.T. units and null detectors near the top are for the control of the temperatures of the jacket cover and the aluminum block. At the top of the second rack are ammeters which indicate the current through the heaters for the shield, the jacket cover, and the aluminum block. A constant voltage power supply below the table top (not visible in the photograph) supplies the power for the three controlled heaters.

The instruments for measuring electrical energy added to the calorimeter during calibrations are shown in the third rack in figure 5. The power is supplied by the constant voltage power supply (at top), and the time of electrical heating is determined by the electronic counter which counts cycles of the 10 kHz standard frequency available at NBS. Recently a solid-state counter replaced the vacuum tube instrument shown here. The six-dial potentiometer and electronic null detector are used for measurements of the current and potential drop across the calorimeter heater. In the last rack are a Pirani gauge and an ionization gauge for measuring pressure in the vacuum system, switches for directing the current through the calorimeter heater or the spill coil, and saturated standard cells against which the working current in the potentiometer is balanced.

Figure 6 is a photograph showing the general setting for the calorimeter. At left is the oil diffusion pump and the copper vacuum line with pressure gauges. On the table at right is the cup of the calorimeter vessel, and at the center is the adiabatic shield. The hydraulic lift (see sec. 3.4) is shown under the calorimeter. The insulated box at the top of the rack contains junctions for thermocouples, heaters, etc.

3. The Calorimeter in Detail

3.1. The Vessel and Its Appendages

This calorimeter was designed to measure heats of reaction in aqueous HF solutions; therefore, all parts in contact with the solution and its vapors are of platinum-iridium alloys or polytetrafluoroethylene (PTFE, Teflon[1]). The platinum alloys containing 10 or 20 percent of iridium were used instead of pure platinum because the greater hardness made them more suitable for machining and more resistant to abrasion.

Details of the construction of the calorimeter vessel are shown in figure 7. The lining of the cup ($Pt + 10\%$ Ir) has an inner diameter of 6.35 cm, a wall thickness of 0.080 cm, and an overall height of 12.1 cm. The width of the flange at the top of the cup is 1 cm. All visible surfaces are highly polished. On the external surface of the cup, 0.32 cm of pure silver was plated

[1]Certain commercial products and instruments are identified in this paper in order to specify adequately the experimental procedure. In no case does such identification imply recommendation or endorsement by the National Bureau of Standards, nor does it imply that the products or equipment identified are necessarily the best available for the purpose.

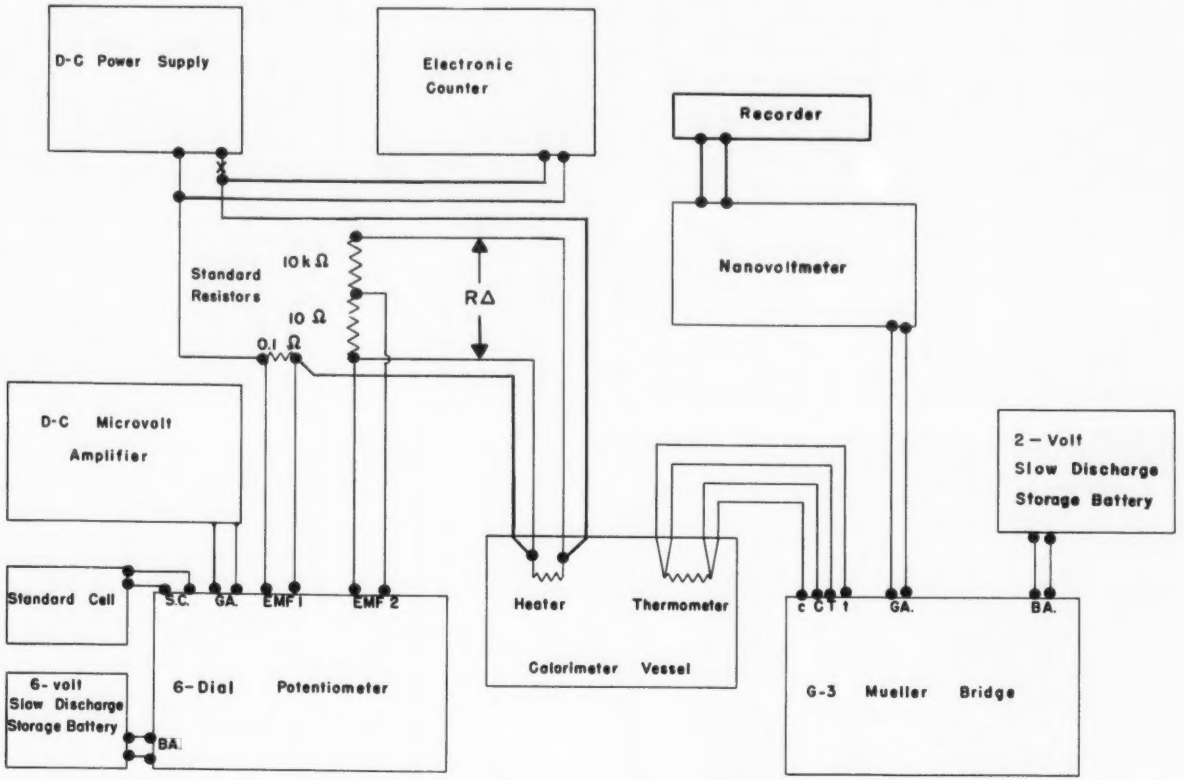

FIGURE 3. *Schematic diagrams of the system for measuring the electrical energy evolved by the 97-Ω calorimeter heater during calibrations, and of the system for measuring the calorimeter temperature with the 25-Ω platinum resistance thermometer.*

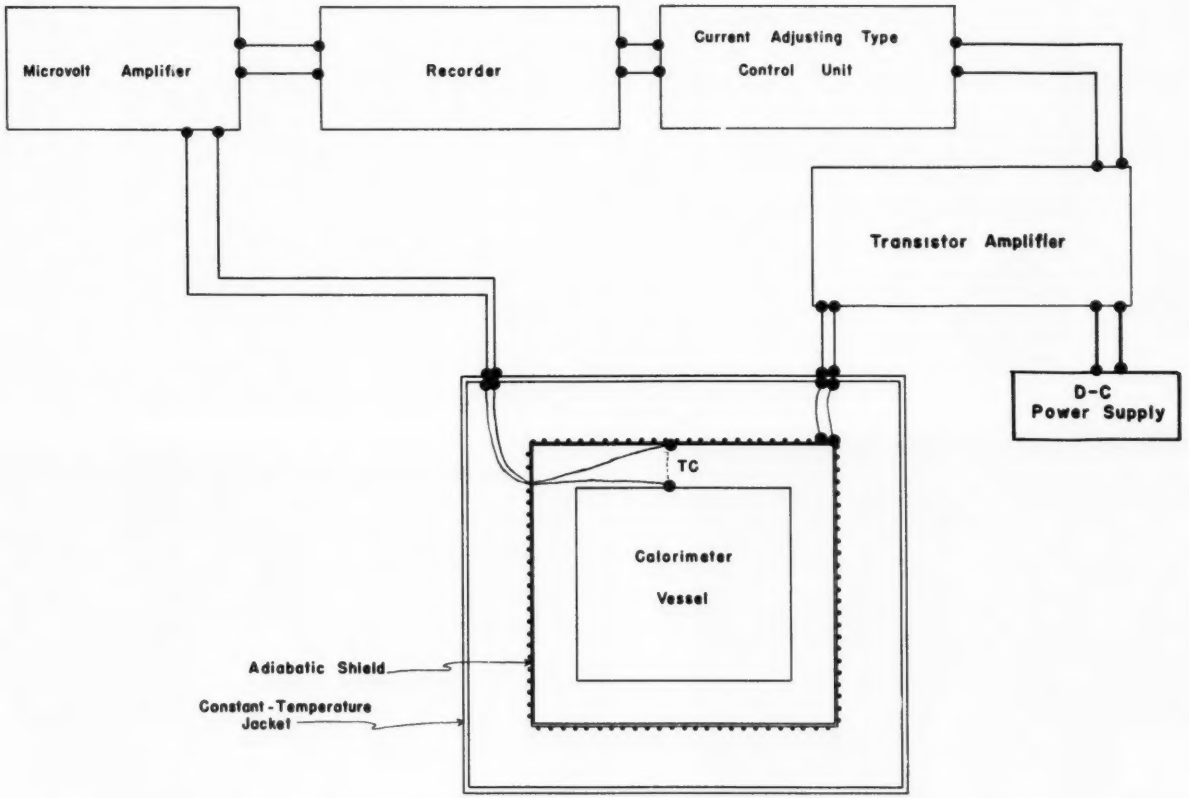

FIGURE 4. *Schematic diagram of the electrical system for controlling the temperature of the adiabatic shield.*

FIGURE 5. *The console for the calorimeter controls and measuring equipment.*

FIGURE 6. *The adiabatic solution calorimeter and the vacuum system, showing the cup of the vessel on the table at right, the adiabatic shield at left, and the hydraulic lift under the case containing the jacket well and insulation.*

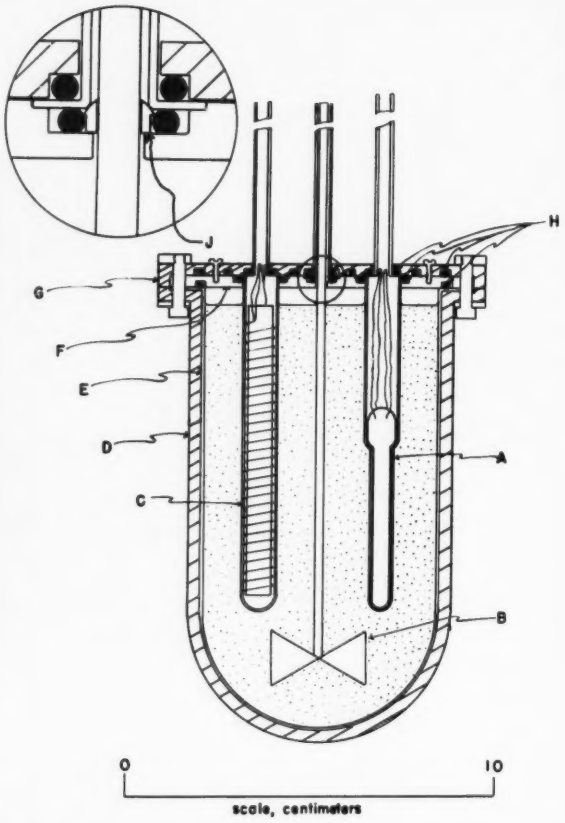

FIGURE 7. *A diagram showing the construction of the calorimeter vessel in detail.*

(A) The well for the resistance thermometer, (B) the stirrer, (C) the well for the calibrating heater, (D) the silver vessel, (E) the platinum lining of the vessel, (F) the platinum cover, (G) the silver cover, and (H) the rubber o-rings which seal against the vacuum surrounding the vessel. The area in the small circle is shown in detail at the upper left, and includes the PTFE bearing, (J), for the stirrer shaft.

by electrodeposition; the high thermal diffusivity of the silver rapidly distributes the heat from within the vessel and provides an essentially isothermal surface. The silver surface was plated with ~ 0.008 cm of gold to prevent oxidation of the silver and to provide a highly polished surface for good reflectivity. The cup of the vessel is attached to the cover by 12 stainless steel screws which tighten on two stainless steel rings—one above and one below the flange on the vessel.

In figure 8, are the various parts of the calorimeter before assembly. At the center are shown (left to right) the stirrer, the well for the calibrating heater, the vent-seal rod, the resistance thermometer and its well, and the first version of the sample holder. The cup of the vessel in its PTFE-lined holder is shown in the upper left, and to the right are the two steel rings used in attaching the cup to the cover with the steel screws shown at the left of the stirrer. Below the cup are the parts of the cover. At lower left is shown the bottom side of the gold-plated pure silver part which fits

FIGURE 8. *The parts of the calorimeter before assembly.*

(Top to bottom) At left, the cup of the calorimeter vessel in its holder, the platinum plate of the vessel cover, and the silver plate of the vessel cover. At top center, the two steel rings used in clamping the cup and the cover of the vessel together. At center (left to right), the stirrer, the well for the calibrating heater, the first vent-seal rod, the resistance thermometer and its well, the first sample holder and cover. At lower center, the five tubes which lead up from the vessel cover. At right, the adiabatic shield and its cover.

tightly over the platinum plate ($Pt+10\%\ Ir$) just above it. These parts are each 0.32 cm in thickness. The flanged wells for the thermometer and the heater (shown near the center) seat on the large o-rings on the platinum plate; the three smaller o-rings form seals under the flanges of the platinum tubes (bottom, center) which lead up from the vessel. The two additional tubes seat in the top of the wells for the heater and the thermometer. In the assembly of the cover, the five holes in the silver part pass around the corresponding tubes seated on the platinum plate; the two parts of the cover are then positioned by means of the aligning pins and holes, located unsymmetrically near the edges of both parts. The two parts are then attached by the 18 small screws with gold-plated brass washers (at left in fig. 8) which tighten against partial taps in the platinum plate. Thus, the five small o-rings shown in the silver part form seals against the vacuum surrounding the vessel above the flanges on the five tubes. The two larger o-rings form a vacuum seal around the flanges on the heater and thermometer wells. A thick layer of Apiezon "N" grease is placed on the top surface of the platinum plate before assembly to improve thermal contact between the plates and to provide an additional supply of lubricant to prevent leakage of the o-ring seals after successive high and low temperature experiments.

The cross-sectional detail of the assembled cover is shown in figure 7. It may also be seen in figure 7 that the platinum lining of the vessel is entirely surrounded by a thick layer of silver in good thermal contact with the platinum. As a result the external surface of the calorimeter vessel may be expected to be effectively isothermal. The vacuum seal between the cup and the cover of the vessel is formed by a Buna N o-ring in a groove on the lower side of the platinum coverplate which seals against the flange on the cup; the outer rim of this flange is also lubricated to improve the thermal contact.

a. The Stirrer Assembly

The platinum stirrer (Pt + 10% Ir) has a four-blade propeller which is 2.5 cm in diameter and is situated 10 cm below the cover of the vessel when assembled. The stirrer shaft passes through the platinum tube in the center of the vessel cover and is driven by a synchronous speed-reducer motor[2] (1/150 hp, Bodine Electrical Type NSY–12R) through a set of pulleys and o-ring belts. Initially Buna-N rubber belts were used, however, an ethylene propylene rubber (Parker Seal Co., Compound E540-8) has been found to be more durable even when operating around 360 K for long periods.

The bearings for the stirrer shaft may be seen by reference to figures 1 and 7. Steel ball-bearings above (not shown) and below the pulley at the top provide permanent alignment at the top of the stirrer shaft. Additional bearing surfaces not shown in figure 1 were provided later because the stirring energy did not remain constant. Variations in the stirring energy were presumed to be due to unpredictable oscillations which developed because the stirrer shaft (0.24-cm diameter) was not supported for a length of approximately 20 cm. Steel ball-bearings could not be used for the additional bearings because of the contact with the vapors from the calorimetric solution; therefore, two PTFE bearings were added. The first was an o-ring located under the fitting below the ball-bearing shown in figure 1. The o-ring was not compressed by the fitting and did not form a seal around the stirrer shaft; its only function was as a bearing. A second PTFE bearing in the form of a collet was added between the two plates of the vessel cover, at a distance of 10 cm above the propeller (see fig. 7). This greatly reduced the oscillation problem, and the uncertainty in the stirring energy is now only 1 or 2 percent of the total. The PTFE collet was first used in November 1968, and stirring energies prior to that were less reproducible. Unfortunately, the PTFE bearings wear and after some months of use, the unpredictable oscillations may reappear. Replacement of the collet in the vessel cover is an operation which should be done infrequently because of the necessity for complete dismantling of the calorimeter; this involves breaking various soldered lead connections and removal of the control thermocouples. A satisfactory substitute for replacement of the collet is to slide a thin PTFE cylindrical sleeve (1.25-cm length) down the annular space between the platinum tube and the stirrer shaft until it is in contact with the collet.

Variations in the stirring speed in the calorimeter are accomplished by changes in the belt positions on a pair of pulleys; the possible combinations result in the following stirring speeds: 200, 250, 300, 350, 450, 550, 700, and 850 rpm. Above 450 rpm, oscillations frequently occur, and these high speeds are used only

[2] The power is the 115-V ac supplied by the public utility in this area. Variations in the 60-Hz frequency are small and slow enough to result in negligible error.

when stirring reproducibility must be sacrificed to achieve more effective mixing in the solution. Below 300 rpm, there is no visible turbulence at the surface of the solution and these slow speeds are used only for reactions which require very little mixing. Of course, the reproducibility of the stirring energy at these low speeds is good.

Rating period slopes were measured near room temperature at various stirring speeds when the calorimeter contained water; the results are as follows: 120 $\mu K \cdot min^{-1}$ at 300 rpm, 290 $\mu K \cdot min^{-1}$ at 450 rpm, 410 $\mu K \cdot min^{-1}$ at 550 rpm, and 1300 $\mu K \cdot min^{-1}$ at 850 rpm. The precision (2 sdm) of these slope measurements ranged from 1 to 10 percent of the mean values; the precision has since been improved as the result of the addition of the PTFE bearings discussed before in this section. At higher temperatures, the rating period slopes are also affected significantly by evaporation of the calorimetric solution.

For special projects such as the measurement of the enthalpy of reaction of ketene gas in aqueous NaOH [1][3] it is necessary to seal the calorimeter by using a lubricated rubber o-ring instead of the usual PTFE o-ring in the top fitting above the jacket cover (fig. 1). In this case the uncertainty in the stirring energy and the slope is greatly increased because the rubber bearing produces less uniform friction at the seal than the PTFE does, and oscillations of the stirrer shaft are more likely to occur. Slopes as great as 700 $\mu K \cdot min.^{-1}$ have been observed at 450 rpm at room temperature, although usually the observed slopes do not vary by more than 5 percent in a single experiment.

b. The Vent and the Wells

The vent was provided as (1) a safety valve in case of unexpected excessive pressure in the calorimeter, (2) an exit for gases when the system is used as a flow calorimeter, and (3) a means of assuring that the vapor space in the calorimeter is at atmospheric pressure at the beginning of an experiment. The original vent seal was a spring-loaded, Pt + 10 percent Ir, rod (center, fig. 8) with the lower end tapered to a point which seated in a PTFE ring in the platinum cover of the vessel. The PTFE seat is shown in the platinum plate (at left center of fig. 8). Later, the spring-loading device was removed and a 100-g brass weight was attached to the top of the platinum rod which was supported by the platinum tube similar to those for the thermometer and heat leads shown in figures 1 and 7. The vent tube is behind the stirrer in these figures on the same radius as the heater and thermometer tubes. Still later it was found that removal of the platinum rod which sealed the vent resulted in improved precision in some reactions. This insured a constant pressure system.

The wells (Pt + 10% Ir) for the calibrating heater and for the thermometer (near center, fig. 8) are centered on a radius of 1.67 cm from the center of the vessel cover. Both wells have a wall thickness of 0.052 cm, are 9.2-cm overall length, have a flange at the top which is 1.5-cm diameter, and have an inner diameter of 0.85 cm. On the well for the resistance thermometer, the inner diameter is reduced to 0.56 cm on the lower 4.4 cm in order to have a close fit to the capsule-type thermometer. A few drops of silicone oil in the well improved the thermal contact with the thermometer.

In the first work with the quartz-oscillator thermometer, the well for the platinum resistance thermometer was used and the quartz-oscillator probe was seated at the place where the diameter was reduced; the lower portion of the well was filled with an aluminum block to maintain good thermal conductivity.

c. The Platinum Sample Holder

The sample holder shown in figures 2 and 8 is the first design and resulted in several problems. The sample was contained in the cylinder and was sealed from the calorimetric solution by the o-rings in the two flat plates. A reaction was initiated by pulling the cylinder up (by means of the rod attached to it) into the area cut out of the end plates where the solution could circulate through the cylinder. This arrangement had the following disadvantages: (1) crystalline samples were trapped between the inner wall of the cylinder and the o-rings causing abrasion of the cylinder rims as well as difficulty in pulling the cylinder up, (2) the frictional energy was large (> 1 J in some cases) for pulling the cylinder up against the resistance of the o-rings, (3) the reproducibility of the opening energy was poor because of the wear and abrasion of the o-rings, and (4) the opened cylinder was near the top of the calorimetric solutions where the stirring turbulence is relatively poor. In July 1967, the final change in design of the sample holder was completed and the improved design includes the following features: (1) the sample unit is inverted to place the open cylinder near the stirrer, (2) the o-ring grooves are in the rim of the cylinder and move with the sample across the flat end plates, and (3) a triggering device opens the sample holder allowing the cylinder to drop by gravity, thus reducing the frictional energy. The sample holder is suitable for solids and liquids of low volatility.

The sample holder was made of platinum containing 20 percent iridium for hardness, hence, resistance to wear and abrasion. The dimensions of the two flat end plates are 5.24 cm (height), 2.70 cm (width), and 0.16 cm (thickness). There are three interchangeable cylinders for the sample holder which have a depth of 0.95 cm, inner diameters of 0.95 cm, 1.59 cm, and 1.90 cm, and contain volumes of approximately 0.7 cm^3, 1.9 cm^3, and 2.7 cm^3, respectively.

When possible, unlubricated PTFE o-rings are used as a seal for the sample holder; however, these have sometimes been unsatisfactory for liquid samples, and lubricated o-rings had to be used. There is always some gas or vapor space with the sample in the container and as thermal expansion occurs during preheating and calibration of the calorimeter, liquid

[3] Figures in brackets indicate literature references at the end of this paper.

samples may be forced through imperfections in the PTFE seals causing prereaction, but with solid samples only small gas bubbles escape. Lubricated o-rings, PTFE or rubber, usually provide satisfactory seals for liquid samples.

The sample holder as it appears before initiating a reaction is shown in figure 9. Holding the two end plates together at the top is the notched trigger bar. (Note that the two top nuts have been loosened and that there is a space between the shoulder of the lower cross-bars and the front end plate which permits the front end plate to pivot when the trigger is released.) To initiate a reaction, the vertical push-rod above the trigger bar is pushed down approximately 3 mm; the trigger bar rotates (because it is connected by a rod at its center to the pin in the end of the forked push rod) and as the notch in the trigger bar is cleared, the front end plate is released allowing the cylinder to drop to the lower cross-bars as shown in figure 10. With the cylinder in this position, the solution can circulate freely through the sample holder without danger of trapping the sample. The notch in the trigger bar can be seen more clearly in figure 10; the fork in the push rod acts as a stop when it reaches the trigger bar. The sample holder is hung on hooks on the lower ends of the two platinum rods which are screwed into the platinum cover of the vessel. When the trigger bar is raised the unit can be removed from the hooks for reassembly.

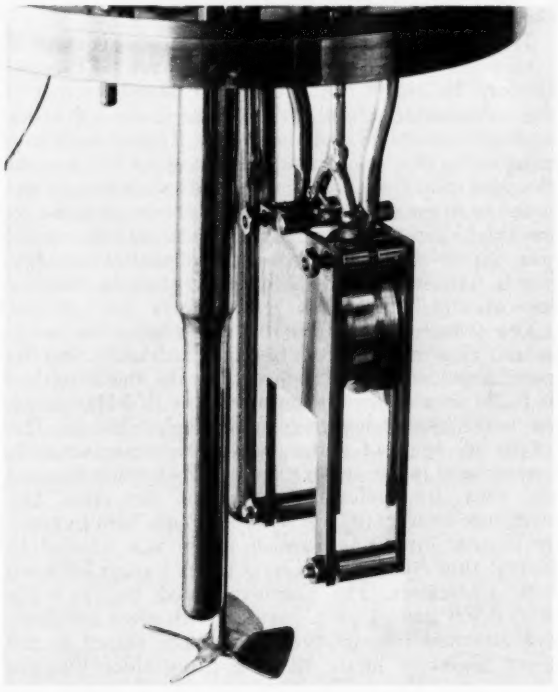

FIGURE 9. *The improved platinum sample holder with trigger set as before opening.*

The sample is contained in the cylinder between the two flat plates. To initiate a reaction, the forked rod is pushed down causing the notch in the horizontal "trigger bar" below it to rotate and release the front plate. This allows the cylinder to drop to the lower cross-bars.

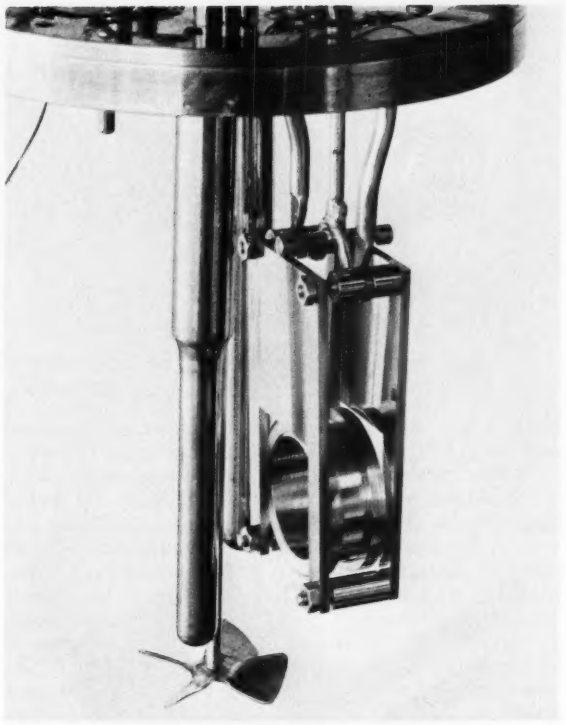

FIGURE 10. *The sample holder after opening.*

The notch in the trigger bar is visible as is the PTFE O-ring which before opening forms a seal with the end plate in front (A similar O-ring is on the other side of the cylinder). The sample holder is supported by the hooks suspended from the vessel cover.

In the assembly of the weighed sample holder, the fixed end plate (at back of figs. 9 and 10) with the four cross-bars attached is placed in a stainless steel clamp as shown at the top of figure 11. The cylinder with the o-rings is placed on the fixed end plate and the two side clamps are tightened to make the lower o-ring seal. Between the lower cross-bars is a steel spacer which is removed after the assembly is completed. The unit may now be placed in a controlled atmosphere such as a dry box if necessary for filling. The sample is added to the cylinder through a funnel or dropper using care to avoid spillage on the o-ring. The second end plate is then placed on top, the four nuts are tightened, the spacer is removed, and the side clamps are released. The sample holder is now ready for weighing in the form shown at the bottom of figure 11. The mass of the empty sample holder is approximately 108 g.

Attempts to measure the opening energy for this improved sample holder gave an average 0.00 ± 0.02 (2 sdm) J in six experiments for which the individual results were: 0.012, 0.021, 0.014, 0.007, −0.051, and 0.016 J. These experiments were at 298 K, used PTFE o-rings in the sample cylinder which was filled with the calorimetric solution (water in this case), and employed the largest, medium-sized, and smallest cylinder, in the stated order and in the reverse order. The precision of the measurements is approximately that of the stirring energy at 250 rpm, and the energy of opening

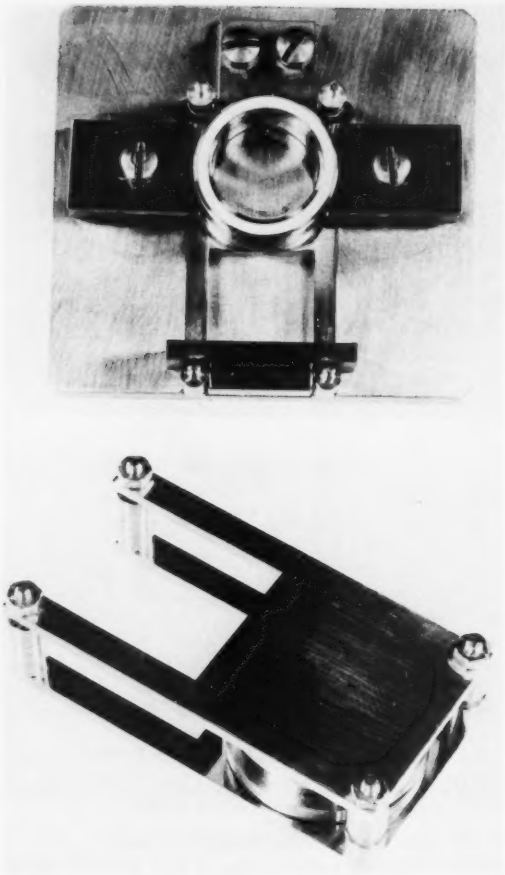

FIGURE 11. *The sample holder.*

At top, in the clamp ready for filling with a sample; at bottom, assembled for weighing after adding a sample.

the sample holder appears to be too small to be detectable. The temperature rises in these experiments were only $\pm 10\ \mu K$ ($\pm 1\ \mu\Omega$) or less. Additional opening energies were measured as follows: −0.006 and 0.065 J using 9.3 *N* NaOH at 298 K; 0.031 and 0.048 J using H_2O at 323 K; −0.049 and 0.018 J using lubricated rubber o-rings; and 0.041, 0.018, and 0.094 J (the last two had only one drop of H_2O in the cylinder) using conditions similar to the six experiments averaged above except that the vent tube was sealed instead of being vented to the atmosphere. The limited number of these measurements does not permit definite conclusions about the opening energies under the various conditions, however, it appears that they would not be expected to exceed 0.1 J.

3.2. The Adiabatic Shield

The adiabatic shield which surrounds the calorimeter vessel is shown at the right in figure 8. It is constructed of vacuum-cast copper which is gold plated and highly polished for reflection of radiant energy. The cover (at lower right) is 0.64-cm thick near the center and 0.32-cm thick near the periphery. It supports the five brass fittings which hold the shield in place on the platinum tubes which rise from the vessel cover. These fittings tighten against wedge-shaped copper rings which not only provide effective support, but also provide good thermal contact between the platinum tubes and the shield cover. On the top surface of the shield cover is a manganin heater which is held in place by Glyptal insulating varnish. Eight steel screws around the edge of the cover are used to attach the base of the shield to the cover; Apiezon lubricant on the rim of the base improves thermal contact between the two metal surfaces.

The base of the shield (fig. 8, upper right) is made of continuous copper with no joints to act as thermal barriers. Its shape conforms approximately to that of the calorimeter vessel, with about 1 cm of space between the shield and the vessel. There are 32 annular holes (0.32-cm diameter) just above the central shoulder of the shield, which permit evacuation of the space between the vessel and the shield. A baffle on the shield between these annular holes and the vessel (see fig. 1) inhibits the passage of radiant energy; this is further reduced by folds of aluminum foil (not shown) in the baffle space.

The temperature of the adiabatic shield is maintained by three separate manganin heaters on the external surfaces: on the cover (115 Ω), on the middle or baffle area above the annular holes (135 Ω), and on the lower base below the annular holes (234 Ω). The length of each of these heaters is approximately proportional to the surface area of the section covered and they are uniformly spaced on the area. The manganin heaters (#36 AWG gauge) are held in place by Glyptal insulating varnish which was applied in several thin coats with several hours baking between each application. The Formvar-coated, copper leads (#26 AWG gauge) were covered with glass spaghetti and attached to miniature connectors shown at the lower center of figure 12. The three shield heaters are operated by a single automatic control system, and initially the current through each heater was adjusted by means of external resistors to minimize temperature differences between the shield and the corresponding location on the calorimeter vessel as indicated by differential thermocouples. Some results of our measurements of the shield temperature profiles are discussed in section 5.2a.

An approximate value was determined for the proportionality factor, k, which is the rate at which heat is transferred between the vessel and its environment per unit temperature difference. For this purpose the control point of the potentiometer in the recorder was offset by − 0.0025 K and by + 0.01 K to produce known temperature differences between the shield and the vessel. The slopes of the time-temperature curves were measured at these two offset points at various pressures and the value of k was equal to the difference in slopes divided by the difference in the control point temperatures. The value of k was about 0.01 min^{-1} at 10.1×10^4 Pa (760 mm Hg), and diminished to 0.003 min^{-1} at about 0.1 Pa (1×10^{-3} mm Hg)

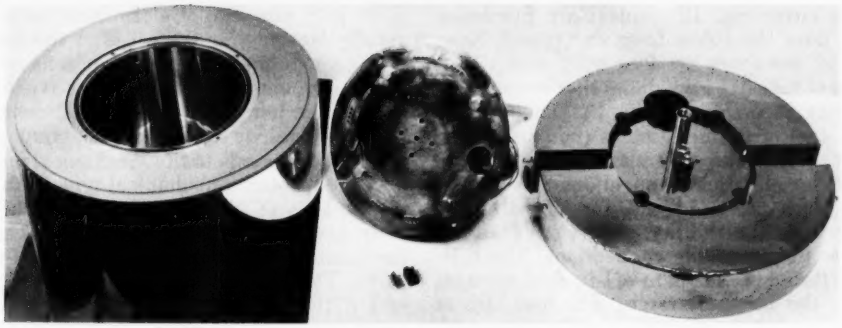

FIGURE 12. *The parts of the jacket.*

At left, the jacket well and insulation; at center, the jacket cover; and at right, the insulation case.

where it became constant. A pressure lower than this is always maintained. The value of k, the heat leak constant, of 0.003 min^{-1} expresses the rate of temperature rise of the calorimeter in degrees K per degree K of temperature difference between the shield and calorimeter per minute. Since the energy equivalent of the calorimeter is approximately 17×10^2 J · K^{-1}, this k corresponds to 5.1 J · K^{-1} · min^{-1}. During rating periods the temperature difference between the shield and calorimeter is typically controlled to within ± 0.0001 K. Thus the heat leak or heat gain during rating periods is less than 0.00051 J · min^{-1} and tends to average out to zero.

During each experiment the difference between the temperatures of the covers of the shield and of the vessel is recorded. Figure 13 illustrates typical curves

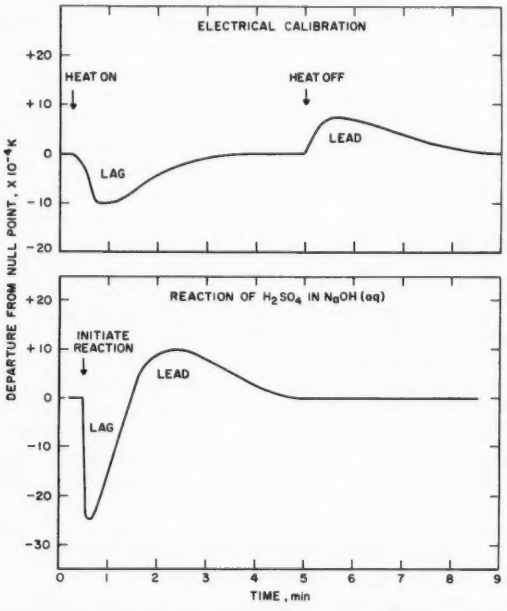

FIGURE 13. *Drawing showing the magnitudes of departures of the temperature of the adiabatic shield from that of the vessel.*

During an electrical calibration (at top), and during a chemical reaction which resulted in a rapid 0.2–K temperature rise in the calorimeter (at bottom).

obtained during an electrical calibration and a rapid chemical reaction (Expt. No. 386, described in section 5.2b) which resulted in a temperature rise of 0.2 K. When the heating is initiated in the calibration there is a "lag" when the calorimeter vessel is warmer than the shield; the maximum departure, ~ 0.001 K, occurs about 0.5 min after the heating is started, and the shield and vessel temperatures are equal about 3 min after initiating heating. When the electrical heating is stopped, a "lead" period results when the cover of the shield is warmer than that of the vessel. It can be seen that the areas of the lag and lead periods are essentially equal but in opposite directions which cancels heat leak errors. In the rapid chemical reaction of H_2SO_4 with NaOH(aq) the temperature difference develops quickly and calls for rapid heating of the shield which, after about 1 min, overshoots the calorimeter temperature. A lead period of about 3 min follows when the shield cover is warmer than the vessel cover. The difference in the lag and lead areas is about 8×10^{-4} K · min. This value is multiplied by our approximate value for k, 0.003 min^{-1}, and the energy equivalent, 17×10^2 J · K^{-1}, to obtain the correction, 0.0003 J, which is not significant in our measurements.

3.3. The Jacket

Another important part of this calorimeter is the jacket which not only confines the vacuum surrounding the calorimeter vessel, but also provides a steady temperature environment for the system. The jacket is surrounded by Fiberglas duct insulation (5-cm thickness), and a coil of copper tubing on the outside which allows the circulation of cold water for measurements below room temperature (see fig. 1).

The jacket consists of two main parts, the well and the cover. The well operates at approximately constant temperature, usually 0.2 to 5 K below the vessel temperature to insure a demand for heat by the adiabatic shield and thus to insure positive shield temperature control. The well (fig. 12, left) has highly polished, nickel-plated, copper walls, 0.64-cm thickness. The inner diameter is 15.5 cm and the depth is 21 cm. In the rim is a groove for a rubber o-ring which forms a vacuum seal with the jacket cover and a thermal barrier between the well and the cover.

In the jacket cover (fig. 12, center) are five holes through which pass the tubes from the vessel. Near the outer edge of the cover are four bolts which hold the stainless steel rods (0.64-cm diam) that support the entire calorimeter assembly (see fig. 2). On the same radius are five sets of hermetic plugs (miniature side mounting connectors, shown separately below the cover in fig. 12) for electrical connections through the jacket. These plugs are used only for shield heater connections because the thermal emfs were found to be excessive for thermocouple connections. The tube at the back of the cover leads to a 1-in dual vacuum coupling and to the vacuum system. The four pins at the rim of the cover are for alignment of the cover with the well. At right in figure 12 is a metal case containing insulation for the jacket cover.

Fittings on the jacket cover around the five platinum tubes are shown in figure 1. Associated with each tube the first fitting above the cover compresses a rubber o-ring around the tube to form a vacuum seal; the second compresses a wedge-shaped, lubricated, copper ring around the tube to support the shield and vessel, and to provide good thermal contact between the tube and the jacket cover; and the third (center tube only) holds an o-ring which provides a bearing and/or a seal for the stirrer (there is a similar fitting for the tube containing the push-rod for the sample holder).

The five platinum tubes above the vessel are the main source of heat leak from the calorimeter. To minimize this heat leak additional heaters, automatically controlled at the shield temperature, were added to the jacket components. One heater (61 Ω) is on the top surface of the jacket cover, and a second independently controlled heater (28 Ω) is on the aluminum block which surrounds the fittings above the jacket cover. In this way, the platinum tubes and their contents are essentially brought to the shield temperature before they enter the calorimeter, and the result is effectively no heat transfer to or from the calorimeter vessel.

Initially when the calorimeter was operated at temperatures above about 300 K, the load was too great on the automatically controlled heaters on the shield and on the jacket. Therefore, additional heaters were added to supply heat at a constant rate and their currents are adjusted by variable transformers to achieve the necessary heat input. They are located on the outer surface of the jacket well, on the connection to the vacuum line, and on the four steel support rods above the jacket cover.

3.4. The Vacuum System and the Hydraulic Lift

This calorimeter does not require a very high vacuum, and the system was designed for dependability and easy maintenance. The pump-down time for the system is relatively long because of the degassing of surfaces of the adiabatic shield and the various insulating materials in the system and the obstructions in the path of the molecular diffusion. About 1 h is required to achieve a pressure of 0.1 Pa (1×10^{-3} mm Hg). Only after several days pumping can the pressure be reduced to about 1×10^{-3} Pa (5×10^{-6} mm Hg). Calorimetric measurements are usually started about 1.5 h after the pumping begins.

The vacuum system is shown in figure 6. The heavy-wall, nitrometer, rubber tubing (visible behind the rack at the left of the jacket well) connects the metal vacuum line via dual vacuum couplings containing rubber o-ring seals to the mechanical pump which is an oil-sealed, rotary, mechanical type, with a rated pumping capacity of $25 \times 10^{-3} m^3 \cdot min.^{-1}$. The other vacuum lines are of copper tubing with soft-soldered joints; the tubing in the lines between the oil diffusion pump (CVC Type MCF–60, capable of an ultimate pressure of 1×10^{-4} Pa or 5×10^{-7} mm Hg at 298 K) and the calorimeter is 2.86-cm outer diameter with 0.086-cm wall thickness, and that leading to the back-up pump is 1.90-cm outer diameter with 0.162-cm wall thickness. The four right-angle, high-vacuum valves in the system are the bellows type with rubber o-ring seals (CVC Type VRA). A valve of this type later replaced the glass stopcock in the line to the ionization gauge tube to reduce the possibility of breakage. The diffusion pump operates with silicone oil (Dow-Corning 704). A line by-passing the diffusion pump permits pumping the system initially with the mechanical pump before switching to include the diffusion pumping.

A hydraulic lift was made to raise the jacket well unit which weighs about 25 kg (see fig. 14). The unit sets on a circular, flat, brass plate attached to a brass rod, 4.76-cm diam, which is a close fit in a stainless steel cylinder, approximately 56-cm height, 5-cm outer diameter, and with 0.165-cm wall thickness. The lower end of the cylinder is welded to a brass plate; near this plate, two copper tubes are welded to the steel cylinder 180 deg apart—one of these connects to the water supply ($\sim 28 \times 10^4$ Pa or $\sim$ 40 psi pressure) and the other to a drain, with valves in each line to control the flow of water. A guide pin (or aligning key) is located near the upper end of the cylinder and slides in a slot in the brass rod (or piston) to maintain alignment as the piston slides up and down in the cylinder; the guide pin also stops the piston from being raised too far. Two lubricated rubber o-rings in grooves near the lower end of the piston form a seal with the cylinder wall. When the well unit has been raised for a calorimetric experiment, a steel pin (safety-stop pin) is set in a hole in the piston at the top of the cylinder to prevent the unit from dropping in case of a failure of the water pressure. The level and rate of movement of this lift may be easily and precisely controlled by operation of the valves in the inlet and exit water lines (shown at the right of the well unit in fig. 6). The cross-sectional area of the piston is 17.8 cm^2, and at the nominal water pressure given above, the lift is capable of raising approximately 50 kg which is about twice that actually required.

3.5. The Calibrating Heater and Control Thermocouples

Because of the important functions of the calibrating heater and the control thermocouples, there was considerable care in their design and fabrication. Some of the features included in the design of this heater

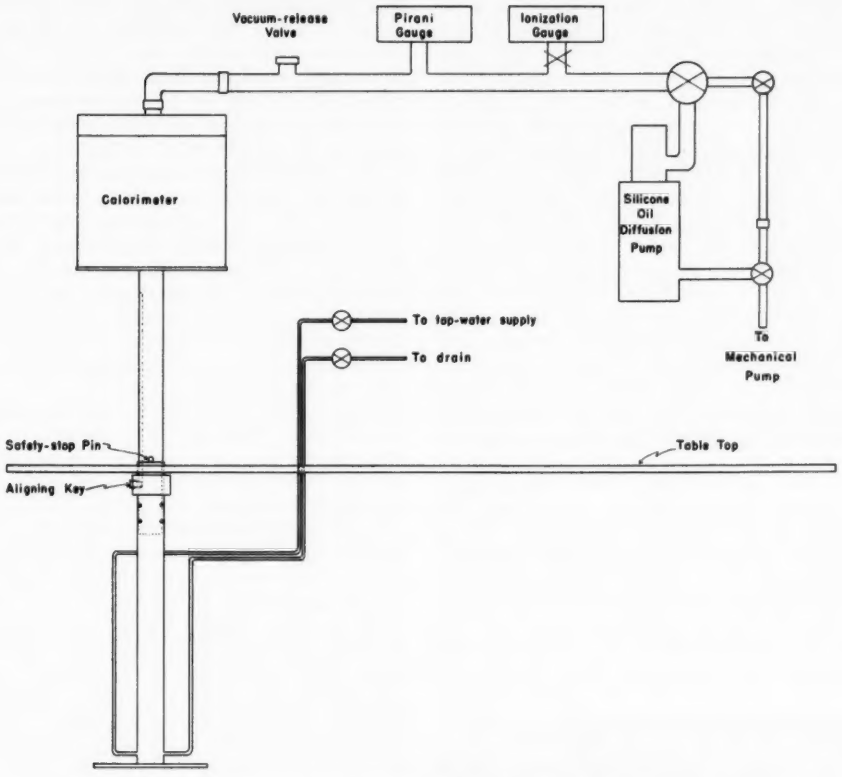

FIGURE 14. *Schematic diagram of the vacuum system and the hydraulic lift for the well of the calorimeter jacket.*

are: the heater wire has a high resistance per unit length to prevent unreasonably long windings, and a low temperature coefficient of resistance to avoid significant changes in the resistance over the temperature range in which it was to be used; the unit has a small heat capacity to reduce thermal lag; the conduction of heat to the well and solution is as rapid as possible compatible with the need for reliable electrical insulation; and possibly most important, the leads to the heater are arranged to minimize the transfer of heat from the calorimeter. The control thermocouples are designed to avoid heat exchange at the point of temperature detection, to achieve maximum thermal contact consistent with electrical insulation, and to provide proper temperature averaging.

The calorimeter heater (approximately 97 Ω, #36 AWG gauge, enamelled, manganin wire) was wound on a stainless steel cylinder (0.81-cm outer diameter and 0.018-cm wall thickness) on which two layers of Glyptal insulating varnish had been baked. The heater was wound noninductively, i.e., at the mid-point of the wire length a loop was formed and secured near the lower end of the cylinder, then the two wires coming from the loop were wound closely together around the cylinder using care to avoid crimping or overlapping the wire. When the winding was complete, the wire was secured with dental floss or silk thread and several layers of Glyptal insulating varnish were applied with baking after each layer. Copper wire (5-cm length, #32 AWG gauge, enamelled, and cotton-covered) was soldered to each end of the manganin heater, and to each of these leads was soldered a pair of #26 AWG gauge copper leads about 25 cm in length. The single copper leads were wrapped around the cylinder twice (the cylinder was indented slightly at the top to allow space for the larger wire and joints), coated with insulating varnish and baked. The unit was pushed into the close-fitting platinum well; the top of the cylinder was about 1 cm below the top of the well. The four Formvar-coated copper leads were looped before leaving the well, and they were held in contact with the well, 90 deg apart, by a balsam disk. The leads were covered with PTFE spaghetti as they passed through the platinum tube and out of the calorimeter.

This heater has given years of stable performance. Its resistance changes only 0.2 Ω between 298 K and 353 K. The rates of heating the calorimeter range from 0.035 K · min^{-1} at 10 V to more than 0.5 K · min^{-1} at 40 V.

To check the heater lead error in this "permanent" heater a series of electrical calibrations were made in which the calibrations alternated between the use of the permanent heater and of a "dummy" heater

which was immersed directly in the calorimetric solution (H_2O) so that the leads were definitely at the temperature of the solution before leaving the calorimeter. The average of 11 electrical energy equivalents measured with the permanent heater was 17,069.88 $\pm$ 1.18 (sdm) $J \cdot \Omega^{-1}$ and with the dummy heater, 17,069.27 $\pm$ 0.58 (sdm) $J \cdot \Omega^{-1}$. The difference between the two is 0.61 $J \cdot \Omega^{-1}$ or 0.004 percent which is within the uncertainty of the measurements. This indicates that no significant amount of heat was transferred from the calorimeter through the heater leads. The possibility of an error due to unmeasured energy generated by current in the copper leads in the area between the shield and the junction point for the potential leads, was considered. The maximum length of the #26 AWG gauge, copper wire involved here is about 6 cm which has a total resistance of about 0.008 Ω. Since this is only 0.008 percent of the heater resistance, the possible error from this source is assumed to be less than 0.01 percent.

The use of the six-junction thermocouple only between the covers of the adiabatic shield and the vessel is justified by the fact that lags in the rest of the system will be reproduced and compensated for in the electrical calibrations. Also, linear heat-flow theory can show that lags in the rest of the shield will cancel out in the calculation of the temperature rise. The placement of some of the thermocouples on the cover of the vessel may be seen in figure 15. Two of

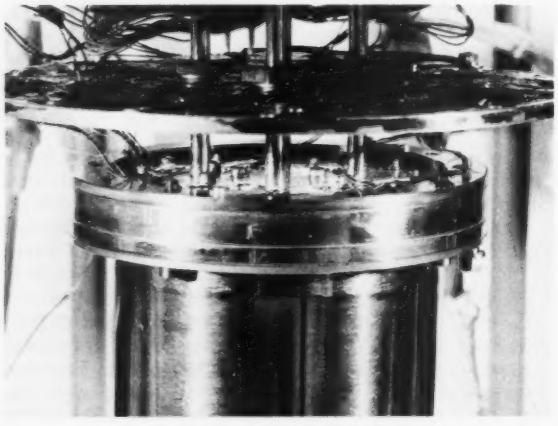

FIGURE 15. *The top of the calorimeter vessel showing the placement of the shield control thermocouples.*

the six junctions on the vessel cover are placed between the platinum tube at the center, and the four platinum tubes which surround it; the remaining four junctions are placed between the radius of the four platinum tubes and the edge of the steel ring. The other junction of each thermocouple pair is placed on the shield cover in the location which corresponds approximately to those on the vessel cover.

The copper and constantan thermocouple wires are #30 AWG gauge, enamelled, and asbestos covered. To form the junction, the insulation is removed on about 3 mm of each wire, the wires are twisted tightly together, and soft soldered with minimal amounts of solder. The junction is cut to a length of about 1.5 mm, placed on a silver disk (about 5-mm diam and 0.08-mm thickness), and attached with a small spot of soft solder. A disk of lens tissue impregnated with epoxy cement is placed between the silver disk and the metal surface to which it is to be attached. Pressure is applied above the silver disk to extrude excess cement (which is removed) until the cement has set. The thin layer of cement insulates the thermocouples electrically without forming a significant thermal barrier. (N,N dimethylformamide is a solvent for the cement when removal of the thermocouples is necessary.) The silver disk covers a large area relative to that of the thermocouple and because of the good thermal diffusivity of silver allows accurate surface temperatures to be measured.

This type of thermocouple is used for detecting the temperature difference between the vessel cover and the shield cover, and between the shield cover and the jacket cover. Thermocouples of the same wire but without the silver disks, using epoxy cement as insulation, were used to indicate the temperature difference between the cover and well of the jacket, and between the jacket cover and the aluminum block at controlled temperature above the jacket.

All of these thermocouples were connected through a solder-type terminal strip under the jacket cover to leads (#28 AWG gauge, enamelled, cotton-covered, copper) which passed through a side arm in the dual vacuum coupling above the jacket cover, and then through a vacuum seal of glass and Apiezon "W" wax

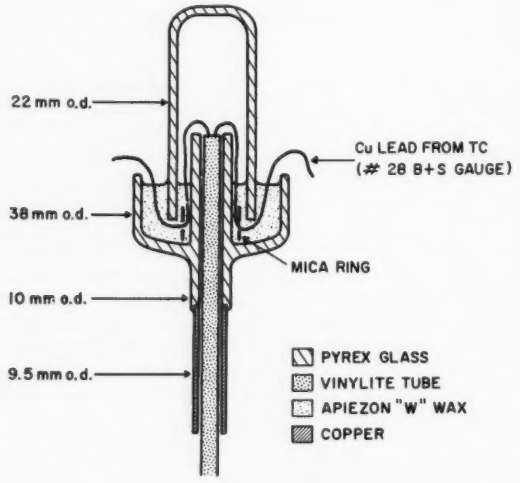

FIGURE 16. *A cross-sectional diagram of the vacuum seal for the thermocouple leads.*

The leads pass through the plastic tubing to the top of the glass tube, then down and through the ring of mica containing holes which insure separation of the leads as they pass under the glass dome and then to the atmosphere. The dome is sealed by the Apiezon wax in the cup.

as shown in figure 16. Then they passed into the insulated terminal box where soldered connections were made to their respective circuits.

3.6. The Electrical Calibration and Electronic Control Instruments

During the 7 years that this calorimeter has been operational, many changes have been made in the electronic equipment used in the various circuits. The conversions, where possible, from vacuum tube units to transistorized and solid-state units greatly improved the dependability of the instruments and reduced the number of experiments lost because of electronic malfunctions. In some cases better instruments are known to be available now, although the additional expense has delayed replacement of the presently adequate equipment. In this section the instruments currently in use will be identified. We wish to emphasize that naming the manufacturer or a trade name is only for specific identification and does not constitute an endorsement of the product by this organization.

The 97-Ω calorimeter heater is used for preheating and electrical calibrations. The pairs of current and potential leads from the calorimeter heater are connected in the insulated junction box (upper right, fig. 6) to leads from the standard resistors, and from the dc constant-voltage power supply (Sorensen Model QR40–2 A; 0–50 V; 0–2.25 A; ripple, 150 μV rms; voltage regulation, $\pm 0.01\% + 1$ mV) through a toggle switch which actuates the electronic counter and directs the current either through the calorimeter heater or through a spill coil with a resistance approximately equal to that of the heater. The current through the heater is calculated from the measured potential drop across a 0.1 Ω standard resistor (Rubicon Ser. No. 117443) in series with and on the low potential side of the calorimeter heater (see fig. 3). The potential drop across the heater is calculated from the measured potential drop across a 10-Ω standard resistor (Rubicon Ser. No. 119222) in series with a 10-kΩ standard resistor (Rubicon Ser. No. 119184), and this combination is in parallel with the calorimeter heater. The potential drops are measured with a six-dial potentiometer (M-H Model 2783; the limit of error in the 0.16 μV range, $\pm 0.005\% + 0.1$ μV) using a null detector (L and N Microvolt Indicating Amplifier Cat. No. 9835-B) which had been modified to increase the sensitivity by a factor of ten (5 μV full scale). The time of heating in electrical calibrations is measured with an accuracy of ± 0.001 s with an electronic counter (H-P Model 5216A, 3 Hz to 12.5 MHz range) which counts cycles of the 10 kHz standard frequency signals available at NBS.

The working current of the potentiometer is balanced against a saturated standard cell (Eppley Group No. 2625) which is maintained at approximately 303 K (constant to ± 0.01 K) in thermostat Box No. 5. These cells are calibrated at intervals of 2 or 3 years as are the standard resistors in the electrical calibration circuit. The records of numerous calibrations over the years provide additional confidence in the values used because of the consistent trend in the calibrated values.

The three standard resistors are in a box protected from abrupt changes in ambient temperatures. The temperatures of the standard resistors are indicated to ± 0.02 K by ten-junction, copper-constantan thermocouples with ice reference junctions, and measured by a millivolt potentiometer. Switching between the thermocouples is done with a rotary selector switch (L and N Cat. No. 8248–16).

The working currents for the G-3 bridge and for the six-dial potentiometer are supplied by 2-V and 6-V, slow-self-discharge, storage batteries (Willard DD-5-1 and DD-5-3). These batteries are recharged annually using 2.5 A for 2 or 3 days, and steady readings with the potentiometer cannot be made for about 2 weeks after charging.

Initially ambient temperature was found to affect the results of the potentiometer measurements. A heater was added to the guard case and controlled by a transistor-circuit temperature controller.[4] This type of temperature controller has also been used with the G-3 bridge and with the standard cell box, and none of them has failed in approximately 7 years of continuous use.

The current in the automatically controlled heaters for the adiabatic shield, for the jacket cover, and for the aluminum block above the jacket is supplied by a dc, constant-voltage, power supply (Sorensen QB28–4; 18–36 V; 0–5 A; voltage regulation accuracy, ± 0.01 %; ripple, < 300 μV rms). The thermocouple emfs for the jacket cover and for the aluminum block are sensed by the dc null detectors (L and N Cat. No. 9834–2; maximum sensitivity, 25 μV full scale or ± 12.5 μV), transmitted to the current-adjusting-type (C.A.T.) control units (Series 60, L and N Part No. 354162) from which the output is dependent not only upon the amount of departure from the null point, but also on the speed with which the null point is approached and the rate at which the demand is changing. Transistor-circuit power amplifiers increase the current output from the C.A.T. control units to the respective heaters. The system for the control of the adiabatic shield heaters (see fig. 4) is essentially the same except that a more sensitive null detector is used (L and N μV Indicating Amplifier Cat. No. 9835B, modified to increase the sensitivity by a factor of ten) and its output is recorded on a strip-chart recorder (L and N Speedomax H, Part No. 077990) with a sensitivity in this system of 0.004 K per chart inch. Thus, departures of the adiabatic shield temperature from the calorimeter temperature are continuously recorded during an experiment. During rating periods, the deflections (or noise) are about ± 0.0001 K; the deflections during electrical calibrations and most chemical reactions result in no significant correction to the heat of reactions. The largest departure from the calorimeter temperature in our records during the 2.5–K temperature rise of a fast chemical reaction resulted in a correction of less than 0.1 percent.

The pressure in the vacuum system is measured with a Pirani vacuum gauge (Consolidated Electrodynamics, Type GP–110) and an ionization vacuum gauge (CVC Type GIC–110B). These gauges are used

[4] Designed by David Brenner Electronic Instrumentation Section.

only for approximate pressure measurements and serve to indicate malfunctions in the vacuum system.

3.7. The Thermometers

Until June 1972, the calorimeter temperature was measured either with a system employing a 25-Ω platinum resistance thermometer or with an experimental system employing a quartz-oscillator thermometer which was used for a period of approximately 8 months. Our preliminary work with the quartz-oscillator thermometer indicated that it is comparable in accuracy and precision with the platinum resistance thermometer.

The platinum resistance thermometer (see fig. 3) was connected directly through thermometer cable (exposed joints were covered with cotton to reduce thermal emfs) to a G-3 Mueller-type thermometer bridge (Rubicon Ser. No. 65471, purchased in 1952 and no longer available). The null detector was an Astrodata nanovoltmeter (Model TDA-121z) with a noise level of < 5 nV and an accuracy of 3 percent of full scale on all ranges; the rating period measurements were made on the 10 μV range. (20 μV full scale). The 3-V output of the nanovoltmeter was reduced by a divider to approximately 5 mV for the input to the strip-chart recorder (L and N Speedomax G, Cat. No. 60614) with a sensitivity in this system of 500 μK per chart inch.

The system which employed the quartz-oscillator thermometer (H-P Model 2801A with the option providing the additional 100-s integration period) used a modified probe-oscillator (H-P 2850D and 2830A). The response time of the probe was improved by removing the protective steel case which surrounded the probe case (8.1-mm diam and 6.4-mm height, with a flange at the top which was about 1-mm width—this is a "TO-5" transistor case). Removal of the protective case was an operation which had to be done with great care to avoid breaking the delicate leads from the quartz oscillator. The probe was placed in the same platinum well used for the resistance thermometer, and it seated just above the point where the diameter of the well was reduced; a close-fitting aluminum block was placed in the bottom of the well to reduce thermal lag and the probe was covered with silicone oil to improve thermal contact with the well.

In order to make the quartz-oscillator case fit into the well used for the resistance thermometer, it was necessary to file down the rim of the case, and in so doing the soldered seal was broken. This caused no problems until after a number of experiments at about 355 K when obviously erratic behavior of the quartz oscillator developed. Some droplets of oil had come in contact with the quartz crystal as a result of replacement of the gas in the case by oil during successive heating and cooling of the calorimeter. After this, the resistance thermometer system was used until a well could be made to fit a new quartz-oscillator case without reducing the diameter of its rim. More than 100 experiments were completed using the quartz-oscillator thermometer before the malfunction developed.

Digital output equipment was not available to us at the time this first probe-oscillator was used, and the temperatures were read directly in °C on the Nixie tube display and recorded manually. On the 100-s integration interval, the temperatures were read to 1×10^{-5} °C, and the standard deviation of rating period points from the mean slope was less than $\pm 10\ \mu$K.

The quartz thermometer system installed in June 1972 (not used in this work) uses only the quartz probe (H-P 2850D), the probe-oscillator (H-P 2830A), and a 15-V power supply. Counting of the frequency is performed directly with a 50 MHz counter (H-P 5326A) using the NBS standard frequency (stable to better than 1 part in 10^{11}) as the time base to obtain 1-s, 10-s, or 100-s integration times. This system eliminates the reference crystal and provides a more stable system. Calibration against a platinum thermometer provides the relation between frequency and temperature.

The stability of the quartz-oscillator thermometer has been found adequate for the relatively short-term requirements of solution calorimetry where the system is calibrated with each experiment, however we have not enough information now to comment on the stability over a period of weeks or months as would be required for some other types of calorimetry.

The platinum resistance thermometer system was used for periodic calibrations of the quartz-oscillator thermometer. For this purpose the resistance thermometer in a platinum well was immersed in the solution close to the well containing the quartz probe; the leads of the resistance thermometer were insulated with Pliobond cement. A few drops of silicone oil were placed in the thermometer well to improve contact between the thermometer and the well.

The NBS certified calibration of the 25-Ω capsule-type platinum resistance thermometer (L and N Ser. No. 769892) in October 1961, provided the following coefficients: $\alpha = 0.00392547$, $\delta = 1.4918$ (estimated value), $\beta = 0$ (for t above 0°C), and $R_0 = 25.547\ \Omega$, for the Callendar equation

$$t = \frac{R_t - R_0}{\alpha R_0} + \delta\left(\frac{t}{100} - 1\right)\frac{t}{100} + \beta\left(\frac{t}{100} - 1\right)\left(\frac{t}{100}\right)^3$$

where t is the temperature in °C. The values for $\Delta R/\Delta t$ are 0.10177 $\Omega \cdot K^{-1}$ at 273.15 K, 0.10104 $\Omega \cdot K^{-1}$ at 298.15 K, and 0.09879 $\Omega \cdot K^{-1}$ at 373.15 K. In January 1968, while the platinum thermometer was mounted in the calorimeter, the resistance at the ice point was measured as $R_0 = 25.5478\ \Omega$. This indicated that the original calibration was unchanged within the uncertainty of the measurements.

Before 1968, our measurements were made using a thermometer current of 8.35 mA to achieve the desired sensitivity with the microvolt amplifier then used as a null detector. The thermometer current remained on continuously during an experiment so that the uniform heat generated by the thermometer became part of the rating period slopes. This large thermometer current caused small fluctuations in the temperature

records which disappeared when the current was reduced to 2.75 mA and a more sensitive null detector was used; the fluctuations were apparently caused by a combination of stirring and thermometer heating effects. Greater stability in the thermometer current was achieved by replacing the variable resistor in the current-measuring branch of the bridge with a fixed resistor. For corrections to the 2.0-mA current used in the thermometer calibration, we measured the 25-Ω thermometer resistance at various currents and found $dR/(dI^2)=46.0\mu\Omega\cdot mA^{-2}$; these corrections are applied to the initial and final temperatures calculated for reactions.

4. Procedures

4.1. Samples and Solutions

The weight of samples in air is usually obtained from the difference in the weights of the sample holder empty and filled with the sample. The weight of the sample in air is multiplied by a buoyancy factor to obtain the mass or weight in vacuum; the buoyancy factor is calculated from the following equation

$$\text{B.F.}=1+\frac{d_{air}}{d_{sample}}-\frac{d_{air}}{d_{weights}}.$$

The weights are calibrated in terms of brass, and $d_{weights}=8.4$ g·cm^{-3}; and the average density of air used is $d_{air}=0.00118$ g·cm^{-3}. This value for the density of air applies within ± 0.00001 g·cm^{-3} at 22.5 ± 0.5 °C, 20 to 50 percent relative humidity, and 745 to 760 mm Hg pressure. The atmospheric pressure at the laboratory is normally not recorded, but a continuous record of the temperature and relative humidity is kept on a Belfort Hydrothermograph. When this calorimeter was first constructed it was located in a laboratory equipped with neither temperature nor humidity controls. In April 1966, the calorimeter was moved to the laboratory in Gaithersburg, Maryland, where the relative humidity was controlled at 30 ± 10 percent and the temperature, at 22.5 ± 0.5 °C. Thus, the density of air in the laboratory is normally within the limits given above.

The calorimetric solutions are usually taken from stock solutions, initially 2000 cm^3 in volume and stored in polyethylene bottles. Approximately 300 cm^3 of the stock solution is transferred to a 500-cm^3 polyethylene bottle, the weight is adjusted to a "standard" weight for the set of experiments, the solution is poured into the cup of the calorimeter vessel which is immediately attached to the cover, the empty polyethylene bottle is weighed, and the weight in air of the solution is obtained from the difference in weights. Typically the stock solutions are prepared from distilled water in equilibrium with air, except alkali solutions for which the distilled water is boiled to remove CO_2 initially. No special precautions have usually been taken to exclude CO_2 from the solutions because during the calorimetric experiments the solutions are exposed to the atmosphere for several hours and the presence of small amounts of carbonate in the calorimetric solutions has little affect on the enthalpy. However, in work requiring the highest accuracy, the stock solutions have been prepared and analyzed a day or two before starting the experiments, and the solution transfers for weighing made quickly with minimal exposure to the atmosphere.

4.2. Temperature Measurements

When the calorimeter temperature is measured with the resistance thermometer, the sensitivity of the measurements is determined at least once in each experiment with the bridge commutator in the normal, *N*, position and readings are recorded for 20-s intervals according to the following procedure: The bridge dials are set to produce a null detector deflection of nearly zero and the first reading, NF_1, is recorded; for the second reading, NB_1, the thermometer current is reversed through a reversing switch; and for the third reading, NF_1, the thermometer current is again switched to the first direction. Then the bridge dials are changed to produce nearly a full scale deflection on the recorder chart, and similar readings are recorded, NF_2, NB_2, and NF_2. The bridge dials are then returned to the values used in the first set of readings and this procedure repeated to produce NF_3, NB_3, and NF_3. The deflections for the NB readings in each set are subtracted from the corresponding average of the two NF readings, and then the average difference, Δ, from the first and third sets is subtracted from the difference for the second set, or $\Delta_D=\Delta_2-1/2\ (\Delta_1+\Delta_3)$. The sensitivity of the measurements is Δ_D divided by the change in resistance between sets 1 and 2.

During rating periods, a single temperature measurement is the average of nine separate readings recorded for 20-s intervals. A measurement is made as follows: three readings are recorded with the commutator in the normal, N, position, NF_1, NB_1, and NF_1, as described above; for the next three readings, RF_2, RB_2, and RF_2, the commutator is in the reverse, R, position, and the bridge dials are adjusted to produce small deflections; for the last three readings, NF_3, NB_3, and NF_3, the commutator is returned to the N position and the bridge dials are again adjusted. The current reversals correct for thermal emfs and zero drifts, and the commutator reversals correct for differences in lead resistances. Three minutes is required for a single temperature measurement and the calculated temperature corresponds to the time at the mid-point of the measurements. To calculate the temperature, the B current deflections are subtracted from the average of the two F current deflections in each of the three groups, and these differences are multiplied by the sensitivity (described above) to obtain the resistance to be added to the dial readings; then half the resistance in the R position plus half of the average of the 2 resistances in the N position, or $R_t=1/2[R_2+1/2(R_1+R_3)]$ gives the thermometer resistance at the mean time of the measurement.

These temperature readings are made at 5-min intervals during rating periods and there are a mini-

491-397 O - 73 - 2

mum of three but usually five readings per rating period. Equations were formulated for our use, by Joan R. Rosenblatt (Statistical Engineering Section), which produce a least squares fit to the slope of a number of *equally spaced* points. These equations are used in our rating period temperature slope calculations. The slope for each pair of obsevations is calculated as the difference in resistance per unit time, $S_1=(R_2-R_1)/\Delta t$, $S_2=(R_3-R_2)/\Delta t$, etc., and the least squares fit is obtained using the following formulae:

$$n=3, \quad (S_1+S_2)/2$$

$$n=4, \quad (3S_1+4S_2+3S_3)/10$$

$$n=5, \quad (2S_1+3S_2+3S_3+2S_4)/10$$

$$n=6, \quad (5S_1+8S_2+9S_3+8S_4+5S_5)/35$$

where n is the number of temperature readings. A more general equation is: slope$=\{6/[nt(n^2-1)]\}$ $[i(n-i)d_i]$ for the summation between the limits $i=1$ to $n-1$, where n is the number of equally spaced points (or temperature measurements), t is the time interval, and d is the difference between successive points.

In figure 17 is a plot of a time-temperature curve for a chemical reaction or an electrical calibration

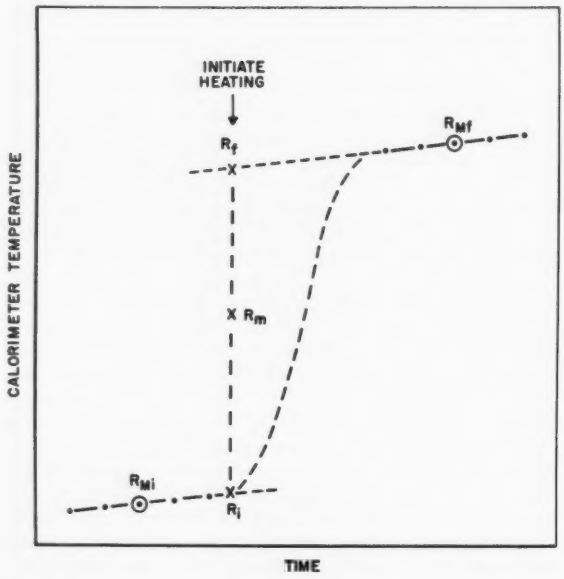

FIGURE 17. *A plot showing various points used in calculating the corrected temperature rise and the mean temperature of reaction.*

R_{Mi} and R_{Mf} are the mean temperatures of the rating periods, R_i and R_f are the initial and final temperatures of reaction, and R_m is the mean temperature of reaction.

showing various points used in the calculation of the corrected temperature rise, ΔR_c, in a normal experiment. Five temperatures for each rating period are calculated as described above, and the mean of these for the initial rating period is R_{Mi} and for the final rating period is R_{Mf}. If S_i and S_f are the slopes of the initial and final rating periods, respectively, then the initial temperature of reaction, R_i, and the final temperature of reaction, R_f, are

$$R_i=R_{Mi}+S_i\,(\Delta t_i) \text{ and } R_f=R_{Mf}-S_f\,(\Delta t_f),$$

where Δt_i is the time interval between the mid-point of the initial rating period and the time of initiating heating (or reaction), and Δt_f is the time interval between the mid-point of the final rating period and the time of initiating heating. The precise time to which the slopes are extrapolated is not important since S_i and S_f are nearly the same and no corrections need to be made for heat exchange with the environment. The corrected temperature rise is $\Delta R_c=R_f-R_i+R_b$ where R_b is a small bridge dial correction; and the mean temperature of reaction is $R_m=[(R_f+c_1)+(R_i+c_2)]/2$ where c_1 and c_2 both include bridge dial corrections and corrections to 2 mA thermometer current.

During our first experiments using the quartz-oscillator thermometer for the calorimeter temperature measurements, the output had not been automated and the temperatures were read directly on the Nixie-tube display in the thermometer chassis. Readings appeared at 100-s intervals for rating periods. This procedure was followed for the experiments to be discussed in section 5. In this case, the temperature slopes of the rating periods were computed as the slopes of the straight lines providing least squares fits of 15 to 20 time-temperature readings.

In very slow reactions, which are frequently measured in this calorimeter, it is impossible to determine precisely the time when the reaction is complete; fortunately, this is not important because the calorimeter is adiabatic and corrections for heat transfer to the surroundings are negligible. The criteria for determining when the reaction is complete are (1) when the slope of the calorimeter time-temperature curve has not changed significantly for 1 h, or (2) when the slope of the time-temperature curve is equal to that preceding the reaction. The first criterion is preferred because small differences in the slopes of the rating periods before and after the reaction may be the result of a change in the stirring energy because of a change in the viscosity of the solution at the higher temperature and a different composition.

4.3. Electrical Calibrations

The voltage across the calorimeter heater may be varied from 0 to 40 V. The highest voltage is used only for preheating the calorimeter at the rate of about 0.55 K · min^{-1} for reactions at high temperatures. Above about 30 V, the current and potential readings are less stable than desired, possibly because the heat transfer through the well is not adequate at the higher temperature. Therefore, electrical calibrations are usually carried out in the range of 10 to 30 V (heating rate, 0.03 K·min^{-1} to 0.30 K·min^{-1}).

In this adiabatic calorimeter it should not be necessary to match the shape of the time-temperature curves in the calibrations with those of the chemical reaction, because there are normally no corrections for heat transfer to the surroundings. However, the voltage and duration of heating in the calibrations are usually chosen so that the temperature rise is approximately equal to that caused by the chemical reaction. The time of heating is not more than 12 min nor less than 2 min, which allows sufficient time to obtain enough readings of current and potential across the heater for a good average. We have not found evidence that variations in the time or voltage selected for calibrations of a given system affect the electrical energy equivalent significantly. However, in some systems, the electrical energy equivalents do change nonlinearly with temperature and it may be necessary to obtain thermal coefficients for the calibrations in order to extrapolate to the mean temperature of reaction. In most systems the change in heat capacities with temperature is negligible and/or linear; therefore, calibrations of the initial and final systems are usually sufficient.

The following procedure is used in the electrical calibrations. Before starting the electrical heating, the temperatures of the three standard resistors are recorded, the working current of the potentiometer is balanced against the standard cell voltage, and the zero readings are made for the "current" and "potential" circuits. A toggle switch directs the current from the spill coil to the calorimeter heater, and starts the electronic counter. After 30 s, the first reading of the current through the heater is made, and 30 s later the first reading of the potential drop across the heater. Alternate readings of the current and potential drop are made at 30-s intervals until the heating is stopped by reversal of the toggle switch which simultaneously stops the counter. Readings are recorded of the time shown on the counter, and again of the temperatures of the three standard resistors, and the zero readings for the "current" and "potential" circuits. The change in the working current is observed and this completes the electrical energy measurements.

The electrical energy measured in the calibrations is calculated as follows: The thermal coefficients for the standard resistors are used to correct the value calibrated at 298.15 K to that at the average temperature of the resistors during the electrical calibration. An additional small resistance (usually less than 0.5 Ω), R_Δ (see fig. 3), is the resistance of the leads included in the circuit for measuring the potential drop across the heater, to the branch points on each side of the heater; this resistance is a constant as long as the circuit remains unchanged. The averages of the voltage readings (corrected for the mean zero readings) for the current, e_i, and for the potential drop across the heater, e_e, are corrected for small changes in the potentiometer working current during the calibration and by addition of potentiometer dial corrections. The current through the heater, I, is equal to the difference between the current through the 0.1-Ω standard resistor and the current through the 10-Ω standard resistor, or $I = (e_i/R_{0.1}) - (e_e/R_{10})$. The voltage drop across the heater, E, is the product of the current through the 10-Ω standard resistor and the total resistance in this branch of the circuit, or $E = (e_e/R_{10})\ (R_{10_k} + R_{10} + R_\Delta)$. The electrical energy equivalent is $(EIt)/\Delta R_c$, where t is the measured time of electrical heating and ΔR_c is the corrected temperature rise. A small correction, 0.40 J · Ω^{-1}, is added to the energy equivalent of the initial system to correct for the heat capacity change when the sample holder is opened (the platinum push-rod is pushed down approximately 3 mm).

In the normal experiment, an electrical calibration of the initial system is followed by the chemical reaction and then by an electrical calibration of the final system. When the product of the corrected temperature rise for the reaction and the energy equivalent of the initial system is divided by the amount of sample, we obtain the enthalpy of reaction referred to the "final temperature" of reaction; similarly, the product of the ΔR_c of reaction and the energy equivalent of the final system divided by the amount of sample gives the enthalpy of reaction referred to the "initial temperature" of reaction. The difference between these two enthalpies is a useful indicator of errors in calculations or measurements, and the mean of these two enthalpies is ΔH_r at the temperature of reaction which we define as the mean temperature of reaction, R_m or $\bar{T}$ reaction.

5. Measurements of a Standard Reaction

An all-purpose, reliable, standard reaction for general solution calorimetry with a known enthalpy value of high accuracy and precision has not yet been established. Gunn [2] has discussed various reactions which have been used for comparison of solution calorimeters. Potassium chloride was objectionable because of the endothermic enthalpy of reaction which may introduce some unknown effects in the heat transfer in some calorimeters, and as Parker has shown [3] there is disagreement as to the best value for the reaction. The reaction of tris(hydroxymethyl)-aminomethane in aqueous HCl has also produced results from various calorimeters which are in poor agreement for reasons not fully explained. We decided to measure the enthalpy of reaction of aqueous H_2SO_4 in NaOH solutions since a sample was given to us of the same H_2SO_4 solution with which Gunn had obtained results with an experimental imprecision of less than 0.01 percent.

In this section will be given the results of our measurements with this sample in two concentrations of NaOH solutions which were also measured by Gunn. Our measurements began in January 1970, and were completed in April 1970.

A quartz-oscillator thermometer calibrated in terms of the 25-Ω platinum resistance thermometer was used for all experiments reported in this section.

Certified NBS calibrations were made as follows: Saturated standard cell No. 2625–2293, July 1969; and standard resistors No. 117443 (0.1 Ω), No. 119222

(10 Ω), and No. 119184 (10,000 Ω), June 1969. The records of numerous calibrations over several years for the standard cell and standard resistors provide additional confidence in the values used because of the consistent trends in the calibrated values.

Calibrations were made in this laboratory of the G-3 resistance thermometer bridge dials in January 1969, and November 1970, and of the six-dial potentiometer in January 1969.

The unit of energy is the joule (J), and 4.1840 J= 1 thermochemical calorie.

5.1. The Sample and Solutions

The sample of $H_2SO_4 \cdot 8H_2O$ as received from Gunn was in a 250-cm³, sealed, glass bottle labeled "18A1". A private communication from Gunn explained that this was one of three bottles into which a batch of quantitatively diluted, constant-boiling acid was divided, and that one of the other bottles was used for his measurements of these reactions. The following additional information was provided:

(1) The composition of the solution corresponds to a molecular weight of 242.204. (The nominal composition corresponds to 242.200 [4] or 242.1968 [5]; Gunn's value was used in our calculations.)

(2) The ratio of the vapor pressure of water above the solution to the vapor pressure of pure water, a_w (or $p/p°$), is 0.5554.

(3) The apparent molar volume, φ_v, is +41.3 $cm^3 \cdot mol^{-1}$.

(4) The density of the sample was given as 1.307 $g \cdot cm^{-3}$. Our buoyancy factor (see sec. 4.1) is 1.000763 using his density for the sample.

(5) Suggestions were given for a procedure to be followed in opening the bottle and in reclosing it to prevent contamination of the sample. (These suggestions were followed closely and carefully.)

Approximately 75 cm³ of the sample was pipeted to a 100-cm³ glass bottle with an inverted, standard-tapered-joint cap. This was then stored in a stainless steel glove box where the calorimetric samples were to be added to the sample holder. In the glove box were three large crystallizing dishes which contained saturated solutions of $Ca(NO_3)_2 \cdot 4H_2O$ to maintain a relative humidity of approximately 53 percent at the laboratory temperature, thus minimizing exchange of water with the sample.

For reaction I, the smallest cylinder (0.7 cm³) with PTFE o-rings for the sample holder was used to contain the samples which were 0.59 to 0.69 g of the acid. In reaction II, the middle-sized cylinder (1.9 cm³) was used for the larger samples of acid which ranged from about 2.0 to 2.4 g. The calorimetric acid samples were transferred in the glove-box-hygrostat to the weighed sample holder by means of a glass dropper, and the sample holder was sealed before removal from the hygrostat for reweighing and installation in the calorimeter.

The 2000-cm³ lots of NaOH stock solutions (from which the calorimetric solutions were taken) were prepared by dilution of 0.1 or 1.0 *N* NaOH solutions with freshly boiled, distilled water which was guarded by Ascarite absorption tubes, and then stored in polyethylene bottles. The stock solutions were analyzed by titration of potassium acid phthalate using a Heath Recording pH Electrometer with calomel and hydrogen reference electrodes. In table 1 are given the average value of three titrations for each stock solution, and the experiment numbers in which the solution was used. The calorimetric solutions were transferred to a polyethylene bottle for weighing and then to the calorimeter vessel; no special precautions were taken to exclude CO_2 during these transfers except to work quickly and to avoid breathing directly on the solutions.

TABLE 1. *Analysis of* NaOH *stock solutions*

NaOH stock soln. No.	Normality	Used in Expt. Nos.
	mol/1000 cm³	
10	0.0207	380–382
11	.0215	384–387
12	.0785	413, 414, 420
14	.0779	416
15	.0770	424, 425
16	.0774	427, 429

5.2. Experimental Results

The adiabatic solution calorimeter described in detail in sections 3 and 4, was used to measure the enthalpy of solution of $H_2SO_4 \cdot 8H_2O$ in ~0.02 *N* NaOH (reaction I), and in ~0.08 *N* NaOH (reaction II). The results of seven experiments for reaction I and eight experiments for reaction II are reported here.

The sample holder (see section 3.1c) functions well with solid samples but problems of prereaction due to leakage at the o-ring seals are sometimes encountered with liquid samples as was true in these measurements; thus, a total of 34 experiments were run and only 15 yielded good values although some were lost for reasons other than prereactions. When there was a large amount of prereaction the rating period slopes were abnormally high and the heats of reaction were abnormally low. Fortunately there was a definite break between the values obtained from reactions which showed no evidence of prereaction and those involving prereaction; i.e., the former values were all 34,185 $cal \cdot mol^{-1}$ and greater and the values rejected because of prereaction were 34,164 $cal \cdot mol^{-1}$ or less. In spite of the problems with liquid samples this sample holder was preferred over the more conventional types, such as glass or plastic containers, because no form of heat-sealing was necessary thus avoiding possible contamination of the sample; also the opening energy for this sample holder has been measured under various conditions and is known to be small and reproducible within ± 0.1 J or less (see section 3.1c). The use of heavily lubricated o-rings in some of the experiments for reaction II may have resulted in slightly higher opening energies

and caused poorer experimental precision than that obtained in reaction I where the o-rings were unlubricated.

Between Expt. No. 388 which completed reaction I experiments and Expt. No. 411 which began reaction II experiments, measurements (to be published later in this journal) were made of the heat of reaction of tris(hydroxymethyl)aminomethane, SRM 724, in 0.1 *N* HCl which showed that higher enthalpy values were obtained when the calorimeter was sealed (unvented) as opposed to the values obtained when the calorimeter was open to the atmosphere through the vent tube or vented to atmospheric pressure through an open-end manometer containing Marcol (mineral oil). This effect was not found in the measurements of $H_2SO_4 \cdot 8H_2O$ in NaOH(aq): all experiments of reaction I were in the unvented calorimeter and all experiments of reaction II were vented to the atmospheric pressure through an open-end manometer containing Marcol, and no "venting" effect was found.

a. Temperature Profiles for the Adiabatic Shield

Some of the experiments for reaction I were lost in respect to enthalpy measurements, but at the same time temperature profiles of the adiabatic shield were recorded which provide some information about the magnitude and duration of departures of the temperature at various locations on the shield from that at the control point.

The permanent control thermocouples (see sec. 3.5) are located between the cover of the vessel and the cover of the shield. For the temperature profile measurements, temporary differential thermocouples were placed between the shield cover (controlled directly) and the center interior wall of the baffle section of the shield about 2 cm below the cover, and the center interior wall of the base section of the shield about 5 cm below the upper end of the baffle (see sec. 3.2). A summary of these temperature profile observations for the shield is given in table 2.

These temperature profiles were recorded during electrical calibrations of the initial (A) or final (B) systems with heating for 4.5 min at 19 V across the calorimeter heater (temperature rise = 0.57 K), or during the $H_2SO_4 \cdot 8H_2O$ reaction in 0.02 *N* NaOH (temperature rise = 0.2 K). This reaction produces an almost instantaneous temperature rise in the calorimetric solution in contrast to the relatively slow dissemination of heat from the electrical heating through the solution. However, in both cases, the heat must be transmitted from the walls of the vessel and the wells to the cover where the control thermocouples are located. This lag tends to smooth the temperature rise and prevent initial shock to the shield controls which can result in an excessive overshoot of the control temperature.

The shapes of the temperature profile curves are similar to those shown for the control thermocouples in figure 13. Initially, there is a period of about 1 min when the shield temperature lags behind that of the vessel (this temperature difference was never more than 0.004 K). As the shield is heated there is an overshoot of the calorimeter temperature to a maximum deflection from the null point and then a period of gradual return to the null point. In table 2 it is shown that for the chemical reactions the lead maximum or the maximum departure from the null point, < 0.008 K, occurred about 1.5 min after initiating the reaction and the total time of departure from the control point was 7 min or less; for the electrical calibrations the maximum departure occurred at 4 to 5 min after starting the electrical heating and the total time of departure from the null point was 10 min or less. In the last four observations given in table 2, the control point was offset by a few thousandths K and no significant effect was apparent on the profiles. The offset was

TABLE 2. *Summary of temperature profile measurements for adiabatic shield during electrical heating for 4.5 min at 19 V, and during* H_2SO_4 *reactions with* NaOH *(0.2 K temperature rise)*

Expt. No.	Calibration or reaction	Thermocouple locations	Length of time for departures from null point after initiating heating			Null point offset	Maximum deflection from null point*	
			Lag	Lead Max.	Total		Lag	Lead
			min	*min*	*min*	*K*	*K*	*K*
374	Calib. A	Cover vs. Base	—	4.0	10.0	0.000	—	0.0092
	H_2SO_4 I-1	do	0.5	1.5	5.0	.000	−0.0023	.0075
	Calib. B	do	—	4.5	8.5	.000	—	.0088
375	Calib. A	Cover vs. Baffle	—	4.5	8.0	.000	—	.0067
	H_2SO_4 I-2	do	0.5	1.5	7.0	.000	−.0028	.0059
	Calib. B	do	0.5	5.0	10.0	.000	−.0010	.0070
376	Calib. A	do	1.5	5.0	9.0	.000	−.0015	.0040
	H_2SO_4 I-3	do	0.8	1.5	5.0	.000	−.0040	.0028
	Calib. B	do	1.5	5.0	9.0	−0.005	−.0013	.0042
388	Calib. A	Cover vs. Base	1.0	5.0	10.0	+0.008	−.0008	.0090
	H_2SO_4 I-15	do	0.5	1.5	5.0	.006	−.0020	.0063
	Calib. B	Cover vs. Baffle	1.5	5.0	10.0	.003	−.0012	.0043

* A negative deflection indicates that the shield is at a lower temperature than the calorimeter cover.

accomplished by addition of a small known emf which opposed or added to that of the thermocouples and resulted in a control point which was less than or greater than zero.

It should be remembered that these temperature differences occur at points on the shield which are separated from the vessel by an evacuated space. At the covers of the vessel and the shield, where heat could be transferred by conduction through the five tubes, the temperature difference rarely exceeds 0.001 K. Even during the most rapid electrical heating, the heat leak corrections are less than 0.001 J (see sec. 3.2). Also, as pointed out earlier, linear heat-flow theory can show that lags in the rest of the system cancel out in the calculation of the temperature rise.

b. Enthalpy of Reaction of $H_2SO_4 \cdot 8H_2O$ with excess NaOH(aq)

The enthalpies of reaction of the $H_2SO_4 \cdot 8H_2O$ in ~ 0.02 *N* NaOH (reaction I) and in ~ 0.08 *N* NaOH (reaction II) were measured and the experimental data are given in table 3. The Expt. No. is a serial number for experiments in this calorimeter. The mass of the H_2SO_4 sample, S, and of the calorimetric solution, NaOH, are in columns 2 and 3; the concentrations of the NaOH solutions were given in table 1. The calculation of the electrical energy equivalents is discussed in section 4.3, and the corrected temperature rise, ΔTc, in section 4.2. The product of the mean electrical energy equivalent and ΔTc is divided by the sample weight to obtain the enthalpy of reaction, $\Delta H_r(T)$, which is equal to the enthalpy of reaction at the mean temperature of reaction, $\bar{T}$ reaction. For the correction to 298.15 K, the value, $\Delta Cp = 0.28\ J \cdot g^{-1} \cdot K^{-1}$ ($16\ cal \cdot mol^{-1} \cdot K^{-1}$) [2] was used. The variations in stirring rates as shown in the table, had no significant effect on the enthalpy of reaction.

In all of the experiments for reaction I unlubricated PTFE o-rings were used for the sample holder. In reaction II a larger cylinder was used for the sample holder and prereaction occurred because of failure of the o-ring seals. Consequently, in the first three experiments for reaction II unlubricated PTFE o-rings were used, in the next three, lubricated PTFE o-rings, and in the last two, lubricated rubber o-rings. The average enthalpy for the first three experiments is smaller than that for the last five experiments, and it is possible that use of the lubricant increased the opening energy in some cases. The sample-holder opening energy using unlubricated PTFE o-rings was measured as 0.00 ± 0.02 J, but with lubricated o-rings less is known about the opening energy. The total heat involved in these experiments was about 1300 J, and an error of 0.010 percent ($3.4\ cal \cdot mol^{-1}$) would result from an opening energy of 0.13 J.

The average enthalpy value measured in the seven experiments for reaction I corresponds to the following equation

$$H_2SO_4 \cdot 8\,H_2O + 2.36(NaOH \cdot 2620\,H_2O) = (Na_2SO_4 \cdot 0.36\,NaOH \cdot 6193\,H_2O)_{soln} \quad (1)$$

$$\Delta H_r(298.15\ K) = -590.692 \pm 0.101\ J \cdot g^{-1} = -34{,}194.1 \pm 5.9\ cal \cdot mol^{-1}$$

and in the eight experiments for reaction II,

$$H_2SO_4 \cdot 8\,H_2O + 2.6(NaOH \cdot 714\,H_2O) = (Na_2SO_4 \cdot 0.6\,NaOH \cdot 1866\,H_2O)_{soln} \quad (2)$$

$$\Delta H_r(298.15\ K) = -590.828 \pm 0.193\ J \cdot g^{-1} = -34{,}203.4 \pm 11.1\ cal \cdot mol^{-1}$$

The precision is twice the standard deviation of the mean of the experimental values. These equations are in excellent agreement with those published by Gunn [6]; in his measurements, the NaOH dilutions were 2580 and 716 H_2O, and for both reactions the excess NaOH was 0.5 mol; the enthalpy values for the mean of eight experiments for reaction I, $34{,}195.9 \pm 2.4$ (2 sdm) $cal \cdot mol^{-1}$, and for the mean of seven experiments for reaction II, $34.200.0 \pm 0.9$ (2 sdm) $cal \cdot mol^{-1}$, agree with ours within 0.01 percent or better. The experimental precision of our measurements is limited by the uncertainty in the stirring energy. Gunn's calorimeter is especially well-designed for measuring heats of fast, easily mixed reactions such as these because the rocking motion of the bomb produces very small and reproducible stirring energy.

The agreement between these two sets of measurements is quite remarkable considering the great differences in the calorimeters. Gunn's is a constant-volume, rocking, isoperibol calorimeter, and ours is a constant-pressure, stirred, adiabatic calorimeter.

The enthalpy of this reaction is not very sensitive to the alkali concentration near 0.05 *N* NaOH as long as a significant excess exists, however, care must be taken to maintain the desired composition of the acid. We believe that this H_2SO_4 neutralization reaction is a good standard reaction for solution calorimetry where highest accuracy is desired.

6. Other Measurements

The range of capabilities of this adiabatic solution calorimeter can be demonstrated by some of the other enthalpies of reactions which have been measured in it. For example, the work leading to the certification of two NBS Standard Reference Materials for solution calorimetry, α-quartz [7] and [8], and tris(hydroxymethyl)aminomethane [9], was done in this calorimeter. The enthalpy of solution of quartz in 24.4 percent HF was measured from 298 to 358 K, and at 353 K in 18 to 30 percent HF, with an experimental imprecision of $\pm 0.4\ J \cdot g^{-1}$ ($\pm 0.017\%$) at the 95 percent confidence level. At 353 K, solution of the sample required approximately 2 h. In contrast, the rapid reactions at 298 K of tris(hydroxymethyl)aminomethane in 0.1 *N* HCl and in 0.05 *N* NaOH resulted in experimental imprecision (2 sdm) of ± 0.017 and 0.08 percent, respectively. The relatively poor precision in the latter

TABLE 3. *Data for the reactions of* $H_2SO_4 \cdot 8H_2O$ *in* 0.02 N NaOH (*Reaction I*) *and in* 0.08 N NaOH (*Reaction II*)

Expt. No.	S	Mass of NaOH soln.	Stirring rate	Stirring corr.	Electrical energy equivalents		ΔT_c	T reaction		$-\Delta H_r(T)$	$-\Delta H_r$ (298.15 K)	
					Initial	Final						
	g	*g*	*rpm*	*K*	$J \cdot K^{-1}$	$J \cdot K^{-1}$	*K*	*K*	°C	$J \cdot g^{-1}$	$J \cdot g^{-1}$	$cal \cdot mol^{-1}$
Reaction I:												
380	0.58854	302.740	350	0.004397	1734.30	1734.22	0.200468	298.437	25.287	590.723	590.803	34,200.5
381	.63605	302.724	.....do	.003736	1734.40	1734.46	.216621	298.446	25.296	590.704	590.786	34,199.5
382	.63773	302.604	.....do	.003227	1734.24	1734.40	.217209	298.435	25.285	590.701	590.780	34,199.1
384	.67947	302.740	250	.001295	1733.86	1733.87	.231489	298.594	25.444	590.710	590.832	34,202.2
385	.68909	302.790	.....do	.001945	1734.86	1734.97	.234531	298.538	25.388	590.478	590.585	34,187.9
386	.67920	302.720	.....do	.001545	1734.32	1734.40	.231218	298.538	25.388	590.427	590.534	34,184.9
387	.69236	302.770	.....do	.001156	1735.09	1734.97	.235610	298.535	25.385	590.425	590.532	34,184.8
										Mean	590.692	34,194.1
										2 sdm	± 0.101	± 5.9
												(± 0.017%)
Reaction II:												
413	2.35981	302.639	450	0.001142	1735.12	1735.75	0.803042	298.166	25.016	590.567	590.571	34,187.1
414	1.95352	302.649	.....do	*.011011	1734.02	1734.58	.665449	298.029	24.879	590.774	590.740	34,196.9
416	2.12442	302.674	.....do	.008227	1734.62	1736.12	.723108	298.151	25.001	590.683	590.683	34,193.6
420	2.18822	302.629	.....do	.001487	1735.59	1736.13	.744967	298.147	24.997	590.962	590.955	34,209.3
424	2.20684	302.699	300	.001345	1736.11	1736.62	.751538	298.129	24.979	591.319	591.313	34,230.0
425	2.22425	302.699	.....do	.003383	1735.42	1736.66	.757410	298.140	24.990	591.163	591.160	34,221.2
427	2.12853	302.730	.....do	.002415	1734.99	1735.59	.724724	298.121	24.971	590.834	590.826	34,201.8
429	2.26004	302.740	.....do	.001074	1735.60	1736.71	.768792	298.140	24.990	590.581	590.579	34,187.5
										Mean	590.828	34,203.4
										2 sdm	± 0.193	± 11.1
												(± 0.032%)

*Before this experiment, a PTFE sleeve was installed between the stirrer shaft and the platinum tube. This increased the stirring energy until it became worn.

reaction was due to in part to the high sensitivity of the enthalpy to the NaOH concentration. This was an endothermic reaction in which electrical energy was added during the reaction in order to maintain a temperature rise in the calorimeter. Details of the work involved in these two certifications are to be published in this Journal.

In the reaction of ketene gas with aqueous sodium hydroxide [1], the calorimeter was modified to function as a flow calorimeter by using the vent tube for the exit gas, and by removing the sample holder and push-rod and replacing them with a metal tube for introducing the ketene gas into the calorimeter. Here the experimental imprecision (2 sdm) was only ± 0.47 percent, but was adequate for this work.

The results will be given [10] for our measurements of the enthalpy of solution of BeO(c) in aqueous HF and in aqueous HCl; the experimental imprecisions (2 sdm) were ± 0.09 and ± 0.4 percent, respectively. The latter measurements were especially interesting calorimetrically because the stirred reaction required approximately 20 h for completion; this caused excessive uncertainties because of the large total stirring energy. This uncertainty was reduced by turning the stirrer off during most of the reaction period and the reaction proceeded unstirred until it was near completion.

7. Conclusions

It has been shown that the optimum experimental imprecision (2 sdm) achieved with this adiabatic solution calorimeter is about ±0.02 percent, and the H_2SO_4 measurements indicate that the accuracy of the calorimetry is probably of the order of 0.05 percent or less where 200 J or more of energy is evolved.

The advantage of the adiabatic calorimeter over isoperibol calorimeters has been proven in its ability to measure heats of slow reactions (of 20 h or more in duration) with relatively high precision. The versatility of this calorimeter has been demonstrated in the ability to make high precision measurements of slow or rapid reactions, exothermic or endothermic, with temperature rises from 0.2 to 2 K or more, over a temperature range of 293 to 363 K, in highly corrosive solutions such as strong acids and bases, and even in a gas flow system.

The calorimeter is limited to reactions occurring at or near atmospheric pressure and to solutions which do not react with the platinum alloys. The limit of energy detection is approximately 0.05 J, and the experimental precision is usually limited by the uncertainty in the stirring energy which is about 1 to 5 percent of the total stirring energy.

Adiabatic solution calorimeters are especially needed in fields, such as biology, geology, and mineralogy, where there is an interest in the properties of materials which react slowly in solutions.

The authors wish to express their gratitude for financial support for the construction of this calorimeter by the U.S. Atomic Energy Commission. We also thank S. R. Gunn, Lawrence Radiation Laboratory, for giving us samples of $H_2SO_4 \cdot 8H_2O$.

8. Prefixes, Symbols, and Abbreviations

Prefixes:

M	mega (10^6)
k	kilo, (10^3)
c	centi (10^{-2})
m	milli (10^{-3})
μ	micro (10^{-6})
n	nano (10^{-9})

Symbols and Abbreviations:

diam	diameter
deg	degree
K	kelvin temperature
°C	Celsius temperature
J	joule
cal	calorie
A	ampere
V	volt
Ω	ohm
Hz	Hertz
m	meter
g	gram
mol	mole
N	normal (equivalents/1000 cm^3 of solution)
S	mass of sample
s	second
min	minute
h	hour
Pa	Pascal, N/m^2, $\sim 1.33 \times 10^2$ mm Hg
psi	pounds per square inch
hp	horsepower
ac	alternating current
dc	direct current
rms	root mean square
rpm	revolutions per minute
No., #	number
%	percent
sdm	standard deviation of the mean
k	proportionality factor for heat leak
Cat.	catalog
Ser.	serial
C.A.T.	current-adjusting-type control unit
PTFE	polytetrafluoroethylene
CVC	Consolidated Vacuum Corporation
H-P	Hewlett-Packard
L and N	Leeds and Northrup Company
M-H	Minneapolis-Honeywell Regulator Company

9. References

[1] Nuttall, R. L., Laufer, A. H., and Kilday, M. V., J. Chem. Thermodynamics **3**, 167 (1971).

[2] Gunn, S. R., J. Phys. Chem. **69**, 2902 (1965).

[3] Parker, V. B., Thermal Properties of Aqueous Uni-univalent Electrolytes, Nat. Stand. Ref. Data Ser., Nat. Bur. Stand. (U.S.), 2, 66 pages (April 1965).

[4] Cameron, A. E. and Wichers, E., J. Am. Chem. Soc. **84**, 4175 (1962).

[5] Commission on Atomic Weights, Pure and Applied Chem. **21**, 91 (1970).
[6] Gunn, S. R., J. Chem. Thermodynamics **2**, 535 (1970).
[7] Nat. Bur. Stand. (U.S.) Certificate, Standard Reference Material 1654, α-Quartz, for Hydrofluoric Acid Solution Calorimetry, Washington, D.C. 20234, April 7, 1971.
[8] Kilday, M. V., and Prosen, E. J., J. Res. Nat. Bur. Stand. (U.S.), **77A** (Phys. and Chem.), No. 2, 205–215 (Mar.–Apr. 1973).
[9] Nat. Bur. Stand. (U.S.) Certificate, Standard Reference Material 724 for Solution Calorimetry, tris(hydroxymethyl) aminomethane, Washington, D.C., 20234, April 14, 1972.
[10] Kilday, M. V., Prosen, E. J., and Wagman, D. D., J. Res. Nat. Bur. Stand. (U.S.), **77A** (Phys. and Chem.), No. 2, 217–235 (Mar.–Apr. 1973).

(Paper 77A2–762)

JOURNAL OF RESEARCH of the National Bureau of Standards—A. Physics and Chemistry
Vol. 77A, No. 2, March–April 1973

The Enthalpy of Solution of Low Quartz (α-quartz) in Aqueous Hydrofluoric Acid

Marthada V. Kilday and Edward J. Prosen

Institute for Materials Research, National Bureau of Standards, Washington, D.C. 20234

(November 9, 1972)

An adiabatic solution calorimeter was used to measure the enthalpy of solution of the NBS Standard Reference Material No. 1654 (α-quartz or low quartz) for use as a reference standard for HF solution calorimetry. The enthalpy of solution of this material at a concentration of 5 grams in 1000 cm^3 of 24.4 weight percent HF(aq) is

$$-\Delta H_{soln}(353.15\ K) = 2362.2 \pm 1.1\ J \cdot g^{-1}.$$

This value also applies to the enthalpy of solution of pure low quartz within the uncertainty limits given. The enthalpy of solution of quartz (in $J \cdot g^{-1}$) as a function of the temperature, T, of reaction in 24.4 weight percent HF in the range 298 to 358 K, is

$$-\Delta H_{soln}(T) = 2275.0 + 1.586\ (T - 298.15).$$

Thus, the average ΔCp for the reaction over the range, 298 to 358 K, is $-1.586 \pm 0.025\ J \cdot g^{-1} \cdot K^{-1}$. As a function of the concentration of HF solution in the range, 18 to 30 weight percent,

$$-\Delta H_{soln}(353.15\ K) = 2362.10 + 1.429\ (wt\%HF - 24.40) + 0.069\ (wt\%HF - 24.40)^2.$$

From measurements of the enthalpies of solution of several samples of quartz and fused silica, the enthalpy difference between low quartz and silica glass at 298.15 K was determined to be $162.2 \pm 4.9\ J \cdot g^{-1}$ ($2.330 \pm 0.070\ kcal \cdot mol^{-1}$).

Key words: Enthalpy of soln, SiO_2; heat of soln, SiO_2(c); quartz, soln in HF(aq); reference material, soln calorimetry; SiO_2(c), soln in HF(aq); thermochemistry.

1. Introduction

The growth of HF solution calorimetry in the past few decades has produced a need for a standard reference material to assist in determining the accuracy and precision of results obtained by calorimeters measuring heats of solution in hydrofluoric acid. This acid is generally used because of its great chemical activity and ability to attack even refractory materials such as oxides and silicates. Thus, by measuring enthalpies of solution in HF of various materials, they can be related even though their properties may be very different.

The reference standards often used in other types of solution calorimetry react rapidly at room temperature and are not suitable for HF work where the reactions are usually slow, and the calorimetrist resorts to higher temperatures and very finely divided samples in order to increase the reaction rate. One of the key compounds relating many systems in this field is SiO_2 (c) or quartz; therefore at the request of the U.S. Calorimetry Conference, the National Bureau of Standards has made available NBS Standard Reference Material No. 1654 (α-quartz) for HF solution calorimetry.[1]

SRM No. 1654 is not intended to be used for calibrating calorimeters, as a replacement for electrical energy calibration. It is intended as a single, uniform sample for comparison of measurements by various calorimeters for establishing the adequacy of measurement techniques.

This quartz sample should prove useful in HF solution calorimetry because it dissolves in well-stirred 24 percent HF in approximately 2 h at 353 K. It is of high purity; it is free from finely divided particles which may introduce surface energy effects; and it requires no special preparation nor techniques in handling.

The purpose of this paper is to describe the preparation and analysis of SRM 1654 and to describe the experimental work which resulted in the certified value for the enthalpy of solution.

[1] This material can be obtained through the Office of Standard Reference Materials, National Bureau of Standards, Washington, D.C. 20234.

The results are also given in section 4 for some of our earlier work with samples of Norwegian and Quebec crystalline quartz and a fused silica glass. This work is not of the high precision achieved in the certification experiments, however, it does add some information about the effects of elutriation of samples and about the enthalpy difference between quartz and the glass.

There has been confusion in the use of the terms α- and β-quartz [1].[2] In this paper, α-quartz refers to the low quartz (stable below 846 K).

2. The Sample

Two pieces of natural Brazilian quartz weighing a total of approximately 4 kg were the starting material for SRM 1654. Surface impurities included in abrasions were removed with a carborundum saw. The surface was washed with a soap solution and then with acetone. At this point the two pieces were clear and colorless with no flaws visible.

The quartz was crushed by hand in a mortar of hardened steel. Bronze sieves separated the material into three portions: (1) passed #100 and retained on #200 sieve (74 to 149 μm), 1.1 kg; (2) passed #200 and retained on #400 sieve (37 to 74 μm), 2.3 kg; and (3) passed #400 sieve (< 37 μm), 0.6 kg. Spectroscopic analysis indicated that a sample from portion (2) contained more than 0.1 wt percent Fe and a trace of Cu. The metallic impurities were removed from all three portions by solution in aqueous hydrochloric acid at approximately 320 K as described in the following paragraph. The three portions of different particle size were kept separate but treated alike, although only portion (2) was to be used for SRM 1654.

The quartz was contained in a 3000-cm^3 Pyrex glass beaker while washing with a 1:1 solution of concentrated hydrochloric acid in distilled water. The contents of the beaker were stirred with a polyethylene stirring rod while being heated to approximately 320 K. The supernatant liquid was decanted and the process repeated once beyond the point where the washings gave no test for iron with 0.25 *M* $K_3Fe(CN)_6$ solution. Then the quartz was repeatedly washed with distilled water heated to 320 K until the washings gave no test for Cl^- with 0.1 *M* $AgNO_3$ solution. The washing was continued with distilled water at room temperature to remove the finest particles from the quartz. When no suspended particles were visible in the water after the mixture remained unstirred for 1 h, the water was decanted, and the quartz was loosened to a fluffy mass before drying for 3 to 5 h at 448 K. Abrasion by the quartz was apparent on the polyethylene stirring rod, but not on the glass beakers.

Spectrochemical analysis[3] of the final products indicated that no detectable amount of Fe or Cu remained in the sample, and only traces (< 0.001 wt%) of Al and Mg were detected. Two samples (3.3 g and 1.9 g) of the SRM 1654 were treated with aqueous HF and evaporated to dryness several times to determine the material inert to HF.[4] The amount found averaged 0.02 percent although the residues were hygroscopic and the weights varied somewhat with atmospheric humidity. No evidence of undissolved residue was ever found in the calorimetric experiments.

Examination of an x-ray diffraction pattern[5] of the SRM 1654 did not indicate the presence of phases other than low quartz. The limit of detection of another form of crystalline SiO_2 was estimated to be between 0.1 and 1.0 percent.

The weight loss by the SRM 1654 on drying at 538 K was determined to be 0.02 percent or less, and on ignition at 1550 K, 0.02 percent. During the remaining measurements the material was stored in glass bottles in the room atmosphere in which a relative humidity of 35 ± 10 percent was maintained.

3. Apparatus and Procedures

In this paper, the 1969 atomic weights [2] were used (H, 1.0080; F, 18.9984; O, 15.9994; Si, 28.086), and 4.1840 joules = 1 calorie. In converting to molar quantities, the samples were assumed to be pure SiO_2, and the possible presence of small amounts of impurities was neglected. The following densities, in g · cm^{-3}, were used to calculate buoyancy factors: quartz, 2.66; SiO_2 glass, 2.20; 18 percent HF, 1.063; 24 percent HF, 1.083; 30 percent HF, 1.101; and air (for average conditions in our laboratory), 0.00118.

The platinum-lined, adiabatic solution calorimeter used in this work was described in detail previously [3]. The stirrer was operated at a speed of 350 rpm, and the sample cylinder, 1.9-cm^3 volume, with polytetrafluoroethylene (PTFE) o-rings was used for the platinum sample holder.

The aqueous HF solutions used in the measurements were taken from stock solutions stored in 2000-cm^3 polyethylene bottles. The solutions were prepared by approximate volumetric dilutions of analytical reagent grade concentrated hydrofluoric acid with distilled water. Weighed aliquots of the stock solutions were analyzed by titration against standard 1 *N* sodium hydroxide solution using phenolphthalein as an end-point indicator.

In each experiment the platinum sample holder containing the weighed sample was installed in the calorimeter, and the HF solution was weighed in a polyethylene bottle and then transferred to the calorimeter vessel. When the calorimeter was completely assembled the jacket was evacuated by means of an oil diffusion pump. A pressure of less than 0.1 Pa (1×10^{-3} mm Hg) was observed in approximately 2 h. During this time the controls for the adiabatic shield were started and the calorimeter was preheated to the desired starting temperature. About 2 h was required for heating to 353 K. Approximately 1 h was allowed for thermal equilibration in the system before starting the temperature measurements. This

[2] Figures in brackets indicate literature references at the end of this paper.

[3] Performed by V. C. Stewart, Spectrochemical Analysis Section, Analytical Chemistry Division.

[4] Analysis by R. A. Paulson, Microchemical Analysis Section, Analytical Chemistry Division.

[5] Performed by H. E. Swanson, Crystallography Section, Inorganic Materials Division.

time period was longer than that following electrical calibrations because the longer time of heating with greater voltage across the calorimeter heater resulted in lags, especially in the temperature of the jacket well and its insulation.

During the 25-min rating periods, calorimeter temperature readings were made at 5-min intervals when the 25-Ω platinum resistance thermometer was used, and at 100-s intervals when the quartz-oscillator thermometer was used. After the first rating period an electrical calibration of the initial system was made using 24 V across the 97-Ω manganin heater for 10.5 min. Alternate measurements of current in the calorimeter heater and the potential across it were made at 30-s intervals during the electrical heating using a high precision potentiometer. Details of the electrical energy measurements were described previously [3]. The time of the electrical heating was measured by an electronic counter which counted cycles of the 10-kHz standard frequency signal available at NBS. The second rating period was started about 12 min after completion of the calibration heating. Following the second rating period, the sample holder was opened and the slow solution reaction began. At 298 K, samples of the finest material (< 37 μm) required 6 h for complete reaction, SRM 1654 (37 to 74 μm) required 10 h, and the coarsest material (74 to 149 μm) required 16 h. At 353 K, these materials required 1, 2, and 4 h respectively. At 353 K, SRM 1654 required for complete reaction 3 h in 18 percent HF, 2 h in 24 percent HF, and 1.5 h in 30 percent HF. The reactions were assumed to be complete when the slopes of the time-temperature curves were approximately the same as those of the initial rating periods and when the slope did not change more than the uncertainty of the readings. The measurements for a third rating period were followed by an electrical calibration of the final system in which the same procedure was used as in the initial calibration. A fourth rating period then completed the measurements.

The slopes in the rating periods were of the order of 200 $\mu K \cdot min^{-1}$ and the uncertainty in the stirring energy was estimated to be ± 5 percent, or less. Thus, for a reaction with a 2-K temperature rise and requiring 2 h for completion, the total stirring energy would be about 24 mK and the uncertainty in ΔT_c, about ± 0.06 percent. However, the experimental imprecision actually observed was about one-third of this uncertainty.

In all experiments the final solutions appeared clear with no evidence of undissolved residue. The solutions were neutralized with soda lime before disposal.

Because this calorimeter is adiabatic, the corrected temperature rise is calculated directly from the projected slopes of the rating periods (the slopes are essentially the same in all rating periods). The only corrections applied were those for the calibrations of the resistance bridge or the quartz-oscillator thermometer.

The quartz-oscillator thermometer, calibrated by comparison with the platinum resistance thermometer, was used for the temperature measurements in Expts. No. 432 through 474. In Expts. No. 479 through 502, the temperature measurements were made with the 25-Ω platinum resistance thermometer and a G-3 resistance thermometer bridge using a nanovoltmeter as a null detector; the nanovoltmeter deflections were recorded on a strip-chart recorder.

4. Preliminary Experiments

The experimental results given in this section are not of the accuracy and precision achieved in the experiments in section 5. However they are useful in estimating the effects of elutriating samples, in comparing the enthalpies of solution of natural quartz from different sources, and in obtaining a value for the enthalpy difference between crystalline quartz and silica glass.

These measurements were made between January and March 1966, before our laboratories were moved to the location at Gaithersburg, Maryland. Since that time, the calorimeter has been modified in a number of ways to improve the precision and accuracy of the measurements. We estimate the experimental imprecision for these measurements to be about 0.05 to 0.1 percent as compared to 0.02 percent in the certification work. The calorimeter as described [3] included the following changes: the sample holder was redesigned; a temperature control was added to the potentiometer; bearings were added to the stirrer; and the temperature and humidity in the new laboratory were automatically controlled.

Three samples of SiO_2 were used in the measurements described in this section: [6]

1. Norwegian crystalline quartz, obtained from Hammill and Gillespie, Inc., New York. Spectroscopic analysis for metallic constituents: Al and Ti, 0.001–0.01 percent; Ag, B, Ca, Cu, Fe, Mg, Mn, less than 0.001 percent. (See footnote 3.)
2. Buckingham, Quebec, crystalline quartz, obtained from International Minerals and Chemical Corp., Buckingham, Quebec. Spectroscopic analysis was the same as for the Norwegian quartz. (See footnote 3.)
3. Suprasil 2, an optical-quality fused silica glass, obtained from Englehard Industries, Amersil Quartz Division, Hillside, New Jersey. Spectroscopic analysis: Fe, 0.01–0.1 percent; Al, Ba, and Mg, 0.001–0.01 percent; and Ag, Ca, Cr, Cu, and Mn, < 0.001 percent (See footnote 3.)

X-ray powder diffraction analysis of these materials indicated that the first two were crystalline low quartz, and that there was no crystalline material in the third sample. (See footnote 5.) The transmission spectra through Suprasil in the ultraviolet, visible, and infrared regions are given in figure 1. In the infrared there are strong absorptions at 2.72 μm and secondary absorption bands at 1.38 and 2.22 μm. According to the manufacturer's specification, the synthetic fused silica, Suprasil, has a density of 2.201 $g \cdot cm^{-3}$ and the annealing point is 1393 K.

[6] Certain commercial products and instruments are identified in this paper in order to specify adequately the experimental procedure. In no case does such identification imply recommendation or endorsement by the National Bureau of Standards, nor does it imply that the products or equipment identified are necessarily the best available for the purpose.

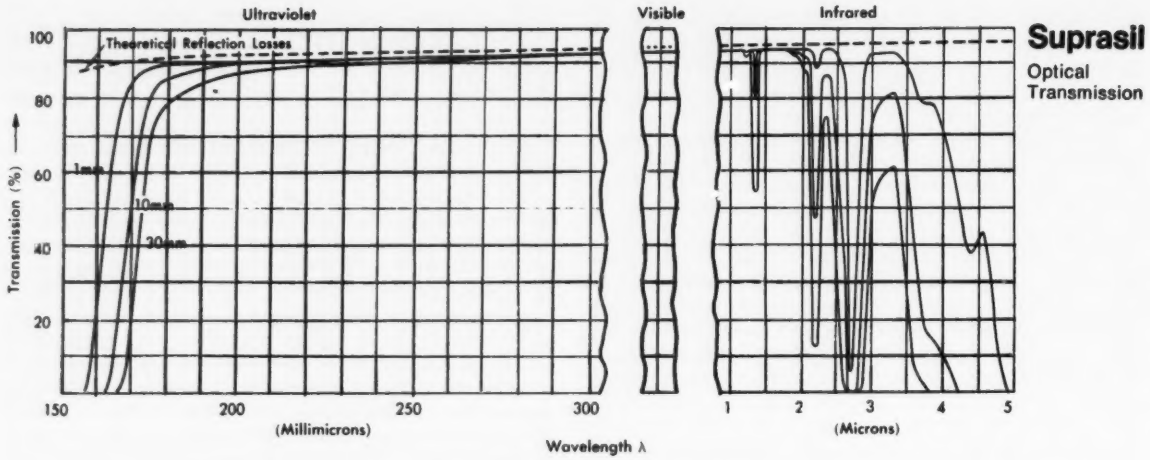

FIGURE 1. *Transmission spectra for Suprasil 2 (reproduced with the permission of Amersil, Inc., from Fused Quartz and Fused Silica, Optics Bulletin EM–9227).*

TABLE 1. *Data for preliminary experiments with samples of crystalline quartz and fused silica glass*

Expt. No.	Stirring rate	Reaction temp.	Duration of reaction	HF Soln. Mass	HF conc.	Amounts of reactants			Mole ratio HF : SiO_2
						HF	H_2O	SiO_2	
	rpm	*K*	*min*	*g*	*wt %*	*mol*	*mol*	*mol*	
I: Norwegian natural crystalline quartz (elutriated)									
89	550	358	50	323.94	22.53	3.64	13.92	0.025840	141
II: Norwegian natural crystalline quartz (passed #200 sieve)									
97	550	353	100	323.11	22.53	3.64	13.88	.025872	141
98	550	353	110	322.19	22.18	3.57	13.90	.025068	142
99	550	353	90	306.78	22.75	3.48	13.14	.025022	139
III: Quebec natural crystalline quartz (elutriated)									
100	550	353	45	319.17	22.75	3.62	13.67	.025312	143
101	550	353	70	322.22	22.75	3.66	13.80	.029548	124
103	550	353	60	311.99	22.75	3.54	13.36	.027322	130
105	550	353	60	316.95	22.75	3.60	13.58	.025431	142
110	450	353	60	317.89	22.21	3.52	13.71	.026429	133
IV: Quebec natural crystalline quartz (passed #200 sieve)									
108	450	353	120	327.11	22.21	3.63	14.11	.025869	140
109	450	353	120	319.89	22.21	3.55	13.80	.025284	140
V: Suprasil 2, fused silica glass (elutriated)									
111	450	353	40	321.97	22.64	3.64	13.81	.024867	146
113	450	353	30	323.62	22.64	3.66	13.88	.025383	144
114	450	353	30	324.03	22.64	3.66	13.90	.026096	140
115	450	—	40	310.26	22.64	3.51	13.31	.024171	145
VI: Suprasil 2, fused silica glass (passed #200 sieve)									
112	450	353	40	316.45	22.64	3.58	13.58	.026174	137
117	450	353	40	331.48	22.64	3.75	14.22	.024628	152

The crushing and purification of the three samples was essentially the same as described in section 2 for SRM 1654 except that all of the portion passing a #200 sieve was used. These materials were heated to approximately 320 K in a similar 1 : 1 aqueous HCl solution. After the mixture had been stirred vigorously, it was allowed to settle for 5 min before decanting the liquid which still contained suspended materials. This supernatant liquid was allowed to settle for 30 min more before again decanting. The portion of the sample remaining after the *first* decantation is called that which "passed #200 sieve," and that remaining after the *second* decantation is called "elutriated." The materials were then washed with distilled water as described in section 2. The finest particles were removed during washing and were not recovered.

Information about stirring rates, reaction temperatures, amounts of materials and duration of reaction for the experiments in which the above samples were dissolved in 22–23 percent HF solutions at about 350 K is given in table 1. The Expt. No. is the serial number for experiments in the adiabatic solution calorimeter. It can be seen that the "elutriated" crystalline samples dissolved in approximately 60 min, but those which "passed #200 sieve" in most cases required nearly twice as long. Reducing the stirring rate from 550 to 450 rpm apparently had little effect on the duration of the reaction, but probably improved the reproducibility of the stirring energy. There appears to be little difference in the duration of reaction for samples of different particle size in the fused silica glass, the time being about half that for the elutriated crystalline samples.

It is apparent from the time required for reaction of these elutriated crystalline materials at 350 K that the particle sizes are considerably larger than those used by most earlier workers who used isoperibol calorimeters where the duration of the reactions had to be limited to around 30 min. For example, Mulert's sample dissolved at room temperature (18°C) in 20 percent HF in 30 min [4]; and Wietzel's, also at room temperature in 35 percent HF, in 15 min [5]. Most later workers used higher reaction temperatures to avoid the use of such extremely fine particles; however, Jeffes et al. [6], and Stevens and Turkdogan [7] used 18.7 percent HF at 25 °C. Also, Hummel and Schwiete [8] used 10 percent HF at 26.5 °C, and the particle size of their sample was reported to be between 2.5 and 5μm.

In table 2 are the calorimetric data for the solution of the six samples of SiO_2 in aqueous HF corresponding to the experiments in table 1. The calorimeter temperatures in all of these experiments were measured with the 25-Ω platinum resistance thermometer. The electrical energy equivalents of the initial and final systems are given. In the stirring energy corrections for the reactions, the uncertainty is estimated to be about 5 percent or less. The methods of calculating the electrical energy equivalents and the corrected temperature rise, ΔR_C, reaction, were described previously [3]. The enthalpy of solution, $\Delta H(T)$, at the temperaof reaction which is the mean temperature of reaction, T reaction, is the product of the mean electrical energy equivalent and the corrected temperature rise divided by the sample mass. The factors as given in section 5, 1.586 J · g^{-1} · K^{-1} and 1.326 J · g^{-1} (wt%HF)$^{-1}$, were used for the corrections to 353.15 K and 24.4 percent HF to obtain the enthalpy of solution under the conditions of the certified value given in section 5.

From the mean enthalpies of solution in table 2 we obtain the following differences between the "elutriated" materials and those which "passed #200 sieve": Norwegian crystal, 115 cal · mol^{-1}; Quebec crystal, 54 cal · mol^{-1}; and Suprasil 2 glass, 60 cal · mol^{-1}. This is an average of about 80 cal · mol^{-1} and the estimated uncertainty[7] is of the same magnitude. It then seems reasonable to assume that an error of a hundred cal · mol^{-1} or more might be expected when samples composed of extremely fine particles are used.

The mean enthalpies of solution in table 2 also serve for comparison of the values obtained from different samples of natural quartz which passed #200 sieve (in kcal · mol^{-1}): Norwegian, 33.80; Quebec, 33.86, and Brazilian, 33.92 (see sec. 5). The latter sample did not contain particles which passed #400 sieve. The three values agree within the experimental uncertainties, 0.10 kcal · mol^{-1} for the first two and 0.02 kcal · mol^{-1} for the third.[7]

The enthalpy difference between quartz and SiO_2 glass from the elutriated samples is 2.318 kcal · mol^{-1}, and from those which passed #200 sieve, 2.343 kcal · mol^{-1}; the average of these two values is 2.330 kcal · mol^{-1} (or 162.2 J · g^{-1}). The estimated uncertainty is about ±0.070 kcal · mol^{-1} (or 4.9 J · g^{-1}). These values agree within the uncertainties with the values of 2.15 ± 0.15 kcal · mol^{-1} determined by Holm, Kleppa and Westrum [9]; 2.27 ± 0.20 kcal · mol^{-1}, by Hummel and Schwiete [8]; 2.21 ± 0.18 kcal · mol^{-1}, by Mulert [4]; 2.32 ± 0.06 kcal · mol^{-1}, by Wietzel [5]; and 2.28 ± 0.02 kcal · mol^{-1}, by Waldbaum [10].

5. Enthalpy of Solution of SRM 1654 in HF(aq)

The experiments reported in this section were completed between May and September 1970. The samples used for measurements of the enthalpies of solution ranged from 1.47 to 1.52 g, and the sample holder was filled in the room atmosphere.

The results of 22 experiments given in table 3 were used to obtain by a least squares regression analysis the following linear equation for the enthalpy of solution of quartz in 24.4 percent HF from 298 K to 358 K (in J · g^{-1}):

$$-\Delta H_{soln}(T) = 2275.0 + 1.586\ (T - 298.15) \quad (1)$$

[7] The uncertainties (based on sdm = ±24 cal · mol^{-1} for the mean enthalpy values in table 2) were based on an analysis of variance by H. H. Ku, Statistical Engineering Laboratory, Institute for Basic Standards.

TABLE 2. *Calorimetric data for the preliminary measurements of the enthalpy of solution of various samples of SiO_2, crystal and glass, in aqueous HF*

Expt. No.	Electrical energy equivalents		React. Stirring Correction	$\Delta Rc_{reaction}$	$\bar{T}$ reaction	Sample Mass	$-\Delta H(T)$[a]	Corr. to 24.4% HF	Corr. to 353.15 K	$-\Delta H$(353.15 K) in 24.4% HF		Mean
	Initial	Final										
	$J \cdot \Omega^{-1}$	$J \cdot \Omega^{-1}$	Ω	Ω	K	g	$J \cdot g^{-1}$	$J \cdot g^{-1}$	$J \cdot g^{-1}$	$J \cdot g^{-1}$	$kcal \cdot mol^{-1}$	$kcal \cdot mol^{-1}$
I: Norwegian natural crystalline quartz (elutriated)												
89	16,998.4	17,031.9	0.00278	0.21602	358.324	1.55260	2367.2	−2.4	8.2	2361.4	33.911	33.911
II: Norwegian natural crystalline quartz (passed #200 sieve)												
97	16,850.7	16,884.3	.00477	.21636	353.179	1.55451	2347.5	−2.4	0.0	2349.9	33.746	
98	16,871.0	16,911.0	.00456	.20982	353.185	1.50622	2352.5	−2.8	0.1	2355.2	33.822	33.795
99	16,332.2	16,374.0	.00475	.21633	353.203	1.50344	2352.9	−2.1	0.1	2354.9	33.818	
III: Quebec natural crystalline quartz (elutriated)												
100	16,769.5	16,807.5	.00179	.21301	353.172	1.52087	2351.2	−2.1	0.0	2353.3	33.795	
101	16,831.6	16,876.7	.00270	.24885	353.318	1.77537	2362.3	−2.1	0.3	2364.1	33.950	
103	16,461.4	16,493.5	.00313	.23541	353.251	1.64165	2362.7	−2.1	0.2	2364.6	33.957	33.909
105	16,635.5	16,674.5	.00249	.21658	353.152	1.52803	2360.4	−2.1	0.0	2362.5	33.927	
110	16,753.9	16,786.6	.00265	.22337	353.084	1.58798	2358.8	−2.7	−0.1	2361.6	33.914	
IV: Quebec natural crystalline quartz (passed #200 sieve)												
108	17,127.1	—	.00546	.21356	353.176	1.55433	2353.0	−2.7	0.0	2355.7	33.829	33.855
109	16,828.2	16,861.6	.00480	.21253	353.035	1.51917	2356.4	−2.7	−0.2	2259.3	33.881	
V: Suprasil 2, fused silica glass (elutriated)												
111	16,961.3	16,990.4	.00205	.22172	353.074	1.49414	2518.9	−2.2	−0.1	2521.2	36.206	
113	16,962.7	17,006.0	.00178	.22638	353.132	1.52513	2520.9	−2.2	0.0	2523.1	36.233	36.228
114	16,956.6	16,995.6	.00186	.23282	353.199	1.56800	2520.5	−2.2	0.1	2522.6	36.226	
115	16,440.8	16,489.2	.00259	.22245	353.051	1.45230	2521.8	−2.2	−0.2	2524.2	36.249	
VI: Suprasil 2, fused silica glass (passed #200 sieve)												
112	16,738.2	16,776.0	.00207	.23601	353.142	1.57263	2514.6	−2.2	0.0	2516.8	36.143	36.168
117	17,212.1	17,243.1	.00244	.21632	353.154	1.47980	2518.2	−2.2	0.1	2520.3	36.193	

[a] The energy for opening the sample holder, 0.24 J, was subtracted in each experiment. This was measured in seven experiments and the average was 0.24 ± 0.32(2sdm) J.

TABLE 3. *Data for experiments showing the relationship of the enthalpy of solution of quartz in 24 percent* HF(aq) *to the temperature of reaction*

Expt. No.	Sample mass	Electrical energy equivalents		Corrected temperature rise	$\bar{Q}_{reaction}$	$\bar{T}$ reaction		$-\Delta H_{soln}(T)$
		Initial	Final					
	g	$J \cdot K^{-1}$	$J \cdot K^{-1}$	*K*	*J*	*K*	°C	$J \cdot g^{-1}$
432[a]	1.48772	1586.0	1590.0	2.13480	3390.0	298.898	25.748	2278.7
437	1.50235	1582.0	1585.8	2.15908	3419.8	298.226	25.076	2276.3
439	1.48326	1596.6	1600.3	2.12282	3393.2	308.348	35.198	2287.7
440[b]	1.47684	1582.0	1586.8	2.11975	3358.5	298.117	24.967	2274.1
463	1.50842	1617.8	1624.2	2.15912	3499.9	323.676	50.616	2320.2
464	1.49148	1648.2	1651.4	2.13083	3515.4	349.026	75.876	2357.0
465	1.50061	1648.6	1650.3	2.13642	3523.9	348.406	75.256	2348.3
466[b]	1.50612	1653.1	1654.7	2.15058	3556.8	352.721	79.571	2361.6
467	1.49116	1653.9	1656.6	2.12867	3523.5	353.153	80.003	2362.9
468[a]	1.49085	1653.5	1656.0	2.12805	3521.4	352.935	79.785	2362.0
469[b]	1.49814	1653.2	1656.5	2.13888	3539.5	352.985	79.835	2362.6
470	1.51161	1653.6	1655.8	2.15700	3569.2	352.983	79.833	2361.2
471	1.49410	1653.4	1655.8	2.13301	3529.3	353.172	80.022	2362.1
473	1.50839	1653.6	1655.9	2.15420	3564.7	353.217	80.067	2363.2
		$J \cdot \Omega^{-1}$	$J \cdot \Omega^{-1}$	Ω				
480	1.51163	16,557.	16,602.	0.215304	3569.6	352.883	79.733	2361.4
481	1.51260	16,560.	16,603.	.215479	3573.0	352.872	79.722	2362.2
482	1.51806	16,571.	16,611	.216067	3584.8	352.888	79.738	2361.4
483	1.49911	16,570.	16,611.	.213384	3540.1	352.865	79.715	2361.5
484	1.50632	16,568.	16,609.	.214454	3557.5	352.892	79.742	2361.7
485	1.50231	16,489.	16,531.	.214070	3534.3	347.857	74.707	2352.6
486	1.51417	16,658.	16,698.	.215352	3591.6	357.910	84.760	2372.0
487	1.51144	16,659.	16,700.	.214945	3585.2	357.894	84.744	2372.1

[a] Particle size of sample: Passed #100 and retained on #200 sieve; finest particles removed in washing.
[b] Particle size of sample: Passed #400 sieve; finest particles removed in washing.

where T is the isothermal reaction temperature in kelvins, the standard error of the estimate is ± 2.4 $J \cdot g^{-1}$, the standard error of the constant term is ± 1.2 $J \cdot g^{-1}$, and the standard error of the slope is ± 0.025 $J \cdot g^{-1} \cdot K^{-1}$. The uncertainty is probably greater at the low temperatures than at the high temperatures because of the longer reaction periods. The average $\Delta Cp = -1.586 \pm 0.025$ $J \cdot g^{-1} \cdot K^{-1}$.

In the tables, the experiment number is the serial number of the experiment in the adiabatic solution calorimeter; omitted numbers are experiments on other compounds, other test reactions, or thermometer calibrations. The electrical energy equivalents (EEE) of the initial and final systems are given in $J \cdot K^{-1}$ where the quartz-oscillator thermometer was used, and in $J \cdot \Omega^{-1}$ where the 25-Ω platinum resistance thermometer[8] was used. The heat evolved during the reaction, in joules, is $Q_{reaction} = [EEE_i + EEE_f)/2] (\Delta T)$. $\bar{T}$ reaction is the mean temperature of the reaction. The isothermal enthalpy at the temperature of reaction is equal to the enthalpy at the mean temperature of reaction, or $\Delta H(T) = \Delta H(\bar{T})$[9]. The corrections to obtain ΔH at 353.15 K were made using $\Delta Cp = -1.586$ $J \cdot g^{-1} \cdot K^{-1}$ or -95.3 $J \cdot mol^{-1} \cdot K^{-1}$.

Figure 2 is a plot on a molar basis of the enthalpies of solution versus the temperatures of reaction given in table 3 (differences from 298.15 K and the corresponding equation are given). Five of the points were measurements on samples of different particle size

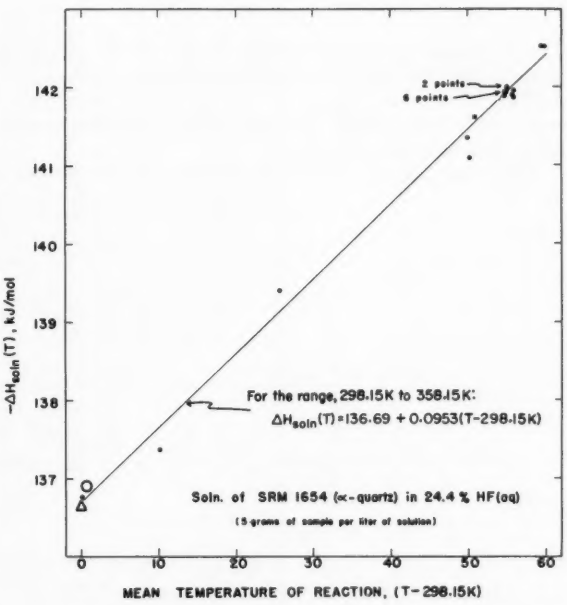

FIGURE 2. *A plot of the data in table 3 showing the relationships of enthalpy of solution of quartz in 24.4 percent* HF *(aq) to the mean temperature of reaction.*

[8] On this thermometer one kelvin is 0.10104 Ω at 298.15 K and 0.09939 Ω at 353 K. (See [3] for thermometer calibration data.)
[9] The use of only EEE_i would give ΔH at the final temperature, and EEE_f would give ΔH at the initial temperature, and the use of $(EEE_i + EEE_f)/2$ gives ΔH at $\bar{T}$.

491-397 O - 73 - 3

than SRM 1654 (37 to 74 μm); the sample 74 to 149 μm, was used for the point in the circle and one of those in the cluster of 6 near $(T-298.15\ \text{K})=55$ K, and the sample which was less than 37 μm was used for the point in the triangle and 2 points in the group just below $(T-298.15\ \text{K})=55$ K. Thus, there appears to be no difference in the results obtained with various particle sizes in this range. The ultrafine material was removed from all three portions of the quartz during the washing. Therefore, since no significant difference was detected in the enthalpies of solution of the three portions, it may be concluded that no change in the enthalpy of solution of the SRM 1654 will result from particle separation within the sample and that surface energy effects are negligible in this sample (which has the ultrafine material removed).

In Expt. No. 490 (not included in the tables or equations), the sample of smallest particle size (< 37 μm) was dissolved in 24.31 percent HF and $\Delta H(352.912\ \text{K})=-2361.1\ \text{J}\cdot\text{g}^{-1}$ which agreed with similar experiments in table 3. In addition three electrical calibrations of the initial system and three of the final system were measured and the following results were obtained:

Initial system		*Final system*	
$\bar{T}$, K	EEE, J · Ω^{-1}	$\bar{T}$, K	EEE, J · Ω^{-1}
346.383	16,493	355.072	16,610
348.570	16,532	357.252	16,647
350.755	16,568	359.428	16,684

These values confirmed the linearity of the energy equivalents (EEE) in this temperature range, and since $d(\text{EEE})/dT$ was the same for the initial and final systems, only one initial and one final calibration was necessary in each experiment.

Two experiments were not included in the tables because low values were obtained and leakage of the sample holder was suspected (this sometimes occurred when sample particles were spilled accidentally on the polytetrafluoroethylene o-ring when filling the sample holder). These were Expt. No. 433 in 24.4 percent HF, $-\Delta H(298.730\ \text{K})=2261.\ \text{J}\cdot\text{g}^{-1}$; and Expt. No. 488 in 29.84 percent HF, $-\Delta H(352.95\ \text{K})=2367.\ \text{J}\cdot\text{g}^{-1}$. Expts. No. 435, 436, and 438 were not used because the stirrer was turned off during the reaction period in an effort to reduce the total stirring energy, however, the resultant uncertainties proved to be larger than expected. Expts. No. 472, 474, and 478 were lost because of electronic problems. Expts. No. 441 through 462 and 492 through 499 were measurements on other reactions.

The results of experiments given in table 4 show the effect of varying concentrations of aqueous hydrofluoric acid on the enthalpy of solution of SRM 1654 at 353 K. A least squares fit of these data gives the following equation for the range of 18 to 30 percent HF (in $J\cdot g^{-1}$):

$$-\Delta H_{\text{soln}}\ (353.15\ \text{K})=2362.10+1.429\ (\text{wt\%HF}-24.40)$$
$$+0.069\ (\text{wt\%HF}-24.40)^2. \qquad (2)$$

The standard error of the constant term is $\pm 0.73\ J\cdot g^{-1}$, of the linear term, $\pm 0.118\ J\cdot g^{-1}$, and of the quadratic term, $\pm 0.028\ J\cdot g^{-1}$. The standard error of the estimate is $\pm 1.6\ J\cdot g^{-1}$. The mean slope is $1.326\ J\cdot g^{-1}\ (\text{wt\%HF}-24.40)^{-1}$.

Figure 3 is a plot on the molar basis of the enthalpies of solution versus the HF concentration as given in table 4. Although a quadratic equation is barely justified over a linear equation, logically the slope should decrease in the more dilute solutions, although there is greater uncertainty in this region because of

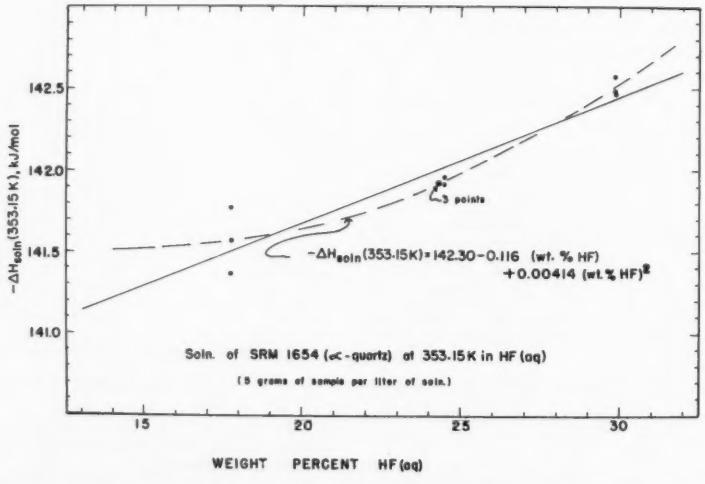

FIGURE 3. *A plot of the data in table 4 showing the relationships of the enthalpy of solution of quartz at 353 K to the concentration of* HF *(aq).*
The straight line represents the mean slope, $0.0796 \pm 0.0084\ \text{kJ}\cdot\text{mol}^{-1}\ (\text{wt\%HF})^{-1}$.

TABLE 4. *Data for experiments showing the relationship of the enthalpy of solution of quartz in aqueous* HF *at 353.15 K to the* HF *concentration*

Expt. No.	Sample mass	Mass HF soln	Conc. of HF soln	Elec. energy equiv.		Corrected temperature rise	Q reaction	$\bar{T}$ reaction		Corr. to 353.15 K	$-\Delta\bar{H}_{soln}$ (353.15 K)
				Initial	Final						
	g	*g*	wt %	$J \cdot \Omega^{-1}$		Ω	*J*	*K*	°C	$J \cdot g^{-1}$	$J \cdot g^{-1}$
479	1.51008	317.66	17.75	17,003	17,035	0.208932	3555.8	352.813	79.663	−0.5	2355.2
480	1.51163	317.58	24.46	16,557	16,602	.215304	3569 6	352.883	79.733	−.4	2361.8
481	1.51260	317.63	24.46	16;561	16,603	.215479	3573.0	352.872	79.722	−.4	2362.6
482	1.51806	317.63	24.31	16,571	16,611	.216067	3584.8	352.888	79.738	−.4	2361.8
483	1.49911	317.64	24.31	16,570	16,611	.213384	3540.1	352.865	79.715	−.5	2362.0
484	1.50632	317.59	24.31	16,568	16,609	.214454	3557.5	352.892	79.742	−.4	2362.1
489	1.51622	317.58	17.75	17,006	17,031	.210117	3575.9	352.799	79.649	−.6	2359.0
491	1.51067	317.53	29.84	16,230	16,283	.220470	3584.1	352.922	79.772	−.4	2372.9
500	1.48970	317.62	17.75	17,014	17,039	.205834	3504.6	353.081	79.931	−.1	2352.7
501	1.49384	317.65	29.82	16,236	16.293	.217811	3542.6	353.260	80.110	+.2	2371.2
502	1.51193	317.55	29.82	16,234	16,286	.220526	3585.8	353.260	80.110	+.2	2371.4

the longer reaction periods. The mole ratio of HF : SiO_2 in the experiments reported here ranges from 111 (No. 489) to 191 (No. 501). This is not sufficient to establish dilution effects over a large range.

TABLE 5. *Results of the experiments on which the certified value for the enthalpy of solution of SRM 1654 is based*

Expt. No.	Concentration of HF soln	$-\Delta H_{soln}(T)$	Correction to 353.15 K	$-\Delta H_{soln}$ (353.15 K)
	wt %	$J \cdot g^{-1}$	$J \cdot g^{-1}$	$J \cdot g^{-1}$
467	24.43	2362.9	0.0	2362.9
470	24.43	2361.2	−0.3	2361.5
471	24.46	2362.1	0.0	2362.1
473	24.46	2363.2	+0.1	2363.1
480	24.46	2361.4	−0.4	2361.8
481	24.46	2362.2	−0.4	2362.6
482	24.31	2361.4	−0.4	2361.8
483	24.31	2361.5	−0.5	2362.0
484	24.31	2361.7	−0.4	2362.1
Mean....	24.40			2362.2
Standard deviation of the mean				±0.2

In table 5 are summarized the results of the nine experiments on which the following certified value for the enthalpy of solution in 24.4 percent HF(aq) of SRM 1654 (α-quartz) is based:

$$\Delta H_{soln}(353.15\ K) = -2362.2 \pm 1.1\ J \cdot g^{-1}.$$

This is for a concentration of 5 g of sample per 1000 cm^3 of HF solution. The enthalpy value also applies to the enthalpy of solution of pure quartz within the assigned uncertainty. The 0.05 percent (1.1 $J \cdot g^{-1}$) uncertainty limit assigned is the square root of the sum of the squares of the following uncertainties: 0.4 $J \cdot g^{-1}$ for experimental precision at the 95 percent confidence level; 1.0 $J \cdot g^{-1}$ for possible inert material (this is about twice the percentage of inert material found in the analysis); 0.3 $J \cdot g^{-1}$ for errors in analysis of HF stock solutions; and 0.2 $J \cdot g^{-1}$ for possible collective errors in values used for calibrations of measuring instruments and reference standards and in heater-lead error. Measurements of the temperature rise in the first four experiments given in table 5 were made with a quartz-oscillator thermometer, and in the last five experiments, with a platinum resistance thermometer.

6. Discussion of Results

Prior to this work very little information was available regarding the effects of temperature and HF concentration on the enthalpy of solution of low quartz. Hummel and Schwiete [8] published plots of their measured values for the enthalpies of solution of quartz versus the temperatures of reaction in 20 percent HF from about 25 to 80 °C, and versus concentration from 10 to 39 percent HF solution. The slope of the straight line from their temperature data is nearly the same as that given in figure 2 although their enthalpy values are about 1 percent smaller than our corresponding values. Their plot showing the effect of HF concentration on the enthalpy includes a greater range than in our measurements and their value at 24 percent HF is only slightly lower than ours corrected to the same temperature. Their value shown in table 6 appears to be about 1 percent lower than other recent measurements of the enthalpy of solution of low quartz.

Some of the other values reported previously for the enthalpy of solution of low quartz in aqueous HF are listed in table 6; also given are these values corrected to the conditions of the certified value for SRM 1654

TABLE 6. *Comparison of some values reported for the enthalpy of solution of low quartz in* HF *(aq)*

Reference	Year	Value reported for $-\Delta H(T)$	T reaction	HF conc.	$-\Delta H$ (80°C) in 24.4% HF	Corrected value minus certified value
		$kJ \cdot mol^{-1}$	°C	wt %	$kJ \cdot mol^{-1}$	$kJ \cdot mol^{-1}$
Mulert [4]	1912	125.23 ± 2.51	18	20	131.48	−10.45
Wietzel [5]	1921	140.79	[b]18	35	145.87	+3.94
Roth and Troitzsch [11]	1932	137.78 ± 0.21	77.2	20.6	*140.79	−1.15
Troitzsch [12]	1936	139.91 ± 0.08	77	20.6	140.50	−1.43
Torgeson and Sahama [13]	1948	138.07 ± 0.08	73.7	20.1	*141.29	−0.64
Sahama and Neuvonen [14]	1951	139.08 ± 0.20	75.1	20.1	*142.23	+0.30
King [15]	1951	139.28 ± 0.33	73.7	20.1	*142.50	+0.57
		137.28 ± 0.38	50	20.1	*141.62	−0.31
Kracek, et al. [16]	1951	139.33 ± 0.17	74.7	20.0	*142.51	+0.58
		138.62 ± 0.12	74.7	20.0	*141.80	−0.13
King [17]	1952	138.36 ± 0.42	60	20.1	*142.23	+0.30
Jeffes, et al. [6]	1954	137.11 ± 0.79	25	18.7	142.80	+0.87
Stevens and Turkdogan [7]	1955	[a]135.56 ± 0.46	25	18.7	141.26	−0.67
Hummel and Schwiete [8]	1959	134.85 ± 0.42	26.5	19.5	140.33	−1.60
Waldbaum [10]	1970	139.00 ± 0.08	49.7	20.1	142.23	+0.30
Waldbaum [10]	1971	138.93 ± 0.40	49.7	20.1	142.17	+0.24
This work	1970	141.93 ± 0.07	80.0	24.4	141.93	—

*Corrected to the isothermal reaction using Cp (quartz) obtained from the JANAF tables [18].

[a] We have used their value before their correction for a hypothetical amount of amorphous SiO_2 since none of the other values have such a correction; their value including the correction is 134.68 $kJ \cdot mol^{-1}$ which becomes 140.36 in 24.4 percent HF at 80 °C.

[b] Temperature not specified but assumed to be 18 °C.

using 0.0953 kJ · mol^{-1} · K^{-1} and 0.0796 kJ · mol^{-1} (wt%HF)$^{-1}$. The corrections may do an injustice to the values for reactions in the lower HF concentrations and near room temperature where our equations are known to have larger uncertainties. However, under those conditions the uncertainty in the measurements must also be large because of the slow reaction rate, and the very finely divided samples which had to be used may have introduced surface energy effects. Except for the value of Hummel and Schwiete, the corrected values are in good agreement for all values reported since 1940.

An adiabatic calorimeter was used in the present work; all other values given in table 6 were measured in isoperibol calorimeters. Waldbaum used a calorimeter previously described by Robie [19]. The values of Troitzsch (1936), Waldbaum, and the present work are for the isothermal reaction where the sample was in a sealed container inside the calorimeter until initiation of the reaction; all other values in table 6 are for the sample at 25 °C (or room temperature) and the solution and products at the mean temperature of reaction, therefore, in order to convert these to the isothermal reactions corrections were made using Cp of quartz at the mean temperature of the excursions, taken from the JANAF Tables [18]. This correction was not made for the reactions at or near 25 °C.

All values in table 6 except the last three were obtained from samples which had been elutriated or extremely finely powdered in order to complete the solution in a short period of time. Both of Waldbaum's samples passed a #400 sieve but fine particles were removed by elutriation, and SRM 1654 used in this work was between #200 and #400 sieve size with fine particles removed by elutriation. The samples were natural Brazilian quartz in this work and in Waldbaum's. The sample for Waldbaum's 1970 value was from the same quartz fragment which he supplied to Holm and Kleppa [9], and for his 1971 value he used a sample from our portion 3 (see sec. 2) which was the same as SRM 1654 except in particle size. Wietzel's sample was Carrara quartz; Kracek's samples were from Sycamore Island and Lisbon, Maryland, respectively; and all other samples were natural quartz of unstated origin.

The corrected values given in table 6 are in good agreement when the variables of time, calorimeters, samples, and procedures are considered. This would suggest that measurements made with a single, uniform sample such as SRM 1654, can serve as an indication of the relative accuracy and precision of measurements by various calorimeters employed in HF solution calorimetry.

We acknowledge with gratitude the advice and information relative to the preparation of this paper supplied by David L. Waldbaum of Princeton University.

7. References

[1] Frondel, C., The System of Mineralogy, **III** (John Wiley and Sons, Inc., New York, N.Y., 1962), pp 1 and 117.
[2] Commission on Atomic Weights, Pure and Applied Chem. **21**, 91 (1970).
[3] Prosen, E. J., and Kilday, M. V., J. Res. Nat. Bur. Stand. (U.S.), 77A (Phys. and Chem.) No. 2, 179–203 (Mar.–Apr. 1973).
[4] Mulert, O., Z. anorg. Chem. **75**, 198 (1912).
[5] Wietzel, R., Z. anorg. allgem. Chem. **116**, 71 (1921).
[6] Jeffes, J. H. E., Richardson, F. D., and Pearson, J., Trans. Faraday Soc. **50**, 364 (1954).
[7] Stevens, C. G., and Turkdogan, E. T., Trans. Faraday Soc. **51**, 357 (1955).
[8] Hummel, von C., and Schwiete, H. E., Glastechn. Ber. **32**, 327 (1959).
[9] Holm, J. L., Kleppa, O. J., and Westrum, E. F., Jr., Geochim. Cosmo. Chim. Acta **31**, 2289 (1967).
[10] Waldbaum, D. R., written communication (1970, 1972).
[11] Roth, W. A., and Troitzsch, H., Arch. Eisenhüttenw. **6**, 79 (1932).
[12] Troitzsch, H., Diss., Technischen Hochschule zu Braunschweig (1936).
[13] Torgeson, D. R., and Sahama, Th. G., J. Am. Chem. Soc. **70**, 2156 (1948).
[14] Sahama, Th. G., and Neuvonen, K. J., Bull. Comm. Geol. Finlande **154**, 177 (1951).
[15] King, E. G., J. Am. Chem. Soc. **73**, 656 (1951).
[16] Kracek, F. C., Neuvonen, K. J., and Burley, G., J. Wash. Acad. Sci. **41**, 373 (1951).
[17] King, E. G., J. Am. Chem. Soc. **74**, 4446 (1952).
[18] JANAF Thermochemical Tables, 2nd Edition, D. R. Stull and H. Prophet, Project Directors, Nat. Stand. Ref. Data Ser. Nat. Bur. Stand. (U.S.), 37, 1141 pages (June 1971).
[19] Robie, R. A., Rev. Sci. Instr. **36**, 484 (1965).

(Paper 77A2–763)

JOURNAL OF RESEARCH of the National Bureau of Standards—A. Physics and Chemistry
Vol. 77A, No. 2, March–April 1973

Enthalpies of Solution of BeO(c) in HF(aq) and in HCl(aq)*

M. V. Kilday, E. J. Prosen, and D. D. Wagman

Institute for Materials Research, National Bureau of Standards, Washington, D.C. 20234

(November 9, 1972)

An adiabatic solution calorimeter was used to measure the enthalpies of the following reactions:

$$BeO(c)+[96\ HF+338\ H_2O](l)\rightarrow[BeF_2+94\ HF+339\ H_2O](l)$$

$$\Delta H \text{ at } 298.15\ K = -101.30 \pm 0.20\ kJ \cdot mol^{-1}$$

$$BeO(c)+[48\ HCl+333\ H_2O](l)\rightarrow[BeCl_2+46\ HCl+334\ H_2O](l)$$

$$\Delta H \text{ at } 352.58\ K = -54.19 \pm 0.22\ kJ \cdot mol^{-1}$$

$$\Delta H \text{ at } 298.15\ K = -53.0 \pm 2.0\ kJ \cdot mol^{-1}$$

ΔCp is $12.5 \pm 2.8\ J \cdot mol^{-1} \cdot K^{-1}$ for the first reaction in the range 298 to 325 K.

Key words: BeO(c), enthalpy of soln in HF(aq); BeO(c), enthalpy of soln in HCl(aq); BeO(c), enthalpy of reaction in HF(aq); beryllium oxide; enthalpy of solution; heat of solution; thermochemistry.

1. Introduction

The value for the enthalpy of formation of beryllium oxide is an important quantity in establishing values for the enthalpies of formation of many other beryllium compounds. Determination of this quantity by direct combustion has been subject to considerable uncertainty, as have the various indirect methods [1].[1] A precision adiabatic solution calorimeter, designed to measure the energy changes in slow reactions, was employed to determine the enthalpies of solution of BeO(c) in both aqueous hydrofluoric and hydrochloric acids as functions of temperature and acid concentration. Effectively complete reaction was obtained in all cases. These values were combined with other data by Parker [1] to obtain a more reliable value for the enthalpy of formation of BeO(c).

2. Sample and Calorimetric Solutions

2.1. BeO(c)

The crystalline beryllium oxide was obtained from the Brush Beryllium Company,[2] Elmore, Ohio. It was identified as UOX grade, −325 mesh. The certificate of analysis supplied with the material indicated 0.33 percent loss on ignition, 0.31 percent loss on drying, 0.23 percent SO_3 and a total of less than 280 ppm of metallic elements identified in spectroscopic analysis. The principal impurities were 50 ppm Al, 15 ppm Fe, 40 ppm Mg, 50 ppm Na, 30 ppm Ca, 50 ppm Si, and <20 ppm Zn. We confirmed the loss on drying at ~540 K, the spectroscopic analysis[3] was confirmed, and the crystallinity of the sample was confirmed by x-ray powder diffraction analysis.[4]

The 1.0-g or 0.3-g samples for the calorimetric experiments were dried overnight at approximately 540 K and stored in a desiccator until they were transferred in a dry box to the weighed sample holder. The determination of the sample mass is estimated to be accurate to ± 0.03 mg.

A slight inhomogeneity in the BeO sample became apparent when traces of undissolved residues were found in the final HCl solutions. There were two types of "undissolved" residue: a very finely divided material which was present at low reaction temperatures and in preliminary experiments of short duration, and coarser particles with diameters of the order of 1 mm which under the microscope appeared to be clusters of crystals. The finely divided material was identified as unreacted BeO by x-ray powder diffraction.[4] The coarser material definitely contributed additional lines to the BeO pattern, but the composition was not identified. Spectroscopic analysis of the material indicated

*This work was supported in part by the Air Force Office of Scientific Research, under the contract series beginning with: AFOSR–ISSA–69–0001.

[1] Figures in brackets indicate literature references at the end of this paper.

[2] Certain commercial material is identified in this paper in order to adequately specify the experimental procedure. Such identification does not imply recommendation or endorsement by the National Bureau of Standards.

[3] Performed by V. C. Stewart, Spectrochemical Analysis Section, Analytical Chemistry Division.

[4] Performed by H. E. Swanson, Crystallography Section. Inorganic Materials Division.

Be as the major constituent with Al and Si as minor constituents, and it was concluded that this coarser material which was insoluble in the HCl solutions even at 363 K was probably mixed oxides of Be, Al, and Si. Further identification of the insoluble residue was not attempted in view of the very small quantities which were not homogeneously distributed in the calorimetric samples. Various final calorimetric solutions contained from zero to five of the "insoluble" particles.

In the hydrofluoric acid calorimetric solutions, solution of the BeO sample appeared to be complete and no undissolved residue was visible.

2.2. Calorimetric Solutions of Aqueous Hydrofluoric Acid

The calorimetric solutions were portions of seven stock solutions prepared by dilution of ACS reagent-grade concentrated hydrofluoric acid (48–51%) with distilled water. The stock solutions were analyzed by titration of weighed samples, 3 to 5 g, with 0.918 *N* standard sodium hydroxide solution using phenolphthalein as an indicator.

The calorimetric solutions were clear after the reactions, with no undissolved residue visible. Analysis of the final solutions was not attempted and the products were assumed to be BeF_2 and H_2O in solution. Soda lime (containing a color indicator) was found to be useful in safely neutralizing the HF solutions from the calorimetric experiments. The neutralization was done in an ice bath with stirring to prevent excessive heating.

2.3. Calorimetric Solutions of Aqueous Hydrochloric Acid

The calorimetric solutions were portions of four stock solutions prepared by dilution of cp reagent-grade concentrated hydrochloric acid (37–38%) with distilled water. The stock solutions were analyzed by titration using anhydrous sodium carbonate prepared from reagent-grade sodium carbonate dried at 543 K for 1 h; bromophenol blue was the indicator.

The final calorimetric solutions were not analyzed and the products were assumed to be $BeCl_2$ and H_2O in solution.

3. Units, Physical Constants, and Calibrations

The masses of samples given in the following tables were obtained using a buoyancy factor calculated from the density, 3.03 $g \cdot cm^{-3}$ [2], for BeO(c).

Values for atomic weights were taken from the 1969 Table of Atomic Weights [3]. Molecular weights used are as follows: BeO, 25.01158; HF, 20.0064; HCl, 36.461; and H_2O, 18.0154.

The unit of energy is the joule (J) and 1 thermochemical calorie = 4.1840 J.

Electrical energy measurements were based on the values of a saturated Weston standard cell last calibrated in April 1968, and of standard resistors last calibrated in October 1966. Temperature measurements are based on the 25-Ω platinum resistance thermometer calibration of 1961.[5] These are all NBS certified calibrations. The history of calibrations of this equipment provided confidence in the values at the actual time of these experiments because of the consistent trend in the calibrated values over the years. The measurements reported in this paper were made between March 1967 and November 1968.

4. Calorimeter and Procedures

The high precision adiabatic solution calorimeter used for these measurements is described in detail by Prosen and Kilday [4]. In this work, the largest cylinder (volume 2.7 cm^3) was used in the sample holder to avoid the necessity for packing the very finely divided sample. In a dry box, the BeO sample was added to the cylinder shown at the top of figure 1 and the sample holder was assembled as shown at the bottom before weighing.

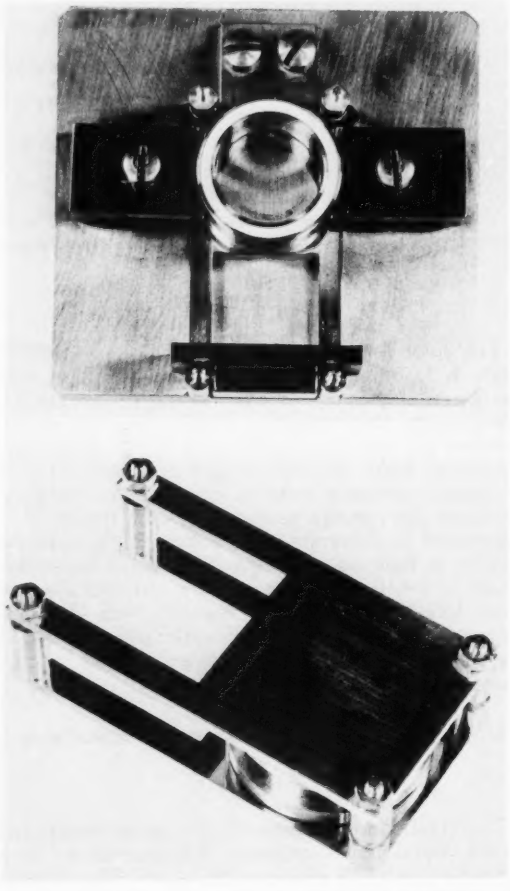

FIGURE 1. *(upper) The sample holder in a clamp ready for filling, and (lower) the assembled sample holder ready for weighing.*

[5] See [4] for thermometer calibration data. On this thermometer, one kelvin is 0.10104 Ω at 298.15 K and 0.09939 Ω at 353.15 K.

The time required for one complete experiment varied from approximately 8 h for the BeO in HF(aq) to 4 days for the BeO in HCl(aq). The duration of the chemical reaction period varied with the concentration of the solvent, the temperature of reaction, and the stirring rate. The four reaction periods plotted in figure 2 show the variations from 1 h to 4.5 h for solutions of BeO(c) in HF(aq). They represent various concentrations of HF(aq) at 298 K and 323 K and a stirring rate of 250 rpm. This stirring rate was used for all of the BeO solutions in HF(aq) except as noted.

The solutions of BeO(c) in HCl(aq) were made with a stirring rate of 350 rpm but only in the first experiment was there continuous stirring during the 20-h reaction period. In all other experiments the stirrer and the thermometer current were turned off for 17.5 h during the chemical reaction. A drift rate for the unstirred system (discussed in sec. 5.3) was measured at the beginning and the end of these experiments. The observed heat loss was assumed to be due to evaporation through the stirrer tube for which approximate corrections were applied. During the stirred portions of the experiments, evaporative heat losses were included in the slopes of the rating periods. The calibrations of the initial and final systems compensate for changes in the heat capacity of the system.

The point at which the reactions were completed was not clearly defined, especially in the very slow reactions, but this is not critical since the calorimeter operates under adiabatic conditions. A reaction was usually assumed to be complete when the slope of the temperature curve was approximately the same as that of the initial rating period, or when the slope of the final time-temperature curve had not changed significantly for 1 h. Although these conditions were met after 8 h in the solution of BeO(c) in HCl(aq) at 358 K, more than 1 percent of the sample remained undissolved in the final solution. When the reaction time was extended overnight, the undissolved sample in the final solution was negligible.

In the solutions of BeO in HF(aq) at 313 and at 323 K, the temperature of the shield lagged behind that of the vessel for several minutes after starting the reaction. Small corrections were calculated for these experiments based on a previously determined value for the heat leak constant, $k = 3.0 \times 10^{-3}$ min^{-1} [4]. The largest of these corrections (Expts. No. 28 and 30) was 0.09 percent of the corrected temperature

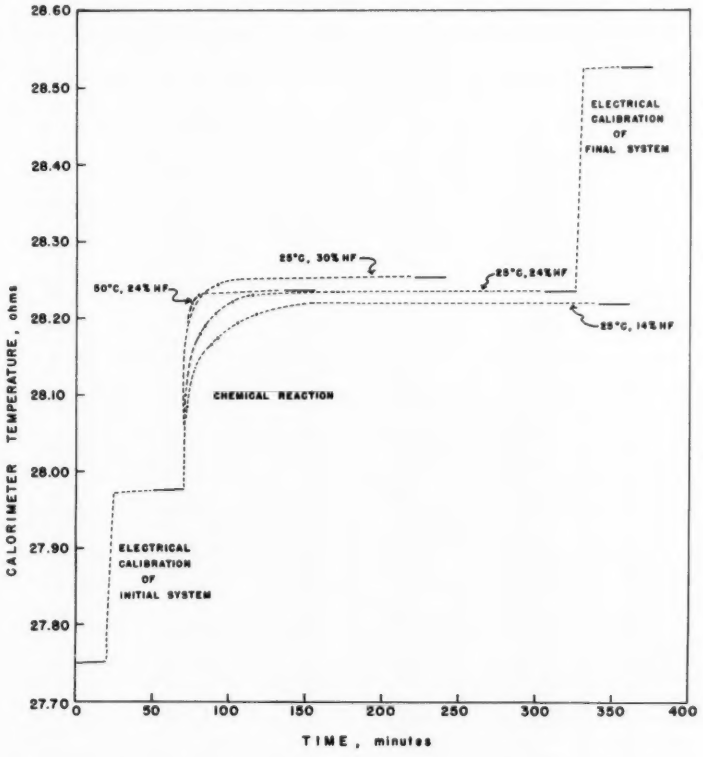

FIGURE 2. *Time-temperature curves for experiments in which samples of* BeO(c) *were dissolved in* HF(aq) *under various conditions.*

The solid lines are rating periods and the dashed lines are reaction or electrical calibration periods. The electrical calibration curves are shown for only one experiment.

rise, ΔRc. The area, 182 $\mu V \cdot min$, was obtained from the record of the difference between the temperatures of the calorimeter vessel and of the adiabatic shield. The six-junction control thermocouples produce 240 $\mu V \cdot K^{-1}$ and the thermal coefficient of the resistance thermometer is 10 $K \cdot \Omega^{-1}$. The correction, 230 $\mu\Omega$, in a total temperature rise of 0.254 Ω is 0.09 percent.

The final calorimeter solutions were not analyzed except by weighing the amounts of undissolved residues in the HCl solutions. The final solutions were allowed to stand at least 1 h after which approximately 250 cm^3 of the solution was siphoned off (to avoid disturbing the solid particles which had settled to the bottom of the vessel). The remaining solution was diluted to approximately 300 cm^3 with distilled water and allowed to stand at least 1 h. Approximately 280 cm^3 of the solution again was siphoned off. The larger "insoluble" particles were removed with a spatula and the finely divided residue was transferred with the solution to a weighed platinum crucible by means of a dropper. The solution was evaporated and the residue was dried for 2 h at 543 K, cooled, and weighed. The mass of the residue was subtracted from the sample mass to give the mass of sample reacted.

5. Experimental Results

5.1. Solution of BeO(c) in HF(aq)

The enthalpies of solution of crystalline beryllium oxide in aqueous hydrofluoric acid solutions were measured in 29 experiments at reaction temperatures ranging from 293 K to 325 K and in 14 to 30 wt percent HF(aq). Most of the BeO samples weighed about 1 g. However, 0.3-g samples were used for the reactions at 293 K in order to obtain the desired mean temperature of reaction with a starting temperature of 291 K, the lower limit of the controlled room temperature. At 298 K, 0.3-g samples were also used in three experiments for comparison with those at 293 K. Unfortunately the use of these small samples resulted in a large reduction in the precision of the measurements because of the smaller temperature rise, and the results were not used in the determination of ΔCp for the reaction. However, they were useful in showing that a change in the ratio of the Be to HF at this concentration has little effect on the enthalpy of solution.

Tables 1 and 2 give the data for the 29 experiments in which the enthalpy of solution of BeO(c) in HF(aq)

TABLE 1. *Composition of reactants in the calorimetric systems for solutions of* BeO(c) *in* HF(aq)

Expt. No.	Initial composition			Conc. of HF soln.	Mass of HF soln.
	BeO	HF	H_2O		
	mol	*mol*	*mol*	*wt %*	*g*
1	0.040166	3.648	12.737	24.13	302.45
2	.039940	3.858	13.326	24.33	317.27
3	.039247	3.826	13.359	24.13	317.21
4	.039186	3.859	13.327	24.33	317.29
5	.035230	3.859	13.328	24.33	317.30
6	.039722	3.117	14.146	19.66	317.20
7	.040649	3.140	14.121	19.80	317.21
8	.040709	3.119	14.152	19.66	317.34
9	.039771	3.826	13.358	24.13	317.18
10	.040045	3.825	13.356	24.13	317.14
11	.013265	3.140	14.122	19.80	317.23
12	.013035	3.117	14.145	19.66	317.18
13	.013414	3.140	14.122	19.80	317.23
14	.039897	2.228	15.139	14.05	317.31
15	.038740	2.227	15.129	14.05	317.12
16	.039486	2.228	15.135	14.05	317.23
17	.012077	3.119	14.152	19.66	317.35
18	.012561	3.140	14.125	19.80	317.29
19	.012302	3.118	14.151	19.66	317.31
20	.041156	4.716	12.361	29.76	317.03
22	.039519	4.719	12.370	29.76	317.27
23	.041010	4.721	12.374	29.76	317.37
24	.040988	4.720	12.372	29.76	317.31
25	.040436	3.844	13.348	24.23	317.36
26	.038455	3.844	13.351	24.23	317.43
27	.039967	3.844	13.348	24.23	317.37
28	.041170	3.843	13.348	24.23	317.35
29	.033059	3.842	13.344	24.23	317.27
30	.040682	3.843	13.347	24.23	317.34

was measured. In this and in subsequent tables, EEE_i and EEE_f are the electrical energy equivalents of the initial and final systems. The methods for calculating the electrical energy equivalents; the stirring energy corrections; the corrected temperature rise, ΔRc; and the mean temperature of reaction, $\bar{T}$, were described previously [4]. The enthalpy of solution at the temperature of reaction, which we define as the mean temperature of reaction, was calculated using the following equation:

$$-\Delta H(T) = \{[1/2(EEE_i + EEE_f)](\Delta Rc)\}/ \text{(moles of sample).}$$

Expt. No. 21 was lost because of a problem with the adiabatic controls and the results are not included in the tables.

A least squares fit of the data from the 13 experiments using 24 percent HF (Nos. 1, 2, 3, 4, 5, 9, 10, 25, 26, 27, 28, 29, and 30) given in table 2 resulted in the following equation for the relationship of temperature (in K) and the enthalpy of solution (in kJ · mol^{-1}) of BeO(c) in 24 percent HF:

$$\Delta H \text{ at } T = -101.20^* + 0.0125\ (T - 298.15\ \text{K}).$$

Thus, ΔCp for the reaction is $+12.5 \pm 2.8$ J · mol^{-1} · K^{-1} (or $+2.99 \pm 0.69$ cal · mol^{-1} · K^{-1}) in the range 298 K to 324 K. The standard error of the estimate of ΔH is ± 0.11 kJ · mol^{-1} and of the constant term, ± 0.04 kJ · mol^{-1}.

The following relationship of HF concentration to the enthalpy of solution (in kJ · mol^{-1}) was obtained for a least squares fit of the data from the 14 experiments near 298.15 K and using ~ 1 g of BeO (Nos. 1, 4, 5, 6, 7, 8, 9, 14, 15, 16, 20, 22, 23, and 24) given in tables 1 and 2:

$$\Delta H \text{ at } 298.15\ \text{K} = -101.30^* - 0.0999\ (\text{wt\% HF} - 24) + 0.00659\ (\text{wt\% HF} - 24)^2.$$

The standard error of the estimate of ΔH is ± 0.12 kJ · mol^{-1} and the standard errors of the constants are ± 0.05, ± 0.0071, and ± 0.00114, respectively.

*These values have been increased by 0.22 percent to correct for the $BeSO_4$ impurity in the sample as described at the end of this section.

TABLE 2. *Calorimetric data for solutions of* BeO(c) *in* HF(aq)

Expt. No.	Sample mass	EEE_i	EEE_f	Duration of reaction	Stirring energy corr.	ΔRc	$\bar{T}$ reaction		$-\Delta H(T)$
	g	$J \cdot \Omega^{-1}$	$J \cdot \Omega^{-1}$	*min*	Ω	Ω	°C	K	$kJ \cdot mol^{-1}$
1	1.00461	15,122.50	15,211.98	215	0.005659	0.267329	26.104	299.254	100.948
2	0.99896	15,709.97	15,809.88	190	.004376	.255894	29.570	302.720	100.973
3	.98164	15,688.63	15,788.83	190	.004158	.251187	29.568	302.718	100.729
4	.98010	15,598.57	15,705.42	220	.004640	.253170	24.743	297.893	101.124
5	.88115	15,590.07	15,692.21	310	.004437	.227897	24.692	297.842	101.181
6	.99350	15,924.52	16,025.89	230	.003311	.250232	25.774	298.924	100.638
7	1.01669	15,887.56	15,988.11	230	.003235	.256641	25.051	298.201	100.626
8	1.01819	15,884.66	15,986.85	230	.003458	.256922	25.050	298.200	100.574
9	0.99474	15,605.42	15,710.15	230	.003443	.256228	25.138	298.288	100.876
10	1.00159	15,696.68	15,793.16	200	.002988	.256612	30.043	303.193	100.895
11	0.33178	15,775.32	15,805.51	190	.004294	.084414	20.115	293.265	100.485
12	.32602	15,775.66	15,808.84	190	.003419	.082964	20.084	293.234	100.515
13	.33549	15,777.37	15,812.70	190	.003907	.084978	20.073	293.223	100.066
14	.99788	16,389.99	16,469.80	435	.007083	.241164	24.298	297.448	99.314
15	.96894	16,390.14	16,469.51	405	.005916	.234906	24.253	297.403	99.626
16	.98760	16,396.71	16,476.73	265	.004225	.238649	24.287	297.437	99.342
17	.30206	15,880.24	15,911.89	195	.003203	.076619	25.426	298.576	100.850
18	.31418	15,883.10	15,908.92	195	.003604	.079494	25.447	298.597	100.597
19	.30770	15,891.29	15,897.92	130	*.011244	.077442	25.496	298.646	100.055
20	1.02937	15,171.25	15,274.16	180	.003963	.274283	25.299	298.449	101.452
22	0.98844	15,169.02	15,270.48	190	.003964	.263342	24.814	297.964	101.419
23	1.02572	15,173.78	15,274.59	180	.003512	.273448	24.868	298.018	101.513
24	1.02517	15,171.86	15,274.00	185	.003936	.273145	24.941	298.091	101.446
25	1.01137	15,970.75	16,067.96	100	.001508	.254713	41.959	315.109	100.908
26	0.96183	15,949.98	16,033.49	120	.002302	.242418	41.872	315.022	100.810
27	.99963	15,858.45	15,949.34	125	.002139	.253236	38.000	311.150	100.770
28	1.02973	16,088.96	16,171.92	65	.001173	.257031	51.885	325.035	100.705
29	0.82687	16,080.54	16,157.78	65	.001160	.206371	51.664	324.814	100.622
30	1.01751	16,082.92	16,167.87	65	.000932	.253897	51.880	325.030	100.640

*Stirring rate changed from 250 rpm to 550 rpm.

Using a multivariable treatment of the data,[6] a least squares fit for the data in all 29 experiments resulted in the following equation (in $kJ \cdot mol^{-1}$ and K):

$$\Delta H = -101.21^* + 0.0125\,(T - 298.15\ \text{K}) - 0.1066\,(\text{wt\% HF} - 24) + 0.0049\,(\text{wt\%} - 24)^2$$

The residual standard deviation of ΔH is ± 0.18 $kJ \cdot mol^{-1}$, and the standard deviations of the four coefficients are 0.05, 0.0040, 0.0095, and 0.0015, respectively. The agreement with the two equations above is good.

The seven experiments which were near 298 K and 24 percent HF given in table 3 are corrected to 298.15 K and 24 percent HF and correspond to the following equation:

$$\text{BeO(c)} + [96\ \text{HF} + 338\ \text{H}_2\text{O}]\,(l) \rightarrow [\text{BeF}_2 + 94\ \text{HF} + 339\ \text{H}_2\text{O}]\,(l) \qquad (1)$$

$$\Delta H \text{ at } 298.15\ \text{K} = -101.30 \pm 0.20\ \text{kJ} \cdot \text{mol}^{-1} = -24.21 \pm 0.05\ \text{kcal} \cdot \text{mol}^{-1}.$$

A correction of 0.22 percent was added to the mean enthalpy value given in table 3 for the SO_3 impurity in the sample (see sec. 2.1) which is probably present as $BeSO_4$. The correction is based on Bear and Turnbull's value for the enthalpy of solution of $BeSO_4$ in HF(aq), -24.05 ± 0.30 kcal/mol [5]. The weight loss on drying the sample, presumably H_2O, was not a source of error because of the initial heating of the calorimetric samples. The maximum error resulting from the presence of oxides or sulfates of the metallic elements found in the spectroscopic analysis was about 0.1 percent, and twice the standard deviation of the mean of the experimental values is 0.09 percent. Therefore, an uncertainty limit of 0.2 percent was assigned to the enthalpy value in eq (1).

TABLE 3. *Enthalpy of solution of* BeO(c) *in 24 percent* HF(aq) *at* 298.15 K

Expt. No.	Corr. to 298.15 K	Corr. to 24% HF	ΔH(298.15 K) in 24% HF
	$kJ \cdot mol^{-1}$	$kJ \cdot mol^{-1}$	$kJ \cdot mol^{-1}$
1	−0.014	+0.012	−100.950
4	+.003	+.026	−101.095
5	+.004	+.026	−101.151
6	−.010	−.558	−101.206
7	−.001	−.536	−101.163
8	−.001	−.558	−101.133
9	−.002	+.012	−100.866
Mean			*−101.080
Standard deviation of the mean			±0.047

*A correction of 0.22 percent should be added to this value for the $BeSO_4$ impurity in the sample.

*These values have been increased by 0.22 percent to correct for the $BeSO_4$ impurity in the sample as described at the end of this section.

[6] Calculated by H. H. Ku, Statistical Engineering Laboratory, Institute for Basic Standards.

5.2. H_2O Dilution of Final Solutions of BeO(c) in HF(aq)

It is important in the correlation of data (see [1]) to have enthalpies of dilution of the final solutions. These enthalpies were measured in experiments where 0.7 g of distilled water was added to final solutions from the reactions of BeO(c) in HF(aq). The data for these experiments are given in table 4. The electrical energy equivalents of the initial systems, EEE, were measured in each of the first four experiments, and an estimated value was used for the last two experiments. The enthalpies derived from these electrical energy equivalents refer to the final rather than the mean temperature of reaction, however the difference is negligible here.

The initial solution for the first experiment was 316.7 g of the final solution (approximately 30% HF) from Expt. No. 24 in the BeO(c) in HF(aq) series. The initial solutions for the last five experiments were each 317 g of a mixture of the final solutions (approximately 24% HF) from Expt. Nos. 25 through 30.

From the average $\bar{T}$ react and $\Delta H(\bar{T})$ from Expt. Nos. 5 and 6 and for Expt. Nos. 2, 3, and 4 (table 4) we calculate a ΔCp for the reaction of $H_2O(l)$ in the 24 percent HF solutions of -1.4 $J \cdot mol^{-1} \cdot K^{-1}$ or -0.34 $cal \cdot mol^{-1}\,K^{-1}$, between 298 and 323 K.

When the enthalpies of reaction for Expt. Nos. 2, 3, and 4 are corrected to 298 K we obtain an average value for reaction (2):

$$\text{H}_2\text{O}(l) + [\text{BeF}_2 + 94\ \text{HF} + 336\ \text{H}_2\text{O}(l) \rightarrow [\text{BeF}_2 + 94\ \text{HF} + 337\ \text{H}_2\text{O}]\,(l) \qquad (2)$$

$$\Delta H \text{ at } 298.15\ \text{K} = -0.334 \pm 0.020\ \text{kJ} \cdot \text{mol}^{-1} = -0.080 \pm 0.005\ \text{kcal} \cdot \text{mol}^{-1}$$

The average deviation from the mean of the three experiments was $\pm 13.$ $J \cdot mol^{-1}$, but the larger overall uncertainty was arbitrarily assigned because of the small number of experiments and the very small temperature rise.

The value for Expt. No. 1 in 30 percent HF was $\Delta H(298.15\ \text{K}) = -0.670$ $kJ \cdot mol^{-1}$ or -0.160 $kcal \cdot mol^{-1}$.

5.3. Solution of BeO(c) in HCl(aq)

In tables 5 and 6 are the data for 11 experiments in which the enthalpy of solution of crystalline beryllium oxide in aqueous hydrochloric acid was measured. The measurements were made in 22.6 percent HCl from 347 K to 362 K, and in 18 percent HCl at 362 K.

In preliminary experiments the reaction was not complete (more than 1% of undissolved sample) after 8 h with stirring at 550 rpm in 18 percent HCl at 358 K. The first experiment of the series reported here showed that the reaction was complete in 18 percent HCl after approximately 20 h with continuous stirring at 350 rpm. Although the completeness of reaction was satisfactory the stirring energy for the long period

TABLE 4. *Data for* H_2O *dilution experiments in* BeO–HF(aq) *solution*

Expt. No.	H_2O sample mass	EEE	Stirring energy corr.	ΔRc	Approx. HF conc.	$\bar{T}$ reaction		$-\Delta H(T)$
	g	$J \cdot \Omega^{-1}$	Ω	Ω	*wt %*	*°C*	*K*	$J \cdot mol^{-1}$
1	0.68925	15,213	0.000613	0.001686	30	24.96	298.11	670.4
2	.68728	15,657	.000634	.000824	24	24.74	297.89	338.1
3	.69654	15,668	.000702	.000775	24	24.62	297.77	313.9
4	.70544	15,651	.000701	.000872	24	24.61	297.76	348.7
5	.70078	*(16,100)	.000402	.000881	24	49.95	323.10	364.6
6	.69473	*(16,100)	.000294	.000894	24	49.95	323.10	373.2

*Estimated, not measured.

TABLE 5. *Composition of reactants in the calorimetric systems for solutions of* BeO(c) *in* HCl(*aq*)

Expt. No.	Initial composition			Concentration of HCl solns.		Mass of HCl soln.
	BeO	HCl	H_2O			
	mol	*mol*	*mol*	$mol \cdot dm^{-3}$	*wt %*	*g*
1	0.040119	1.568	14.444	5.375	18.01	317.37
3	.040519	1.543	14.218	5.375	18.01	312.41
4	.032737	1.493	13.755	5.375	18.01	302.24
5	.039980	1.906	13.206	6.874	22.61	307.42
6	.039615	1.906	13.206	6.874	22.61	307.42
7	.039344	1.909	13.224	6.874	22.61	307.83
8	.040995	1.907	13.207	6.874	22.61	307.44
9	.039431	1.906	13.204	6.874	22.61	307.37
10	.039862	1.907	13.207	6.874	22.61	307.45
11	.039492	1.902	13.226	6.852	22.54	307.61
12	.040870	1.902	13.228	6.852	22.54	307.64

TABLE 6. *Calorimetric data for solutions of* BeO(c) *in* HCl(*aq*)

Expt. No.	Sample mass	Undissolved sample	EEE_i	EEE_f	Stirring energy corr.	ΔRc	Drift corr.	$\bar{T}$ react		$-\Delta H(T)$
	g	*g*	$J \cdot \Omega^{-1}$	$J \cdot \Omega^{-1}$	Ω	Ω	Ω	*°C*	*K*	$kJ \cdot mol^{-1}$
1	1.00421	0.00077	15,168.8	15,210.2	0.01099	0.14458	—	89.348	362.498	54.740
3	1.01394	.00051	14,964.1	15,012.5	.00336	.13757	0.01032	89.159	362.309	54.706
4	0.81943	.00063	14,639.6	14,678.7	.00303	.11390	.00835	89.121	362.271	54.742
5	1.00179	.00183	14,341.6	14,393.0	.00249	.14437	.00600	89.303	362.453	54.037
6	0.99084	—	14,194.8	14,245.2	.00304	.14595	.00575	79.648	352.798	54.453
7	.99957	.01551	14,122.5	14,158.0	.00296	.14829	*.00365	74.320	347.470	54.607
8	1.02790	.00256	14,152.7	14,189.4	.00291	.15246	*.00396	76.307	349.457	54.071
9	0.98864	.00241	14,151.5	14,189.9	.00367	.14741	.00437	76.275	349.425	54.547
10	.99701	—	14,195.0	14,233.4	.00311	.14728	.00424	79.713	352.863	54.030
11	.98865	.00088	14,198.6	14,234.2	.00441	.14494	.00420	80.107	353.257	53.688
12	1.02341	.00118	14,187.5	14,223.2	.00327	.15180	.00377	79.748	352.898	54.072

*Drift rate calculated from equation.

of time would have resulted in a large uncertainty. It was found that the stirrer and thermometer current could be turned off about 1.5 h after initiating the reaction, and the reaction proceeded slowly without stirring; the stirrer and thermometer current were turned on again about 1.5 h before the final rating period. Thus, the stirring energy was reduced to about one-seventh of that in stirring for the full reaction period, and the uncertainty was reduced accordingly. This procedure could be used only because the calorimeter is adiabatic and has an approximately isothermal surface.

The calorimeter temperature dropped slightly during long periods of unstirred drift when there was no chemical reaction. This was apparently caused by small evaporative losses through the stirrer tube. Unfortunately, these unstirred drift rates varied somewhat from one experiment to another and it was necessary to measure the drift rate for the initial system and for the final system in each experiment, and the mean of the two drift rates was used in the correction to ΔRc for the chemical reaction. After the first experiment, the stirrer and thermometer current were off 17.5 h during the chemical reaction

periods and the initial drift measurements, and 20 h during the final drift measurements.

The drift rates varied with the calorimeter temperature and ranged from 200 to 400 $\mu\Omega \cdot h^{-1}$. The difference between initial and final drift rates ranged from 10 to 30 $\mu\Omega \cdot h^{-1}$. The drift rates for Expt. Nos. 7 and 8 were not measured, but corrections were calculated from a linear equation obtained from a least squares fit of the drift rate and temperature data in Expt. Nos. 5, 6, 9, 10, 11, and 12.

The results of Expt. No. 2 of this series were not included because the drift rates were not measured and there was insufficient data from the experiments in 18 percent HCl to calculate drift corrections.

In table 6, $\Delta H(T)$ is the enthalpy of solution at the temperature of reaction,

$$-\Delta H(T) = \frac{(25.01158)(\mathrm{EEE}_i + \mathrm{EEE}_f)\,(\Delta Rc + \text{Drift corr.})}{2(\text{Sample mass-Undissolved sample})}$$

The "Undissolved sample" was actually the insoluble residue discussed in section 2.1 except in Expt. No. 7 where the reaction was not complete at 347 K (presumably more sample would have dissolved in a longer reaction period). However, the results were used because the reaction was proceeding so slowly that the small amount of heat evolved during the final calibration was insignificant, and the calorimeter was opened immediately after the final calibration. The same procedure was followed in Expt. No. 8 at 349 K and there was no undissolved BeO. This was a good indication of the lower temperature limit for this reaction for complete solution in a reasonable length of time.

The following equation corresponds to the average value for the enthalpy of solution in 22.6 percent HCl for Expt. Nos. 5 through 12 given in table 6.

$$\mathrm{BeO(c)} + [48\,\mathrm{HCl} + 333\,\mathrm{H_2O}](\ell) \rightarrow [\mathrm{BeCl_2} + 46\,\mathrm{HCl} + 334\,\mathrm{H_2O}](\ell) \qquad (3)$$

$$\Delta H \text{ at } 352.58\ \mathrm{K} = -54.19 \pm 0.22\ \mathrm{kJ \cdot mol^{-1}} = -12.95 \pm 0.05\ \mathrm{kcal \cdot mol^{-1}}.$$

The uncertainty is twice the standard deviation of the mean of the experimental values. A correction for the SO_3 impurity in the BeO(c) was estimated to be less than 0.2 percent and was based on data for the enthalpies of formation of $BeSO_4$(c) and $BeSO_4$ in various aqueous HCl solutions [6]. This correction was not applied to the enthalpy value in equation (3) since it was small, uncertain, and well within the experimental uncertainty.

It was apparent from the experiments in table 6 that the ΔC_p for the reaction was small but the temperature range of the measurements was not sufficient to justify an extrapolation to 298 K. A value of ΔC_p for correcting the measured enthalpy of solution to 298 K was obtained from preliminary experiments in which electrical calibrations of the initial systems were made over the range of 298 K to 358 K and similar calibrations of the final systems were made over the same temperature range. The data are given in table 7. The Calib. No. indicates P for preliminary series and I for series I, the experiment no., and a letter for the electrical calibration, i.e., P-4b corresponds to a preliminary series, experiment no. 4, and the second electrical

TABLE 7. *Electrical calibration data from which* ΔCp *for the reaction of* BeO(c) *in* HCl(*aq*) *was obtained*

Initial systems			Final systems		
Calib. No.	EEE_i	$\bar{T}$	Calib. No.	EEE_f	$\bar{T}$
	$J \cdot °C^{-1}$	°C		$J \cdot °C^{-1}$	°C
P-4a	1480.416	66.5852	P-4d	1495.879	86.1536
4b	1481.343	67.7193	4e	1496.646	87.2714
4c	1482.621	68.8526	4f	1497.893	88.3897
			4g	1439.480	24.7156
I-1a	1438.757	24.7999	4i	1440.981	27.1328
1b	1440.981	25.9647	4j	1455.042	40.5510
1c	1471.129	54.5756	4k	1456.187	41.7084
1d	1470.605	55.7152	4l	1457.813	42.8631
1e	1497.052	84.5474	4m	1469.360	55.1328
			4n	1469.966	56.2840
I-2a	1497.360	84.5705	4p	1481.379	69.5224
			4q	1483.103	70.6512
I-3a	1497.090	84.5573	4r	1484.511	71.7776
			4s	1495.152	84.5557
I-4a	1439.499	24.7450	4t	1495.904	85.6762
4b	1440.666	25.9212			
4c	1495.660	84.5768	I-1g	1441.472	24.8196
			1h	1470.806	54.5654
I-5a	1439.197	24.7129	1i	1497.772	84.5620
5b	1438.877	25.8833			
5c	1496.842	84.5628			
I-6a	1495.070	84.6242			
I-7a	1496.248	84.5620			

calibration of the system. A least squares fit of the data resulted in the following equations (in °C and $J \cdot °C^{-1}$): EEE_i at $(T) = 1411.22 + 1.180(T) - 0.00202(T)^2$, and EEE_f at $(T) = 1413.24 + 1.108(T) - 0.00166(T)^2$. The standard error of the estimate for the first equation is ± 0.78 $J \cdot °C^{-1}$ and for the second equation ± 1.04 $J \cdot °C^{-1}$. Integrating the two equations between the limits of 25 and 79.43 °C we obtain a difference of -31 J which corresponds to an average of 0.0266 mol BeO(c) in 317 g of 18 percent HCl solution, or $\Delta(H_{352.58K} - H_{298.15K}) = -1.2 \pm 2.0$ $kJ \cdot mol^{-1}$ or -0.28 ± 0.48 $kcal \cdot mol^{-1}$. The large uncertainty is partly the result of evaporative losses at the high temperatures. Heat capacity data for aqueous HCl solutions are not available at the temperatures and concentrations of our measurements, however, we assume from the data given by Parker [7] that the corrections obtained in 18 percent HCl solutions would be the same in 22.6 percent HCl solutions within the uncertainty given. When the correction is added to eq (3), $\Delta H(298.15\ K) = -53.0 \pm 2.0$ $kJ \cdot mol^{-1}$ or -12.67 ± 0.48 $kcal \cdot mol^{-1}$.

From Expt. Nos. 1, 3, and 4 (table 6) we obtain a value of $\Delta H(362.4\ K) = -54.73$ $kJ \cdot mol^{-1}$ or -13.08 $kcal \cdot mol^{-1}$ for the enthalpy of solution of BeO(c) in 18 percent HCl. The average deviation of the three experiments was ± 0.027 percent.

5.4. H_2O Dilution of Final Solutions of BeO(c) in HCl(aq)

The enthalpy of dilution of the final solution was measured when 0.7 g of water was added to a mixture of the final solutions of Expt. Nos. 11 and 12 (tables 5 and 6). The data for the two experiments are given in table 8. The electrical energy equivalents, EEE, were measured for only the initial systems. Therefore, the enthalpies refer to the final rather than the mean temperature of reaction; however, the difference is negligible here. The following equation corresponds to the average for the two experiments:

$$H_2O(\ell) + [BeCl_2 + 46\ HCl + 331\ H_2O](\ell) \rightarrow [BeCl_2 + 46\ HCl + 332\ H_2O](l) \qquad (4)$$

$$\Delta H \text{ at } 298.15\ K = -1.14\ kJ \cdot mol^{-1} = -0.27\ kcal \cdot mol^{-1}.$$

TABLE 8. *Data for* H_2O *dilution in final solutions of* BeO–HCl(aq)

Expt. No.	Wt. of calor. soln. (in air)	H_2O sample mass	EEE	Stirring energy corr.	ΔRc	$\bar{T}$ reaction		$-\Delta H(T)$
	g	*g*	$J \cdot \Omega^{-1}$	Ω	Ω	°C	K	$J \cdot mol^{-1}$
1	297.18	0.70431	13,147.	0.001168	0.003351	25.09	298.24	1127.
2	269.68	.72752	12,353.	.000755	.003756	25.09	298.24	1149.
				Mean of 2 = 1138. $J \cdot mol^{-1}$ or 272.0 cal $\cdot mol^{-1}$				

6. Conclusions

Kolesov, et al., measured the enthalpy of reaction of BeO(c) in 22.6 percent HF(aq) at 21 °C as -24.17 ± 0.12 $kcal \cdot mol^{-1}$ [8]. This value corrected for temperature and acid concentration using our equations in section 5.1 is $\Delta H(298.15\ K) = -24.19$ $kcal \cdot mol^{-1}$ which is in good agreement with our value, -24.21 ± 0.05 $kcal \cdot mol^{-1}$, given in eq (1). No values have been reported previously for the enthalpy of reaction of BeO(c) in aqueous HCl.

The values for the enthalpies of solution of BeO(c) in HF(aq) and in HCl(aq) as well as the temperature and dilution effects reported here were used with comparable enthalpies of solution of Be(c) and the enthalpy of formation of $H_2O(l)$ to obtain values for the enthalpy of formation of BeO(c). These results are discussed in detail in the paper by V. B. Parker which follows this.

7. References

[1] Parker, V. B., J. Res. Nat. Bur. Stand. (U.S.) 77A (Phys. and Chem). No. 2, 227–235 (Mar.–Apr. 1973).

[2] Thermophysical Properties of High Temperature Solid Materials, Y. S. Touloukian, editor, **4**, 55 (The Macmillian Co., New York, 1967).

[3] Commission on Atomic Weights, Pure and Applied Chem. **21**, 91 (1970).

[4] Prosen, E. J., and Kilday, M. V., J. Res. Nat. Bur. Stand. (U.S.)–77A (Phys. and Chem.), No. 2, 179–203 (Mar.–Apr. 1973).

[5] Bear, I. J., and Turnbull, A., J. Phys. Chem. **70**, 711 (1966).

[6] Parker, V. B., Wagman, D. D., and Evans, W. H., Nat. Bur. Stand. (U.S.), Tech. Note 270–6, 5 (November 1971).

[7] Parker, V. B., Thermal Properties of Aqueous Uni-univalent Electrolytes, Nat. Stand. Ref. Data Ser. Nat. Bur. Stand. (U.S.), **2**, 3 and 42 (April 1965).

[8] Kolesov, V. P., Popov, M. M., and Skuratov, S. M., Zh. Neorg. Khim. **4**, 557 (1959).

(Paper 77A2–764)

JOURNAL OF RESEARCH of the National Bureau of Standards—A. Physics and Chemistry
Vol. 77A, No. 2, March–April 1973

The Enthalpies of Formation of BeO(c) and BeF_2(c)

Vivian B. Parker

Institute for Materials Research, National Bureau of Standards, Washington, D.C. 20234

(November 9, 1972)

Two of the key compounds in the evaluation and synthesis of a consistent set of thermodynamic values for the Be compounds are BeO(c) and BeF_2(c). The available measurements on the enthalpies of formation of these two compounds are presented with a detailed outline of the approach used to select the "best" values, $\Delta Hf^\circ_{298.15K}$ [BeO(c)] $= -145.7 \pm 0.6$ kcal · mol^{-1} (-609.6 ± 2.5 kJ · mol^{-1}) and $\Delta Hf^\circ_{298.15K}$ [BeF_2(c, quartz)] $= -245.4 \pm 0.8$ kcal · mol^{-1} (-1026.8 ± 3.3 kJ · mol^{-1}).

Key words: BeF_2(c); BeO(c); beryllium fluoride; beryllium oxide; enthalpies of formation; $\Delta Hf^\circ_{298.15K}$ [BeF_2(c)]; $\Delta Hf^\circ_{298.15K}$ [BeO(c)]; thermochemistry.

1. Introduction

Two of the key compounds in the evaluation and synthesis of a consistent set of thermodynamic values for the Be compounds are BeO(c) and BeF_2(c).

One approach used in the preparation of compilations of thermochemical data is to start with a compound for which ΔHf° (or ΔGf°) is definitive and independent of ΔHf° of any other compound of that element and preferably involves a minimum of auxiliary ΔHf°'s, and to build from the selected value for this compound. An example of this is the direct oxidation of the metal to the oxide, e.g., BeO(c), or the halogenation of the metal to the halide, e.g., BeF_2(amorp), or a set of reactions that can be combined in such a way that only one ΔHf° is unknown, e.g., $Be(c) + 2HF(aq) \rightarrow H_2(g) + BeF_2(aq)$ and $BeO(c) + 2HF(aq) \rightarrow BeF_2(aq) + H_2O(liq)$ so that by difference we can write the possible reaction, $Be(c) + H_2O(liq) \rightarrow BeO(c) + H_2(g)$; similarly $Be_3N_2(c) + 3/2O_2(g) \rightarrow 3BeO(c) + N_2(g)$ and $3Be(c) + N_2(g) \rightarrow Be_3N_2(c)$ giving $Be(c) + 1/2O_2(g) \rightarrow BeO(c)$. We may then relate the ΔHf°'s of other compounds of that element to the selected compound by enthalpies of reaction.

If however every subsequent ΔHf° calculated is dependent upon the value selected for one compound, although we have internal consistency, we have no crosscheck as to how good the original value is. We should then have a second compound whose ΔHf° can also be obtained independently and an enthalpy of reaction relating the two to corroborate the choices and to close the cycle.

Until the recent measurements of Kilday, Prosen, and Wagman [1][1] on the enthalpies of solution of BeO(c) in aqueous HF solutions and the measurements of Churney and Armstrong [2] on the direct determination of the ΔHf°[BeF_2(amorph)], the data available on the direct enthalpies of formation of BeO(c) and BeF_2(c) and the data linking these values were discordant. These new investigations are a significant aid in establishing the values for BeO(c) and BeF_2(c) with more certainty. Our main efforts then, after considering the direct determinations, center upon the use of the solution measurements of BeO(c) in HF(aq) together with the solution measurements of Be(c) in HF(aq) which previously could not be fully utilized to obtain indirectly a definitive value for the ΔHF°[BeO(c)] and to relate that value to the determinations on the ΔHF°[BeF_2(c)]. Figure 1 schematically presents the reactions and paths discussed in this paper.

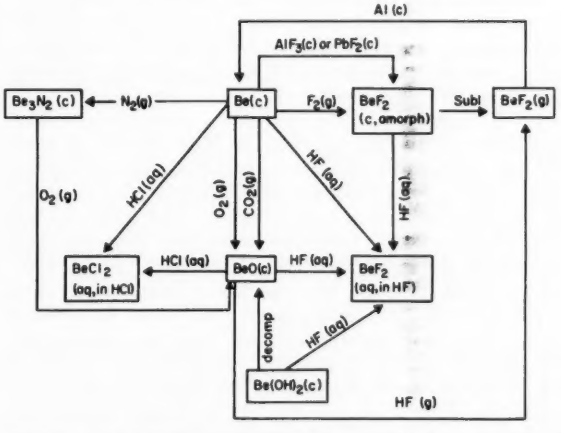

FIGURE 1: *The schematic presentation of the relationships involved in the evaluation of* ΔHf°[BeO(c)] *and* ΔHf°[BeF_2(c)].

[1] Figures in brackets indicate the literature references at end of this paper.

All auxiliary data and constants used in the calculations are given in Wagman et al. [3]. Unless otherwise specified the values quoted are at, or have been corrected to, 298.15 K. Our final selections are reported in both kJ · mol^{-1} and kcal · mol^{-1}. However, since this evaluation is included in Parker, Wagman, and Evans [3], where values are expressed in kcal · mol^{-1}, we report the individual values and their corrections in the same units in order to preserve the consistency of the relationships.

2. Discussion of Data on BeO(c)

2.1. Bomb Combustion

The following values of ΔH(kcal · mol^{-1}) for the oxidation of Be(c) have been reported: Moose and Parr [4], −134.4; Roth, Börger, and Siemonsen [5], −147.3; Neumann, Kröger, and Kunz [6], −145.3; Mielenz and v. Wartenberg [7], −136.2; and Cosgrove and Snyder [8], −143.1. Neumann, Kröger, and Kunz [6] measured the enthalpy of combustion of Be_3N_2 (crystal form unspecified) to form BeO(c) and N_2(g) as −300.6 kcal·mol^{-1} of Be_3N_2(c). Neumann, Kröger, and Haebler [9] directly determined $\Delta Hf°[Be_3N_2(c)] = -134.1$. By difference we obtain $\Delta Hf°[BeO(c)] = -144.9$. Of these determinations the Cosgrove and Snyder measurement appeared to be the best value and had been generally accepted; however, the measurements of Kolesov, Popov, and Skuratov [10] on the enthalpies of reaction of BeO(c) in aqueous HF and BeF_2(c) in aqueous HF indicate that the value for $\Delta Hf°$ [BeO(c)] should be more negative. This is in line with the fact that Cosgrove and Snyder did not determine the completeness of the reaction; incomplete combustion would cause the value, based on the weight of metal taken, to be too positive. We turn therefore to the indirect determinations of $\Delta Hf°$ [BeO(c)].

2.2. The Enthalpies of Solution of Be(c) and BeO(c) in Aqueous HF Solutions

Matignon and Marchal [11] measured the enthalpies of solution of Be(c) and BeO(c) in 30 percent HF solutions, as have Copaux and Philips [12]. By difference, we obtain for Be(c) + H_2O(liq) → BeO(c) + H_2(g), $\Delta H° = -70.9$ and −62.1 kcal, or $\Delta Hf°$[BeO(c)] = −139.2 and −130.4 kcal · mol^{-1}, respectively. The individual ΔH's for solution of Be(c) in 30 percent HF are −94.2 from Matignon and Marchal and −82.2 kcal · mol^{-1} from Copaux and Philips. For solution of BeO(c) they are −23.3 and −20.1 kcal · mol^{-1}, respectively. More recently, Bear and Turnbull [13] measured the enthalpy of solution of Be(c) in 12, 22.6, 30, and 40 percent HF solutions. The values are −101.5, −101.0, −100.5, and −100.5 kcal. Armstrong and Coyle [14] reported −99.6 kcal for solution in 25 percent HF. For solution of BeO(c) in aqueous HF we also have the results of Kilday et al., e.g., −24.2 kcal in a 30 percent HF solution, the results of Kolesov et al., in a 23 percent HF solution, −24.1 kcal, and Fricke and Wüllhorst [15] −24.3 kcal in 12 percent HF. It appears that the measurements of Matignon and Marchal and Copaux and Philips are not reliable; they give little information as to the experimental details and purity of materials. We cannot rely upon the values for $\Delta Hf°$[BeO(c)] obtained from the data of either Matignon and Marchal [11] or Copaux and Philips [12], but a judicious combination of the other measurements can yield a more reliable value.

One of the problems associated with combining reactions of Be(c) and BeO(c) in aqueous HF is that in most cases the final solutions are not the same. Not only are there no quantitative data on what Be species are in the final solutions or the percent of each, there are also no direct data on the ΔH_{dil^n} or ΔH_{mix} of these species in HF solutions. The measurements of Kilday et al., however, provide some insight into the effect of having solutions that do differ in both the amount and concentration of the excess HF(aq).

They have also measured the differential enthalpy of dilution in two of their final solutions,

$$H_2O(liq) + [BeF_2 \text{ in excess HF} \cdot nH_2O] \rightarrow [BeF_2 + H_2O \text{ in excess HF} \cdot nH_2O].$$

These measurements are important since H_2O(in $BeF_2 + HF \cdot nH_2O$) is formed in the reaction of BeO(c) with HF(aq), i.e.,

$$BeO(c) + 2HF(aq) \rightarrow [BeF_2 + H_2O] \text{ in excess HF.}$$

We have compared the experimental data with those calculated from the slope $d\varphi_L/dm^{1/2}$ of φ_L HF at n_f H_2O from the values[2] tabulated by Parker [16]. These values are: at $n_f = 2.68$, $\bar{L}_1$ (cal · mol^{-1}) = −178 (calc.), and −160 ± 10 (experimental); at $n_f = 3.57$, $\bar{L}_1 = -110$ (calc.) and −85 ± 5 (experimental). Since the agreement is good, we decided to ignore the presence of the BeF_2 in the final solutions and treat the solutions as if they were HF solutions. Since X (the ratio of HF to BeF_2 in the final solution) ≧ 50 this is not an unreasonable approach.

We can now set up the equation for the reaction[3] in the form,

$$BeO(c) + (X+2)(HF + n_iH_2O) \rightarrow [BeF_2 + H_2O + X(HF + n_f'H_2O)]$$

and use the experimental $\bar{L}_1$ values and the φ_L values at the appropriate concentrations from [16] to calculate $\Delta(\Delta Hf°)$ which represents $\Delta Hf°$[BeO(c)] − ΔHf [BeF_2(aq)]. Table 1 shows the results as a function of n_f where n_f is the final ratio of H_2O to HF. It includes the mole of H_2O formed. All of their experimental ΔH's

[2] φ_L is the relative apparent molal enthalpy. It is the negative of the integral enthalpy of dilution per mole of solute of a solution at concentration m to an infinitely dilute solution. L_1 is the partial or differential enthalpy of dilution, per mole of solvent, when it is added to a large volume of solution at the given concentration.

[3] $n_f' = n_i(X+2)/X$; it excludes the mole of H_2O formed. n_i is the initial mole ratio of H_2O to HF. X is the mole ratio of HF to BeF_2 in solution.

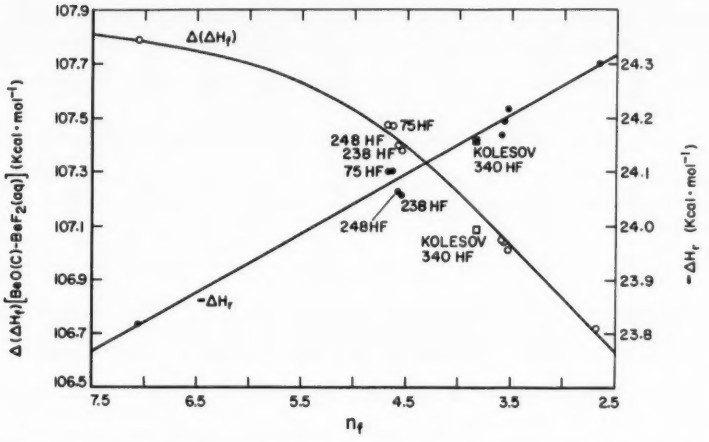

FIGURE 2: *The* ΔHr[BeO(c)] *and* Δ(ΔHf)[BeO(c)−BeF_2(aq)] *(uncorrected for the variation in* X*) as a function of the concentration of* HF *in the final solution* (HF + $n_f H_2O$).
For ΔHr: ● data of Kilday et al. ■ data of Kolesov et al.
For $\Delta(\Delta Hf)$: ○ data of Kilday et al. □ data of Kolesov et al.

are included, corrected to 298.15 K where necessary, using the temperature coefficient given in their work. The number in the first column corresponds to the number of the Kilday et al., experiment.

The values for $\Delta(\Delta Hf)$ within each group are in excellent agreement with one another, within the precision of the experimental data although there are some differences in X and n_f in the final solutions. The values appear to be primarily dependent upon the concentration of HF within the range $50 \leqq X \leqq 250$. Figure 2 shows a plot of $\Delta(\Delta Hf)$ as a function of n_f. For the $\Delta(\Delta Hf)$ we obtain a smooth curve. The smoothed values are also given in table 1. The variation of ΔH as a function of the concentration of HF without regard to the variation of X may be expressed as $\Delta H = -24.092 - 0.113(4.50 - n_f)$ kcal · mol^{-1} for $7.1 > n_f > 2.6$.

Kolesov, Popov, and Skuratov [10] also measured the enthalpy of solution of BeO(c) in aqueous HF. Their reaction corresponds to:

$$BeO(c) + 342(HF + 3.801\ H_2O) \rightarrow$$
$$[BeF_2 + H_2O + 340(HF + 3.823\ H_2O)].$$

The $\Delta H = -24.158$ kcal · mol^{-1} of BeO(c) results in $\Delta(\Delta Hf) = 107.085$ kcal · mol^{-1} (using the same treatment as before). From our straight line plot of ΔH from Kilday et al.'s data, we obtain -24.168 kcal · mol^{-1} where the final solution contains BeF_2 in 90(HF+3.826 H_2O). From our plot of $\Delta(\Delta Hf)$ versus n_f we obtain $\Delta(\Delta Hf) = 107.185$ kcal · mol^{-1}. The agreement in ΔH is excellent, fortuitously so; in $\Delta(\Delta Hf°)$ it is not, but still within the experimental uncertainties. In addition X differs by 250 moles HF in the two solutions.

Kilday and Churney, private communication (1971), also made some measurements on the enthalpy of solution of BeF_2(amorph) in HF concentrations of 3.63 H_2O and 5.06 H_2O where X varied from 400 to 2700. From these measurements we obtain the following:

$$\Delta H_{soln} = -8{,}430 + 0.50\,X \text{ cal} \cdot \text{mol}^{-1} \text{ for } n = 3.63$$

$$\Delta H_{soln} = -8{,}680 + 0.60\,X \text{ cal} \cdot \text{mol}^{-1} \text{ for } n = 5.06.$$

Although the precision of these measurements is not high they do enable us to obtain an approximate correction to $\Delta(\Delta Hf)$ for the variation in X. As a reference solution we have chosen this X to be 100 and have added $-0.55(100 - X)$ cal · mol^{-1} (an

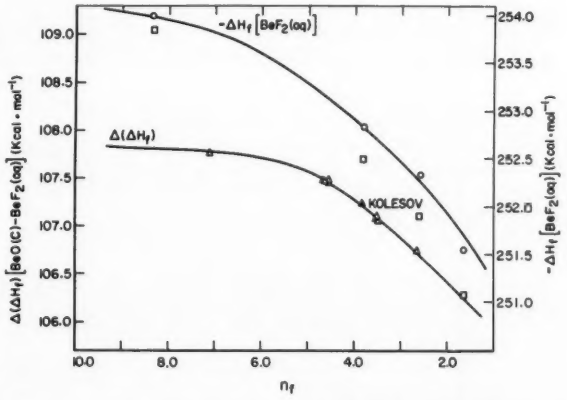

FIGURE 3: *The* Δ(ΔHf)[BeO(c)−BeF_2(aq)] *and the* ΔHf[BeF_2(aq)] *as a function of the concentration of* HF *in the final solution* (HF + $n_f H_2O$).
For $\Delta(\Delta Hf)$: △ Kilday et al. data, corrected to $X = 100$. ▲ Kolesov et al. data, corrected to $X = 100$.
For ΔHf[BeF_2(aq)]: ○ Bear and Turnbull data, corrected to $X = 100$. □ Bear and Turnbull data, uncorrected for variation in X.

TABLE 1. *Data derived from measurements of Kilday et al.*

1	2	3	4	5	6	7	8	9	10	11	12
No.	%HF in initial solution	$-\Delta H^{a}_{298.15K}$	X	n_f	$\Delta(\Delta Hf)$ [BeO(c)- $-BeF_2(aq)$]	Mean $\Delta(\Delta Hf)$	Mean n_f	$\Delta(\Delta Hf)$ from smooth curve, fig. 2	$\Delta(\Delta Hf)$ corrected to $X=100$	Mean $\Delta(\Delta Hf)$	$\Delta(\Delta Hf)$ from smooth curve, fig. 3
		kcal · mol^{-1}			*kcal · mol*$^{-1}$	*kcal · mol*$^{-1}$		*kcal · mol*$^{-1}$	*kcal · mol*$^{-1}$	*kcal · mol*$^{-1}$	*kcal · mol*$^{-1}$
20	29.76	24.301	112.58	2.6765	106.710				106.717		
22		24.292	117.42	2.6742	106.707	106.716	2.676	106.70	106.717	106.723	106.71
23		24.315	113.12	2.6762	106.731				106.738		
24		24.299	113.16	2.6762	106.714				106.721		
2	24.33	24.200	94.60	3.5374	107.041				107.038		
4		24.221	96.47	3.5359	107.055	107.051	3.534	107.07	107.053	107.051	107.07
5		24.235	107.53	3.5274	107.057				107.061		
25	24.23	24.221	93.05	3.5581	107.109				107.105		
26		24.197	97.97	3.5538	107.082				107.081		
27		24.176	94.17	3.5571	107.064	107.080	3.555	107.08	107.061	107.078	107.08
28		24.202	91.36	3.5597	107.096				107.091		
29		24.182	114.23	3.5423	107.057				107.065		
30		24.187	92.47	3.5586	107.071				107.067		
1	24.13	24.183	88.82	3.5817	107.113				107.112		
3		24.141	95.48	3.5753	107.070	107.090	3.578	107.09	107.068	107.087	107.09
9		24.163	94.19	3.5765	107.103				107.100		
10		24.183	93.52	3.5771	107.072				107.068		
7	19.80	24.103	75.23	4.6310	107.475	107.475	4.631	107.46	107.461	107.461	107.47
11	19.80	24.055	234.68	4.5407	107.389				107.463		
13		23.955	232.05	4.5412	107.296	107.378	4.540	107.43	107.369	107.454	107.44
18		24.089	247.99	4.5384	107.448				107.529		
6	19.66	24.108	76.47	4.6699	107.473	107.468	4.672	107.47	107.460	107.456	107.48
8		24.091	74.60	4.6731	107.462				107.452		
12	19.66	24.062	237.12	4.5806	107.397				107.472		
17		24.158	256.22	4.5773	107.497	107.404	4.579	107.44	107.583	107.485	107.46
19		23.968	251.47	4.5781	107.318				107.401		
14	14.05	23.787	53.85	7.0644	107.753				107.728		
15		23.862	55.49	7.0563	107.830	107.782	7.061	107.78	107.806	107.758	107.78
16		23.794	54.42	7.0616	107.764				107.739		

[a] Corrected for $BeSO_4$ impurity.

TABLE 2. *Data derived from the measurements of Bear and Turnbull and the corresponding values from Kilday et al.*

1	2	3	4	5	6	7	8	9	10	11
% HF	X	n_f	$\Delta Hr°$ Be(c)	ΔHf [BeF_2(aq)]	$\Delta Hr°$ of BeO(c) st. line plot, fig. 2	X for (6)	$\bar{L}_1$ H_2O	$\Delta(\Delta Hf)$ [BeO − BeF_2(aq)] fig. 2	ΔHf [BeF_2(aq)] corrected to $X = 100$	$\Delta(\Delta Hf)$ [BeO(c)−BeF_2(aq)] fig. 3
			kcal · mol⁻¹	*kcal · mol⁻¹*	*kcal · mol⁻¹*		*kcal · mol⁻¹*	*kcal · mol⁻¹*	*kcal · mol⁻¹*	*kcal · mol⁻¹*
12	358	8.184	− 101.47	− 253.84	− 23.68	50	0	107.81	− 253.98	107.78
22.6	677	3.811	− 101.02	− 252.51	− 24.17	90	− 0.07	107.18	− 252.83	107.18
30	899	2.597	− 100.52	− 251.89	− 24.31	115	− 0.18	106.68	− 252.33	106.68
40	1079	1.670	− 100.5	[a]− 251.0	− 24.42	130	− 0.3 (est'd)	106.2	− 251.54	106.2

[a] This is based on an estimate for $\Delta H_{dilu} = -0.9$ kcal · mol⁻¹ for 1079(HF + 1.666H_2O) → 1079(HF + 1.670H_2O) and φ_L for HF + 1.666H_2O = 3.8 kcal · mol⁻¹.

TABLE 3. ΔHf°[BeO(c)] *in kcal · mol⁻¹ as calculated by various methods from data in table 2*

Method 1 (4, 6, and 8)	Method 2 (5 and 9)	Method 3 (10 and 11)
− 146.11	− 146.03	− 146.20
− 145.24	− 145.33	− 145.65
− 144.70	− 145.21	− 145.65
− 144.7	− 144.8	− 145.3

average value) to the $\Delta(\Delta Hf)$'s (see table 1, columns 10, 11, and 12 and fig. 3). The new $\Delta(\Delta Hf)$'s are in slightly better agreement with one another. For the $\Delta(\Delta Hf°)$ from Kolesov et al., we obtain 107.217 kcal · mol⁻¹ as compared to 107.180 from figure 3, in much better agreement; this lends support to the use of this treatment on the Bear and Turnbull measurements [13] on Be(c) in excess HF solutions, where the final ratio of HF to BeF_2 is greater than 340.

Bear and Turnbull used solutions of 12, 22.6, 30, and 40 percent HF. Their results can be treated three ways:

(1) using their ΔH_r with the ΔH_r from our straight line plot of the Kilday et al., data on BeO in HF at the appropriate n_f, with the experimental $\bar{L}_1$, obtaining the reaction, Be(c) + H_2O(aq) → BeO(c) + H_2(g);

(2) calculating the $\Delta Hf°$[BeF_2 in X(HF + $n_f H_2O$)] and using the appropriate $\Delta(\Delta Hf)$ [BeO − BeF_2(aq)] at n_f from figure 2;

(3) correcting ΔHf[BeF_2(aq)] to $X = 100$ and using the comparable corrected $\Delta(\Delta Hf)$ from figure 3.

The results are summarized in tables 2 and 3. It is obvious that the values for $\Delta Hf°$[BeO(c)] are in better agreement using the third way of calculating. Figure 3 shows a plot of ΔHf[BeF_2(aq), in 100(HF+$n_f H_2O$)] and also the uncorrected values derived from the Bear and Turnbull measurements.

For confirmation of the above values we may use the enthalpy of solution of the samples of BeF_2(amorph) cited earlier whose $\Delta Hf°$ is known (−244.3 kcal · mol⁻¹, directly determined by Churney and Armstrong [2]) from which we obtain ΔHf[BeF_2(aq) in 100(HF + 3.63H_2O)] = −252.68 kcal · mol⁻¹ and ΔHf[BeF_2(aq) in 100(HF+5.06 H_2O)] = −252.92 kcal · mol⁻¹ (cf −252.75 and −253.38 kcal · mol⁻¹ from the smoothed curve (fig. 3) of Bear and Turnbull's corrected ΔHf's). Using $\Delta(\Delta Hf) = 107.11$ and $\Delta(\Delta Hf) = 107.57$ kcal · mol⁻¹ from figure 3, we obtain $\Delta Hf°$ BeO(c) = −145.57 and −145.35 kcal · mol⁻¹, respectively.

In all the above cases we have used the $\Delta(\Delta Hf)$ [BeO(c)−BeF_2(aq)] derived from the Kilday et al. measurements. If we use $\Delta(\Delta Hf) = 107.217$ kcal · mol⁻¹ from the Kolesov et al. measurements and ΔHf BeF_2(aq) = −252.93 kcal · mol⁻¹ from figure 3 we obtain $\Delta Hf°$ BeO(c) = −145.71 kcal · mol⁻¹.

There is another reaction involving the enthalpy of solution of Be(c) in HF(aq), that by Armstrong and Coyle [14]. They reported that there was an unexplained deficiency of H_2 on the order of 0.5 percent. They ascribe an uncertainty of not more than 0.2 percent to the enthalpy of reaction for this contribution. The measurements are on the reaction: Be(c) + 6.470(HF + 3.309 H_2O) → [BeF_2 + 4.470(HF + 4.789 H_2O)] + H_2(g) for which $\Delta H = -99.64$ kcal · mol⁻¹ and ΔHf[BeF_2(aq) in 4.470(HF + 4.789 H_2O)] = − 251.1 kcal · mol⁻¹. Using the same three approaches as for Bear and Turnbull's data we obtain $\Delta Hf°$[BeO(c)] = −143.9 (1); −143.6 (2); and −143.5 kcal · mol⁻¹ (3), where X is corrected to 100. In all cases we assume that the species in the two solutions are the same; in the third case we also assume our correction is applicable to $X = 4.47$, which is probably not justified.

There are two other approaches we can use on their data:

(4) Heretofore we have neglected the effect of the BeF_2 on the HF dilution correction. If we assume that the BeF_2 present in the solution may be replaced by an equivalent number of moles of HF solution, then we may consider the HF to be in 3.913H_2O. This results in ΔHf[BeF_2(aq)] = −251.4 kcal · mol⁻¹ and $\Delta Hf°$ [BeO(c)] = −143.9 kcal · mol⁻¹.

(5) We can calculate a ΔH_{mix} for the addition of more of the initial solution, [HF + 3.309 H_2O], to their final solution, using the ϕ_L values of HF, and obtain:

[BeF_2(aq) + 4.470(HF + 4.789H_2O)] + 95(HF + 3.309H_2O) → [BeF_2(aq) + 99.470(HF + 3.375H_2O)]; $\Delta H_{mix} = -0.264$ kcal · mol⁻¹. Combining this with their reported ΔH leads to:

Be(c) + 101.470(HF + 3.309H_2O) → [BeF_2(aq) + 99.470 (HF + 3.375H_2O)] + H_2(g); $\Delta H = -99.95$ kcal · mol⁻¹. This value is now in closer agreement with Bear and

Turnbull's measurements. For the same reaction with BeO(c) we obtain $\Delta H = -24.22$ kcal · mol^{-1}, so that $\Delta Hf°[BeO(c)] = -144.1$ kcal · mol^{-1}. A variation of this would be to use a ΔH_{mix} based on our fourth approach, i.e., to assume the HF is in 3.913 H_2O, then $\Delta H = -100.23$ and $\Delta Hf°$ [BeO(e)] = − 144.4 kcal · mol^{-1}.

2.3. The Enthalpies of Solution of Be(c) and BeO(c) in Aqueous HCl Solutions

The problem of nonidentical final solutions is also present in the Be(c) − BeO(c) − HCl aqueous systems. Kilday et al. [1] have obtained $\Delta H = -12.8$ and -12.7 kcal · mol^{-1} for the solution of BeO(c) in 18 and 22.6 percent HCl, respectively. The complete reactions are:

$$BeO(c) + 40.9(HCl + 9.21H_2O) \rightarrow [BeCl_2(aq) + H_2O(aq) + 38.9(HCl + 9.69H_2O)]$$

and

$$BeO(c) + 47.8(HCl + 6.93H_2O) \rightarrow [BeCl_2(aq) + H_2O(aq) + 45.8(HCl + 7.23H_2O)].$$

(The experimental $\bar{L}_1$ value=−272 cal · mol^{-1} of H_2O (see ref. [1], sec. 5.4) checks well with the $\bar{L}_1$ calculated from the ϕ_L values of HCl [16] at $n = 7.23H_2O$).

From these reactions we obtain for $BeCl_2$(aq) in 38.3(HCl + 9.72H_2O) $\Delta(\Delta Hf)$[BeO(c) − $BeCl_2$(aq)] = 18.6 kcal · mol^{-1} and 16.6 kcal · mol^{-1} for $BeCl_2$(aq) in 45.8(HCl + 7.25H_2O).

Thompson, Sinke, and Stull [17] reported $\Delta H = -89.61$ kcal · mol^{-1} for Be(c) + 8.38(HCl + 8.111H_2O) → [$BeCl_2$(aq) + 6.38(HCl + 10.654H_2O)] + H_2(g), from which we obtain ΔHf [$BeCl_2$(aq)] = −163.79 kcal · mol^{-1}. Blachnik, Gross, and Hayman [18] reported $\Delta H_{383K} = -90.00$ kcal/mol for:

$$Be(c) + 8.86(HCl + 7.991H_2O) \rightarrow H_2(g) + [BeCl_2(aq) + 6.86(HCl + 10.320H_2O)].$$

This value, corrected to 298.15 K is in good agreement with the Thompson et al. value.

Using the same approaches as for HF we have:

(1) With ΔH of solution of BeO(c) ≈ −12.8 kcal · mol^{-1} when $n_f = 10.65$, $\Delta Hf°$ [BeO(c)] = −145.2 kcal · mol^{-1}.

(2) From an extrapolation of $\Delta(\Delta Hf°)$[BeO(c) − $BeCl_2$(aq)] we obtain $\Delta(\Delta Hf°) = 19.4$ kcal · mol^{-1} where the $BeCl_2$ is in 34(HCl + 10.65H_2O) and $\Delta Hf°$ [BeO(c)] = −144.4 kcal · mol^{-1}.

(3) Not used since we have no correction for the variation in X.

As in our treatment of the Armstrong and Coyle [14] results we may try the following:

(4) If we assume that the $BeCl_2$ present may be replaced by an equivalent number of moles of HCl solution we may consider the HCl to be in 9.21H_2O. Then ΔHf[$BeCl_2$(aq)] = −165.0 and ΔHf[BeO(c)] = −145.6 kcal · mol^{-1}.

(5) We can calculate a ΔH_{mix} by adding more of the initial HCl solution to the final solution. We obtain:

$$[BeCl_2(aq) + 6.38(HCl + 10.654H_2O)] + 35.54(HCl + 8.111H_2O) \rightarrow [BeCl_2(aq) + 41.92(HCl + 8.499H_2O)]; \Delta H = -0.64 \text{ kcal} \cdot \text{mol}^{-1}$$

and $\Delta H = -90.3$ kcal · mol^{-1} for:

$$Be(c) + 43.92(HCl + 8.111H_2O) \rightarrow H_2(g) + [BeCl_2(aq) + 41.92(HCl + 8.499H_2O)].$$

For the reaction with BeO(c) we can say $\Delta H = -12.7$ kcal · mol^{-1} for BeO(c) + 43.92(HCl + 8.111H_2O) → [$BeCl_2$(aq) + H_2O + 41.92(HCl + 8.499H_2O)], so that $\Delta H = -77.56$ kcal · mol^{-1} for Be(c) + H_2O(aq) → BeO(c) + H_2(g) and $\Delta Hf°$BeO(c) = −146.0 kcal · mol^{-1}. A variation of this would be to calculate a $\Delta H_{mix} = -1.81$ kcal · mol^{-1} on the basis of (4). Then ΔH for the reaction with Be(c) = −91.4 and $\Delta Hf°$[BeO(c)] = −147.2 kcal · mol^{-1}.

Averaging these five values we obtain −145.7 kcal · mol^{-1} for $\Delta Hf°$ [BeO(c)].

2.4. Other data

From the cell measurements of Smirnov and Chukreev [19] in the temperature range 955 to 1313 K, we obtain a second law $\Delta H° = -94.6$ kcal · mol^{-1} and a third law $\Delta H° = -93.7$ kcal · mol^{-1} for Be(c) + 1/2CO_2(g) → BeO(c) + 1/2C(graphite), or $\Delta Hf°$ [BeO(c)] = −141.6 and −140.8 kcal · mol^{-1}, respectively.

2.5. The Selection of the $\Delta Hf°$[BeO(c)]

It is appropriate at this point to tabulate the values of $\Delta Hf°$BeO(c), both the direct and indirect determina-

TABLE 4. *Summary of values of* $\Delta Hf°$ [BeO(c)]

Investigator	$\Delta Hf°$
Direct Determinations	*kcal · mol*$^{-1}$
Moose and Parr [4]	−134.1
Roth et al. [5]	−147.3
Neumann et al. [6]	−145.3
Mielenz and v. Wartenberg [7]	−136.2
Cosgrove and Snyder [8]	−143.1
Indirect Determinations	
Neumann et al. [6, 9]	−144.9
Smirnov and Chukreev [19]	−141.1
Kilday et al. [1] and Bear and Turnbull [13]	−146.20 −145.65 −145.65 −145.3
Kilday et al. [1], Kilday and Churney, private communication (1971) and Churney and Armstrong [2]	−145.6 −145.4
Kolesov et al. [10] and Bear and Turnbull [13]	−145.7
Kilday et al. [1] and Armstrong and Coyle [14]	−143.9
Kilday et al. [1] and Thompson et al. [17]	−145.7

tions (table 4). As is evident, except for the Smirnov and Chukreev value, all the indirect determinations support a more negative value than that of Cosgrove and Snyder. The "best" value now appears to be -145.7 kcal · mol^{-1} in good agreement with the Neumann et al. [6] direct determination. The uncertainties are discussed in section 4.

2.6. The Decomposition of Beryllium Hydroxide as Supporting Evidence

Bear and Turnbull [13] have also measured the enthalpy of solution of $Be(OH)_2$ (β, orthorhombic) and $Be(OH)_2$ (α, tetragonal) in 22.6 percent HF, [679($HF + 3.80H_2O$)]. From these measurements and their measurements on Be(c) we obtain $\Delta H = -79.83$ kcal · mol^{-1} for $Be(c) + 2H_2O(liq) \rightarrow Be(OH)_2(\beta) + H_2(g)$ and $\Delta Hf° = -216.5$ kcal · mol^{-1}; similarly for $Be(OH)_2(\alpha)$ we obtain $\Delta H = -79.10$ kcal · mol^{-1} and $\Delta Hf° = -215.7$ kcal · mol^{-1}. Using these values for $\Delta Hf°$ and our tentative "best" value for BeO(c) we obtain:

$$BeO(c) + H_2O(liq) \rightarrow Be(OH)_2(c, \beta);\ \Delta H° = -2.5 \text{ kcal} \cdot \text{mol}^{-1}$$

$$BeO(c) + H_2O(liq) \rightarrow Be(OH)_2(c, \alpha);\ \Delta H° = -1.7 \text{ kcal} \cdot \text{mol}^{-1}.$$

Fricke and Wüllhorst [15] measured the enthalpies of solution of BeO(c), $Be(OH)_2(c, \beta)$, and $Be(OH)_2(c, \alpha)$ in 11.59 percent HF. From these measurements we obtain $\Delta H° = -2.5$ and -1.8 kcal · mol^{-1}, respectively, in excellent agreement with our $\Delta H°$. Matignon and Marchal [20, 21], from measurements in 30 percent HF, obtained $\Delta H°_{hyd}$ ($Be(OH)_2$, form unspecified) $= -3.2$ kcal · mol^{-1}, in fair agreement. Fricke and Severin [22] measured the equilibrium vapor pressure at 378 K to be 100 mm $H_2O(g)$ over $Be(OH)_2(c, \beta)$. Using a Nernst equation they calculate $\Delta H = 15.5$ kcal · mol^{-1} of $H_2O(g)$, which results in $\Delta H° = -5.0$ kcal · mol^{-1} for the hydration of BeO(c). However they reported that the BeO formed had a distorted lattice which should require a $\Delta Hf°$ more positive than -145.7 kcal · mol^{-1}. Also since the ΔH calculated is based on only one point it can not be considered a definitive value.

It is evident that the related data are supportive of our value for $\Delta Hf°[BeO(c)] = -145.7$ kcal · mol^{-1}.

3. The Enthalpy of Formation of BeF_2(c)

3.1. The Enthalpy of Transition of BeF_2(gl) and BeF_2(amorph) to BeF_2 (α, quartz)

There are no published direct determinations of the $\Delta Hf°[BeF_2(c)]$ from combustion of Be(c) in F_2(g); the combustion of Be(c) in F_2(g) results in amorphous material. The indirect reactions, in which BeF_2 forms, produce a glassy state.

Taylor and Gardner [23] determined the enthalpy of solution of both the α, quartz form, and the glassy form in acetic acid-sodium acetate solutions to be -3.64 and -4.76 kcal · mol^{-1}, respectively. This leads to a ΔH_{trans} quartz → glass $= 1.12$ kcal · mol^{-1}. If we assume that the amorphous and glassy states are equivalent we can convert both to $\Delta Hf°[BeF_2(\alpha, \text{quartz})]$.

3.2. The Reaction of Be(c) With F_2(g)

Churney and Armstrong [2] measured the enthalpy of reaction of Be(c) in F_2(g) to be -244.3 kcal · mol^{-1}. They report BeF_2(amorph) to be their product. This results in $\Delta Hf°[BeF_2(c)] = -245.4$ kcal · mol^{-1}. In a preliminary report (1965) they cite the unpublished measurements of Simmons (1961) on the conversion of Be(foil) to partially glassy BeF_2, leading to $\Delta Hf°[BeF_2(c)] = -257.0$ kcal · mol^{-1}.

3.3. The Reaction of Be(c) With PbF_2(c)

Gross [24] reported $\Delta H° = -84.0$ kcal for the reaction of Be(c) with PbF_2(c) to form BeF_2(c) and Pb(c). Although no crystallographic identification was made the direction of the results under varying conditions indicates that the value is for the formation of BeF_2(c). Since there is some uncertainty in our selection for PbF_2(c) we will avoid its use by relating the reaction to the reaction from Gross, Hayman, and Levi [25]:

$3/2PbF_2(c) + Al(c) \rightarrow AlF_3(c) + 3/2Pb(c)$; $\Delta H = -118.53$ kcal from which we obtain:

$3/2Be(c) + AlF_3(c) \rightarrow Al(c) + 3/2BeF_2(c)$; $\Delta H = -7.47$ kcal and using $\Delta Hf°[AlF_3(c)] = -359.5$ kcal · mol^{-1} [3], $\Delta Hf°[BeF_2(c)] = -244.6$ kcal · mol^{-1}. However, a more recent direct determination of $\Delta Hf°[AlF_3(c)] = -361.0$ kcal · mol^{-1} by Rudzitis et al. [26] would lead to $\Delta Hf°[BeF_2(c)] = -245.6$ kcal · mol^{-1}.

3.4. Other Data

There is a path to $\Delta(\Delta Hf°)$ [BeO(c) − BeF_2(c)] and another to $\Delta Hf°[BeF_2(c)]$ both of which involve BeF_2(g) in high temperature gas phase equilibria. These can be referred to BeF_2(c) with the enthalpy of sublimation of BeF_2. Table 5 summarizes the second

TABLE 5. *Summary of values for* $\Delta H°_{sub}[BeF_2(c)]$ *at 298 K*

Investigator	Temp. Range of Measurements	Second Law $\Delta H°$	Third Law $\Delta H°$
	K	*kcal · mol*$^{-1}$	*kcal · mol*$^{-1}$
Cantor [28]	1146–1372	56.03	55.70
Khandamirova et al. [29]	846–950	58.7	56.07
Sense and Stone [30]	1075–1293	55.37	55.65
Sense, Snyder, and Clegg [31]	1019–1076	60.8	55.58
	1076–1241	55.9	
Hildenbrand and Theard [32]	821–942	55.98	55.40
Blauer et al. [33]	713–795	58.1	53.70
Greenbaum et al. [34]	823–1053	56.66	54.86
Nososelova et al. [35]	1040–1376	52.3	55.8

and third law ΔH°_{subl} BeF_2 calculated from the vapor pressure measurements on the crystal and liquid. From these data we have chosen $\Delta H^\circ_{subl} = 55.7$ kcal $\cdot$ mol^{-1}. Because the thermal functions of BeF_2(g) are based on an estimate for one of the three vibrational frequencies and the thermal functions of the condensed phases at high temperature are only approximate, we estimate an uncertainty of ± 2.0 kcal $\cdot$ mol^{-1}. The gas phase equilibria calculations are summarized in table 6. Because of the many uncertainties inherent in these data, we have not assigned any weight to these measurements. The thermal functions used are given in [27].[4]

TABLE 6. *Gas phase equilibria involving* BeF_2(g)

Reference	Reaction	$\Delta(\Delta Hf^\circ)$[BeO(c) − BeF_2(c)]		ΔHf° [BeF_2(c)]	
		2d Law	3d Law	2d Law	3d Law
		kcal · mol^{-1}		*kcal · mol*$^{-1}$	
[36].....	$BeO(c) + 2HF(g) \rightarrow BeF_2(g) + H_2O(g)$	105	101		
[32].....	$BeF_2(g) + 2Al(c) \rightarrow Be(c) + 2AlF(g)$			−242	−238

3.5. The Selection of ΔHf°[BeF_2(c)] and $\Delta(\Delta Hf^\circ)$[BeO(c) − BeF_2(c)]

From the values for ΔHf°[BeF_2(c)] in 3.2 and 3.3 our "best" value for BeF_2(c, quartz) appears to be -245.4 kcal $\cdot$ mol^{-1}. Tentatively, then our $\Delta(\Delta Hf^\circ)$ [BeO(c) − BeF_2(c)] = 99.7 kcal $\cdot$ mol^{-1}.

As cited earlier the data from Kolesov et al. [9] yielded $\Delta(\Delta Hf)$ [BeO(c) − BeF_2(aq)] = 107.085 kcal $\cdot$ mol^{-1}, where the BeF_2(aq) is in 340($HF + 3.826H_2O$). They also measured the enthalpy of solution of BeF_2(c, β-cristobalite) to the same final solution, $\Delta H = -8.07$ kcal $\cdot$ mol^{-1}. If we combine these results with our selected value for BeO(c), $\Delta Hf^\circ = -145.7$ kcal $\cdot$ mol^{-1} we obtain for BeF_2(c, β-cristobalite) -244.7 kcal $\cdot$ mol^{-1}. This indicates an enthalpy of transition of 0.7 kcal $\cdot$ mol^{-1} between the two forms. Reported values for similar transitions in SiO_2 [3], CaF_2 [37], and $BeCl_2$ [38] are 0.37, 1.14 and 1.32 kcal $\cdot$ mol^{-1}, respectively.

4. Assigned Uncertainties

We have tried to indicate some measure of the uncertainty in the reported values of ΔH and in the derived ΔHf°'s by the number of significant figures given, following the convention that the overall uncertainty lies between 2 and 20 units of the last figure. The uncertainty in the ΔHf°'s depends on the uncertainties of all the determinations in the total chain of reactions used to establish the value. But the values also are given so that the experimental data from which they are derived may be recovered with an accuracy equal to that of the original experimental quantities.

The overall uncertainties in the ΔH's are based on many factors—the experimental technique used, the details given, the number of measurements, the standard deviation of the reported results, the magnitude and reliability of the corrections to 298.15 K, and the reliability of previous work of the investigators. A strictly mathematical evaluation can therefore not be made. For this reason we shall consider only the discussion of the assignment of uncertainties to our "best" values for ΔHf°[BeO(c)] and ΔHf°[BeF_2(c)].

Kilday et al. reported the uncertainty in their measurements of ΔH of solution of BeO(c) in aqueous 24 percent HF to be ± 0.05 kcal $\cdot$ mol^{-1}. Kolesov et al. state their uncertainty to be ± 0.12 kcal $\cdot$ mol^{-1}. Bear and Turnbull state the uncertainties in their measurements to be ± 0.6, ± 0.3, ± 0.6, and ± 0.9 kcal $\cdot$ mol^{-1} for the solution of Be(c) in 12, 22.6, 30, and 40 percent HF solutions, respectively. In calculating the $\Delta(\Delta Hf)$ [BeO(c) − BeF_2(aq)] and ΔHf[BeF_2 aq)] we introduced errors due to the uncertainties in our values for ΔHf° F^-(aq) and φ_L HF, but these errors essentially cancel in obtaining ΔHf°[BeO(c)]. We introduce a ± 0.05 kcal $\cdot$ mol^{-1} uncertainty by our correction of ΔHf [BeF_2(aq)] to $X = 100$. This is negligible. The overall uncertainty obtained from the combined results of Bear and Turnbull and Kilday et al. is ± 0.6 kcal $\cdot$ mol^{-1}; similarly from the results of Kolesov et al. and Bear and Turnbull. The ΔHf° [BeO(c)] derived from the combination of the results of Kilday et al., and Churney and Armstrong, is dependent upon ΔHf°[F^-(aq)]; hence the overall uncertainty must be ± 1.2 kcal $\cdot$ mol^{-1}.

The uncertainty in the Armstrong and Coyle measurement is ± 0.2 kcal $\cdot$ mol^{-1}. However, the final solution here is not dilute with respect to the BeF_2(aq). Even with the estimated mixing correction to the measured ΔH, the uncertainty in the derived ΔHf° [BeO(c)] must be ± 1.5 kcal $\cdot$ mol^{-1}. Similarly, although the uncertainty in the measurements of Thompson et al., on Be(c) in HCl is ± 0.1 kcal $\cdot$ mol^{-1} (for BeO in HCl from Kilday et al. it is ± 0.5 kcal $\cdot$ mol^{-1}) the overall uncertainty in the derived ΔHf° [BeO(c)] is $+1.5$ kcal $\cdot$ mol^{-1}. For our "best" value for ΔHf° [BeO(c)] we assign an uncertainty of ± 0.6 kcal $\cdot$ mol^{-1}. Churney and Armstrong assigned ± 0.8 kcal $\cdot$ mol^{-1} to their value for ΔHf°[BeF_2(amorph)]. The indirect determination from the measurements of Gross et al. have an overall uncertainty of ± 0.8 kcal $\cdot$ mol^{-1}. We assign an overall uncertainty of ± 0.8 kcal $\cdot$ mol^{-1} to our "best" value for ΔHf°[BeF_2(c)].

5. A Key Assumption

The interpretation of the data and the values given are internally consistent with our value for ΔHf° [HF(aq, std. state)] [3], and lend support to this value; eg., the values for $\Delta(\Delta Hf^\circ)$ [BeO(c)−BeF_2(quartz)] from our 'selected' values, independent of HF(aq) are in excellent agreement with that derived from the Kolesov et al. difference, HF dependent, if one assumes a ΔH_{trans} of 0.7 kcal $\cdot$ mol^{-1} for the β cristobalite to the quartz form. Also the ΔHf[BeF_2(aq, in HF)] from the Bear and Turnbull measurements, dependent upon HF

[4] Use of a more recent set of thermal functions [40], also based on an estimate, could change ΔH°_{subl} of BeF_2 by a few tenths of a kcal, well within the assigned uncertainty.

are in excellent agreement with that derived from the ΔH_{soln} (measured by Kilday and Churney) of a BeF_2 (amorph) sample whose $\Delta Hf°$ was measured directly by Churney and Armstrong and is thus independent of $\Delta Hf°$[HF(aq)]. However there is also evidence [39, 40, 41] that the 'selected' value for HF may be too positive by 0.3 to 0.4 kcal · mol^{-1}. If so, this would involve a reinterpretation of the data.

In summary:

$$\Delta Hf°[BeO(c)] = -145.7 \pm 0.6 \text{ kcal} \cdot \text{mol}^{-1}$$
$$(-609.6 \pm 2.5 \text{ kJ} \cdot \text{mol}^{-1})$$

$$\Delta Hf°[BeF_2(c, \text{quartz})] = -245.4 \pm 0.8 \text{ kcal} \cdot \text{mol}^{-1}$$
$$(-1026.8 \pm 3.3 \text{ kJ} \cdot \text{mol}^{-1}).$$

6. References

[1] Kilday, M. V., Prosen, E. J., and Wagman, D. D., J. Res. Nat. Bur. Stand. (U.S.) **77A2** (Phys. and Chem.) No. 2, 217–225 (Mar.–Apr. 1973).

[2] Churney, K. L., and Armstrong, G. T., J. Res. Nat. Bur. Stand. (U.S.) **73A,** (Phys. and Chem.), No. 3, 281–297 (May–June 1969).

[3] Wagman, D. D., Evans, W. H., Parker, V. B., Halow, I., Bailey, S. M., and Schumm, R. H., Selected Values of Chemical Thermodynamic Properties, Nat. Bur. Stand. (U.S.), Tech. Note 270–3. 264 pp. (Jan. 1968); Parker, V. B., Wagman, D. D., Evans, W. H., Nat. Bur. Stand. (U.S.), Tech. Note 270–6, 106 pp. (Nov. 1971).

[4] Moose, J. E., and Parr, S. W., J. Am. Chem. Soc. **46,** 2656 (1924).

[5] Roth, W. A., Börger, E., and Siemonsen, H., Z. anorg. u. allgem. Chem. **239,** 321 (1938).

[6] Neumann, B., Kröger, C., and Kunz, H., Z. anorg. u. allgem. Chem. **218,** 379 (1934).

[7] Mielenz, W., and v. Wartenberg, H., Z. anorg. u. allgem. Chem. **116,** 267 (1921).

[8] Cosgrove, L. A., and Snyder, P. E., J. Am. Chem. Soc. **75,** 3102 (1953).

[9] Neumann, B., Kröger, C., and Haebler, H., Z. anorg. u. allgem. Chem. **204,** 81 (1932).

[10] Kolesov, V. P., Popov, M. M., and Skuratov, S. M., Zhur. Neorg. Khim. **4,** 1233 (1959).

[11] Matignon, C., and Marchal, G., Compt. rend. **183,** 927 (1926).

[12] Copaux, H., and Philips, C., Compt. rend. **176,** 579 (1923).

[13] Bear, I. J., and Turnbull, A. G., J. Phys. Chem. **69,** 2828 (1965).

[14] Armstrong, G. T., and Coyle, C. F., U.S. AEC AED–Conf–65–358–1, 35 pp. (1965).

[15] Fricke, R., and Wüllhorst, B., Z. anorg. u. allgem. Chem. **205,** 127 (1932).

[16] Parker, V. B., Nat. Stand. Ref. Data Ser., Nat. Bur. Stand. (U.S.), 2, 66 pp. (Apr. 1, 1965).

[17] Thompson, C. J., Sinke, G. C., and Stull, D. R., J. Chem. Eng. Data **7,** 380 (1962).

[18] Blachnik, R. O. G., Gross, P., and Hayman, C., Fulmer Research Inst. Scientific Rept. No. 5, Contract AF 61(052)–863 (July 1968).

[19] Smirnov, M. V., and Chukreev, N. Ya., Zhur. Neorg. Khim. **3,** 2445 (1958).

[20] Matignon, C., and Marchal, G., Bull. soc. chim. France [4] **39,** 167 (1926).

[21] Matignon, C., and Marchal, G., Compt. rend. **181,** 859 (1925).

[22] Fricke, R., and Severin, H., Z. anorg. u. allgem. Chem. **205,** 287 (1932).

[23] Taylor, A. R., and Gardner, T. E., U. S. Bur. of Mines Rept. Invest. **6664,** 15 pp. (1965).

[24] Gross, P., Hayman, C., and Bingham, J. T., Fulmer Research Inst. Ltd. Sci. Rept. No. **7,** Contract AF 61(052)–447, 10 pp. (Feb. 1971).

[25] Gross, P., Hayman, C., and Levi, D. L., Met. Soc. Conf. **8,** 903 (1961).

[26] Rudzitis, E., Feder, H. M., and Hubbard, W. N., J. Inorg. Chem. **6,** 1716 (1967).

[27] Dow Chemical Company, JANAF Thermochemical Tables PB 168 370 (Clearinghouse for Federal Scientific and Technical Information, Springfield, Virginia, August 1965).

[28] Cantor, S., J. Chem. Eng. Data **10,** 237 (1965).

[29] Khandamirova, N. E., Evseev, A. M., Pozharskaya, G., et al., Zhur. Neorg. Khim. **4,** 2192 (1959).

[30] Sense, K. A., and Stone, R. W., J. Phys. Chem. **62,** 453 (1958).

[31] Sense, K. A., Snyder, M. J., and Clegg, J. W., J. Phys. Chem. **58,** 223 (1954).

[32] Hildenbrand, D. L., and Theard, L. P., J. Chem. Phys. **42,** 3230 (1965).

[33] Blauer, J. A., Greenbaum, M. A., and Farber, M., J. Phys. Chem. **69,** 1069 (1965).

[34] Greenbaum, M. A., Foster, J., Arin, M. L., and Farber, M., J. Phys. Chem. **67,** 36 (1963).

[35] Novoselova, A. V., Muratov, F. Sh., Reshetnikova, L. P., and Gordeev, I. V., Vestnik Moskov, Univ., Ser. Mat., Mekh., Astron., Fiz. i Khim, No. **6,** 181 (1958).

[36] Greenbaum, M. A., Arin, M. L., and Farber, M., J. Phys. Chem. **67,** 1191 (1963).

[37] Naylor, B. F., J. Am. Chem. Soc. **67,** 150 (1945).

[38] McDonald, R. A., and Oetting, F. L., J. Phys. Chem. **69,** 3839 (1965).

[39] Armstrong, G. T., Hydrogen Fluoride and the Thermochemistry of Fluorine, Nat. Bur. Stand. (U.S.), Tech. Note. 513, 32 pp. (Oct. 1970).

[40] Stull, D. R., and Prophet, H., Eds. JANAF Thermochemical Tables, 2nd ed., Nat. Stand. Ref. Data Ser., Nat. Bur. Stand. (U.S.), 37 (1971).

[41] Domalski, E. S., and Armstrong, G. T., J. Res. Nat. Bur. Stand. (U.S.) **71A,** (Phys. and Chem.) No. 3, 195–202 (1967).

(Paper 77A2–765)

JOURNAL OF RESEARCH of the National Bureau of Standards—A. Physics and Chemistry
Vo. 77A, No. 2, March–April 1973

Vapor Pressure and Heat of Sublimation of Tungsten

E. R. Plante and A. B. Sessoms

Institute for Materials Research, National Bureau of Standards, Washington, D.C. 20234

(November 30, 1972)

The vapor pressure of tungsten was measured by the Langmuir method in the temperature range 2600 to 3100 K using a vacuum microbalance. Four series of data gave concordant results and three of the four series gave second and third law heats of sublimation in excellent agreement. A vapor pressure equation representing the data is log P(atm)$=-45385/T+7.871$, based on our mean third law heat and tabulated entropies at 2800 K. The mean third law heat of sublimation at 298.15 K is 205.52 ± 1.1 kcal mol^{-1} (859.90 ± 4.6 kJ mol^{-1}) where the uncertainty is an overall estimated error. Rates of vaporization are about 1/2 those previously accepted for tungsten.

Key words: Heat of sublimation; Langmuir vaporization; rate of vaporization; tungsten; vapor pressure.

1. Introduction

This study was undertaken as part of an NBS contribution to a program involving the measurement of vapor pressures of selected standard materials in various cooperating laboratories. The object of these measurements is to determine reliable standard vapor pressure data and to reveal, if possible, any systematic differences in vapor pressures which might be attributable to different methods of measurement. Currently, gold, and cadmium and silver [1][1] have been certified as standard reference materials for vapor pressure measurements. Certification of standards for platinum and tungsten are in process and are expected to be available in the near future [2].

Data leading to vapor pressures or heats of sublimation of tungsten have been reported by a number of investigators [3–9] using the Langmuir method. In addition, Golubtsov and Nesmeyanov [8] measured the vapor pressure by the Knudsen method. Thermodynamic data resulting from these and the current measurements are summarized in table 2 and discussed in section 4 of this paper.

2. Experimental Method

Data were obtained by Langmuir rate of sublimation measurements using a vacuum microbalance. Vacuum in the range 10^{-7} to 10^{-9} torr was maintained and indicated by a commercial sputter-ion pump. Techniques and procedures were similar to those outlined previously [10].

The tungsten SRM–749 stock material is in excess of 99.99 percent purity. Additional information will be included in the provisional NBS Certificate of Analysis. Samples were machined by arc erosion into right circular cylinders having nominal diameters of 0.25 and 0.20 cm and length of 1.9 cm. A hole 0.1 cm in diameter and 1.5 cm long, assumed to represent blackbody conditions, was drilled along the cylinder axis and a suspension hole was drilled along a diameter about 0.20 cm from the other end.

The sample was suspended from one arm of an equal-arm quartz[2] beam microbalance by a chain of 0.025 cm diameter sapphire or quartz rods connected together by V-shaped hooks made by heating and bending the rods. The lower 10 cm of the suspension was 0.005 cm tungsten wire which passed through the suspension hole in the samples and over the hook on the lowest suspension rod.

The appendage of the vacuum chamber in which the sample hung was a 20 mm O.D. Vycor[3] tube made with a fused silica window at the bottom. The window could be protected during sublimation experiments by a magnetically operated shutter; however, because the shutter must be kept open for a large fraction of the time during short experiments when the rate of vaporization is highest, the shutter was left open during all the experiments reported here. To afford some additional protection to the window, the side arm was extended so that the bottom of the sample was about 22.5 cm from the window. With this experimental arrangement changes in the window correction factor are not significantly larger than in those cases where an attempt was made to protect the window.

Data were designated as belonging to a new experimental series when new window correction values were determined and when a sample was changed. The purpose of changing samples was to

[1] Figures in brackets indicate the literature references at the end of this paper.

[2] The terms quartz and fused silica are used interchangeably in this paper for fused silica.

[3] Reference to trade names is made only for completeness of description and does not imply in any way the endorsement of the product by the National Bureau of Standards.

check on reproducibility of the measurements and to see if changes in the rate of sublimation could be detected for slightly different length to radius ratios of the samples because of temperature inhomogeneity.

Prior to experiments, a thin platinum coating which did not heat inductively was deposited on the interior surface of the Vycor tube, and a grounding device, consisting of a split circular stainless steel ring with a magnetically actuated wire hinge, was positioned in the Vycor tube so that it made contact with the platinum coating. The Vycor tube was connected to the vacuum system by means of a standard taper joint using Apiezon W sealant. A wire connected the grounding device to an electrical ground. With the sample in place the hinge of the grounding device could be magnetically deflected until it made contact with the wire supporting the sample. This allowed for removal of any static charge generated during the high temperature heating. Heating was accomplished by induction of 450 kHz. The metal sample served as its own susceptor.

Temperatures were measured with an NBS-calibrated optical pyrometer through a calibrated window and mirror. Calibration corrections for the window and mirror were determined in separate experiments using a band lamp. Corrections were determined in terms of "A" values where $A=(1/T)-(1/T_w)$; T is the brightness temperature of the source and T_w is the brightness temperature of the source with the window or mirror in the optical path. Window corrections were determined before and after each series of measurements and the average value accepted. Mirror corrections were determined less frequently; an average of two independent sets of determinations was used. Corrections applied to the observed temperature because of the change in the window "A" value during an experimental series were less than 4 K at 2800 K.

In obtaining each datum point the following sequence of operations was followed: (1) the rest point of the balance was determined, (2) the sample was heated to the base temperature, a temperature about 100 K below the lowest temperature where sublimation rate measurements were practicable, (3) an operating temperature of the sample was attained by adjusting the heater power and holding it constant at a predetermined setting, (4) the power was turned off, (5) the sample and platinum coating on the Vycor sleeve were grounded, and (6) the rest point of the balance was redetermined.

The mass change of the sample was determined from the displacement of the beam of the microbalance and the previously determined sensitivity which was about 0.5 $\mu g/\mu m$. The change in sensitivity with load is negligible for the weight change (about 2 mg) during a series of experiments. Data during these experiments were obtained with a gold plated balance used in previous experiments. This balance exhibited excellent zero point stability in contrast to some previous drift problems [11]. This is attributed to a more nearly constant room temperature at our new facility, use of a narrower slot on the kinematic table which supported the balance, and the grounding procedure which eliminates static charge on the sample and its surroundings.

Initial time for an experiment was taken when the brightness of the blackbody hole matched the brightness of the pyrometer filament previously set for a temperature 50 K below the expected operating temperature for a particular power setting. Final time was taken as the time the power was turned off. The first temperature measurement was usually obtained within the first minute of the experiment, at which time the sample had attained its operating temperature. This method of determining the duration of the experiment was used because the rate of heating is slower than the rate of cooling.

Experimentally it is observed that the time required to heat from the base temperature to the operating temperature is shorter, the greater is the temperature difference between them. This probably is due to the fact that the power input can be changed almost instantaneously, the power loss is proportional to T^4, and the energy absorbed by the sample during warm up becomes a smaller fraction of the energy input as the temperature difference gets larger. For low temperature runs the length of time to go from the base temperature to 50 K below the operating temperature would be about 15 seconds while for high temperature runs about 3 seconds would be required. This method of timing tacitly assumes that the excess weight lost in heating from the base temperature to 50 K below the operating temperature exactly balances the deficiency in weight lost in going from 50 K below the operating temperature to the operating temperature. We have assumed that systematic error resulting from this approximation is negligible.

3. Thermodynamic Treatment of Data

Vapor pressures were calculated using the equation [4]

$$P=\frac{m}{\alpha a t}\left(\frac{2\pi RT}{M}\right)^{1/2} \tag{1}$$

where m is the mass of material sublimed, t is the duration of the experiment, a is the projected surface area of the sample, T is the temperature on the IPTS-68 scale [12], R is the gas constant, M is the atomic weight of the vaporizing species, monatomic tungsten, and α is the vaporization coefficient which we assumed is equal to unity. The value of the sample area at temperature, A_T, was calculated using the equation

$$A_T=A_R[1+2\beta(T-300)]$$

where A_R is the area calculated from measurements made at room temperature and β is the linear thermal expansion coefficient. For tungsten β was taken to be 6.0×10^{-6} K^{-1}. This correction amounts to an increase in the sample surface area of 2 to 4 percent at sublimation temperatures.

[4] Values of constants used in the equation were: $R=1.98717$ cal mol^{-1} K^{-1} or 8.3143 $Jmol^{-1}$ K^{-1}, atomic weight of tungsten = 183.85; one standard atmosphere = 101,325 Nm^{-2}.

Areas at room temperature were 1.30 cm^2 and 1.64 cm^2 for the nominal 0.20 cm and 0.25 cm diam samples respectively.

A linear equation was fitted to the data by least squares solution of the approximate integrated form of the Clausius-Clapeyron equation

$$\log P(\text{atm}) = -\frac{\Delta H^\circ}{R'T} + \frac{\Delta S^\circ}{R'} \qquad (2)$$

where ΔH° and ΔS° are the heat and entropy changes at an average temperature and R' is $R \ln 10$.

In addition, third law heats of sublimation were calculated using the equation

$$\Delta H^\circ_{298} = T\left[\Delta\left(-\frac{G^\circ_T - H^\circ_{298}}{T}\right) - R \ln P(\text{atm})\right] \qquad (3)$$

where $\Delta -(G^\circ_T - H^\circ_{298})/T$ is the difference in free energy functions of product and reactant. Free energy function data were from JANAF [13]. Finally, accurate second law heats and entropies were obtained using a method suggested by Horton [14] which is similar to Cubicciotti's method [15]. This consists of fitting by

TABLE 1. *Compilation of tungsten data* [a]

Temp Kelvins	Time Seconds	Wgt loss Micrograms	Pressure Atmospheres	$\Delta H(298)$ cal/mol	$\Delta H(298)$ J/mol
Vapor pressure of tungsten SRM 749, 0.20 cm sample series I					
2879	300	53.7	1.19000E−8	205932	861620
2691	3600	56.1	1.01000E−9	205533	859949
2946	300	127	2.85000E−8	205656	860463
2756	3600	139	2.52000E−9	205544	859998
2627	10800	68.9	4.07000E−10	205334	859116
2990	240	160	4.52000E−8	206014	861965
2799	1200	80.8	4.43000E−9	205650	860438
2880	600	123	1.37000E−8	205198	858549
2567	14400	31	1.36000E−10	206179	862652
3026	180	190	7.20000E−8	205715	860712
2843	900	103	7.58000E−9	205879	861400
2876	600	98.7	1.10000E−8	206165	862593
Vapor pressure of tungsten, SRM 749, 0.25 cm sample series II					
2760	1200	67	2.89000E−9	205095	858116
2927	240	98.8	2.19000E−8	205850	861275
2796	1200	102	4.43000E−9	205427	859505
2865	480	88.8	9.74000E−9	206061	862159
2983	120	100	4.47000E−8	205594	860204
2710	2400	68.4	1.46000E−9	205016	857785
2667	4500	69.3	7.84000E−10	205021	857807
2590	10800	49.4	2.30000E−10	205346	859166
2628	7200	57	4.00000E−10	205503	859826
Vapor pressure of tungsten SRM 749, 0.20 cm sample series III					
2857	600	93	1.03000E−8	205162	858400
2796	1200	81.4	4.46000E−9	205389	859349
2931	180	63	2.35000E−8	205723	860744
2633	10800	76.6	4.53000E−10	205248	858756
2983	180	128	4.32000E−8	205147	858335
2712	3000	68.2	1.47000E−9	205132	858271
2733	2100	62.6	1.94000E−9	205231	858685
2670	5400	67	7.98000E−10	205160	858390
2569	16200	44.1	1.72000E−10	205143	858316
3008	180	180	6.80000E−8	204824	856983
Vapor pressure of tungsten SRM 749, 0.25 cm sample series IV					
2812	600	68.1	5.93000E−9	204985	857655
2955	240	144	3.21000E−8	205591	860192
2637	7200	62	4.36000E−10	205763	860914
2895	300	89.4	1.58000E−8	205457	859633
2734	2400	77.8	1.67000E−9	206121	862410
2688	3600	65.3	9.27000E−10	205759	860895
2775	1500	91.2	3.16000E−9	205729	860771
2577	10800	39.4	1.83000E−10	205472	859696
3067	120	248	1.12000E−7	205831	861197
3013	180	196	5.87000E−8	206047	862103

[a] Data are listed in experimental sequence.

least squares $\Delta-(G_T^\circ-H_{298}^\circ)/T-R\ln P$ versus $1/T$ and allowing for nonzero intercept. The slope corresponds to an accurately adjusted second law heat while the intercept corresponds to ΔS_{298}° (3d law) $-\Delta S_{298}^\circ$ (2d law) [10].

4. Results

Basic data, the vapor pressures calculated using eq (1) and individual third law heats calculated using eq (3) are listed in table 1. Table 2 lists the second law heat and entropy change at 298.15 K calculated by Cubicciotti's method and their standard errors, the coefficients of eq (2) and their standard errors, the standard deviation in the pressure in log units, and the average third law heat and its standard error for each series of data. The mean third law heat at 298.15 K, calculated as the average of the means for each run, is 205.52 kcal mol^{-1} (859.90 kJ mol^{-1}) while the average second law heat and entropy change at 298.15 K based on the four series of data are 204.15 kcal mol^{-1} (854.16 kJ mol^{-1}) and 33.25 cal mol^{-1} K^{-1} (139.08 J mol^{-1} K^{-1}) respectively. As usual, the third law heat is considered more reliable than the second law heat.

It may be of interest to indicate the uncertainty in the pressures, temperatures, mean third law heat, and the second law heat and entropy change. The standard deviation in P as computed by the law of propagation of errors [17] applied to equation (1) has components of error due to random error in m, t, T and systematic error in a. For a typical experiment at 2800 K, respective standard deviations of 2 percent, 2 percent, 0.07 percent (2K), and 1 percent are reasonable estimates based on the experimental observations for the above quantities. These combine to give a standard deviation in the pressure of 3 percent. It is important to note that this estimated standard deviation will be too small because it applies to an experiment in which T is constant and in which only estimates of the value of T vary. However, in practice, some real fluctuation in T may occur and the rate of evaporation is not independent of real fluctuations in T.

A more realistic estimate of the error in P is given by the standard deviation obtained by least squares fit of eq (2). For the four runs reported here, standard deviations in the range 4–7 percent are observed. Application of the law of propagation of errors to eq (2) shows that a standard deviation in T of 1 K would result in a standard deviation in P of 1.3 percent at 2800 K. The standard deviation in P, calculated from the least squares fit of eq (2), can be considered as arising from two sources. Part is due to measurement errors in the pressure itself which was estimated as 3 percent and the remainder is due to error in the temperature measurements. If the resultant error in the pressure is calculated as the square root of the sum of the squares, a standard deviation of 4 K in the mean temperature would give a standard deviation of 6 percent which agrees well with the observed range of 4–7 percent.

The standard deviation in the mean temperature of an experiment can be computed from the temperature observations for each experiment and these show that standard deviations in the mean temperature of an experiment seldom exceed 2 K. The standard deviation in the temperature of an experiment thus

TABLE 2. *Derived quantities for tungsten* [a]

	Second law values									Third law values	
	$\Delta H°(298)$ kcal mol^{-1}	S.E.[b] kcal mol^{-1}	$\Delta S°(298)$[c] cal mol^{-1} K^{-1}	S.E. cal mol^{-1} K^{-1}	$-\Delta H_T^\circ/R'$ K	S.E. K	$\Delta S_T^\circ/R'$	S.E.	S.D.[b] (log P)	$\Delta H°(298)$ kcal mol^{-1}	S.E. kcal mol^{-1}
Series I .20 cm	205.33	1.94	33.60	0.69	45345	428	7.840	0.152	0.026	205.73	0.09
Series II .25 cm	201.12	2.28	32.18	.83	44427	502	7.531	.181	.025	205.44	.12
Series III .20 cm	205.16	1.41	33.72	.51	45307	305	7.866	.110	.018	205.22	.07
Series IV .25 cm	204.98	1.96	33.49	.70	45255	431	7.812	.154	.027	205.68	.10
Means, this work	204.15	[d] 2.0	33.25	[d] .70						205.52	[d] 1.1
Swarcz et al. [6]	202.55	2.74	34.14	.96	44706	601	7.773	.212	.045	203.69	.18
Deadmore [7][e]	216.43	9.19	37.94	3.22	47737	2004	8.777	.702	.102	204.39	.50
Zwikker [5]	214.95	1.41	38.10	.50	47445	306	8.821	.109	.037	202.54	.33
Langmuir [3, 4]	204.51	3.80	34.67	1.30	45141	819	8.064	.280	.070	201.78	.27
G and N [8]					45526		8.074				
Knudsen data [8]					44766		7.845				
ZIT [9]					43333						

[a] All temperatures were converted to IPTS–68 scale.
[b] S.D. = Standard deviation of a single measurement; S.E. = standard error (standard deviation in the mean).
[c] Based on tabulated data, $\Delta S°(298) = 33.74$ cal mol^{-1} K^{-1}.
[d] These errors are based on twice the standard error.
[e] Original data were supplied by author.

appears to be 2 to 3 times larger than that estimated from the temperature observations. This is probably due in part to the gradual increase in A value of the window during an experimental series which biases the observed temperatures toward lower values as an experimental series progresses, but which will show up as a random error because of random selection of temperatures. A second contributing factor is that the operator's judgment of what constitutes a match in brightness of the pyrometer filament with the blackbody hole varies with temperature and from day to day.

Estimates of the errors in second law heats and entropy changes can be made using several methods. Assuming that the effect of systematic error is negligible as compared to random error for the second law method, errors based on twice the standard error in the average of the four series are 2.0 kcal and 0.7 cal mol^{-1} K^{-1} respectively.

Experience has shown that the uncertainty in the third law heat arising from systematic errors is usually greater than or comparable to the uncertainty arising from random errors. Thus, an estimate of the error in the mean third law heat will have to include both. An estimate of the random error can be made by applying the law of propagation of errors to eq (3). In doing so, we assume that there is no significant error in the free energy functions and their variation with temperature is negligible. Based on estimates of a 3 percent standard deviation in pressure and a 4 K standard deviation in temperature, the standard deviation in ΔH°_{298} evaluated from data at 2800 K is 340 cal. For 10 data points this corresponds to a standard error of 110 cal in the mean third law heat, which agrees well with values derived from the individual series. If there were no between run bias, the standard error in the mean third law heat derived from all four series and based on within run uncertainty would be 100 cal while the observed value is 200 cal. This discrepancy is due to a between run systematic error of 2.5 K in the window and mirror correction factors which leads to an additional uncertainty of 170 cal. The largest uncertainty is due to systematic error in temperature measurement. Part of this error results from the uncertainty in the NBS calibration but most results from our inability to transfer this scale to laboratory measurements without error. The uncertainty in the pyrometer calibration at 2800 K is 7 K and we assume an additional systematic error of 14 K results in the process of carrying out measurements. These errors are presumed to represent 2 standard deviations and lead respectively to uncertainties of 500 cal and 1000 cal in the mean third law heat. If we use 2 standard deviations as the measure of uncertainty, then the uncertainty is $(200^2 + 340^2 + 500^2 + 1000^2)^{1/2} = 1100$ cal (4600 J). If this error is expressed in terms of temperature or pressure, it corresponds to an error in temperature of 15 K or an error in pressure of 22 percent.

This procedure for estimating the uncertainty in the third law heat deviates from some of our previous estimates (6, 10, 11) because it assumes a much larger component of systematic error than we have previously estimated. The present method however, appears justified since it is well known that mean third law heats measured in different laboratories frequently disagree within the stated error limits when these limits are based on random error only.

Pressures obtained in this work are about one half those previously reported from this laboratory. This pressure difference corresponds to temperatures in the present work being systematically higher than those previously measured by about 30 K at 2800 K. An error of this magnitude is most likely due to an error in temperature measurement and could result from an improperly determined A value, deposition of tungsten on the window, or temperature inhomogeneity of the sample. Duplicate determinations as well as variation in the length to radius ratio of the two samples should prevent such an error from being important in the present work.

The spread in the average third law heats in these series amounts to 0.5 kcal and this appears reasonable considering the standard errors and the small component of systematic error resulting from different window and mirror factors. Comparison of second law heats with third law heats shows good agreement in three of the four series with series 2 showing questionable agreement depending on ones interpretation of the significance of the standard errors. The vapor pressure data of tungsten is adequately represented by

$$\log P\ (\text{atm}) = -\frac{45385}{T} + 7.871$$

based on our mean third law heat and entropy data from JANAF [13] centered on 2800 K. This equation gives pressures agreeing within 10 percent of pressures derived from least squares equations of each of the experimental series in the experimental temperature range.

Analysis of the older tungsten data was made by Szwarc et al. [6]. In the present work temperatures were converted to the IPTS–68 scale using data given in [12], and free energy function data from JANAF [13] were used to compute the value of the properties listed in table 2. These corrections increase the average third law heat by about 300 cal but have little effect on the second law heats.

Other data listed in table 2 shows quite good agreement with the present results. Considering the time span and the temperature range involved the agreement is quite satisfactory. Deadmore [7] measured rates of sublimation of tungsten to use as a standard for comparison with rates of evaporation of TaC, HfC, and HfC-TaC solid solutions. His third law results are in good agreement with those presented here while his second law heat indicates some systematic error. Golubstov and Nesmeyanov [8] measured rates of sublimation by both the Langmuir and Knudsen method using nuclear activation analysis and studied the apparent vapor pressure as a function of ambient pressure in the system. They concluded that the apparent pressure was not a function of ambient pressure at pressures below 10^{-7} torr and the second law values for these conditions derived from their log P versus $1/T$ equations agree well with those in the present study. It is of interest to note also that

their data indicate unit sublimation coefficient for tungsten which all Langmuir measurements have previously only assumed. Values for the heat of sublimation determined mass spectrometrically by Zandberg et al. [9] are in satisfactory agreement for second law results. The older results of Langmuir [3, 4] and Zwikker [5] are in reasonable agreement with our results considering their experimental difficulties of measuring surface temperatures and establishing a temperature scale.

Our experiments indicate a heat of sublimation of tungsten about 2 kcal mol^{-1} higher than any of the previous results. Because of this difference, we have considered likely sources of systematic error very carefully. The effect of temperature gradients in a freely radiating cylindrical sample is without doubt the greatest unknown.

For an inductively heated, cylindrical specimen, the highest temperature should occur halfway up the cylinder axis. Temperatures above and below this should gradually decrease because of end effects. If a 1.0 mm diam blackbody hole terminated halfway up the cylinder axis, it would have a length to radius ratio of 18 and would give an excellent approximation to blackbody conditions if the specimen were isothermal. If the specimen is not isothermal and a blackbody hole extends beyond the center of the sample, the experimental temperature would probably be lower than that observed with a blackbody hole terminating at the center. Assuming a linear temperature gradient and neglecting the end areas which constitute only about 5 percent of the sample area, the optimum depth for a blackbody hole would be about 0.75 of the sample length. This depth would give an average temperature approximately equal to the average surface temperature of the sample. Our samples had blackbody holes about 79 percent of the sample length. Previous measurements by Szwarc et al. [6] used a sample having a blackbody hole extending 67 percent of the sample length. On the basis of the above arguments one would expect slightly lower apparent rates of vaporization in the measurements of Szwarc et al., than in our work. However, the reverse is true. This indicates either that temperature gradients in the samples were not important or that insufficient changes in geometry were made to expose their effects.

It is worth noting that because tungsten is the least volatile of all materials, it is difficult to imagine any experimental error which would lead to insufficient volatility. Thus, the most common errors such as reaction with ambient gases, deviation from blackbody conditions, and window contamination would all result in higher volatilities. This tends to support the lower volatilities obtained in the present work.

5. References

[1] Paule, R. C., and Mandel, J., Nat. Bur. Stand. (U.S.) Spec. Publ. 260–19 (1970), and Spec. Publ. 260–21 (1971).

[2] Cadmium, silver and gold standard reference materials (SRM 746, 748, and 745 resp.) may be purchased from the Office of Standard Reference Materials, National Bureau of Standards, Washington, D.C. 20234. Platinum (SRM 747) and tungsten (SRM 749) will be available after certification.

[3] Langmuir, I., Phys. Rev. **2**, 329 (1913).

[4] Jones, H. A., Langmuir, I., and Mackay, G. M. J., Phys. Rev. **30**, 201 (1927).

[5] Zwikker, C., Arch Ne'erl, Serie IIIA, **9** 207–339 (1925).

[6] Szwarc, R., Plante, E. R., and Diamond, J. J., J. Res. Nat. Bur. Stand. (U.S.), **69A** (Phys. and Chem.), No. 5, 417–421 (Sept.–Oct. 1965).

[7] Deadmore, D. L., J. Am. Ceram. Soc. **48**, 357 (1965).

[8] Golubtsov, I. V., and Nesmeyanov, A. N., Vestn. Mosk. Univ., Ser. II, Khim [5], 31 (1965).

[9] Zandberg, E. Ya., Ionov, N. I., and Tontegode, A. Ya., Zh. Tekhn. Fiz. **35**, 1504 (1965).

[10] Plante, E. R., Sessoms, A. B., and Fitch, K. R., J. Res. Nat. Bur. Stand. (U.S.), **74A** (Phys. and Chem.), No. 5, 647–653 (Sept.–Oct. 1970).

[11] Plante, E. R., and Szwarc, R., J. Res. Nat. Bur. Stand. (U.S.) **70A**, (Phys. and Chem.), No. 2, 175–179 (Mar.–Apr. 1966).

[12] The International Temperature Scale of 1968, Metrologia **5**, 35 (1969).

[13] JANAF. Thermochemical Tables, The Dow Chemical Company, Midland, Michigan. Tungsten (c, g) tables dated June 30, 1966.

[14] Horton, W. S., J. Res. Nat. Bur. Stand. (U.S.) **70A** (Phys. and Chem.) No. 6, 533–539 (Nov.–Dec. 1966).

[15] Cubicciotti, D., J. Phys. Chem. **70**, 2410 (1966).

[16] Kostkowski, H. J. and Lee, R. D., Nat. Bur. Stand. (U.S.), Monogr. 41, 31 pages (March 1962).

[17] Mandel, J., The Statistical Analysis of Experimental Data (Interscience Publishers, New York, 1964), pp. 72–75.

(Paper 77A2–766)

JOURNAL OF RESEARCH of the National Bureau of Standards—A. Physics and Chemistry
Vol. 77A, No. 2, March–April 1973

Gas Phase Far Ultraviolet Photolysis and Radiolysis of Vinyl Chloride*

P. Ausloos, R. E. Rebbert

Institute for Materials Research, National Bureau of Standards, Washington, D.C. 20234

M. H. J. Wijnen

Hunter College of the City University of New York, New York, N.Y. 10021

(November 30, 1972)

Quantum yields of the major products formed in the far ultraviolet photolysis of CH_2CDCl (C_2H_2, C_2HD, C_2H_3D, $C_2H_2D_2$, and 1,3-$C_4H_4D_2$) have been determined at 147 nm (8.4 eV), 123.6 nm (10.0 eV), and 104.8–106.7 nm (11.6–11.8 eV). The quantum yield of the stable vinyl radicals which can be unambiguously ascribed to the primary process ($CH_2CDCl + h\nu \rightarrow CH_2CD + Cl$) is 0.3 and 0.05 at 147 and 123.6 nm, respectively. The sharp decrease in the yield of vinyl radicals with the increase in energy of the incident photon beam is in part attributed to the decomposition of internally excited vinyl radicals to give acetylene as a product. At 147 nm, the combined yield of acetylene plus vinyl radicals is 0.95 ± 0.05. At the shorter wavelengths, approximately one acetylene molecule is formed per electronically excited vinyl chloride molecule. It is concluded that the dissociative process: $C_2H_3Cl^* \rightarrow C_2H_2 + H + Cl$, occurring via a C_2H_3 or C_2H_2Cl intermediate adequately accounts for the reactive neutral species formed at higher photon energies. Isotopic labeling experiments show that the hydrogen atoms are detached from both positions of the parent molecule. Ethylene which is a product over the entire wavelength range is in part formed via the reaction: $H^* + C_2H_3Cl \rightarrow C_2H_4 + Cl$, where H^* represents a translationally excited hydrogen atom. The $C_2H_2DCl^+$ ions formed at 104.8 – 106.7 nm with a quantum yield of 0.47 do not contribute to the formation of acetylene or vinyl radicals. In the gas phase radiolysis of vinyl chloride, acetylene ($G \sim 1.5$) is mainly formed in the dissociation of neutral electronically excited vinyl chloride molecules. From this value, we may estimate that the ratio of neutral excited molecules formation to ionization in the radiolysis of vinyl chloride is 0.39. Vinyl ions, which are also produced ($G \sim 0.28$–0.35) react mainly by addition to vinyl chloride.

Key words: Gas phase; photolysis; quantum yield; radiolysis; vinyl chloride; vinyl radical.

1. Introduction

Radiation-induced polymerization of vinyl chloride has been investigated extensively, mainly because vinyl chloride is often used in industrial polymerization processing [1–2].[1] In contrast, the fragmentation of excited vinyl chloride monomer molecules formed by photon absorption or electron impact has received little attention [3].

The present study deals with the decomposition of neutral vinyl chloride molecules excited by absorption of photons whose energy (8.4 to 11.8 eV) brackets the ionization potential of vinyl chloride (I.P.=9.99 eV) [4]. Information gained from these photochemical experiments enables us to assess the contribution of neutral excited molecule precursors to the formation of low molecular weight products formed in gas phase radiolysis experiments.

2. Experimental Procedures

2.1. Materials

The vinyl halides used in this study were purified by gas chromatography. The major ions in the 70 eV mass spectrum of the purified CH_2CDCl were as follows: $C_2H_2DCl^+$ – 39.2 percent, ($C_2HDCl^+ + C_2H_3Cl^+$) – 2.05 percent, $C_2H_2D^+$ – 32.7 percent, ($C_2H_3^+ + C_2HD^+$) – 8.4 percent, ($C_2H_2^+ + C_2D^+$) – 4.2 percent. The mass spectrum did not show any evidence for the presence of higher deuterium labeled vinyl chloride molecules ($C_2HD_2Cl < 0.1\%$). Mass 27 in the 70 eV mass spectrum can mainly be ascribed to C_2HD^+ rather than to $C_2H_3^+$ in view of the fact that a low electron energy mass spectrum of the CH_2CDCl material contained less than 2 percent C_2H_3Cl. The HI and NO were purified by low temperature distillation.

The 200 ml reaction vessel and light sources used in the photochemical experiments have been described in a previous report from this laboratory [5]. The xenon and argon resonance lamps were provided with LiF windows, while the krypton resonance light source

*Work supported in part by the U.S. Atomic Energy Commission.

[1] Figures in brackets indicate the literature references at the end of this paper.

491-397 O - 73 - 5

was fitted with a CaF_2 window transmitting only the 10 eV resonance line. The number of photons transmitted through the LiF window (diameter: 2.1 cm) of the resonance lamps were as follows: xenon, 3×10^{13} photon/s (97% 147 nm; 3% 129.5 nm); krypton, 1 to 4×10^{14} photon/s; argon, 1 to 4×10^{13} photon/s (45% 104.8 nm; 55% 106.7 nm). Because of polymer formation on the fluoride window, the output of the resonance lamps diminishes from one experiment to the next. At a vinyl chloride pressure of 1 torr, the drop in transmission was most severe when argon resonance radiation was used (30% after a total output of 4×10^{15} photons) and was least pronounced in the xenon resonance experiments (1% after a total output of 4×10^{15} photons).

The quantum yields of hydrogen at 147 nm given in the Results section were based on the yield of CO produced in the photolysis of CO_2 (taking $\Phi(CO)=1$) [6]. The quantum yields of the other products were determined by using ethylene (1.5 torr) as a chemical actinometer. The quantum yield of acetylene at 147 and 123.6 nm was established [7–8] to be 1 ± 0.05. At 104.8–106.7, $\Phi(C_2H_2)$ has been estimated [9] to be 0.75 ± 0.05. In the present study ethylene offers an advantage as an actinometer in that the product acetylene can be measured on the same gas chromatograph column as that used for analyzing the products formed in the photolysis of the vinyl halides. Because of the drop in transmission of the window occurring during the vinyl halide experiments, actinometry experiments were performed after each argon resonance photolysis experiment. In the case of the xenon resonance experiments, actinometry had to be performed only after every 3 to 5 experiments. Because the ionization potential of vinyl chloride is slightly below 10 eV, the drop in transmission during radiation with the 10 and 11.6–11.8 eV photons could also be determined by monitoring the saturation ion current as a function of time. Such ion current measurements concurred with the chemical actinometer determinations. The photoionization quantum yields (Φ_+) given in table 1 are based on the saturation ion currents measured in NO as a standard ($\Phi_+(NO)_{123.6}=0.77$, $\Phi_+(NO)_{104.8\text{-}106.7}=0.70$) [10]. These measurements were carried out at pressures at which all incident light is absorbed by the vinyl halides (0.2 to 1.0 torr). The absorption coefficient of vinyl chloride at 147 nm is 355 ± 25 atm^{-1} cm^{-1}.

The NBS cobalt-60 gamma-ray source was used for the radiolysis experiments. Cylindrical 100 ml borosilicate glass reaction vessels were provided with break seals. The dose rate was 12.4×10^{19} eV/g-s.

TABLE 1. *Photoionization quantum yields 300 K*

	10 eV	11.6–11.8 eV
C_2H_3F	0.00	0.28
C_2H_3Cl	.037	.47
C_2H_3Br	.167	.61

Product yields in the photolysis experiments are given in terms of quantum yields. The precision estimated from the scatter of the results is ±5 percent. Products observed in the radiolysis experiments are expressed in G-values (molecules per 100 eV absorbed). Taking a $W-$ value of 24.7 eV [11] for vinyl chloride, ion pair yields can be obtained by multiplying the G-values by 0.247.

3. Results

Acetylene and ethylene are the major hydrocarbon products in all vinyl halide photolysis and radiolysis experiments (tables 2 to 5). 1,3-Butadiene is also produced, but only in the xenon resonance photolysis of pure vinyl chloride could the quantum yield of this product be determined with a better than 10 percent accuracy (table 2). At the shorter wavelengths and in the radiolysis, the yield of butadiene relative to that of acetylene was a factor of 10 less than in the xenon resonance experiments and therefore no attempt was made to obtain quantitative measurements of this product. The quantum yield of 1,3-butadiene in the xenon resonance photolysis of pure vinyl chloride (1 torr) diminishes nearly 30 percent when the number of photons absorbed by vinyl chloride in the course of one experiment is increased from 10 to 20×10^{15} photons (table 2). C_2HCl is observed as a product in the photolysis of vinyl chloride, with quantum yields of 0.012 ± 0.002 and 0.02 ± 0.005 at 147 and 123.6 nm respectively. Addition of O_2 or HI to vinyl chloride did not alter these quantum yields. In the radiolysis, $G(C_2HCl)=0.045\pm0.005$.

The quantum yields of H_2 and HD in the 147 nm photolysis of CH_2CDCl were 0.047 ± 0.005 and 0.01 ± 0.002 respectively. In the photolysis of C_2H_3F

TABLE 2. *Photolysis of vinyl halides at 147 nm*

C_2H_3X pressure	Additive (Torr)[a]	Photons absorbed $\times10^{15}$	Acetylene	Ethylene	1,3-Butadiene
			Quantum yields		
Vinyl chloride					
0.2	.....	20	0.59	0.113	n.d.
1.0	.....	10	.60	.084	0.17
1.0	.....	20	.59	.097	.12
1.0	HI–0.1	20	.59	.377	.00
5.3	.....	16	.59	.071	.16
5.3	.....	60	.58	.070	n.d.
5.3	He–100	60	.57	.008	n.d.
5.3	O_2–0.1	20	.58	.065	.00
5.3	HI–.01	10	.57	.368	.00
5.3	HI–.04	10	.59	.388	.00
5.3	HI–.10	10	.59	.385	.00
5.3	HI–.50	10	.58	.394	.00
5.3	HI–5.6	10	.60	.384	.00
22.6	.....	20	.58	.070	n.d.
22.6	HI–2.0	20	.59	.385	.00
Vinyl bromide					
5.3	.....	20	.89	.140	< .02
5.3	HI–0.5	20	.91	.186	.00
44.4	.....	20	.91	.125	n.d.

[a] 1 Torr = 1.33×10^2 newton/meter^2.

at 147 nm, $\Phi(H_2)$ was determined to be 0.079 ± 0.01. These hydrogen quantum yield determinations were within experimental error, independent of pressure over the range 5 to 50 torr. Quantum yields of hydrogen could not be determined at shorter wavelengths because of the sharp drop in transmission of the LiF window as a function of radiation time.

4. Discussion

4.1. Photolysis in the Subionization Region

It is firmly established [3] that electronically excited vinyl chloride molecules produced in the vapor phase photolysis over the wavelength range ~ 190–220 nm dissociate by cleavage of the C–Cl bond

$$C_2H_3Cl \rightarrow C_2H_3 + Cl \qquad (1)$$

and by the molecular elimination of HCl

$$C_2H_3Cl \rightarrow C_2H_2 + HCl. \qquad (2)$$

Φ_1/Φ_2 was found to be 1.4, independent of pressure (2 to 600 torr) and temperature (– 78 to 40 °C).

At the shorter wavelength (147 nm) used in the present study the occurrence of process 1 is indicated by the presence of 1,3-butadiene as a significant product (table 2) and the enhanced quantum yield of ethylene when HI is added as a free radical scavenger to vinyl chloride. The independence of $\Phi(C_2H_4)$ over a 500-fold concentration range of HI indicates that all stable C_2H_3 radicals are intercepted by HI via the abstraction reaction

$$C_2H_3 + HI \rightarrow C_2H_4 + I. \qquad (3)$$

On the assumption that the difference in $\Phi(C_2H_4)$ measured in the presence and absence of HI represents the contribution of reaction 3 to the ethylene formation, a value of 0.31 ± 0.02 is obtained for the quantum yield of stable vinyl radicals at 147 nm over the pressure range 1 to 22.6 torr.

The ethylene observed in the absence of HI can at least in part be accounted for by the decomposition of the internally excited C_2H_4Cl radicals formed in the reaction [12]

$$H + C_2H_3Cl \rightarrow C_2H_4Cl^* \rightarrow C_2H_4 + Cl. \qquad (4)$$

At pressures above 1 torr, $\Phi(C_2H_4)$ is essentially independent of the pressure of vinyl chloride, indicating that the C_2H_4Cl radicals must be highly excited. Apparently, the C_2H_4Cl are formed by addition of translationally excited H atoms to vinyl chloride. This is confirmed by the observation that addition of 100 torr of helium, which is an efficient remover of kinetic energy to 5.3 torr of vinyl chloride (table 2) reduces $\Phi(C_2H_4)$ nearly 10-fold.

In principle, the quantum yield of 1,3-C_4H_6 also provides a measure of the yield of C_2H_3. However, in a study of the Hg–sensitized photolysis of vinyl chloride, it was such that $\Phi(C_4H_6)$ diminishes rapidly with an increase in conversion (table 2). Furthermore there is evidence [13] that besides the recombination reaction

$$CH_2CH + CH_2CH \rightarrow 1,3\text{-}C_4H_6 \qquad (5)$$

the displacement reaction

$$C_2H_3 + C_2H_3Cl \rightarrow 1,3\text{-}C_4H_6 + Cl \qquad (6)$$

should be considered as a source of 1,3-C_4H_6. Both reactions are quenched by the addition of HI (through interception of vinyl radicals in reaction 3) and by the addition of 2 percent oxygen to vinyl chloride (table 2).

At 147 nm $\Phi(C_2H_3)/\Phi(C_2H_2)$ is nearly a factor of three lower than in the 190–220 nm photolysis, but this does not necessarily reflect a higher probability for the HCl elimination process 2 over the C–Cl cleavage process 1 at higher photon energies. It may indeed be expected that at 147 nm a fraction of the internally excited C_2H_3 radicals formed in the C–Cl cleavage process dissociate to give C_2H_2 as a product. The overall process

$$C_2H_3Cl \rightarrow C_2H_2 + H + Cl \qquad (7)$$

requires only 5.5 eV, which is 2.9 eV less than that available to the parent molecule absorbing a 147 nm (8.4 eV) photon. There are actually a number of observations which are consistent with the occurrence of process 7. For instance, approximately 90 percent of the acetylene formed in the 147 nm photolysis of CH_2CDCl consists of CHCD (table 6), as compared to only 50 percent at longer wavelengths (~ 200–220 nm) [14]. At lower photon energies (5.6–6.2 eV) there is barely enough energy for the occurrence of the overall process

$$CH_2CDCl \rightarrow H + C_2HD + Cl \qquad \Delta H = 5.5 \text{ eV} \qquad (8)$$

and the high relative yield of C_2H_2 can definitely be ascribed to the elimination of DCl from a single carbon atom:

$$CH_2CDCl \rightarrow C_2H_2 + DCl. \qquad (9)$$

Formation of acetylene by decomposition of excited vinyl radicals is also indicated by the C_2H_3Br experiments (table 2) where the weaker carbon-halogen bond causes a drastic reduction in the quantum yield of stable vinyl radicals to about 0.04 as compared to 0.31 in the case of vinyl chloride. The data given in table 2 show that the lower yields of C_2H_3 radicals observed in the photolysis of C_2H_3Br, compared to C_2H_3Cl, is entirely compensated by an increase in the yield of C_2H_2. Finally, the C_2H_3Cl–HI experiments given in table 3 demonstrate that an increase in the photon energy from 8.4 eV to 10.0 eV lowers the yield of C_2H_3 and increases that of C_2H_2. A primary process such as:

$$C_2H_3Cl \rightarrow C_2H_2Cl + H \qquad (10)$$

followed by decomposition of the C_2H_2Cl radical, should also be considered to account for these results. The net result of such a sequence is indistinguishable from process 1 followed by the dissociation of C_2H_3.

It is intriguing that stable C_2H_3 radicals are observed in the 147 nm photolysis of C_2H_3Cl while in the photolysis of C_2H_4 at the same wavelength, C_2H_3 radicals are essentially absent even though the overall process

$$C_2H_4{}^* \rightarrow C_2H_2 + H + H \qquad (\Phi = 0.6) \qquad (11)$$

requires 6.4 eV as compared to only 5.5 eV for the analogous process 7. Stable vinyl radicals are also absent in the 147 nm photolysis of CH_2CHF. The sum of the quantum yields of C_2H_2 (~ 0.8) and C_2HF (0.2) in the O_2 scavenged photolysis of C_2H_3F is equal to 1 ± 0.05 over the pressure range from 5 to 200 torr.

As already pointed out above, the low yield of C_2H_2 in the CH_2CDCl experiments (table 6) indicates that elimnation of hydrogen chloride from a single carbon atom in vinyl chloride occurs only to a minor extent [$\Phi(C_2H_2) \sim 0.07$] at 147 nm. Furthermore, the quantum yield of H_2 [$\Phi(H_2) = 0.05$] and HD [$\Phi(HD) = 0.01$] in the photolysis of CH_2CDCl at 147 nm shows that elimination of molecular hydrogen from vinyl chloride is even less probable. The latter is substantiated by the low yield of C_2HCl ($\Phi \sim 0.01$) at 147 nm. The low quantum yield of "molecular" H_2 in vinyl chloride as compared to that reported in the photolysis of C_2H_4 [$\Phi(H_2) = 0.4$] can be attributed to the weak C-Cl bond strength or to localization of electronic excitation in that bond [15].

TABLE 3. *Photolysis of vinyl chloride at 123.6 nm*

CH_2CDCl pressure	Additive (torr)	Photons absorbed $\times 10^{15}$	Acetylene	Ethylene
			Quantum yields	
1.1	.....	35	0.82	0.175
1.1	NO – 0.3	30	.83	.093
1.1	NO – 2.1	30	.87	.072
1.1	NO – 5.0	30	.84	.044
5.3	O_2 – 0.3	30	.84	.107
5.3	HI – 0.2	20	.86	.166
5.3	HI – 1.6	20	.87	.174
5.3	HI – 5.3	20	.87	.174
24.0	.....	70	.86	.120

4.2. Photolysis in the Photoionization Region

The photon energies corresponding to the krypton (10 eV) and argon (11.6–11.8 eV) resonance lines are above the photoionization threshold of vinyl chloride (9.99 eV) and vinyl bromide (9.8 eV). Because the photoionization quantum yields (Φ_+) are below unity (table 1), dissociation of superexcited vinyl halide molecules will occur over the 10–11.8 eV photon energy range. The quantum yield of the superexcited molecules which do not autoionize is simply given by $(1 - \Phi_+)$.

In order to derive information concerning the primary modes of decomposition of the superexcited molecules from an analysis of the final products formed, one has to substract out the yields of products formed in unimolecular and bimolecular ionic processes. For the wavelength range covered here (10 eV–11.8 eV), this is relatively simple in view of the fact that the parent ion is the only reactive primary ion in the system. The threshold for the formation of the vinyl ion, which is the major fragment ion observed in the 70 eV mass spectrum of the vinyl halides, is 12.5 eV and 12 eV for vinyl chloride and vinyl bromide respectively [4, 16].

On the basis of the high rate for disappearance of the parent ion reported in two recent low pressure mass spectrometric studies [17–18] it can be concluded that under our experimental conditions neutralization of the parent ion is to be ruled out. Instead the vinyl halide ion will react with its neutral counterpart to yield product ions such as $C_4H_6Cl^+$, $C_4H_5Cl^+$ and $C_3H_4Cl^+$. The relative abundances of these ions which are formed in a relatively long lived collision complex are dependent on the internal energy content of the parent ion. It has also been shown that these product ions react further with vinyl chloride to form higher molecular weight ions. Several of these reactions occur with the explusion of HCl as a neutral unity and it can be surmised that they account in part for the high G-value of HCl observed [2] in the gas phase radiolysis of vinyl chloride ($G(HCl) \sim 10$).

From the foregoing it can be expected that at 10 eV and 11.6–11.8 eV only the dissociation of neutral excited molecules will contribute to the formation of the major hydrocarbon product, acetylene. There is strong support for this view in that, in the argon resonance photolysis experiments, the quantum yield of ionization plus the yield of acetylene ($\Phi(C_2H_2) + \Phi_+$) is approximately equal to unity for both vinyl chloride and vinyl bromide (table 4). The HI additive experiments given in table 4 indicate that stable vinyl radicals are apparently formed with a relatively low quantum yield at 1048–67 Å ($\Phi(C_2H_3) < 0.04$). At 10 eV, $\Phi(C_2H_3)$ can be estimated to be 0.06. The actual primary dissociative processes responsible for the formation of acetylene cannot be ascertained from the present results. The isotopic analysis of the ethylene product formed in the photolysis of CH_2CDCl does however indicate that the reaction

TABLE 4. *Photolysis of vinyl chloride and vinyl bromide at 104.8–106.7 nm*

C_2H_3X pressure	Additive (torr)	Photons absorbed $\times 10^{15}$	Acetylene	Ethylene
			Quantum yields	
Vinyl chloride				
0.5	–	2	0.51	0.093
1.2	–	2	.50	.095
5.3	–	2	.51	.099
5.3	HI–0.5	3	.49	.125
5.3	HI–1.6	3	.49	.137
Vinyl bromide				
1.0	–	3	.34	.110
5.6	–	3	.35	.092
5.6	HI–0.2	3	.35	.190

$$D^* + CH_2CDCl \rightarrow C_2H_2D_2 + Cl \qquad (12)$$

(where D* represents a D atom with excess translational energy) increases in importance with increase in photon energy. This points to the increased importance of the overall process

$$CH_2CDCl + h\nu \rightarrow C_2H_2 + D + Cl \qquad (13)$$

as a function of energy. Also, the fractional yield of C_2H_2 in the acetylene increases gradually from 8.4 to 11.6–11.8 eV (table 6). Process 13 can be looked upon as the elimination of excited DCl (process 9) or the cleavage of the C-D bond in the superexcited vinyl chloride molecule followed by decomposition of the internally excited C_2H_2Cl radical. The latter is a mechanism which is more probable in view of the fact that a sharp drop is noted in the abundance of process 9 from 200–220 to 147 nm.

4.3. Radiolysis

There is experimental evidence which indicates that polymerization in gaseous vinyl chloride proceeds via a free radical as well as an ionic reaction mechanism [2]. Radicals formed in the decomposition of neutral excited vinyl chloride molecules, parent ions and their main dissociation fragments ($C_2H_3^+$, Cl) have to be considered as potential chain initiators. In the light of what we learned about the primary dissociative processes in neutral excited vinyl chloride an examination of the data given in tables 5 and 6 provides quantitative information about the yields and sources of the reactive species formed in the gas phase radiolysis.

TABLE 5. *Radiolysis of vinyl chloride*

CH_2CDCl pressure	Additive (torr)	Dose eV/g $\times 10^{-22}$	Acetylene	Ethylene
			G-values [a]	
28.7	.....	2	1.52	0.254
28.7	.....	6	1.50	.275
28.7	.....	24	1.48	.326
28.7	HI – 1.15	2	1.56	.479
85.2	.....	2	1.47	.234
196.3	.....	2	1.36	.221

[a] Number of molecules of product formed per 100 eV energy absorbed.

The only major reactive entity which is present, in addition to those already considered in the 104.8–106.7 nm photolysis, is the $C_2H_3^+$ ion formed in the fragmentation process

$$C_2H_3Cl^+ \rightarrow C_2H_3^+ + Cl \text{ (appearance potential 12.5 eV).} \qquad (14)$$

Ion pair formation may also contribute to the formation of $C_2H_3^+$

$$C_2H_3Cl + e \rightarrow C_2H_3^+ + Cl^- + e \qquad (15)$$

but is apparently of minor importance [16].

TABLE 6. *Isotopic composition of the acetylene and ethylene in the Photolysis and radiolysis of* CH_2CDCl

Radiation	CH_2CDCl pressure	Additive (torr)	$C_2H_2D_2$	C_2H_3D	C_2HD	C_2H_2
			Relative yields			
200–220 nm [a]	5.0	–			100	100
147 nm	5.3	–	9.5	100	100	13.5
	5.3	HI–0.2	2.8	100	100	13.3
123.6 nm	5.3	–	16.2	100	100	22.0
	5.3	HI–0.2	10.0	100		
104.8–106.7 nm	5.3	–	27.5	100	100	31.0
	5.3	HI–0.2	24.0	100	100	32.0
γ-ray	28.7	–	27.4	100	100	40.5
	183.0	–	17.0	100	100	37.3

[a] M.H.J. Wijnen, unpublished results.

Mass spectrometric investigations [17–18] have shown that the $C_2H_3^+$ ion reacts with vinyl chloride in the following manner

$$C_2H_3^+ + C_2H_3Cl \rightarrow C_2H_4Cl^+ + C_2H_2$$

$$k = 5.6 \times 10^{-10} \text{ cm}^3 \text{ molecule}^{-1}\text{s}^{-1} \qquad (16)$$

$$\rightarrow C_4H_5^+ + HCl$$

$$k = 1.5 \times 10^{-10} \text{ cm}^3 \text{ molecule}^{-1}\text{s}^{-1}. \qquad (17)$$

Experiments carried out in the NBS photoionization mass spectrometer [19] confirm the occurrence of these reaction channels and show that in the case of CH_2CDCl the $C_2H_2D^+$ ions react to give both C_2H_2 (30%) and C_2HD (70%) as neutral products

$$C_2H_2D^+ + CH_2CDCl \rightarrow C_2H_2D_2Cl^+ + C_2H_2 \qquad (18)$$

$$\rightarrow C_2H_3DCl + C_2HD. \qquad (19)$$

In order to estimate $G(C_2H_2D^+)$ in the gas phase radiolysis of CH_2CDCl, i-C_4D_{10} was added as a vinyl ion interceptor. Vinyl ions would contribute to the formation of $C_2H_2D_2$ via the D^- transfer reaction [20]:

$$C_2H_2D^+ + i\text{-}C_4D_{10} \rightarrow C_2H_2D_2 + C_4D_9^+$$

$$k = 11.4 \times 10^{-10} \text{ cm}^3 \text{ molecule}^{-1}\text{s}^{-1}. \qquad (20)$$

From the rate constants for the individual reactions, it can be calculated that at the highest concentration of i-C_4D_{10} (table 7) approximately 75 percent of the vinyl

TABLE 7. *Radiolysis of* $CH_2CDCl - i\text{-}C_4D_{10}$ *mixtures*

CH_2CDCl pressure	i-C_4D_{10} (torr)	C_2DH_3	$C_2D_2H_2$	C_2HD	C_2H_2
		G_{CH_2CDCl} [a]			
28.7	.....	0.11	0.06	1.06	0.44
28.7	14.4	.10	.17	1.07	.42
28.7	28.7	.09	.22	1.06	.44
28.7	56.5	.08	.27	1.08	.44

[a] Number of molecules per 100 eV absorbed by vinyl chloride.

ions should be intercepted. It follows from the $G(C_2H_2D_2)$ values given in table 7 that $G(C_2H_2D^+)$= 0.28–0.36. The lower value applies if one assumes that reaction 12 resulting in the formation of $C_2H_2D_2$ in the absence of i-C_4D_{10} is not affected by the presence of i-C_4D_{10}.

The yield of $C_2H_2D^+$ in the radiolysis is well below the value one would estimate from the 70 eV mass spectral cracking pattern of vinyl chloride. Apparently, because of the short time interval between collisions in the radiolysis experiments the parent ion may be collisionally deactivated or react before dissociating. A variation in pressure also affects the mode of reaction of the vinyl ion with vinyl chloride. If indeed the proton transfer reaction were the main reaction channel under these conditions, then contrary to the data given in table 7, a decrease of $G(C_2HD)$ and $G(C_2H_2)$ should be observed when the fraction of $C_2H_2D^+$ intercepted by i-C_4D_{10} increases. The apparent non-occurrence of reactions 18 and 19 under the radiolysis conditions indicates that these reactions occur via a long lived complex which can be collisionally deactivated, favoring a condensation type reaction such as 17. There is evidence in the literature [21] to show that if for a particular reactant pair, proton transfer competes with condensation reaction, the latter will be favored at low kinetic or internal energy.

Because neither the parent ion (see previous section) nor the vinyl ion contributes to the formation of acetylene as a neutral product in the radiolysis it follows that only the decomposition of neutral excited vinyl chloride and the fast charge transfer reaction

$$C_2H_2^+ + C_2H_3Cl \rightarrow C_2H_2 + C_2H_3Cl^+ \qquad (21)$$

are plausible modes of acetylene formation. Upon addition of i-C_4D_{10} reaction 21 would compete with

$$C_2H_2^+ + i\text{-}C_4D_{10} \rightarrow C_2H_2 + C_4D_{10}^+ \qquad (22)$$

so that there would be no net change in G (acetylene). However, in the 70 eV mass spectrum of C_2H_3Cl, $C_2H_2^+$ is only 10 percent of the total ionization ($G = 0.4$). Furthermore, in view of its high appearance potential (13.8 eV) as compared to that of $C_2H_3^+$ (12.8 eV) one may expect the yield of this fragment to be diminished even more at high pressure than $C_2H_3^+$. It is reasonable therefore to assume that acetylene coming from the C_2H^+ ion has a yield smaller than 0.4. By elimination, we conclude that fragmentation of neutral excited vinyl chloride accounts for most of the observed acetylene, $G \sim 1.2$–1.4.

The increment in G (C_2H_4) upon addition of HI to C_2H_3Cl provides an approximate value of 0.25 ± 0.05 for G (C_2H_3) which can be entirely ascribed to process 1, the dissociation of the neutral excited molecule. The low yield of C_2H_3 relative to that of C_2H_2 is consistent with the photolysis experiments. Although the optical excitation spectrum of vinyl chloride is not known, if one takes other organic molecules as examples [22] it may be expected that a considerable fraction of the excitation occurs in the ionization region. Comparison of the isotopic analysis of the acetylene and ethylene formed in the radiolysis of CH_2CDCl with those observed in the photolysis substantiates this view (table 6). Summation of the yield of acetylene not accounted for by reaction 21 and of the vinyl radicals gives a G-values of 1.55 ± 0.1 of neutral excited molecules in the gas phase radiolysis. That is, the ratio of neutral excited molecule formation to ionization in the radiolysis of vinyl chloride is 0.39.

5. References

[1] Chapiro, A., Radiation Chemistry of Polymeric Systems, Interscience, New York (1962).
[2] Grossoleil, J., and Herman, J. A., Can. J. Chem. **49**, 363 (1971) and references cited therein.
[3] Fujimoto, T., Rennert, A. M., and Wijnen, M. H. J., Ber. Bunsenges. Physik Chem. **74**, 282 (1970).
[4] Franklin, J. L., Dillard, J. G., Rosenstock, H. M., Herron, J. T., Draxl, K., and Field, F. H., Ionization Potentials, Appearance Potentials and Heats of Formation of Gaseous Positive Ions, Nat. Stand. Ref. Data Ser., Nat. Bur. Stand. (U.S.) 26, 289 pages (1969).
[5] Gorden, R., Jr., Rebbert, R. E., and Ausloos, P., Nat. Bur. Stand. (U.S.), Tech. Note 496, 55 pages (1969).
[6] Yang, J. Y., and Servedio, F. M., Can. J. Chem. **46**, 338 (1968).
[7] Ausloos, P., unpublished results.
[8] Potzinger, P., Glasgow, L. C., and von Bunau, G., Z. Naturforsch. **27a**, 628 (1972).
[9] Gorden, R., Jr., and Ausloos, P., J. Chem. Phys. **47**, 1799 (1967).
[10] Watanabe, K., Matsunage, F. M., and Sakai, H., Appl. Opt. **6**, 391 (1967).
[11] Leblanc, R. M., and Herman, J. A., J. de Chim. Phys. **63**, 1055 (1966).
[12] Rennert, A. M., and Wijnen, M. H. J., Ber Bunsenges. Physik. Chem. **72**, 222 (1968).
[13] Bellas, M. G., Wan, J. K. S., Allen, W. F., Strausz, O. P., and Gunning, H. E., J. Phys. Chem. **68**, 2170 (1964).
[14] Wijnen, M. H. J., to be published.
[15] Walsh, A. D., Trans. Faraday Soc. **41**, 35 (1945).
[16] Lossing, F. P., Can. J. Chem. **49**, 357 (1971).
[17] Herman, J. A., Myher, J. J., and Harrison, A. G., Can. J. Chem. **47**, 647 (1969).
[18] Hughes, B. M., Tiernan, T. O., and Futrell, J. H., J. Phys. Chem. **73**, 829 (1969).
[19] Sieck, L. W., Searles, S. K., and Ausloos, P., J. Amer. Chem. Soc. **91**, 7627 (1969).
[20] Munson, M. S. B., J. Phys. Chem. **71**, 3966 (1967).
[21] Sieck, L. W., and Ausloos, P., J. Res. Nat. Bur. Stand. (U.S.), **76A** (Phys. and Chem.), No. 3, 253–262 (1972).
[22] Platzman, R. L., Radiation Research, Siline, G., Editor (North-Holland Publishing Co.) (1967), p. 20.

(Paper 77A2–767)

JOURNAL OF RESEARCH of the National Bureau of Standards—A. Physics and Chemistry
Vol. 77A, No. 2, March–April 1973

Pulse Radiolysis of Methane*

R. E. Rebbert, S. G. Lias, and P. Ausloos

Institute for Materials Research, National Bureau of Standards, Washington, D.C. 20234

(December 6, 1972)

The pulse radiolysis of methane has been studied in the absence and presence of electron scavengers such as SF_6 and CD_3I and positive ion scavengers such as i-C_4D_{10} in order to define the role of the intermediates H, C, CH, CH_2, CH_3, CH_5^+, and $C_2H_5^+$ in product formation. The dose rate was varied from 0.68 to 15.2×10^{19} eV/g-s, the dose (number of pulses) was varied, and the duration of the pulse was changed from 3 ns to 100 ns. The variation of the yields of the ethylene and ethane products with dose is explained by the reaction of H-atoms with accumulated ethylene product. The fast reacting C, CH, and $^1CH_2$ species insert into methane to form acetylene, ethylene, and ethane products, but all of the reactions of these species cannot be completely specified since they may originate in upper electronic states, whose reactions with methane are unknown. Product formation by the slow reacting $^3CH_2$ and CH_3 radicals is also examined; for instance, evidence is presented for the occurrence of the reaction: $^3CH_2 + CH_3 \rightarrow C_2H_4 + H$. Results indicate that the ions CH_5^+ and $C_2H_5^+$ undergo neutralization mainly through the processes

$$CH_5^+ + e \rightarrow CH_4 + H$$

$$C_2H_5^+ + e \rightarrow (C_2H_4)^* + H \rightarrow C_2H_3 + H + H_2(2H).$$

When i-C_4D_{10} is added, a fraction of the CH_5^+ and $C_2H_5^+$ react with the additive rather than undergo neutralization. A calculation demonstrates that the fraction of ions undergoing reaction with a given concentration of i-C_4D_{10} can be correctly predicted by assuming that the rate constant for neutralization of CH_5^+ and $C_2H_5^+$ is the same as that determined recently for the t-butyl ion.

Key words: Electron scavengers; gas phase; ion-molecule reactions; methane; neutralization; pulse radiolysis.

1. Introduction

The gas phase radiolysis of methane has been investigated extensively [1],[1] but is still not entirely understood. Three previous communications [2–4] have dealt with the yields of products formed in the pulse radiolysis of methane. The yields of the C_2 products were in poor agreement, even though in one of the studies, the conclusion was reached that the yields of these products were independent of the dose. Spectroscopic studies of the pulse radiolysis of methane have also appeared; in these studies $C(^1S)$ atoms [4] and $CH(^2\pi)$ [5] were shown to be formed.

An important question in the radiolysis of methane has been the ultimate fate of the major ions in the system, $C_2H_5^+$ and CH_5^+, which do not react with methane to produce any chemically different species at ambient temperatures. In the radiolysis at low dose rates, these ions will undergo many hundreds of collisions before being neutralized, and therefore will have a good chance of being intercepted first by small amounts of impurities or with accumulated radiolysis products [6]. Therefore, at low dose rates the chemical identities of the positive ions which eventually undergo neutralization will vary with dose, dose rate, condition of the wall, the purity of the CH_4, etc. At the high dose rates attained in pulse radiolysis experiments, on the other hand, the $C_2H_5^+$ and CH_5^+ ions will have a relatively short lifetime with respect to neutralization, and therefore are less likely to be intercepted by impurities or product molecules. The present investigation is essentially a continuation of an earlier study [7] which examined in detail the neutralization mechanism of the $C_2H_5^+$ ion in methane. The present investigation examines in more detail the effects of dose, dose rate, electron scavengers, and positive ion scavengers on the yields of the radiolytic products formed in methane under pulse radiolysis (high dose rate) conditions.

2. Experimental Procedure

2.1. Irradiation

The experimental procedure was identical to that described in two previous publications from this laboratory [7–8]. Two field emission sources (Febetron 705 and 706) [9] were used in this investigation. The dose per pulse (dose rate) was varied by (a) changing the charging voltage of the diode tube, or (b) inserting

* Work supported in part by the U.S. Atomic Energy Commission.

[1] Figures in brackets indicate the literature references at the end of this paper.

an aluminum plate (0.1 cm thick) between the face of the diode tube and the reaction vessel. These procedures result in changes in the pulse shape. However as will be shown later, the pulse shape or duration has no obvious effect on the product yields in the pulse radiolysis of CH_4. All irradiations carried out with the Febetron 705 and 706 will be henceforth designated as 60–100 ns and 3–5 ns pulse radiolysis, respectively. An accurate determination of the pulse shape is however required in the case of the $CH_4-i\text{-}C_4D_{10}$ experiments, where a quantitative treatment of the data in terms of the ion-molecule reactions is needed. The pulse shape for these experiments which were carried out with the 705 Febetron has been determined with a Faraday cup, and is given in a previous publication [8].

Nitrous oxide at 1 atm was used as a dosimeter. It was assumed that in the pulse radiolysis of nitrous oxide 12.4 molecules of N_2 are produced per 100 eV [10–11]. Relative stopping powers per electron relative to nitrous oxide were calculated from the tables of Berger and Seltzer [12].

2.2. Materials and Analysis

Methane and NO were purified by repeated low temperature distillation until the impurity level was less than 1 ppm. Isobutane-d_{10} was purified by gas chromatography. Mass spectrometric analysis showed that the methane-d_4 contained 5 percent CD_3H while the $i\text{-}C_4D_{10}$ contained 9 percent C_4D_9H.

Hydrogen was analyzed by low temperature distillation using liquid hydrogen as a refrigerant. All other products were analyzed by gas chromatography and in those experiments where deuterium labeled compounds were used, the different hydrocarbon products were collected at the exit of the gas chromatograph and subsequently analyzed by mass spectrometry.

3. Results

3.1. Product Yields

The yields of the measured products are given as molecules, M, of product X produced per ion pair, N_+, formed as a result of the absorption or radiation by methane ($M(X)/N_+$). A W-value of 27 for methane was chosen [13] to convert the number of molecules per eV to the number of molecules per ion pair.

Figure 1 shows the effect of the number of pulses on the major products. These experiments were carried out with the 705 Febetron (60–100 ns) at dose rates ($\sim 10^{26}$ eV/g-s) which were at least a factor of 20 below the maximum dose rate obtainable from a Febetron 705. Product yields obtained at higher dose rates are given in table 1. It can be noted that it is the total dose rather than the dose rate which determines the product yields. The product yields observed for one pulse at a dose per pulse of $3.3\ \text{eV/g} \times 10^{19}$ (second row of table 1) corresponds roughly to that observed for five pulses delivered at a five fold lower dose rate (fig. 1). Apparently the duration of the pulse has no effect on the product yields as long as the total dose is the same. Indeed, the experiments carried out with a 706 Febetron (3–5 ns) given in table 1, show that an increase in the number of pulses has qualitatively and quantitatively the same effect on the product yields as that observed for the 60–100 ns pulse experiments (fig. 1); the dose per pulse in the two series of experiments was comparable.

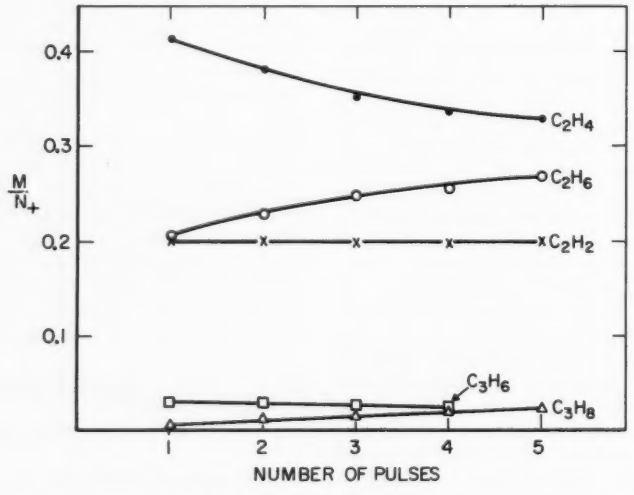

FIGURE 1. *Ion pair yields of* C_2H_4, C_2H_6, C_2H_2, C_3H_6, *and* C_3H_8 *formed in 300 torr of methane as a function of dose (number of pulses).*

Dose/pulse = 0.68×10^{19} eV/g and pulse duration = 60–100 ns.

TABLE 1. *Pulse radiolysis of pure methane*

Duration of pulse ns	Dose/pulse eV/g × 10^{-19}	Number of pulses	Pressure torr	C_2H_2	C_2H_4	C_2H_6	C_3H_4	C_3H_6	C_3H_8	Reference
				Molecules per ion pair (M/N_+)						
60–100	0.68	1	300	0.205	0.420	0.202	0.010	0.029	0.008	This work
60–100	3.3	1	300	.210	.326	.262	.012	.024	.018	
60–100	15.2	2	100	.210	.191	.284	.011	.016	.024	This work
60–100	~ 70	1	400–700	.185	.258	.258				2
60–100	~ 70	10	400–700	.148	.185	.332				2
3–5	0.83	1	300	.218	.432	.212	.011	.029	.008	This work
3–5	0.83	2	300	.204	.370	.230	.011	.025	.012	This work
3–5	0.83	4	300	.210	.343	.279	.012	.024	.019	This work
3–5	0.49	1 to 16	760	.23	.28	.52				3
3–5	0.58		100	.162	.324	.567			.019	5
Low Dose Rate			731	.00	.001	.595		.00	.097	26

The main effect of an increase in total dose is to raise $M(C_2H_6)/N_+$ and $M(C_3H_8)/N_+$ and to diminish $M(C_2H_4)/N_+$. Comparable effects of dose on yields of C_2H_6 and C_2H_4 were also reported by Cahill et al. [2] (table 1). In addition, the latter investigators did observe a decrease of $M(C_2H_2)/N_+$ with increasing dose while none was seen in the present study. The dose range in the study of Cahill et al. was however higher than in our investigation. In contrast, Hummel and Hearne [3] did not find any obvious effect of dose on the yields of C_2H_6, C_2H_4, and C_2H_2 (table 1). The fact that the dose per pulse, the methane pressure and the reaction vessel design were comparable in the two studies, makes it difficult to provide any clues as to the cause of these conflicting observations. The scatter in the product yield data reported by Hummel and Hearne [3] is however unusually high, if one considers the reproducibility of the dose per pulse delivered by the 706 Febetron (see Experimental Procedure of Ref. [19]).

In the last row of table 1 we presented a typical product distribution observed in the radiolysis of CH_4 at the relatively low dose rates provided by a 3 MeV Van de Graaff electron accelerator. In certain other low dose rate studies which were carried out at extremely low doses, higher ion pair yields of ethylene (up to 0.2) have been obtained than in the example given, but in all of the published investigations the ion pair yield of acetylene in pure methane was found to be no higher than 0.07.

Figure 2 shows the effect of pressure on the product yields obtained with the 705 Febetron (60–100 ns). The samples were exposed to only one pulse.

The effect of electron scavengers, SF_6 and CD_3I, and free radical scavengers, O_2 and NO, on the products was explored. The CH_4-SF_6 and CH_4-CD_3I experiments were performed with a 705 Febetron, while the CH_4-O_2 and CH_4-NO experiments were carried out with the 706 Febetron. The electron scavengers inhibit the formation of acetylene, allene, and propyne and increase the yield of ethylene. A threefold increase of the pressure of SF_6 has no noticeable effect on the product yields, while an increase of the pressure of CD_3I raises the yield of ethane. The free radical scavengers, oxygen and nitric oxide diminish the yields of essentially all products. The effect on the production of acetylene and ethylene is however much less

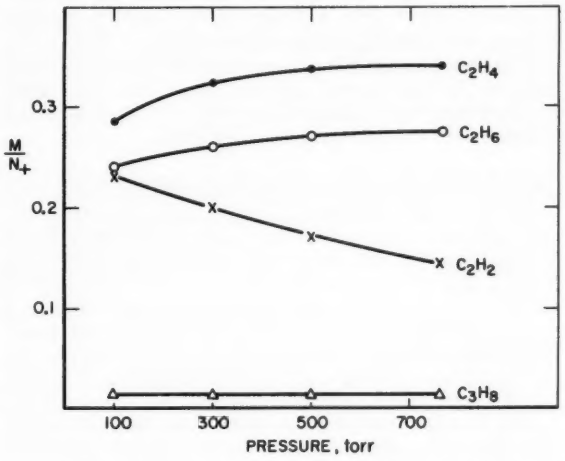

FIGURE 2. *Ion pair yields of* C_2H_4, C_2H_6, C_2H_2, *and* C_3H_8 *formed in methane by one* 3.3×10^{19} *eV/g pulse of* 60–100 ns *duration, as a function of pressure.*

pronounced than on that of ethane and propane. An increase in the number of pulses from 1 to 4 had no noticeable effect on the product yields produced in the pulse radiolysis of the $CH_4 - O_2$ or $CH_4 - NO$ mixtures. Product yields reported in a conventional NO scavenged radiolysis experiment carried out with a 3 MeV Van de Graaff electron accelerator are included in table 2 for comparison.

3.2. Deuterium Labeling Experiments

We determined the isotopic composition and ion pair yields of the hydrogen formed in the pulse radiolysis (dose/pulse: 0.68×10^{19} eV/g, pulse duration 60–100 ns, total pressure: 300 torr) of CH_4-CD_4 (1:1) mixture in the presence and absence of SF_6. These results are represented in table 3. Because of their complexity, the isotopic compositions of the ethane formed in these experiments could not be established. They were however quite similar to those obtained in low dose rate experiments. In contrast, the mass spectrum of the ethane fraction formed in the pulse radiolysis of a CH_4-CD_4-NO (1:1:0.06) mixture was easy to interpret. The small contributions of

TABLE 2. *Effect of electron and free radical scavengers*

Duration of pulse ns	Dose/pulse eV/g × 10^{-19}	CH_4 pressure, torr	additive	C_2H_2	C_2H_4	C_2H_6	C_3H_4	C_3H_6	C_3H_8
				Molecules per Ion Pair (M/N_+)					
60	0.68	300		0.205	0.420	0.202	0.010	0.029	0.008
60	0.68	300	SF_6 − 3.0	.028	.575	.333	.002	.033	.025
60	3.3	100		.240	.286	.241	.011	.021	.016
60	3.3	100	SF_6 − 1.0	.034	.623	.261	.004	.027	.017
60	3.3	100	SF_6 − 3.2	.034	.651	.295	.003	.026	.018
60	3.3	300		.195	.305	.245	.010	.022	.016
60	3.3	300	CD_3I − 1.0	.042	.424	.744	.001	.018	.039
60	3.3	300	CD_3I − 3.6	.042	.479	1.11	.001	.015	.048
Low Dose Rate [a]		731	NO − 7		.190	.043		.011	.008

[a] Reference [26].

C_2D_5H, C_2DH_5, and $C_2D_3H_3$ found in the ethane fraction (C_2D_6 − 22%, C_2D_5H − 2%, $C_2D_4H_2$ − 23.5%, $C_2D_3H_3$ − 2.7%, $C_2D_2H_4$ − 22%, C_2DH_5 − 2%, C_2H_6 − 25.8%) shows that 3 mol percent NO scavenged the majority of the methyl radicals under the conditions of this experiment (dose/pulse: 0.83 × 10^{19} eV/g, pulse duration 3–5 ns, total pressure: 500 torr).

TABLE 3. *Radiolysis of* $CH_4 - CD_4$ (1:1). *The formation of hydrogen*

	Methane pressure	Additive (torr)	H_2	HD	D_2
			M/N_+		
Pulse radiolysis (60–100 ns).	300		0.67	0.36	0.44
	300	SF_6, 3	.57	.23	.37
(Difference)			.10	.13	.07
^{60}Co-Gamma radiolysis	39	NO, 0.06	.45	.20	.36

The isotopic composition of the hydrogen formed in the pulse radiolysis of $CH_4 - CD_4$ (1:1) both in the presence and absence of SF_6 is given in table 3. The total yield of hydrogen was within 5 percent independent of pulse duration (3–100 ns) and dose (0.78–15.2 eV/g × 10^{19}).

4. Discussion

4.1. Formation of Products in the Pulse Radiolysis of Methane

Before beginning our discussion of the specific modes of product formation in irradiated methane, it is useful to summarize the major processes which are known to occur in this system. Products will, of course, originate from the dissociation of the parent CH_4^+ ion, i.e.:

$$CH_4^+ \rightarrow CH_3^+ + H \tag{1}$$

from ion-molecule reactions [1] such as:

$$CH_3^+ + CH_4 \rightarrow C_2H_5^+ + H_2 \tag{2}$$

$$CH_4^+ + CH_4 \rightarrow CH_5^+ + CH_3 \tag{3}$$

and from the neutralization of positive ions [7]. (The CH_4^+ and CH_3^+ ions comprise at least 90 percent of the initially formed positive ions in methane; CH_2^+ may be formed but in small yield.) Since ion-molecule reactions 2 and 3 occur at essentially every collision, the major ions which will undergo neutralization in methane at high dose rates (where reaction with impurities or accumulated products can not compete with neutralization) will be $C_2H_5^+$, which is neutralize according to the mechanism:

$$C_2H_5^+ + e \rightarrow [C_2H_4]^* + H \rightarrow C_2H_2 + H_2 + H \tag{4}$$

and CH_5^+ whose neutralization mechanism is unknown. We will present evidence in this paper that CH_5^+ is neutralized to give mainly methane and an H atom:

$$CH_5^+ + e \rightarrow CH_4 + H. \tag{5}$$

In addition to these ionic processes, products formed in irradiated methane will originate from the decomposition of neutral excited methane molecules [1]:

$$CH_4^* \rightarrow CH_2 + H_2\ (2H) \tag{6}$$

$$\rightarrow CH + H + H_2\ (2H) \tag{7}$$

$$\rightarrow C + H_2\ (2H) + H_2\ (2H) \tag{8}$$

and from the subsequent reactions of the radical intermediates formed in dissociation reactions 6 through 8 as well as in reactions such as 1, 3, 4 and 5. (We exclude from this discussion product formation through reaction with accumulated products.) The prediction of the modes of reaction of these radical intermediates is complicated by the fact that we do not know in which excited states they may be formed. For instance CH_2 may be formed [14] in the ground $\tilde{X}^3\sum_g$ state, which is unreactive with methane, in the lowest singlet state, $\tilde{a}\,^1A_1$, which will insert into methane [15]:

$$^1CH_2 + CH_4 \rightarrow (C_2H_6)^* \begin{matrix} \rightarrow 2CH_3 \\ \underrightarrow{M}\ C_2H_6 \end{matrix} \tag{9}$$

as well as undergo conversion to the triplet upon collision with methane [16]:

$$^1CH_2 + CH_4 \rightarrow {}^3CH_2 + CH_4 \quad (10)$$

or in a higher excited state [17] such as $\tilde{b}\ ^1B_1$ or $\tilde{c}\ ^1A_1$ whose reactions with methane are unknown. It is not inconceivable that these excited species undergo some reaction other than reaction (9), possibly H atom abstraction. Similarly, the CH species from reaction (7) is formed [17] not only in the ground $X^2\pi$ state, but also in the $A^2\Delta$ and $B^2\ \Sigma^-$ states. It has been shown that some of the ethylene formed in irradiated methane originates in a reaction in which a CH species inserts into methane [18]:

$$CH + CH_4 \rightarrow C_2H_4 + H. \quad (11)$$

The ground state CH does undergo reaction (11), but the reactions of the excited CH species are unknown. Finally, the C atoms may be in the unreactive ^3P state, or in the ^1S or ^1D states. It has recently been demonstrated that the insertion of C atoms into methane results in the formation of acetylene [7]:

$$C(^1S \text{ or } ^1D) + CH_4 \rightarrow C_2H_2 + H_2. \quad (12)$$

It is interesting to consider the various intermediate species generated in methane in terms of their lifetimes in the pulsed system. As mentioned before, it is to be expected that the primary ions will react at the first collision to give CH_5^+ and $C_2H_5^+$, most of which, under our conditions will be neutralized (reactions 4 and 5) during the duration of the pulse, generating H atoms and stable product molecules. At least some of the $^1CH_2$, CH, and ^1C species (depending on the electronic state, as discussed above) will disappear by reaction with methane at essentially every collision (through reactions 9–12), so these species also will have effectively disappeared by the end of the pulse. On the other hand, the H atoms, methyl radicals, and the triplet CH_2 species, do not react to any appreciable extent with methane under these conditions, and therefore will survive in the system until they encounter a species with which they can react. This means that we should expect to see reactions among these long-lived intermediate species as major sources of product formation.

Unfortunately, it is difficult to accurately predict the yields of the long-lived H, CH_3, and triplet CH_2 species, so a quantitative unraveling of all the mechanisms of product formation in the pulse radiolysis of methane is not actually feasible at the present time. Although the yields and reactions of the ionic species are well understood, the initial yield of excited CH_4 can only be estimated in a rough way.

We can, however, predict that most H atoms will combine with polyatomic radicals, mostly CH_3:

$$H + CH_3 \rightarrow CH_4^* \quad (13)$$

$$CH_4^* + M \rightarrow CH_4 + M \quad (14)$$

H–H recombination will be very slow because of the third body requirement and will not effectively compete with reaction with polyatomic radicals as long as such species remain in the system. The occurrence of reaction (13) as the most probable fate of H atoms on the pulse radiolysis of neopentane has been demonstrated [19]. That reaction (13) is important in this system is qualitatively confirmed by the results of experiments in which the yield of H atoms is reduced. It has recently been shown [7] that the addition of SF_6 as an electron scavenger in the pulse radiolysis of methane eliminates reaction (4) as a source of ethylene and H atoms, probably through the occurrence of a reaction such as:

$$C_2H_5^+ + SF_6^- \rightarrow C_2H_4 + HF + SF_5. \quad (15)$$

Thus, in the presence of SF_6, a major source of H atom formation is eliminated. Under these conditions, the yield of ethane is increased (table 2) because of the increased importance of methyl-methyl combination:

$$CH_3 + CH_3 \rightarrow C_2H_6. \quad (16)$$

The same interpretation explains the fact that in the low dose rate radiolysis of methane (where neutralization processes 4 and 5 will not occur to any appreciable extent, and where the steady state concentration of H atoms will be much lower, so that diffusion to the wall and recombination there to form H_2 will be much more important), the yield of ethane and hydrogen is much higher than in the pulse radiolysis experiments. It is difficult to explain the high ethane yields obtained in a recent pulse radiolysis study [3], which, fortuitously, agreed with the low dose rate ethane yield.

4.2. The Formation of Ethylene and Acetylene Products

As discussed above, it is expected that ethylene and acetylene should be formed in the radiolysis of methane under high dose rate conditions [7] from the neutralization of the ethyl ion according to reaction (4), as well as from reaction (11) (ethylene formation) and reaction (12) (acetylene formation). Also, it is possible that other sources of these products exist, for instance, reactions of excited CH_2 species with methane, or reactions of triplet CH_2 with other radicals. There is actually some experimental evidence for the formation of ethylene from a reaction involving triplet CH_2 (which is unreactive with methane) and methyl radicals. In one experiment, CD_3I was added to methane as an electron and H atom scavenger:

$$CD_3I + H \rightarrow CD_3 + HI \quad (17)$$

$$CD_3I + e \rightarrow CD_3 + I^-. \quad (18)$$

In this experiment, it was seen that about 15 percent of the ethylene consisted of $C_2D_2H_2$ and C_2D_3H, formed in a ratio of 4.3:1. This demonstrates that some reaction involving methyl radicals contributes to ethylene formation. A plausible reaction is:

$$^3CH_2 + CD_3 \rightarrow (C_2D_3H_2)^* \begin{matrix} \rightarrow C_2D_2H_2 + D \\ \rightarrow C_2D_3H + H. \end{matrix} \quad (19)$$

An isotopic analysis of the ethane formed in this experiment indicated that the ratio of CH_3 to CD_3 radicals was 2.38. Thus, if one accepts the occurrence of reaction 19, it can be estimated (table 2) that the ion pair yield of $^3CH_2$ reacting to give ethylene is about 0.1. It should be pointed out that this methyl radical reaction leading to ethylene formation is more plausible than the reaction suggested earlier [20]:

$$CH_3 + CH_3 \rightarrow C_2H_6^* \rightarrow C_2H_4 + H_2. \quad (20)$$

It is well known [21] that ethylene is not a product in systems where methyl radicals are the major intermediate reactants.

As pointed out before [7], the substantial reduction of the yield of acetylene on addition of electron scavengers such as SF_6 and CD_3I (table 2) can be accounted for by a change in the neutralization mechanism of the $C_2H_5^+$ ion (reactions 4 and 15). The reduction in the yield of acetylene observed when the pressure is increased (fig. 2) can at least in part be explained by the collisional deactivation of the ethylene precursor in reaction (4).

4.3. The Formation of Hydrogen Product

The most important sources of unscavengeable hydrogen in the radiolysis of methane [22] would be expected to be reactions (2) and probably (6–8), with additional contributions from reactions such as (12). In the high dose rate pulse radiolysis [7], an additional source of unscavengeable hydrogen will be the neutralization of the $C_2H_5^+$ ion through reaction (4). (As mentioned before, this ion will react with impurities or accumulated products before undergoing neutralization under low dose rate conditions [6].) However, if SF_6 is added to pulse-irradiated methane, the ethyl ion will be neutralized through reaction (15) and will not produce H_2 as a neutralization product. Since the other hydrogen-forming reactions would not be expected to be dependent on dose rate, it is not surprising that the isotopic distribution and total yield of the hydrogen produced in the low intensity gamma radiolysis [22] of a $CH_4 - CD_4$ (1:1) mixture in the presence of a radical scavenger (NO) is quite similar to that of the hydrogen produced in the pulse radiolysis of such a mixture in the presence of SF_6 (tab. 3). These distributions and yields are compared with those observed in the pulse radiolysis of a $CH_4 - CD_4$ mixture in the absence of added SF_6, where neutralization mechanism 4 would be expected to prevail. Although the drop in the total yield of hydrogen product (0.30) when SF_6 is added is somewhat larger than the corresponding drop in the yield of acetylene, i.e., the yield of reaction (4) in the absence of SF_6 (0.18), it should be remembered that H atom reactions may contribute to hydrogen formation to some extent in the absence of SF_6.

4.4. Neutralization of CH_5^+

As mentioned above, the neutralization mechanism of CH_5^+ has been a matter of speculation in the past. For instance, it has been suggested [23] that CH_5^+ neutralization results in the formation of CH_2 radicals:

$$CH_5^+ + e \rightarrow CH_2 + H_2 + H \quad (21)$$

The occurrence of this reaction to give three H atoms as products can be excluded on energetic grounds; this process would be 25 kcal/mol endothermic. However, the formation of CH_2 species in a neutralization reaction can be excluded entirely on the grounds that the yield of CH_2 species is the same in the pulse radiolysis (where CH_5^+ undergoes neutralization) as in the low dose rate radiolysis (where it does not). That is, the yield of stabilized ethane formed in CH_2 insertion reaction (9) is 0.054 in the low dose rate radiolysis of a methane – NO mixture at a pressure of 500 torr; the yield of this product in the pulse radiolysis of a $CH_4 - CD_4 - NO$ mixture (see Results) is 0.058. (The insertion product will consist of C_2D_6, $C_2D_4H_2$, $C_2H_4D_2$, and C_2H_6, as more than 90 percent of the ethane formed in this experiment did.) The occurrence of process (21) was suggested [23] on the basis of an analysis of C_5 product yields formed in the low dose rate radiolysis of CH_4 containing 10 percent 2-butene. In such a mixture, neutralization of CH_5^+ could not possibly compete with the fast exothermic proton transfer reaction:

$$CH_5^+ + C_4H_8 \rightarrow CH_4 + C_4H_9^+. \quad (22)$$

Another plausible neutralization process which CH_5^+ could undergo would be:

$$CH_5^+ + e \rightarrow CH_3 + H_2. \quad (23)$$

We cannot exclude the occurrence of this process on the basis of our results, but can conclude that this is not the major neutralization mechanism of this ion since the hydrogen which is formed in the pulse radiolysis can largely be accounted for by reactions (2, 4, 6–8), and 12). Also, if we consider that when SF_6 is added, the energy available to the neutralization process is reduced, and one generally observes a change in neutralization mechanism [7] (as seen for $C_2H_5^+$, reaction (4) being replaced by reaction (15)). Thus, it is pertinent that when SF_6 is added to methane (at a pressure of 300 torr), the total yield of hydrogen is reduced from 1.47 to 1.16, a drop of 0.31. Of this, 60 percent can be accounted for by the elimination of reaction (4) (as evidenced by the drop in the acetylene yield). Thus, the maximum yield which could be attributed to process (21) or (23) is 0.13 (i.e., not more than 30% of the CH_5^+). However, if one examines the isotopic distribution of the differential hydrogen, given in table 3, one notices that HD is the main component; such a distribution would be inconsistent with the loss of a molecule of hydrogen from the various

isotopically labeled CX_5^+ ions (where X is H or D). Even if we assume that SF_6 does not affect the occurrence of neutralization mechanism (23), we can say that the maximum yield which could be attributed to this process would be the difference between the hydrogen yield in the low dose rate radiolysis [22] of a CH_4—NO mixture (0.95) where neutralization processes do not contribute, and that observed in the pulse radiolysis in the presence of SF_6 (1.16), a difference of 0.21.

By elimination, then, we write as the most probable neutralization reaction of CH_5^+, process (5), the formation of an H atom and a methane molecule. It is interesting to note that the maximum amount of energy which can be contained in this product CH_4 molecule is 8.1 eV; this is about 0.4 eV below the onset for singlet-singlet excitation, so we may conclude that the CH_4 is excited to the triplet state (onset at 7.5 eV) or is a vibrationally excited ground state molecule. In the latter case, further dissociation would involve cleavage of a C-H bond.

4.5. Effect of Dose on the Product Yields

Figure 1 shows the yields of the ethylene, ethane, acetylene, propylene, and propane products formed in methane as a function of the total absorbed dose (number of pulses). It is seen that the yields of some of these products do change with the number of pulses. Additional results confirming this observation are given in table 1. Since this observation is in contradiction to results reported in a recent pulse radiolysis study of methane [3], the effect of dose on product yields merits some examination.

At the high dose rates and relatively low total dose used in pulse radiolysis studies, nearly all of the unreactive ions (mainly $C_2H_5^+$ and CH_5^+) formed in pure methane will undergo charge recombination, and will not survive long enough to undergo reactions with accumulated products, so this can be discounted as a possible source of the dose effects shown in figure 1 and table 1. On the other hand, it is to be expected that as the total dose is increased, accumulated products, especially ethylene, will begin to intercept H atoms formed in the system. In the low dose rate radiolysis of methane, the formation of propane and *n*-butane is ascribed [23–25] to the reaction sequence:

$$C_2H_4 + H \rightarrow C_2H_5 \tag{24}$$

$$C_2H_5 + CH_3 \rightarrow C_3H_8 \tag{25}$$

$$C_2H_5 + C_2H_5 \rightarrow n\text{-}C_4H_{10}. \tag{26}$$

The observed dose effects given in figure 1 and table 1 can in part be accounted for by the occurrence of this reaction sequence in the pulse radiolysis of methane. For instance, the yield of ethylene decreases with increasing dose, while the yield of propane increases (and the yield of *n*-butane increases also, but the total ion pair yield of this product was less than 0.01 so it has not been included in the figure). The fact that the increment in the yield of propane is less than the decrease in the yield of ethylene can be explained by the combination reaction

$$C_2H_5 + H \rightarrow C_2H_6. \tag{27}$$

Reaction (27) would also account in part for the increase in the yield of ethane with increasing dose. As mentioned before, the high concentration of free radicals in the pulse radiolysis experiments favors reactions such as (27) over the termolecular combination of H atoms [19].

$$H + H + M \rightarrow H_2 + M. \tag{28}$$

The inhibition of the formation of propane in the presence of a free radical scavenger such as NO is consistent with the formation of this product is a free radical reaction (reaction 25).

The lack of any noticeable effect of dose on $M(C_2H_2)/N_+$ can easily be explained, since the rate constant for the addition of H to C_2H_2 is nearly a factor of ten lower than that of reaction (24) [27]. Therefore, for a 30 percent decrease of $M(C_2H_4)/N_+$ as a function of dose (fig. 1) one can only expect an ~ 3 percent decrease of $M(C_2H_2)/N_+$. Although such a minor decrease would go unnoticed over this limited dose range it might account for the low yields of $M(C_2H_2)/N_+$ reported by Cahill et al. [2] (table 1) for their experiments performed at a relatively high total dose.

4.6. Pulse Radiolysis of CH_4—*i*-C_4D_{10} Mixtures

As discussed in the foregoing sections of this paper, the major change in the radiolytic mechanism of methane which occurs in going from low dose rate conditions (i.e., gamma radiolysis) to high dose rate conditions (pulse radiolysis) is the change in the fate of the two major ions in the system, $C_2H_5^+$ and CH_5^+. At low dose rates, the steady state concentration of electrons is low, and the ions, consequently, will survive many collisions before undergoing neutralization (at one atmosphere and a dose rate such that 10^{10}-ions/s-ml are formed, it can be estimated that these ions would undergo 10^5 to 10^6 collisions before being neutralized), and consequently will have ample opportunity to react with accumulated products or any other foreign compounds which may be present in small concentrations. This was illustrated in an earlier radiolysis study [6], where it was shown that at a dose rate of 4×10^{17} eV/g-s, addition of 0.01 mol percent propane resulted in the interception of all $C_2H_5^+$ and CH_5^+ ions, through the reactions:

$$C_2H_5^+ + C_3H_8 \rightarrow C_2H_6 + C_3H_7^+ \tag{29}$$

$$CH_5^+ + C_3H_8 \rightarrow (C_3H_9^+)^* + CH_4. \tag{30}$$

Reactions of this type were shown [6] to be of general occurrence for all higher hydrocarbon additives. (This was later confirmed mass spectrometrically [28–31]; the occurrence of such ion molecule reactions in gas mixtures in high pressure mass spectrometers now finds application as an analytical technique called

"chemical ionization mass spectrometry".)

At high dose rates, on the other hand, the $C_2H_5^+$ and CH_5^+ will undergo neutralization before being able to react with small amounts of foreign compounds. In a recent pulse radiolysis study [8], the rate of neturalization of unreactive ions (*t*-butyl ions in neopentane) was examined by allowing the neutralization process to compete with a reaction between the ion and a reactive additive. In this section we report the results of similar experiments in methane, in which the neutralization of $C_2H_5^+$ and CH_5^+ competes with their reactions with isobutane-d_{10}:

$$C_2H_5^+ + i\text{-}C_4D_{10} \rightarrow C_2H_5D + C_4D_9^+ \quad (31)$$

$$CH_5^+ + i\text{-}C_4D_{10} \rightarrow (C_4D_{10}H^+)^* + CH_4 \quad (32)$$

$$(C_4D_{10}H^+)^* \rightarrow CD_3H + C_3D_7^+ \quad (33)$$

$$C_3D_7^+ + i\text{-}C_4D_{10} \rightarrow C_3D_8 + C_4D_9^+. \quad (34)$$

At low dose rates [6], where every $C_2H_5^+$ ion can be expected to undergo reaction (31), the ion pair yield of C_2H_5D observed in a $CH_4-i\text{-}C_4D_{10}$ mixture (at a total sample pressure of 460 torr) was 0.32. The CH_5^+ ions reacting with $i\text{-}C_4D_{10}$ will lead mainly to the formation of C_3D_8 as a neutral product through reactions (33) and (34) (although a fraction of the $C_4D_{10}H^+$ ions formed in reaction (32) undergo fragmentation reactions other than (33)); under low dose rate conditions [6], the observed ion pair yield of C_3D_8 was 0.36. At the highest dose rates used in that study (4×10^{17} eV/g-s), all the $C_2H_5^+$ and CH_5^+ ions were intercepted by the isobutane, as evidenced by the fact that the yields of C_2H_5D and C_3D_8 were independent of isobutane concentration from 0.01 to 1 mol percent.

Similar $CH_4-i\text{-}C_4D_{10}$ mixtures were irradiated here at high dose rates in the presence and absence of the electron scavenger, SF_6. As the results given in figure 3 show, neutralization does compete with reactions (31) and (32) under these conditions; not only are the yields of C_2H_5D and C_3D_8 strongly dependent on the concentration of $i\text{-}C_4D_{10}$ at high dose rates, but also, even at an isobutane concentration of 1 percent, the yields of these products are lower than the corresponding yields in the low dose rate radiolysis.

In order to evaluate these results, the yields of C_2H_5D and C_3D_8 which one would expect in these experiments were calculated using a modified WR-16 computer program [32]. In the calculation, reaction mechanism (31–34) was assumed to occur, and in addition it was assumed that $C_2H_5^+$, CH_5^+, $C_3D_7^+$ (formed in reaction (33)), and $C_4D_9^+$ (formed in reactions (31) and (34)) will undergo neutralization in competition with reaction. The neutralization rate constants for all these ions were assumed to be equal to those recently determined [8] for the *t*-butyl ion; that is, the rate constant for neutralization by an electron was taken to be 1.9×10^{-6} cm^3/molecule-s, while that for neutralization by SF_6^- (for experiments in the presence of SF_6) was taken to be 0.4×10^{-6}. In the presence of SF_6, a calculation indicates that more than 99 percent of the electrons will attach to SF_6 to form SF_6^-, taking a rate constant of 2.6×10^{-7} cm^3/molecule-s for thermal electron attachment [33–34]. The rate constants for the ion-molecule reactions (31) and (34) were taken to be 0.7×10^{-9} cm^3/molecule-s and 0.33×10^{-9} cm^3/molecule-s respectively [35–36]. Reaction (32) was assumed to occur at every collision ($k_{30}=1.1\times10^{-9}$ cm^3/molecule-s). Finally it was assumed that the $(C_4D_{10}H^+)$ species formed in reaction (32) does not survive long enough to be neutralized.

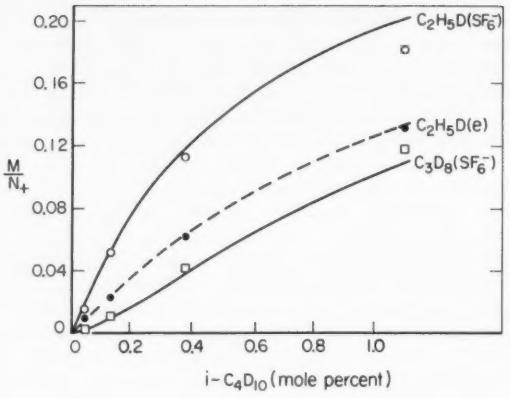

FIGURE 3. *Ion pair yields of* C_2H_5D *formed in* 300 *torr of methane to which various concentrations of* $i\text{-}C_4D_{10}$ *have been added, in the absence and presence of* SF_6*, and the yield of* C_3D_8 *in the presence of* SF_6.

Dose/pulse = 3.3×10^{19} eV/g. Lines represent yields of these products predicted by by calculation (see Discussion).

The yields of C_2H_5D and C_3D_8 predicted by these calculations are shown by the lines in figure 3. (The yield of C_3D_8 was not measured in the absence of SF_6 so this line has not been given in the plot.) Considering the fact that the mechanism here is fairly complicated, and several assumptions or approximations had to be made in the calculations (i.e., the lifetime of $(C_4D_{10}H^+)^*$, the neutralization rate constants, the rate constant of reaction (32)), the calculations predict the observed yields of C_2H_5D and C_3D_8 as a function of $i\text{-}C_4D_{10}$ concentration remarkably well. This indicates that the neutralization rate constants of these ions probably are not much different from those determined [8] for the neutralization of the *t*-butyl ion.

It is interesting that the calculation actually predicts the observed slight *s*-shaped curvature of the plot of C_3D_8 yield as a function of $i\text{-}C_4D_{10}$ concentration (fig. 3).

5. References and Note

[1] For a review up to 1968 see: Meisels, G. G., in Fundamental Processes in Radiation Chemistry, P. Ausloos, Editor (Interscience, N.Y., 1968).

[2] Cahill, R. W., Seeler, A. K., and Glass, R. A., J. Phys. Chem. **71**, 4564 (1967).

[3] Hummel, R. W., and Hearne, J. A., J. Phys. Chem. **75**, 1164 (1971).

[4] Meaburn, G. M., and Perner, D., Nature **212,** 1042 (1966).
[5] Bosnali, M. W., and Perner, D., Z. Naturforsch **26a,** 1768 (1971).
[6] Ausloos, P., Lias, S. G., and Gorden, R., Jr., J. Chem. Phys. **39,** 3341 (1963).
[7] Rebbert, R. E., and Ausloos, P., J. Res. Nat. Bur. Stand. (U.S.), **77A** (Phys. and Chem.), No. 1, 109–114 (Jan.-Feb. 1973).
[8] Lias, S. G., Rebbert, R. E., and Ausloos, P., J. Chem. Phys. **57,** 2080 (1972).
[9] "Certain commercial equipment, instruments, or materials are identified in this paper in order to adequately specify the experimental procedure. In no case does such identification imply recommendation or endorsement by the National Bureau of Standards, nor does it imply that the material or equipment identified is necessarily the best available for the purpose."
[10] Willis, C., Miller, O. A., Rothwell, A. E., and Boyd, A. W., Advan. in Chem. Ser. **81,** 539 (1968).
[11] Willis, C., Boyd, A. W., and Miller, O. A., Radiat. Res. **46,** 428 (1971).
[12] Berger, M. J., and Seltzer, S. M., NASA Report SP-3012 (1964).
[13] Klots, C. E., Energy Deposition Processes, Chapter 1 in Fundamental Processes in Radiation Chemistry, P. Ausloos, Editor (Interscience, N.Y., 1968).
[14] Herzberg, G., Molecular Spectra and Molecular Structure (D. Van Nostrand Co., Inc., Princeton, New Jersey, 1967).
[15] Ausloos, P., Gorden, R., Jr., and Lias, S. G., J. Chem. Phys. **40,** 1854 (1964).
[16] Braun, W., Bass, A. M., and Pilling, M., J. Chem. Phys. **52,** 5131 (1970).
[17] Welch, A. R., and Judge, D. L., J. Chem. Phys. **57,** 286 (1972).
[18] Gorden, R., Jr., and Ausloos, P., J. Chem. Phys. **46,** 4823 (1967).
[19] Rebbert, R. E., and Ausloos, P., J. Res. Nat. Bur. Stand. (U.S.), **76A** (Phys. and Chem.), No. 4, 329–336 (July–Aug. 1972).
[20] Hummel, R. W., Int. J. Radiat. Phys. Chem. **2,** 119 (1970).
[21] Steacie, E. W. R., Atomic and Free Radical Reactions (Reinhold, New York, 1954).
[22] Ausloos, P., and Lias, S. G., J. Chem. Phys. **38,** 2207 (1963).
[23] Hummel, R. W., Int. J. Radiat. Phys. Chem. **2,** 31 (1970).
[24] Ausloos, P., Gorden, R., Jr., and Lias, S. G., J. Chem. Phys. **40,** 1854 (1964).
[25] Yang, K., and Manno, P., J. Amer. Chem. Soc. **81,** 3507 (1959).
[26] Sieck L. W., and Johnsen, R. H., J. Phys. Chem. **67,** 2281 (1963).
[27] Cowfer, J. A., Keil, D. G., Michael, J. V., and Yeh, C., J. Phys. Chem. **75,** 1584 (1971) and references cited therein.
[28] Munson, M. S. B., Field, F. H., and Franklin, J. L., J. Chem. Phys. **42,** 442 (1965).
[29] Munson, M. S. B., and Field, F. H., J. Amer. Chem. Soc. **87,** 3294 (1965).
[30] Haynes R. M., and Kebarle, P., J. Chem. Phys. **45,** 3899 (1966).
[31] Munson, M. S. B., and Field, F. H., J. Amer. Chem. Soc. **91,** 3413 (1969).
[3] Schmidt, K. H., AEC Research and Development Report NAL–7199 (1969).
[33] Davis, F. J., and Nelson, D. R., Chem. Phys. Letters **3,** 461 (1969).
[34] Mothes, K. G., and Schindler, R. N., Ber. Bunsenges fur Phys. Chemie **75,** 938 (1971).
[35] Munson, M. S. B., J. Phys. Chem. **71,** 3966 (1967).
[36] Sieck, L. W., Searles, S. K., and Ausloos, P., J. Res. Nat. Bur. Stand.) (U.S.), **75A** (Phys. and Chem.), No. 3, 147–153 (May–June 1971).

(Paper 77A1–768)

JOURNAL OF RESEARCH of the National Bureau of Standards—A. Physics and Chemistry
Vol. 77A, No. 2, January–February 1973

Relation of Vitron Theory to 2-Layer-Liquid Immiscibility in Binary Silicate and Borate Glass Melts*

Leroy W. Tilton**

(August 1, 1972)

Silica-rich and boron-rich binary glasses resemble clathrates in having host cavities in which modifier oxides may be inclosed without stress as inactive guests until the cavities are approximately filled. Additional modification results in stress both in the holes of the matrix and the cavities of vitrons. Then the structure begins to disintegrate and mixing takes place. The required mole-percent modification is expressed by an equation of the form

$$100r_h=\frac{100(A-\alpha)\cdot q/5}{(L-\delta-\alpha)+(A-\alpha)\cdot q/5} \tag{4}$$

where A and α are the diameters of vitron cavity and matrix hole, respectively, L is the linear extent of a modifier, and q the proportion of glass-maker that forms vitrons. Computations for 66 glasses have been made to constitute a unified system covering approximately the gamut of typical modifiers.

The identity of parameters A and α for silicates and borates leads to the suggestion that the vitron structure in boric-oxide glass is the regular icosahedron of 20 triangular faces to accommodate a neutral molecule of $(B_4O_6)_5$. Regular octahedra of $(B_4O_6)_2$, if present in the matrix, would provide matrix holes of approximately α in diameter.

Key words: Binary borates; binary silicates; boron glass; glass; homogenization of glass melts; immiscible glass melts; immiscibility gaps; silica glass; structure of glass; vitron theory.

1. Introduction

These studies of glass were made in part several years ago and brief references to some of the results were mentioned in a summary of vitron theory published in 1963 [12g].[1] Meanwhile Levin [5, 28, 37] and co-workers at the National Bureau of Standards had continued their classic reports in the field of glass immiscibility (2-layer liquid type) according to the random-network theory of glass. It was not readily evident how such divergent views of glass structure could lead, almost without exception, to satisfactory agreements in the computation of degree of modification for the termination of immiscibility in binary silicates and borates when the modifiers were known to be mono- and divalent oxides. Also, until certain recent publications on rare-earth oxides, it seemed impossible to understand how unsatisfactory results appeared to follow in many cases when the modifiers were trivalent.

Delay, however, has led to clarification of vitron theory. Now, in the language of a certain class of nonstoichiometric substances, it is possible to consider silica-rich and borate-rich binary melts as similar to clathrates, or huge molecules within which one type of cage structure imprisons smaller unionized and therefore inert molecules. In silicate glass the guest molecules, or modifying oxides, are imprisoned in the dodecahedral host cavities or vitrons of the silica structure. These vitron cavities are similar to the dodecahedral cavities of liquid hydrates [36].

Silica-rich glass also has additional and smaller (distorted) holes predominantly of a tetrahedral nature within the matrix silica. The holes are considered as bounded by four faces each formed of rings of four, five, or six silicon-oxygen tetrahedra.

As usual in clathrates, host and guest show little or no mutual reaction whether or not they are otherwise compatible. In other words, the forces existing between host and guest molecules are not specifically chemical in nature but only of a general type.

It now becomes clear that only a definite structure theory can apply to glass-former-rich glasses, and only a random theory can cope with conditions after the structure is in great measure destroyed. This dual aspect of the structure of glass was not earlier appreci-

*Vitron theory relates only to the short-range order in glasses and glass melts that distinguishes glass from crystal and is not concerned with submicroscopic but relatively gross heterogeneities that are currently being studied in complex glasses or in simple binaries that contain even small percentages of homogenizers.

**An invited paper. The author was formerly a member of the staff of the Optics Section, National Bureau of Standards, Washington, D.C. Present address: 300 Ocean Avenue, A-41, Ocean City, N.J. 08226.

[1] Figures in brackets indicate the literature references at the end of this paper.

ated because most experimental processes in the glass field took place on melts that were well modified. Complete modification now is interpreted as meaning melts in which structure has been destroyed or is fine grained.

Furthermore, it is now understandable how the destruction is so early produced by large oxide molecules like the alkalies, whereas it can be so long delayed by using only small alkaline earths as modifiers. Were it not for the use of homogenizers like Al_2O_3 the practical range of vitron theory would extend to higher modifications and perhaps would have been accepted more readily.

The tremendous change that takes place during silicate glass making is the breakup of tenacious structure. This is evidenced by the rapid and extensive fall in liquidus temperature when and as modification progresses. During borate glass modification the major change may be the replacement of a relatively weakly connected molecular structure by one with stronger network, and the rise in liquidus temperature is the evidence.

Vitron theory is applicable chiefly to the range from unmodified glass-former glass to the composition at which the liquidus ceases to be horizontal or ceases to show a continuing tendency thereto. Although this is a very restricted region if only large modifiers are used, it becomes a wide one whenever modification is solely dependent on small alkaline earths. Similarly, *random-network theory* applies principally from that degree of modification where the liquidus completes its first small but rapid rise beyond the eutectic and extends into the region where compounds are formed.

Inbetween lies the important and complex region of glass formation where either or both theories may be helpful. This glass-formation region is often narrow, and more so the wider the vitron region.

Thus, the two theories are complementary rather than antagonistic, and it seems reasonable that boundary conditions, such as the incidence of miscibility, may be predictable from a proper understanding of conditions on either side of the boundary. Also, definite understanding of the modification process should help in the prediction of glass properties and minimize repeated trials in the design and production of glasses suitable for specific purposes.

After Greig [1] in 1927 defined the extent of immiscibility in some simple silicate systems, Kracek [2] combined in a single provocative illustration the silica-rich portions of the temperature-composition curves in the phase diagrams of the alkaline-earth and alkali silicates. He announced that on a mole-percent basis decreasing extent of immiscibility (or a tendency thereto) followed the order of basicity of the modifier oxides. It is herein shown that one can equally well say that it follows the order of maximum linear extension of the oxides. Figure 1 shows Kracek's curves as modified and republished by Levin and Block in 1957 [5].

Warren and Pincus [3] used bonding energies, Z/r, where r = radius of cation, and also used some geometrical ideas from infinite network theory in computing reasonable values for the approximate limiting compositions of immiscibility in some silicate glasses, but Deitzel [4] favored $Z/(r_1+r_2)^2$ for expressing the limits.

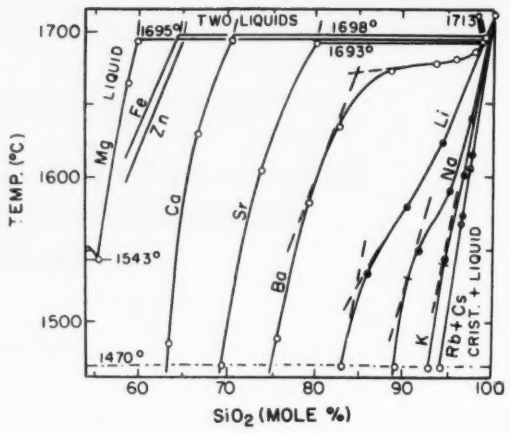

FIGURE 1. *Cristobalite melting-point curves, mostly after Kracek* [2].
Tangents to alkali silicate S-shaped liquidus curves indicate compositions of postulated metastable modifier-rich liquids. This diagram is unexcelled as an introduction to the study of structure and 2-liquid immiscibility in silicate glasses. (Reproduced as modified by Levin and Block [5]).

Levin and Block [5] extended the work of Warren and Pincus and applied crystal chemistry in using not only valence and ionic radii but also coordination number for meticulously and successfully computing limiting compositions of immiscibilities for both silicate and borate glasses.

It was suggested by Glasser, Warshaw, and Roy [6] that the limiting compositions could best be computed by use of Z/r with the introduction of a suitable "valence correction."

The investigators mentioned used chiefly concepts of the random-network theory of the structure of glass. Meanwhile, Preston [7] disagreed with the ideas and interpretations given by Warren and Pincus. He stated that immiscibility is plausibly due to segregations of different types of structure. This last idea, of course, is logically inferable because in all immiscible silicate melts positive departures from ideality are shown by the liquidus curves. Esin [8] concluded that microheterogeneous structure in liquid silicates was consistent with observed experimental tendencies in immiscibility, surface tension, electrical conductivity, and viscosity.

Relative to this is the work of Forland [9] who studied freezing point depressions and found a remarkably low value of 0.93 units for the entropy of fusion of silica and concluded that "at the melting point the liquid state has almost as much order as the solid state." He states that SiO_2 must have a highly ordered and inflexible structure. "By mixing into it a second oxide, this oxide has to be incorporated without major disturbances in the structure . . . This property of liquid SiO_2 seems to cause the formation of certain groups in the liquid and may be the cause of the liquid immiscibility in some silicate systems."

An important principle that was noticed and announced early in the course of vitron study was the existence of a modificational threshold for ionization in glasses. A strong note in favor of delayed ionization was sounded by R. W. Douglas [17] at the conference on noncrystalline solids at Alfred, New York, in 1958 when he said concerning positive departures from ideality and immiscibilities in silica-rich binary silicates: "This clearly indicates that the ionization of the network-modifying oxides is incomplete . . ." In retrospect, it can be realized that the electrical experiments on which ionization theory [16] rests do not show that the theory can extend with equal validity to *low degrees* of modification.

Moreover, it has been reported [20] that the thermal expansion of alkali silicate melts increases very sharply when alkali content exceeds 12 ± 2 mole percent. White [21], in particular, recognized this as "the first direct proof that a fundamental change in liquid (alkali) silicates occurs near 12 percent R_2O." For the alkaline-earth silicates the corresponding percentages for onset of "typically ionic" thermal expansion can be estimated from the curves of Tomlinson [22] et al. (their fig. 4 reproduced here as fig. 2). For BaO the modification is certainly as high as 15 percent before expansion begins in quantity; for SrO, CaO, and MgO it may be inferred that the percentage modification at incidence is near or above 20, 29, and 40 percent, respectively.

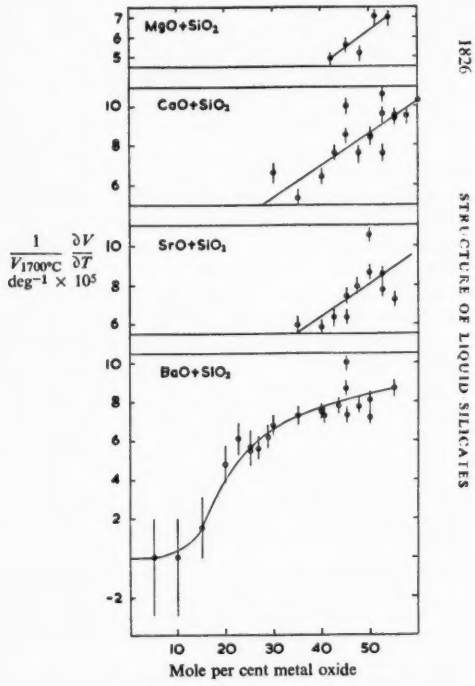

FIGURE 2. *Expansivity curves published by Tomlinson et al.* [22].
One may infer that typically ionic thermal expansion begins in quantity for alkaline-earth binary silicates at or above modifications of 15, 20, 29, and 40 mole percent, where vitrons begin to disintegrate.

Regardless of evidence, many investigators of silicate glasses still accept not only the conventional idea that modifier *cations* enter the "voids" but also the idea that the oxygens enter the network itself by the immediate "breaking of oxygen bridges" between network silicon and oxygen.[2] Furthermore it has been assumed, according to the uniform random-network theory, that the voids in glass are more or less of one average size.

In contrast, the writer [12] developed the vitron theory according to which silica glass itself is a composite of 0.305 "vitron" having nearly regular pentagonal dodecahedral cavities and 0.695 matrix having much smaller and irregular (probably roughly tetrahedral) holes.[3] The structure in each case is basically of connected silicon-oxygen tetrahedra, but whereas the vitron portion has the definite (but slightly distorted) structure of pentagonal dodecahedra (as evidenced by the *peaks* on the various radial distribution curves) the denser matrix corresponds to the general blurred background of the scattering in the x-ray diffraction patterns. Thus, the matrix may have rings other than penta and considerable variation in the Si–O–Si angles, and perhaps in the shape of matrix holes which are predominantly very small as compared with the vitron cavities.

Obviously the Si–O–Si angles in such a dual silica cannot be comprehensively determined by x-rays. The characteristics of only the vitron or regular portion can be measured and here the evidence is consistent with the assumption of 180° as originally made by Warren [13] for a nearly unstressed high-temperature condition in tetrahedra.

These proposed vitrons are, from a structural viewpoint, somewhat similar to pseudonuclei more recently described in general terms by Bernal [14] for certain liquids and by Ginell [15] for the basis of his "asymetric cluster picture of glass structure."

From the volume proportion of vitron (computed density 1.986) in fused silica (density 2.203), one may compute (by additivity of specific volumes) a density of 2.31 for the matrix. This exceeds all values reported for the end product of the neutron irradiation of either quartz or vitreous silica and is about as dense as crystobalite in which the cavities might be able to include, at maximum, one oxygen atom. The matrix can be considered as the solvent in which the vitrons are immersed. The matrix probably has a melting range not far above 1700 °C, but silica vitrons may persist to temperatures above 2000 ° (see sec. 5). Internal stresses and small quantities of modifiers and impurities, say 0.5 percent, may reduce the matrix liquidus temperature by several degrees C.

[2] Interpenetration of cation and network was quantitatively discussed by Dietzel [10] in 1943 and by Dietzel and Sheybany [11] in 1948. On the conventional basis alone, they came to the less than satisfactory conclusion that 142 percent (sic) of the Li ions must be lost in the voids in silica-rich glasses in order to account in this way for the observed densities of the binary glasses. Vitron theory early suggested as an alternative that oxygen as well as cation can and does enter the voids.

[3] The volume proportion of vitron, i.e., the somewhat regular structure in silica glass, was first estimated graphically (see L. W. T. paper [12(e)], p. 16) from interpenetration data on alkali silicates as at least 28 percent. Later, from a vitron model and published immiscibility data on $SiO_2 \cdot MgO$, an independent and probably more reliable computation led to 30.5 percent vitron. (See L.W.T. paper [12(g)], p. 433.)

A probable structure for the matrix is a network of some rings of 6 and 7 tetrahedra in addition to the more probable penta rings. The Si–O–Si angles in this matrix are necessarily variable over a considerable range and probably considerably smaller than 180°. Perhaps the majority of holes in the matrix may be irregularly tetrahedral in form with the four distorted faces, each consisting, on average, of rings of 5 tetrahedra.[4] It is unlikely that many representative holes in the matrix can have both the spherical size to accommodate an oxygen atom and also the added linear dimension to accommodate any commonly used glass modifying oxide without serious stresses in the matrix network. In other words, BeO may be the only modifying oxide molecule small enough to enter freely into holes in the matrix.

The method used here in studying immiscibility is primarily geometrical in nature. The general question is simply: Can we compute how much oxide can be added to molten silica and remain so concealed and inclosed in vitron cavities that the silica-rich portion of the liquidus remains horizontal (or tends to be that way) until the vitron cavities are so reduced in residual capacity as to equal the matrix holes in their original capacity? To answer, it is necessary to evaluate or estimate:

(a) The vitron geometry and density. (See L.W.T. [12(b)] 1959.)
(b) The threshold for ionization. (See sec. 2, this paper.)
(c) Relative volumes of vitron and matrix. (See footnote 3, this paper.)
(d) The matrix geometry. (See footnote 3, this paper.)

In particular, the procedures make use of computations of the sizes of modifier oxides as compared with cavities in silica-rich and boron-rich glasses.

2. Maximum Extension of Glass Modifiers

In preliminary work on some silicates during this investigation of immiscibility, the concept of maximum individual oxide extension, L, at high temperatures was tried graphically as a measure of the effectiveness of each of a group of similar modifier oxide molecules in causing damaging stress when inclosed within vitron cavities. Later it was found that L is very satisfactory, but not perfect, for use in computing the termination of immiscibility in borates as well as in silicates. Some of the difficulties of precise computation are mentioned in connection with eq (3) in section 3.

L may be simply expressed as the sum of diameters of atoms for monovalent oxides R_2O and divalent oxide modifiers RO. That is, $L = (D_O + 2D_R)$ and $L = (D_O + D_R)$ respectively.

For R_2O_3 modifiers (not reduced at glass-processing temperatures), the diameter of the circumsphere is the corresponding maximum extension. If the radius of the cation is less than 1.10 Å, the maximum extension is constant at the diameter of a sphere that incloses the three touching oxygens, namely

$$L = 2r_O(1 + (2/3)\sqrt{3}) \qquad (1)$$

or 5.7 Å for $R_O = 1.32$ Å.

If trivalent cation radii are larger than approximately 0.85 Å, one must consider the overall cation extension. Each continues to touch 3 oxygens, but cannot touch the other cation. The cation centers lie on opposite sides of a central plane determined by the three oxygens. In such cases, the maximum cation extension becomes larger than the diameter for the circumsphere for the three touching oxygens, that is in excess of 5.7 Å, which is also the maximum inscribed sphere inside a vitron. Thus it appears that trivalent modifiers, acting as such, would not be of interest in 2-layer-liquid immiscibilities for silicate or borate glasses. Even single molecules of trivalent modifiers should produce some stress ionization and miscibility starting almost immediately if they can withstand high temperatures, and some of them are well known as homogenizers.

From eq (1) and discussion above it might be thought, as already indicated, that trivalent oxides (sesquioxides) would be of little interest in studies of immiscibility in silicates. On the contrary, immiscibilities have been reported for about as many sesquioxides as for all mono- and divalent oxides.

The highly refractory Al_2O_3 has a molecular size (maximum-extent) of 5.7 Å, which places it among oxides that have an S-shaped liquidus, a temperature-composition curve with a tendency toward metastable immiscibility terminating near 13 mole percent of modification. Experimentally, Aramaki and Roy [27] found only a nearly flat liquidus. No reports have been made of any immiscible liquids and the use of Al_2O_3 as an homogenizer is well known. A similar example is the strong glass former B_2O_3 which shows no 2-liquid layer in binary silicate melts.

A third trivalent oxide modifier of the same maximum extent, 5.7 Å, but different character is Fe_2O_3. In this case it is commonly said that the 2-liquid layer produced in the binary melt arises from FeO as the only modifier even though ferric iron was introduced and FeO is known to be of little stability in air.

A fourth trivalent oxide is Cr_2O_3 and here the results are somewhat ambiguous. This oxide also is said to be at least partially reduced at high temperatures. There is some discrepancy among experimental reports, but it seems probable that only one 2-liquid area of immiscibility is formed. The miscibility gap is usually labeled as that for Cr_2O_3, but the

[4] If the holes of the matrix have tetrahedral character and four faces of 5-ring tetrahedra each, there would be 0.8 SiO_2 per hole; if the faces are of 6 rings, there would be one SiO_2 per hole, and if of 7 rings there would be 1.2 SiO_2 per hole. Thus a group of 5 holes of the matrix would require about as much SiO_2 as is required for a vitron cage, namely 5 SiO_2. This estimate, of course, accords with the assumption made in constructing table 3 on p. 151 of L.W.T. paper [12(b)] for use with R_2O modifiers, namely that in miscible glasses the modifiers would be approximately uniformly distributed with respect to silica (whether in vitron or matrix). As a consequence, all the inferences that were drawn concerning numbers of R_2O molecules per vitron cavity at the "breaks" and special points on the curves of property versus composition that were discussed in former papers on vitron theory, are approximately as valid as would have been the case if said table 3 had been made with present ideas of the matrix and the value of $q = 0.305$ as the volume proportion of silica that forms vitrons.

gap itself is almost exactly that predicted by vitron theory for (CrO) in silicate melts and the same is true for borate melts.

The author of this paper suggests that similar partial reduction in the furnace in the course of glass melting has occurred when many other sesquioxides have been used as glass modifiers; that only one 2-liquid region is present in such cases in binary melts; and that the termination of the gap has usually been adequately determined but erroneously assigned to the sesquioxide that was used in the batch rather than to the divalent oxide (RO) to which it was partially reduced. Furthermore, it seems that numerous analyses of cation in glasses quenched from terminal conditions have been made without regard to its valence condition.

Indeed, one confirmatory experiment is of record, as published by Shafer and Suits [44] in which mention is made of a region of liquid immiscibility in the system $EuO-B_2O_3$ appearing to extend "to about 15 to 20% EuO." In a private communication, Shafer says: "After looking at some of our data again, I am convinced that compositions of 20–24% EuO could easily be within the immiscibility region." The best value for termination of the gap in "Eu_2O_3" is 26.7 mole percent, and the vitron prediction for (EuO) is 25.5 mole percent. The finding of this gap was a side issue in the Shafer-Suits paper, but they state: "All glass specimens were chemically analyzed for divalent europium, total europium, boron, and aluminum."

If large glass-forming quadrivalent oxides are used in silica-rich or boron-rich binary glasses, immiscibility cannot result because networks may interpenetrate or the sizes of the large oxides may be such that probably no one of them can be contained within an unstressed vitron wherein the maximum diameter of an inclosable sphere is only 5.7 Å. Nor does it seem probable that strong glass-former oxides would be reduced in the furnace to smaller modifier oxides that might enter silicate or borate glasses. These quadrivalent oxides are appreciably larger than SiO_2. Thus, they may be expected to form larger vitrons than does SiO_2 or B_2O_3, and have correspondingly larger holes in their matrices. It is interesting to surmise that some of the small modifiers would be completely miscible in large-cation quadrivalent glasses for the same reason that BeO is miscible in SiO_2.

Before announcing the above conclusions, it seemed advisable to place miscibility computations on a precise quantitative basis.

3. Equations for Limit of Immiscibility

As mentioned in the Introduction, glass maker-rich glasses are similar to clathrates within which one type of structure imprisons another. Immiscibility results if modifiers can be enclosed in the large cavities of vitrons but not in the small holes in the matrix. Ionization which induces miscibility begins in quantity only when the guests start to disrupt the host walls, either because of large guest size or their collective effect. In either case, ionization begins after it becomes about equally difficult for vitron or matrix to inclose an additional oxide molecule without significant stress and strain. This is called the condition of equal voids.

In an earlier paper (L.W.T. [12(g)] footnote, p. 433) N, the number of oxide molecules per cavity, was expressed as

$$N=5r/q(1-r) \qquad (2)$$

where q is the proportion of silica molecules available for the formation of vitrons at any proportion of modifier molecules, r, and 5 is the number of molecules of interior SiO_2 forming the walls of a vitron cavity (and thus not part of the walls of adjacent cavities or of the matrix). In other words, the number of cavities is $C=(1-r)(q/5)$. For computing the modification corresponding to any particular N, eq (2) is conveniently used as $r=(q/5)N/[1+(q/5)N]$.

The value of q can be determined from eq (2) if any pair of reliable corresponding values of N and r are available. For a modifier with sufficiently small cation, $N_{max}=13$ can be found from the known vitron geometry and a model consisting of 13 spheres representing oxygens in central packing—12 touching one at their center to form a loosely packed cluster in which the outer 12 do not necessarily touch each other. The three touching oxygens on each of 6 axes have a combined extension of 7.92 Å which exceeds the face-to-face distance within the vitron cavity, but protrudes insignificantly beyond the 7.8 Å diameter of the volume-equivalent sphere. The looseness of packing may provide space for small cations.

From the experimental data listed in this paper (table II), a few values of r_h for modifiers having small cations were plotted versus $(L-\alpha)$. Then a smoothed value of r_h for (GaO) was read from a smooth curve for use with N_h for (GaO) assuming that $N_h=N_{max}$.[5] From eq (2) the values $q=0.31$ for silicates and $q=0.38$ for borates were then obtained.

Precise computation of extent of immiscibility, even in simple binary glasses, seems difficult because the incidence of homogeneity is dependent not only on differential volumes but also on peripheral cavity strain which may be introduced at a single point long before volume filling is concluded. Either way, the host structure is vulnerable. There is no problem about computing total volumes of the vitron cavities and no important problem about the host holes of the matrix, but a real problem seems present in the accidental packing of the guest oxides. Futile studies of packings and porosities were made, and various trials were unsuccessful with actual oxide volumes, with their spherical envelopes, and also with volumes of their inclosing parallelopipeds. The matter is further complicated by possibilities that parts of some oxides may protrude through common interfaces and into adjacent cavities or holes without damaging stress that will break Si–O bonds.

[5] Precise data are not available for $\Delta N=N_{max}-N_h$. It is estimated as 0.2 or 0.3. The parameter α is defined below and in table I.

In view of a successful graphic use of maximum extent (M.E.) of oxides in preliminary tests, it seemed that linear distance, L = M.E., might be useful also in computations as a measure of ability to cause damaging stress. For a beginning, the average linear effective or "pseudo capacity" of a tetrahedral matrix hole was represented by diameter α Å and estimated to be greater than 2.6 or 2.8 (diam. of oxygen atom), perhaps about 3.5 Å (linear extent of BeO which is miscible in all proportions in silica glass). Next, the effective or pseudo capacity of a vitron cavity was represented by a diameter of A angstroms and estimated to be 7.81 Å, the diameter of the vitron cavity's volume-equivalent sphere. Then $(A-\alpha)$ is the total available pseudo capacity of a vitron for oxide storage before equalization of voids in cavities of vitrons and holes of matrix and the incidence of homogenization. At this stage one might try to express the required number, N_h, of modifier oxides per vitron cavity at incidence of homogenization as $N_h=(A-\alpha)/L$, but this would neglect the cooperative protrusion of part of an oxide into the holes of the matrix. By using $(L-\alpha)$ instead of L, $N_h=(A-\alpha)/(L-\alpha)$. The usefulness of this expression can be tested by a trial computation of N_h for the oxide (GaO), the smallest modifier that seems available for the test. The value of N_h so obtained is 8.3 as compared with about 13 that should be found, as will be understood from the discussion in the first three paragraphs of this section. Further improvement in N_h may result from arbitrary changes in parameters A or α, or by a decrease in the computed value of L, which is merely a conveniently variable property of the modifying oxides. Accordingly L is reduced by $\delta=0.05L$ (a packing factor) and

$$N_h=(A-\alpha)/(L-\delta-\alpha) \qquad (3)$$

which gives as N_h for (GaO) the reasonable value 12.9 molecules per cavity.

After substituting eq (3) in (2), the value of modification in mole percent at incidence of homogenization is

$$100r_h=\frac{100\,(A-\alpha)\cdot q/5}{(L-\delta-\alpha)+(A-\alpha)\cdot q/5} \qquad (4)$$

which was found to be valid for values of L between those for K_2O and (GaO).

A surprising thing about miscibility gaps in binary glasses is the close agreement between the gaps in silicates and borates for the same oxides. Because of this, the equations (3) and (4) were used for both sets of published experimental data, and the parameters are listed in table I.

Values of atomic radii by Ahrens [54] were preferred and used throughout[6] except that for Bi the value of 1.20 Å was used, following Levin [28, 30] and associates at the National Bureau of Standards, and that for oxygen 1.32 was used as in glass technology.

TABLE I. *Parameters for Equations* (3) *and* (4)

	A	δ	α	q
	angstroms		*angstroms*	
For silicates.....	7.81	$0.05L$	3.34	0.31
For borates.....	7.81	$0.05L$	3.34	0.38

A is diameter of spheres each equivalent in volume to a vitron cavity;
δ is a correction to oxide extension, L, perhaps a packing factor;
α is diameter of spherical holes in matrix each capable of holding one molecule of BeO;
q for silica is the vitron proportion thereof, independently computed and published in 1963, and for borates the value obtained from eq (2) as mentioned in section 3.

Equations (3) and (4) with the parameters of table I were used for computing the required conditions, N_h and r_h, for incidence of homogenization of silicate and borate glasses, and the computed values are given in columns (1), (4), (10), and (11) of table II for comparison with experimental results (as selected by Levin and associates, columns (3) and (13), and by them adequately referenced). The values Δ, column (9) for borates minus silicates, speak for the precision of the computations which were made with a slide rule.

In table II the formulae for numerous divalent oxides known to be unstable in air are inclosed in parentheses. The corresponding values of $100r_h$ are for divalent modifiers preserved in the glasses. In one instance, (EuO), in borate glass, the predicted value has been approximately confirmed [44]. (See sec. 2 above.) In most other cases of unstable divalent modifiers, the only observed values available for listing in the table are those which have been published for the sesquioxides of the same cations. In all cases, except for (CoO), these published observed values for R_2O_3 agree very well with the predicated values for (RO). In only five cases, CaO, CdO, ZnO, MgO, and (CoO), are the observed values discordant—all too high—and the cause may be evaporation during melting or modifier acting in part as glass former.

Columns (4) and (10) are of course equal because the silicate and borate cavities are equal in size. The plus signs appear exclusively in column (9) because there are more cavities in borates than in silicates at any given mole-percent composition. It is to be expected that columns (2) and (12) should show predominently negative signs. Even the accepted values of observed $100r_h$ are somewhat higher than the computed values because some small amounts of modifier are found in the predominently glass-maker-rich liquids, not in the modifier-rich liquids. To this extent, perhaps 1 or 2 percent of mix, there is loss of modifier as such, and the total modification actually required exceeds the amount judged as necessary according to the composition of the modifier-rich liquid.

In brief, vitron theory predicts that all sesquioxides of rare earths, including Ce_2O, and also the oxides

[6] In computations the values of radii for R^{2+} were used even for those modifiers assumed to be reduced in the melts from R^{3+} to a divalency. In a few cases, the R^{2+} radii were tried and found to yield values of $100r_h$ only 10 percent lower than with the R^{3+} values. Cationic behavior of this nature has been reported among rare-earth nitrides [38]. Another evidence of divalency of rare-earth cations with $^{3+}$ radii may be the report that some of these atoms can be substituted for Ca^{2+} crystal sites [39].

Bi_2O_3, Cr_2O_3, and Ga_2O_3, are at least partially reduced to divalency in the furnace at glass-melt temperatures and preserved in the glass from reoxidation [40].[7]

The use of eqs (3) and (4) in computing the degree of modification necessary for homogenization in binary silicates and borates is the most simple and direct evidence so far produced for the existence of vitrons in glass.

In this connection it should be emphasized that the parameters of these equations were taken from vitron theory approximately as published some years ago and fixed within relatively narrow limits. Only one constant, $q=0.38$, for borates, was adjusted to fit data. The residuals c−o (columns 2 and 12) of table II do not exceed the imprecision of the experimental data. Only small systematic trends indicate that the form of eq (4), or the values for its parameters, are not perfectly suitable for the use made thereof.

That vitron geometry may be used in the formulation of glasses of specified densities is indicated by the computations in the next section. Also a correlation between vitron theory and neucleation is shown in section 5.

4. Density of Molten Binary Silicate Glasses at Homogenization

If one knows the degree of modification, $100r_h$, at which immiscibility (or tendency thereto) terminates, it is possible to approximately compute the density of

[7] Here it may be mentioned that Cohen [41] has published papers on the partial reduction by x-irradiation of trivalent rare-earth cations to divalency and their preservation in glasses.

TABLE II. *Mole-Percent Modification for Incipient Homogenization*
(Computed by equations 3 and 4)

	Binary silicates			Modifiers					B−S (11) minus (1)	Binary borates			
	Mol percent r_h			N_h	$L-\delta-\alpha$ (ang)	Oxide	Ionic radii (ang)	$L=$ M.E. (ang)		N_h	Mol percent r_h		
	Comp.	c−o	Obs.								Comp.	c−0	Obs.
	(1)	(2)	(3)	(4)	(5)	(6)	(7)	(8)	(9)	(10)	(11)	(12)	(13)
S-shape ↕ TC curves	6.1	+0.6	5.5	1.0	4.22	K_2O	1.33	7.96	+1.3	1.0	7.4		
	9.1	−0.4	9.5	1.5	2.74	Na_2O	0.94	6.40	+1.9	1.5	11.0		
	13.5	−1.8	15.3	2.4	1.75	Li_2O	.68	5.36	+2.7	2.4	16.2		
	13.7	−1.5	15.2	2.4	1.72	BaO	1.34	5.32	+2.8	2.4	16.5	+0.1	16.4
	15.8			2.9	1.45	PbO	1.20	5.04	+3.6	2.9	19.4	+0.4	19.0
	15.1			2.9	1.48	(BiO)	1.20	5.04	+2.8	2.9	17.9	−1.1	19.0
	16.2	−2.3	18.5	3.1	1.36	(LaO)	1.14	4.92	+3.0	3.1	19.2	−2.3	21.5
	16.6	−3.2	19.8	3.2	1.32	SrO	1.12	4.88	+3.1	3.2	19.7	−1.3	21.
	18.2			3.6	1.18	(CeO)	1.05	4.74	+3.2	3.6	21.4		
	18.5	−2.3	20.5	3.7	1.16	(NdO)	1.04	4.72	+3.3	3.7	21.8	−2.2	24.0
	19.6	−1.7	21.3	3.9	1.08	(SmO)	1.00	4.64	+3.4	3.9	23.0	−3.5	26.5
	19.9		28.9?	4.0	1.06	CaO	0.99	4.62	+3.4	4.0	23.3	−3.8	27.1
	20.5	−1.5	22.0	4.2	1.02	(EuO)	.97	4.58	+3.5	4.2	24.0	−2.7	26.7
	20.5			4.2	1.02	CdO	.97	4.58	+3.5	4.2	24.0		39?
	20.5	−3.0	23.5	4.2	1.02	(GdO)	.97	4.58	+3.5	4.2	24.0	−3.3	27.3
	22.2	−2.8	25.0	4.6	0.92	(DyO)	.92	4.48	+3.8	4.6	26.0	−3.0	29.0
	22.8	−2.2	25.0	4.8	.89	(YO)	.91	4.45	+3.8	4.8	26.6	−3.4	30.0
	23.0	−3.0	26.0	4.8	.88	(HoO)	.90	4.44	+3.8	4.8	26.8	−3.1	29.9
	23.7	−3.3	27.0	5.0	.85	(ErO)	.89	4.41	+3.8	5.0	27.5	−2.8	30.3
	24.3	−1.0	25.3	5.2	.82	(TmO)	.87	4.38	+4.0	5.2	28.3	−2.2	30.5
	24.7	−1.6	26.3	5.3	.80	(YbO)	.86	4.36	+4.1	5.3	28.8	−2.2	31.
	25.2	−3.8	29.0	5.5	.78	(LuO)	.85	4.34	+4.1	5.5	29.3	−2.7	32.
	27.2	−1.8	29.0	6.1	.70	(ScO)	.81	4.26	+4.4	6.1	31.6	−2.4	34.
	27.8			6.3	.68	MnO	.80	4.24	+4.4	6.3	32.2		
	32.0	−3.8	35.8	7.6	.56	FeO	.74	4.12	+4.6	7.6	36.6		
	32.0	−3.0	35.0	7.6	.56	ZnO	.74	4.12	+4.6	7.6	36.6		48?
	32.7			7.9	.54	CoO	.73	4.10	+4.7	7.9	37.4		
	33.5			8.2	.52	CuO	.72	4.08	+4.8	8.2	38.3		
	39.1	−1.0	40.1	10.3	.41	MgO	.67	3.97	+4.9	10.3	44.0		48?
	39.6	−1.4	41.0	10.6	.40	(MnO)	.66	3.96	+5.1	10.6	44.7		
	43.5		48.3?	12.5	.34	(CoO)	.63	3.90	+5.2	12.5	48.7		
	43.5	+1.5	42.	12.5	.34	(CrO)	.63	3.90	+5.2	12.5	48.7		
	45.0	+5.0	40.	13.3	.32	(GaO)	.62	3.88	+5.2	13.3	50.2		
						O	1.32 (used by glass technologists)						
						Be	0.35	3.34					

Observed values of columns (13) and (3) are listed by Levin [5].

a glass from the molecular weights of silica and modifier, the volume (251.2 Å^3) of a vitron, the density (2.203g/cm^3) of vitreous silica, and the volume ratio (2.28) of matrix to vitron therein. Since the atomic weight of silicon is 28.086 and of oxygen 15.9995, the weight of 5 SiO_2 in the framework of a vitron is 300.4 gfw/avogadro's number or 498.8 g $\times 10^{-24}$. After adding the corresponding weight of the N_h modifiers and dividing by the volume of a vitron, one obtains the density of the vitron portion ($q=0.305$) of the glass. The deduction of 2.31 g/cm^3 as the density of the matrix portion ($1-q=0.695$) of the glass was mentioned in section 1 of this paper. The glass densities in table III were computed as outlined above and by use of the additivity of specific volumes.

The observed densities for the alkaline-earth glasses are extrapolated from values given by Tomlinson, Heynes, and Bockris [22] for 1700 °C. Those for the alkali silicates are from Bockris, Tomlinson, and White [20] for 1400 °C.

Note that at melt temperatures the densities of the oxides Li_2O, Na_2O, and K_2O (which show only tendencies toward immiscibility in binary silicate glasses) are about the same as or only slightly different from that of silica; whereas the oxides MgO, CaO, and SrO (which produce definite immiscibility) are all of considerably greater density than silica. Whenever by chance a vitron becomes modified to the extent of containing one or two molecules of one of these denser oxides, it tends to sink in the melt where it has greater probability of further modification, whereas the empty vitrons tend to float where the probability of modification is lowest. In this way, modifier-rich liquid tends to become richer and forms a lower layer and nearly pure silica forms a top layer, as has been observed and reported.

TABLE III. *Densities at Incipient Homogenization*

Oxide	MgO	CaO	SrO	BaO	Li_2O	Na_2O	K_2O
Computed.....	2.74	2.61	2.72	2.75	2.27	2.24	2.23
c–o.....	+.29	+.17	.0	+.03	+.08	+.02	.0
Observed.....	2.45	2.44	(2.7)	2.72	2.19	2.22	2.23

5. Nucleation

According to vitron theory, the pseudonuclei short-range structure forms at high temperatures and persists to distinguish a glass melt from one of cristobalite. The Si–O–Si angles of 180° are to be expected as the highest temperature form of connected tetrahedra, and pentagonal rings of such tetrahedra (all centers of Si–O–Si atoms being in one plane) require angles of 178.5° so that such connections are very likely to form. If it be recalled that the interior angle O–Si–O in a tetrahedron is 109° 28′, it will be realized why connected tetrahedra are almost naturally adapted for the 108° interior angles of plane pentagonal ring systems at the highest temperatures for the existence of connected tetrahedra. A very slight stress must exist if the 180° angles tend to be maintained. Furthermore, any departure from planeness would increase rather than relieve this slight stress which prevents the extension of micro-order to crystal growth. The micro-network so formed is uniquely that of necessarily stressed small clusters of otherwise regular pentagonal dodecahedra. This is characteristic of silica-glass structure.

Another possible ring-type structure at fairly high temperatures is hexagonal. For unstressed planar rings the angles at Si–O–Si must be 169.5° so that the favorable temperature for high probability of connecting tetrahedra into the form of hexagonal rings, would be appreciably lower than for forming pentagonal rings. In important contrast with pentagonal rings, the hexagonal rings, even if perchance formed with Si–O–Si angles larger than 169.5°, can easily become crooked and nonplanar to release the stress and thus permit the unlimited 3-dimensional growth of crystals in silicate melts.

Zarzycki [31] says that a typical infrared quartz band remains in vitreous silica held for 30 minutes at temperatures of 1750 to 1900 °C and only after treatment to above the latter temperature is the band weakened. Sosman [32] says: "Both quartz and tridymite can be melted at temperatures lower than the stable melting point of 1723 °C, but unless further heated to a higher temperature, the fused silica so produced would gradually change over into crystobalite." Also, it is known that fused silica of density 2.20 is obtained after cooling a silica melt from temperatures of 2000 °C or higher to holding-period temperatures at or near 1800 °C for 30 minutes.

From the above, it may be surmised that for nucleation of crystals in silica melts the coolings should be rapid through temperatures near 2000 ° and perhaps down to about 1800 ° or lower. On the other hand, for "nucleation" of vitron structure the maximum temperature should be near 2000 ° or higher with slow cooling to, say, around 1900 ° and with cooling, rapid if possible, below 1800 ° and lower temperatures where nucleation of hexagonal structure probably occurs.

Usually nucleation means incipient crystallization in or from a well-modified essentially glassy melt. It has long been observed that heterogeneous nucleation starts and spreads rapidly from surfaces, edges, cracks, defects, flaws, fissures, or veritable crystallites with some of which melts are usually well supplied. A very small "free volume" permits "cooperative maneuvers" necessary for change of structure, step-

wise. It is noteworthy that any contraction of Si–O–Si angles would rapidly increase free volume. It has also been insistently inferred that homogeneous nucleation can start more or less simultaneously anywhere within the body of melts.

In a discussion of nucleation (with a comprehensive bibliography), Brown and Ginell [33] conclude that good glass structure is so metastable with respect to crystal that homogeneous nucleation rarely if ever occurs. Instead, they stress the great prevalence in all real systems of heterogeneous sites at which crystallization may start.

Dietzel and Wickert [34] measured rates of crystallization as a function of modification for the Na_2O–SiO_2 system and expressed glass tendencies as reciprocals of such rates. Their results (as shown in their fig. 1) are reproduced here as figure 3. The

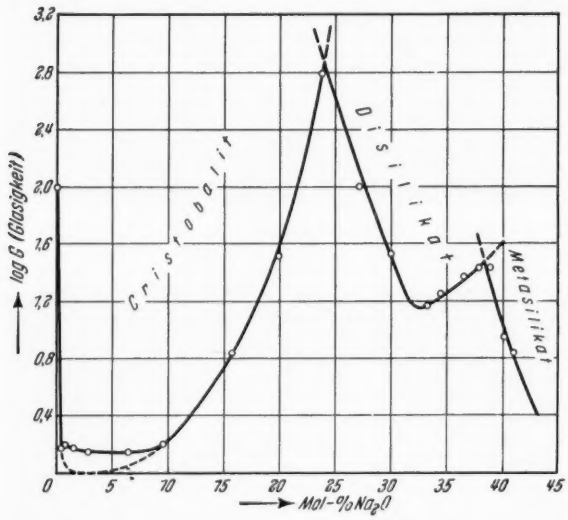

FIGURE 3. *Curve of glasigkeit in* Na_2O *binary silicates, reproduced from Bild by Dietzel and Wickert* [34], *may be used to illustrate the relation of vitron theory to nucleation. (See text.)*

maxima of rates of glasigkeit occur at 0, 24, and 38 mole percent Na_2O, with a wide minimum at about 0.5 to 10, and a sharper one at 33 mole percent. The authors mention but do not explain the *unexpected* abrupt fall from 100 percent silica and the wide minimum from 0.5 to 10 percent. From a vitron viewpoint, the abrupt fall, like a similar fall in viscosity, is attributable to "fissuring" and to the incipient predisposition to free volume at the peripheries of all vitrons. The maximum in glass tendency at 24 percent corresponds to oxide saturation at the glass eutectic (25 or 26 percent), and the less prominent one at 38 corresponds to the cation (and last) saturation before essentially complete vitron destruction. At both peaks the saturation offers maximum steric hindrance to formation of free volumes.

As pointed out by various investigators and mentioned by this writer [12(f), p. 125] in a discussion of viscosity, the conventional concept of a loosened structure by the breaking of oxygen bridges as modifiers are added, is too slow and delayed to explain the first precipitate fall in viscosity or in glasigkeit. For the extreme case of only 0.5 percent Na_2O, only one bridge in about 400 can be broken; yet for 9 percent where one in 20 might be broken the curve of glasigkeit stands at the same very low level. The narrower valley at 33 percent marks the condition where cation concentration begins to outrun the relaxation that followed oxide saturation. The rise near 17 mole percent may be even more sudden and abrupt than appears in figure 3. Some evidence of this is found in data by Jenckel and Schwittman [35] which was discussed by this writer [12(c), pp. 362, 363]. At 16.7 mole percent Na_2O one molecule of that oxide becomes available for each vitron cage and can strengthen and stiffen it by a "deep potential well" position therein.

The concept of fissuring which the writer now suggests as of great importance in nucleation of glass is essentially the same as previously postulated [12(e), p. 10]; [12(f), p. 118] to explain the maximum in partial molar volume for silica at 12 or 13 mole percent, as found by Callow [24].

Innumerable fissures can probably supply free volume permitting rearrangements necessary for the change of 5-ring tetrahedra to hexagonal linking and thus to further crystal nucleation. If one thinks of about 5 SiO_2 tetrahedra involved near each vulnerable fissure (or stressed region), it follows that such vulnerability can be effectively lowered by 16.7 percent modification, or about one oxide per vitron, to give steric support.

6. Tentative Vitron Structure of Borate Glasses

The remarkable similarity in the data of immiscibility for silicate and borate glasses stimulates a search for vitron structure in borates. Despite the similarity, there are extreme differences between silicates and borates. In silicates, after the termination of immiscibility, the liquidii fall precipitately, whereas in borates they rise. Apparently modification weakens a strong structure in silicates, but slowly substitutes a partial network instead of a molecular structure in borates. Possibly the vitron structures in B_2O_3 glass are neutral discrete molecules in large part, held together by very weak forces, and their destruction allows formation of a moderately stronger 3-dimensional network.

In 1952 Fajans and Barber [42] published a scholarly paper on boron trioxide. They concluded that a 3-dimensional network is incompatible with the low melting point and molar refraction of (pure) boron oxide, that the expansibility, surface tension, and viscosity below 1400 °C prove that the glass below about 300 °C consists of units held together by "weak" forces, and that with increasing temperature the structure changes gradually toward a "strong" one. They give consideration to a molecule of B_4O_6. A more recent paper by Ottar and Ruigh [43] also gives consideration to B_4O_6 cage molecules, held to each other by (weak) directed

dative bonds between oxygen of one molecule and boron of another.

In published speculations regarding the structure of borate glasses, the equilateral triangle has often been discussed. With trivalent B at the center, the three half oxygens may be located at the midpoints of the sides. Planar and lamellar structures have been proposed with the half oxygens at the apices. With oxygen at the mid sides, as in figure 4, and dihedral

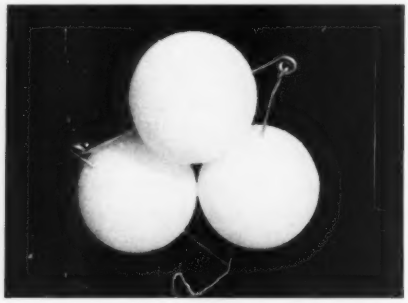

FIGURE 4. *The boron-oxygen equilateral triangle.*
This is a widely accepted unit of boric-oxide glass. Each midside is the locus of (one-half) oxygen. The boron atom (not shown) lies at the triangle center.

angles of 138°16′ between the triangle surfaces, a vitron cage of triangles called an icosahedron is formed with 20 triangular faces and 30 edges. Obviously, this could be a model for a neutral-free molecule of $(B_4O_6)_5$. Figures 5, 6, and 7 show a model so constructed.

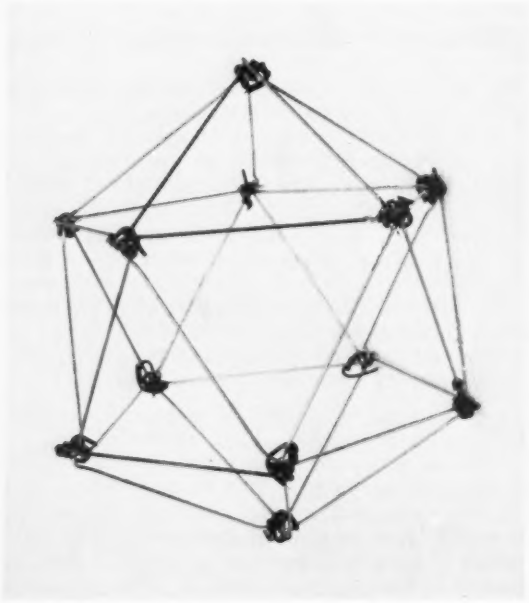

FIGURE 5. *Framework of icosahedral vitron proposed for boric-oxide glass.*
View along one of ten 3-fold boron axes. There are 20 triangles united by the sharing of oxygen atoms.

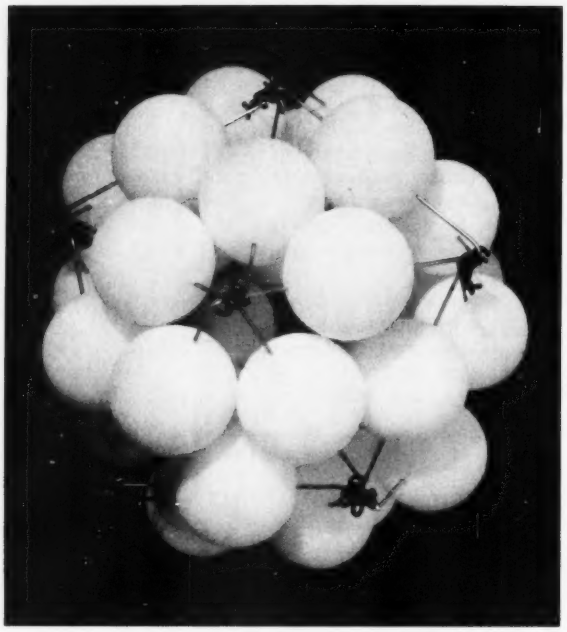

FIGURE 6. *Proposed empty vitron for boric-oxide glass.*
Thirty oxygens are mounted on the framework of figure 5. With twenty borons (not shown) this forms a neutral molecule of $(B_4O_6)_5$.

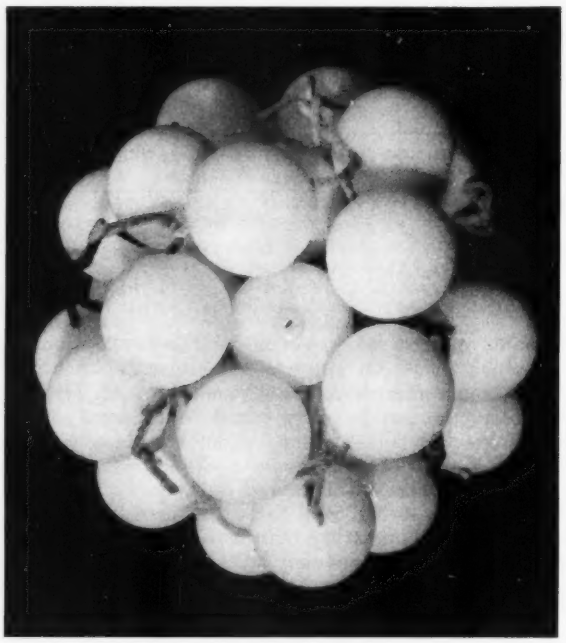

FIGURE 7. *Proposed vitron fully modified by an oxide having very small cations (not shown).*
Thirteen oxide molecules at most may be placed in the cavity of figure 6. (The wire framework has been replaced by tie lines which are regrettably in evidence.)

Radial-distribution data from diffraction patterns on borates are not numerous and not very consistent, but

there seems to be a consensus for a B–O distance of 1.39 or 1.40 Å (which is less than Σ radii) in boric-oxide glass (with a spread toward higher values, up to 1.48, depending on degree of modification).

If the scale factor for the icosahedron is taken from 1.40 for the B–O distance, the edge length is 4.85 Å and the volume is 249 cu Å. This compares with 251 cu Å as published in 1957 for the volume of the dodecahedral vitron of silica. This would show why eqs (3) and (4) of section 3 in this paper with the same values for parameter A and for α can be used for borates as well as silicates.

A second regular solid made up of 8 equilateral triangles is the octahedron, figure 8. This might serve as the secondary structure in the matrix of boric-oxide glass. With the same arrangement of B at 8 face centers and oxygen at the 12 midedges, it would be a model for $(B_4O_6)_2$ and again a free neutral molecule, figure 9.

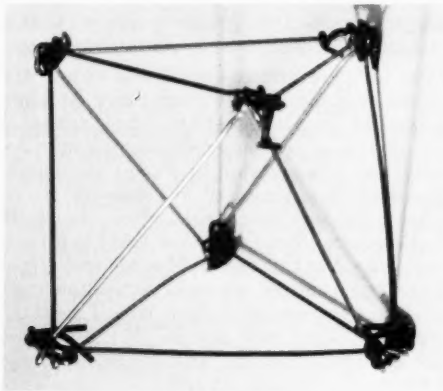

FIGURE 8. *Framework of octahedral structure proposed for part of matrix of boric-oxide glass.*
There are 8 triangles united by the sharing of oxygen atoms at the midedges.

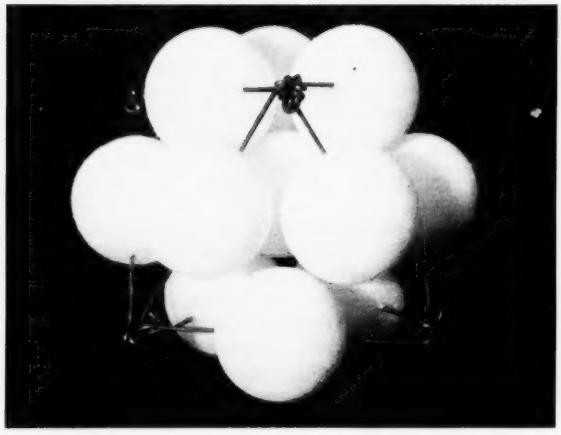

FIGURE 9. *Proposed octahedral structure for part of the matrix of boric-oxide glass.*
Twelve oxygens are mounted on the framework of figure 8. With eight borons (not shown) this forms a neutral molecule of $(B_4O_6)_2$. An oxygen atom is inclosed at center to show that the hole is somewhat larger than 2.8 Å in diameter. According to eq (4) of Section 3 above, the hole should have a diameter of approximately $\alpha = 3.56$ Å.

Remembering that the dihedral angle is only 109.5°, the scale factor may become larger than for the triangles of the icosahedron in order, after modification, to make room inside the octahedra for the oxygens and leave at the center of the cluster an aperture, or hole, approximately α Å in effective diameter and capable of inclosing an oxygen and a small cation like beryllium.

When soda modifiers are added not in excess of those retainable as guests in the icosahedra, it has been said that the boron may become 4-coordinated and some triangles add oxygen and become boron-oxygen tetrahedra joined by bridges into a coordinative network. However, there seems no direct evidence that tetrahedra are actually formed in borate glasses, or that a really *strong* coordinative network exists at any temperature or degree of modification.

Warren and associates [45] measured the (B–O) distance in boric-oxide glass as 1.39A which he compared with 1.36 in some crystalline borates. A boron-oxygen equilateral triangle, even with (B–O) = 1.40 Å, certainly means interpenetration of electron clouds of adjacent atoms. Warren also found a peak at 2.42 Å for (O–O) distance which likewise indicates interpenetration. Then for (B–2dO) he found 3.75. In the icosahedra, or large molecules, the last distance is 4.16 for the scale adopted and in the octahedra 3.13 Å. These results are tabulated below.

TABLE IV

Distance	Octahedra	Icosahedra	Average	Warren
(B–O)	1.40	1.40	1.40	1.39
(B–B)	2.27	2.61	2.44	2.42
(O–O)	2.42	2.42	2.42	
(B–2dO)	3.13	4.16	3.65	3.75
(B–2dB)	3.23	4.21	3.72	
(O–2dO)	3.42	3.92	3.67	

All initial distances of near-neighbor atoms in B_2O_3 glass seem to indicate a state of *compression*. Shartsis, Capps, and Spinner [47] remark, from other considerations, that "the glass should act as if it were under pressure." Biscoe and Warren [46] reported that the (B–O) distance first decreased and then increased progressively from 1.37 to 1.48 Å as modifier content of Na_2O in B_2O_3 was increased from 10 to 31 mole percent, and that the coordination of boron [8] also increased. This may mean merely that some (B–O) bonds decreased in strength and that the concentration of oxygen atoms in the cavities must increase the apparent coordination of boron. These and other reported effects and the so-called boron-oxide anomalies, such as maxima and minima on property composition curves, are probably explainable in terms of some of the following:

[8] If the 4-coordination of boron is supposedly affected by an oxygen bridge from B of one molecule to B of another molecule and the B atoms pulled out of their original triangular plane so that the new (B–O) distances are increased from 1.40 to 1.48 Å (Briscoe and Warren's report), then each boron need be displaced only 0.44 Å from the original plane instead of 0.96 Å for a symmetrical tetrahedron.

(1) Increasing concentration of modifiers isolated in cavities as their respective capacities are approached (see $100r_h$ as specified by eq (4) and listed in table II);
(2) Dearth of ionization and expansion before cavity capacities are reached;
(3) Stress of B–O bonds beginning with 4-coordination of boron and rapidly increasing at cavity capacity;
(4) Continuous breakup of vitrons and increase in ionization and in volume expansion that begins near cavity capacity and extends to much higher modifications.

To test the proposed models for density is difficult, particularly because of the unknown packing factor. According to eq (4), the value for q, that is the percentage of (B_2O_3) in icosahedral form, is 38. If it be assumed that the atoms in an icosahedral molecule are all contained in the circum circle of $D=9.2$A, then the density of the vitron portion is 2.83. Similarly, an estimate of the octahedral portion is 2.73, but all suggested about its extent in boric-oxide glass is that it forms a part of the matrix of 62 mole percent—perhaps a large part. If the remainder is loosely connected random fragments of B_2O_3, the whole matrix might have a density of 2.73, which gives about 2.76 for the combination. This, of course, would require almost perfect packing of approximately spherical molecules and particles of 2 or 3 sizes. For a reasonable estimate of one-third of total volume as very small interstitial voids, the computed density reduces to 1.83 in agreement with measured values [52] at room temperature.

The cavities of vitrons are soon effectively filled when modification is caused by alkalies. Moreover, some ionization starts early for alkalies and for barium oxide because immiscibility is not complete but only a metastable tendency. Consequently, some modifier O^{2-} is soon trapped at the octahedral centers so that in effect some atoms of B^{3+} become 4-coordinated (perhaps with one bond longer than the others) and thus share their charge with 4 oxygen atoms. Some oxygens of the octahedral molecule are therefore not fully satisfied and the modifier alkali or barium atoms may become loosely attached at apices of the octahedra. Each such molecule will have a residual plus charge that can be useful in establishing weak connections with other elements of the matrix during subsequent degradation of the orderly arrangements in icosahedra.

The distance between extreme apices of octahedra in borates is 6.5 Å, and that between adjacent apices is 4.8 Å. Bienenstock, Posner, and Block [48] reported (Ba–Ba) distances of 6.76 Å in a 20 mole-percent barium borate glass in 1960; and, similarly, Piermarini and Block [49] reported 6.8 and 4.7 Å in a 24 mole-percent barium borosilicate glass in 1962. Also, Krogh Moe [50] reported a (Ba–Ba) distance of 6.9 Å in a barium borate glass in 1962.

BaO resembles the alkalies in that the miscibility is metastable and there is only a tendency thereto, and some ionization probably starts before vitron capacity is reached. For example, when BaO is the modifier, no 2-liquid layer appears. Inflection of the S-shaped liquidus occurs near 16 mole-percent modification for borates and near 15 percent for silicates. Icosahedral disintegration is well underway at 24 percent. Krogh Moe [50] refers to similar experiments with cesium oxide which should be even more conclusive on this point.

The experimental evidence just cited suggests that the octahedral molecules are more stable than the icosahedra and exist intact after the latter are partially broken up by modification.

Unquestionably the destruction of order in glasses can be caused by high temperature as well as by the process of modification. At present, experiments do not permit so precise an account of temperature effects as have been given for the modification process which has been empirically practiced for many decades. Possibly, in terms of the models herein presented, a temperature hypothesis may be formulated.

At room temperatures the molecular vitrons of boric-oxide glass may be held to each other by numerous intermolecular bonds, perhaps the dative bonds between oxygen of one molecule and boron of an adjacent molecule, as suggested by Fajans and Barber [42] and discussed in more detail by Ottar and Ruigh [43]. When temperatures are held below about 300 °C, borate glass is in a rigid state and there is little expansion in volume. For this region Macedo and Napolitano [51] have reported an apparent activation energy of some 90 kcal per mole for viscous flow. This may be, as suggested by Ottar and Ruigh [43], the combined simultaneous breaking of a number of intermolecular dative bonds.

Then rather suddenly, as the glass softens at higher temperatures, rapid expansion takes place because some of the icosahedral bonds, which have been stressed beyond their breaking length, begin to part. Because of the varying stresses in different parts of these vitrons, there may be a distribution of activation energies with an average value steadily decreasing as the disordering process proceeds at ever-increasing temperatures while the volume expansion gradually slows at temperatures above softening. Then the end of the non-Arrhenius region is reached and activation energies again tend toward constancy at 700 or 800 °C. The (computed [51]) terminal value of say 18 kcal may relate to flow within the matrix consisting of octahedral molecules $(B_4O_6)_2$, immersed in a proportionately much larger matrix including fragments of the disrupted icosahedra. This is in accord with modern theories of structure of glass in that there is a growing tendency to consider that some glass structures are already well formed in the melt above liquidus temperatures.

At present, experiments do not permit desirably direct examination of this high-temperature hypothesis. The successful quantitative use of eq (4) of this paper does reveal the nature of a close relation between such different glasses as silicates and borates. It is also quantitatively consistent with the fundamental nature

and function of glass modifiers and indicates methods for investigating structure in other glass-former glasses.

7. Concluding Remarks

This paper concludes the detailed reports on vitron theory as developed chiefly between 1955 and 1958. Its publication has been delayed partly in futile attempts to arrange for experiments leading to pertinent quantitative high-temperature studies of details of immiscibility and related manifestations of departures from ideality in silicate and borate melts, including the size, shape, and location of domes of immiscibility above liquidus temperatures for the several modifying oxides, and under conditions for possible variations in the existing vitron-to-matrix equilibrium.

From the vitron viewpoint, the report by Dietzel and Wickert on glasigkeit, and especially their curve therefor in figure 3 (above), is very significant. It stimulates a few very comprehensive remarks about glass.

The presence of vitrons, which initially tend to make it difficult for crystals to form, is later not advantageous in their undamaged state for making the best glasses. The example is pure silica glass which is easily made without crystallization, but is somewhat lacking in ultimate uniformity. The best silicate glasses are made by modifications of vitrons carried to a limit that alters the vitrons and thus slowly, without completely destroying them, reduces the abruptness of transition from vitron to matrix. Immediately and suddenly after oxide saturation near or at the eutectic, the ionization and bridge-breaking seriously damage the vitrons and this begins to favor the rearrangements of crystallization. Probably some Si–O–Si angles contract. This and/or the pressure of increased cation particles briefly outrun the loosening tendencies, reduces free volume, and thus continues to favor glass formation for a short range in added modification. Thereafter, with further modification, *good* glassmaking is very soon ended. Rigidity and/or particle pressure seem to oppose formation of free volume, low temperatures reduce nucleation rates, and remaining goodly proportions of pentagonal ring structure of the tetrahedra greatly retard the formation of hexagonal rings and hence of crystals.

With this concept of glass, it can be said that glass formers, of the SiO_2 and B_2O_3 types, are those that can and do form distorted cages (such as pentagonal dodecahedra and icosahedra) that are almost but not exactly of crystalline form. Glass modifiers are oxides that can by mere quantity progressively (and advantageously) modify the properties of such noncrystal structures and can even partially (and advantageously) disrupt their quasi-crystalline degree of order.

Can it be that crystallization would predominate at all degrees of modification if elemental arrangements of quasi-crystalline structures were not present? The series of seven papers of which this one is the last is founded upon that hypothesis. Without some phenomenon to block the iterative processes of crystallization, inorganic glasses would not exist. Their characteristically small molecules would fit instead into one of a large number of potential repetitive crystalline structures.

8. References

[1] Greig, J. W., Am. J. Sci. **73,** 1 (1927).
[2] Kracek, F. C., J. Am. Chem. Soc. **52,** 1436 (1930).
[3] Warren, B. E., and Pincus, A. G., J. Am. Ceram. Soc. **23,** 301 (1940).
[4] Dietzel, A., Z. Electrochem. **48,** 9 (1942).
[5] Levin, Ernest M., and Block, Stanley, J. Am. Ceram. Soc. **40,** 95 (1957). Levin, E. M., Phys. and Chem. of Glasses **7,** 92 (1966).
[6] Glaser, F. P., Warsaw, J., and Roy, R., Phys. and Chem. of Glasses **1,** 39 (1960).
[7] Preston, Eric, J. Soc. Glass Techn. Trans. **26,** 82 (1942).
[8] Esin, O. A., J. Phys. Chem. **22,** 617 (1948).
[9] Forland, Tormond, Techn. Report No. 63, Office of Naval Research, NR 032–264; Penna. State Univ., College of Mineral Industries. pp. 11, 16, 23 (1955).
[10] Dietzel, A., Naturwis. **31,** 110, 112 (1943).
[11] Dietzel, A., and Sheybany, H. A., Verres et Réfractaires **2,** 63–80 (1948).
[12] Tilton, L. W..
(a) J. Soc. Glass Techn. **40,** T338 (1956);
(b) Opt. Soc. Am. Annual Meeting, Oct. 1956. J. Opt. Soc. Am. Abst. **47,** 115 (1957); J. Research NBS **59,** 139 (1957) RP2782;
(c) J. Research NBS **60,** 351 (1958) RP2854;
(d) J. Research NBS **61,** 463 (1958) RP2915;
(e) J. Am. Ceram. Soc. **43,** 9 (1960);
(f) J. Res. Nat. Bur. Stand. (U.S.), 65A (Phys. and Chem.), No. 2, 117 (Mar.–Apr. 1961);
(g) Encyclopedia of X-Rays and Gamma Rays, Ed. George L. Clark, 430–436, (Reinhold Publ. Corp., N.Y., 1965).
[13] Warren, B. E., Z. Krist. **86,** 349 (1933); J. Am. Ceram. Soc. **17,** 249 (1934).
[14] Bernal, J. D., Nature **185,** 68 (1960).
[15] Ginell, R., J. Chem. Physics **34,** 999 (1961).
[16] Mackenzie, J. D., Chemical Reviews **56,** 456 (1956).
[17] Douglas, R. W., Non-Crystalline Solids, 382. (John Wiley & Sons, Inc., N.Y., 1960).
[18] Kracek, F. C., J. Am. Chem. Soc. **52,** 1438–42 (1930).
[19] Moore, Walter J., Physical Chemistry, 317 (Prentice-Hall Inc., 1958).
[20] Bockris, J. O'M., Tomlinson, J. W., and White, J. L., Trans. Faraday Soc. **52,** 299 (1956).
[21] White, J. L., PhD thesis, Univ. of Cal. 1955.
[22] Tomlinson, J. W., Heynes, M. S. R., and Bockris, J. O'M., Trans. Faraday Soc. **54,** 2218 (1958).
[23] Simon, I., and McMahon, H. O., J. Am. Ceram. Soc. **36,** 160–164 (1953).
[24] Callow, R. J., J. Soc. Glass Techn. **36,** T137–41 (1952).
[25] Hill, O. F., and Audrieth, L. F., J. Phys. & Colloid Chem. **54,** 690–96 (1950).
[26] White, J., Howat, D. D., and Hay, R., J. Roy. Tech. Coll. Glasgow **3,** 239 (1933–36).
[27] Aramaki, Shigeo, and Roy, Rustum, J. Am. Ceram. Soc. **42,** 644 (1959).
[28] Levin, Ernest M., and McDaniel, Clyde L., J. Am. Ceram. Soc. **45,** 355 (1962).
[29] Toropov, N. A., The Structure of Glass (Translated from Russian), 285. Acad. Sci. USSR Press, Moscow-Leningrad 1953.
[30] Bergman, A. G., The Structure of Glass (Translated from Russian), 246. Acad. Sci. USSR Press, Moscow-Leningrad 1953.
[31] Zarzycki, J., Verres et Réfractaires **11,** 3 (1957).
[32] Sosman, R. B., Encyl. Britannica, 1955.
[33] Brown, S. D., and Ginell, Robt., Preprint, Am. Ceram. Soc. Toronto Meeting, 1961.

[34] Dietzel, Adolf, and Weikert, Helmut, Glastechn. Berichte **29**, 3 (1956).
[35] Jenckel, E., and Schwittman, A., Glastechn. Berichte **16**, 168 (1938).
[36] Mandelcorn, Lyon, Non-stoichmetric Compounds, 309, 314 (Academic Press, New York, 1964).
[37] Levin, Ernest M., Robbins, Carl R., and Waring, Jon L., J. Am. Ceram. Soc. **44**, 87 (1961).
[38] McClure, J. H., J. Phys. Chem. Solids **24**, 871 (1963).
[39] Nassau, K., J. Phys. Chem. Solids **24**, 1511 (1963).
[40] Moeller, Therold, The Chemistry of the Lanthanides, 44 (Reinhold Publ. Corp., New York, 1963).
[41] Cohen, A. J., VII International Congress on Glass, Brussels, 1965.
[42] Fajans, K., and Barber, S. W., J. Am. Chem. Soc. **74**, 2761 (1952).
[43] Ottar, B., and Ruigh, W. L., Phys. and Chem. of Glasses **3**, 95 (1962).
[44] Shafer, M. V., and Suits, J. C., J. Am. Ceram. Soc. **49**, 262 (1966).
[45] Warren, B. E., Krutter, H., and Morningstar, O., J. Am. Ceram. Soc. **19**, 202 (1936).
[46] Biscoe, J., and Warren, B. E., J. Am. Ceram. Soc. **21**, 287 (1938).
[47] Shartsis, L., Capps, W., and Spinner, S., J. Am. Ceram. Soc. **36**, 40 (1953).
[48] Bienenstock, A., Posner, A. S., and Block, Stanley, J. Research N.B.S. **64A**, 229 (1960).
[49] Piermarini, G. J., and Block, S., J. Res. Nat. Bur. Stand. (U.S.), **67A** (Phys. and Chem.), No. 1, 37 (1963).
[50] Moe, J. Krough, Physics and Chemistry of Glasses **3**, 208 (1962).
[51] Macedo, P. B., and Napolitano, A., J. Chem. Physics **49**, 1887 (1968).
[52] Macedo, P. B., Caps, W., and Litovitz, T. A., J. Chem. Physics **44**, 3357 (1956).
[53] Olshansky, Ya., Proc. Acad. Sci. USSR **75**, 93 (1951).
[54] Aherns, L. H., Geochim. Cosmochim. Acta **2**, 155 (1952).

(Paper 77A2–769)

JOURNAL OF RESEARCH of the National Bureau of Standards—A. Physics and Chemistry
Vol. 77A, No. 2, March-April 1973

Publications of the National Bureau of Standards*

Citations with Selected Abstracts

J. Res. Nat. Bur. Stand. (U.S.), **76A** *(Phys. and Chem.),* No. 4, (July-Aug. 1972), SD Catalog No. C13.22/sec.A:76/4.

The EMF-temperature coefficient of "acid" standard cells of the saturated cadmium sulfate type from 15 to 40 °C, W. J. Hamer, A. Skapars,and B. F. Field.

Pulse radiolysis of neopentane in the gas phase, R. E. Rebbert and P. Ausloos.

Anatomy and thermal history of laser self-focusing damage tracks in glass, W. Haller and J. H. Simmons.

Normal emissivity of an isothermal, diffusely reflecting cylindrical cavity (with top) as a function of inside radius, W. B. Fussell.

Lattice vibrations of antiparallel chain sheet structures, B. M. Fanconi.

J. Res. Nat. Bur. Stand. (U.S.), **76A** *(Phys. and Chem.),* No. 5, (Sept.-Oct. 1972), SD Catalog No. C13.22/sec.A:76/5.

High accuracy spectrophotometry at the National Physical Laboratory, F. J. J. Clarke.

An accurate spectrophotometer for measuring the transmittance of solid and liquid materials, R. Mavrodineanu.

Absolute spectroradiometric measurements, G. A. W. Rutgers.

Accurate measurements of and corrections for nonlinearities in radiometers, C. L. Sanders.

Physical parameters in high-accuracy spectrophotometry, K. D. Mielenz.

Liquid absorbance standards, R. W. Burke, E. R. Deardorff, and O. Menis.

Accurate measurement of molar absorptivities, R. W. Burnett.

Problems associated with the need for standardization in clinical spectrophotometric and fluorometric measurements, J. R. Penton, G. M. Widdowson, and G. Z. Williams.

The role of spectrophotometric standards in the clinical chemistry laboratory, R. N. Rand.

Spectrophotometric standards, W. H. Venable, Jr.

An alternative to accurate pyrometry in distinguishing concurrent vaporization reactions. Postulated results using the vaporization of gold in analyzing the vaporization of beryllium oxide in water vapor, T. B. Douglas.

The determination of iron, titanium, and nickel in Apollo 14 samples by cathode ray polarography, E. J. Maienthal.

The Stark splitting of millimeter wave transitions of water, Y. Beers and G. P. Klein.

J. Res. Nat. Bur. Stand. (U.S.), **76A** *(Phys. and Chem.),* No. 6, (Nov.-Dec. 1972), SD Catalog No. C13.22/sec.A:76/6.

Absolute spectrofluorometry, W. H. Melhuish.

Absolute quantum efficiencies, G. A. Crosby.

Phosphorimetry, J. D. Winefordner.

Measurements of absolute values in biochemical fluorescence spectroscopy, R. F. Chen.

Newer fluorometric methods for the analysis of biologically important compounds, G. G. Guilbault.

Inorganic ions in glasses and polycrystalline pellets as fluorescence standard reference materials, R. Reisfeld.

Development of a new fluorescent reagent and its application to the automated assay of amino acids and peptides at the picomole level, S. Udenfriend.

Considerations on organic compounds in solution and inorganic ions in glasses as fluorescent standard reference materials, R. A. Velapoldi.

Ion-molecule reactions in isopropanol: Implications for its radiolysis, R. Gorden, Jr., and L. W. Sieck.

Excitation of $O_2{}^1\Delta_g$ by electron impact, P. S. Julienne and M. Krauss.

Vibrational and electronic oscillator strengths of LiO, M. Marchetti, P. S. Julienne, and M. Krauss.

J. Res. Nat. Bur. Stand. (U.S.), **76B** *(Math. Sci.),* Nos. 1 and 2, SD Catalog No. C13.22/Sec.B:76/1&2.

Minimax-based selection, adjustment and disaggregation for incompletely specified univariate distributions, A. J. Goldman.

Three results for trees, using mathematical induction, W. A. Horn.

Abstract groups as doubly transitive permutation groups, R. Merris.

Covariances of two sample rank sum statistics, P. V. Tryon.

Efficient techniques for unbiasing a Bernoulli generator, J. A. Lechner.

Checks of the algebraic matrices for the configurations ($d+s^2p$, C. Roth.

J. Res. Nat. Bur. Stand. (U.S.), **76C** *(Eng. and Instr.),* Nos. 1 and 2, SD Catalog No. C13.22/sec.C:76/1&2.

National Bureau of Standards one kilogram balance (NBS No. 2), H. E. Almer.

Ball and cylinder interferometer, J. B. Saunders, Sr.

Precision reference specimens of surface roughness: Some characteristics of the Cali-Block, R. D. Young and F. E. Scire.

Absorption of sound in liquids by the resonator-decay technique: A critique, M. Greenspan.

Ductile fracture by development of surfaces of unstable cavity expansion, C. A. Berg.

Friction and wear of graphite fiber composites, C. A. Berg, S. Batra, and J. Tirosh.

A note on construction of the equivalent plastic strain increment, C. A. Berg.

Monogr. 25, Section 10. **Standard x-ray diffraction powder patterns. Section 10—Data for 84 substances,** H. E. Swanson, H. F. McMurdie, M. C. Morris, E. H. Evans, B. Paretzkin, J. H.

deGroot, and S. J. Carmel, Nat. Bur. Stand. (U.S.), Monogr. 25, Sec. 10, 161 pages (Nov. 1972) 60 cents, SD Catalog No. C13.44:25/Sec. 10.

Key words: Crystal structure; integrated intensities; lattice constants; peak intensities; powder patterns; reference intensities; standard; x-ray diffraction.

Standard x-ray diffraction patterns are presented for 84 substances. Forty-seven of these patterns represent experimental data and 37 are calculated. The experimental x-ray powder diffraction patterns were obtained with an x-ray diffractometer. All d-values were assigned Miller indexes determined by comparison with computed interplanar spacings consistent with space group extinctions. The densities and lattice constants were calculated, and the refractive indexes were measured whenever possible. The calculated x-ray powder diffraction patterns were computed from published crystal structure data. Both peak height and integrated intensities are reported for the calculated patterns.

Monogr. 124. **Reference tables for low-temperature thermocouples,** L. L. Sparks, R. L. Powell, and W. J. Hall, Nat. Bur. Stand. (U.S.), Monogr. 124, 61 pages (June 1972) 60 cents, SD Catalog No. C13.44:124.

Key words: Cryogenics; homogeneity tests; liquid helium; liquid hydrogen; liquid nitrogen; thermocouples.

The experimental program to establish low-temperature reference tables for the commonly used thermocouples has been completed. Details of the experimental system, instrumentation, data analysis, error analysis, and materials tested are given in order to allow the user to better evaluate and apply the results. The results presented here include: (1) Reference tables for thermocouple types E, K, and T, both as $E=f(T)$ and $T=f(E)$. The shorter $f(E)$ tables have a 0 °C (273.15 K) reference temperature while all other tables have a 0 K reference temperature; (2) Reference tables for Pt and *Ag*-28 at % Au vs the materials used in thermocouple types E, K, and T. These data are presented as $E=f(T)$ only; (3) Orthogonal polynomials and the associated coefficients necessary to generate the data with reduced order approximations; and (4) Power series coefficients for full precision reproduction of the reference data.

The data presented in the $E=f(T)$ tables cover the temperature range from 0 to 280 K. The $T=f(E)$ tables cover temperature ranges from 273.15 K down to the lowest temperatures allowed by table resolution.

Monogr. 128. **Corrosion rates on underground steel test piles at Turcot Yard, Montreal, Canada—Part 1,** W. J. Schwerdtfeger and M. Romanoff, Nat. Bur. Stand. (U.S.), Monogr. 128, 17 pages (July 1972)30 cents, SD Catalog No. C13.44:128.

Key words: Average penetration rate; H-piles; instantaneous corrosion rate; linear polarization; pit depth; polarization curve.

In 1966, isolated steel H-piles allocated for underground corrosion tests were installed in three locations at the Turcot Yard Interchange of the Transcanadian Highway at Montreal. The reason for the installation was to furnish answers to some questions concerning the corrosion characteristics of piles, 12 in-74 lb/ft(30.5 cm-110 kg/m), which are identical with the piles supporting the concrete piers under the highway. Polarization measurements have been made once every year since installation.

This paper describes the determination of corrosion rates based on the polarization measurements made up to the time of removal of the first group of piles in 1969. The piles, placed underground at the three locations, differ mainly in that at one site all the piles are bare, at the second site the upper ends of the piles are coated with an epoxy paint and at the third site the upper ends are encased in concrete. Physical measurements made on the cleaned piles after removal are correlated with corrosion rates calculated from the polarization measurements. Also, penetration rates on the piling based on the polarization data are compared with average penetration rates (based on actual weight losses) on relatively small pipe specimens. The pipe specimens were removed from 28 underground sites having a range of soil resistivities comparable to those of the three piling sites.

Using one of the polarization techniques applied to the individual test piles, polarization measurements were also carried out on 32 interconnected piles supporting one of the concrete piers. The calculated average corrosion rate of the 32 piles was found to compare favorably with that of the separate test piles in the same area.

Monogr. 129. **The development of Loran-C navigation and timing,** G. Hefley, Nat. Bur. Stand. (U.S.), Monogr. 129, 144 pages (Oct. 1972) $4.50, SD Catalog No. C13.44:129.

Key words: Cyclan; cytac; Loran; Loran-C; low frequency; navigation; pulse propagation; radio positioning; time dissemination; time transfer system.

The Loran-C timing and navigation concept and its implementation in the form of the Loran-C system has taken on considerable importance in a variety of military and civilian applications such as microsecond clock synchronization, precision tactical or civil navigation, etc. Future applications like tying together continental surveys, aircraft collision avoidance, etc., have yet to be explored in detail. This work traces the development of the Loran-C concept from its inception as a 100 kHz pulse hyperbolic navigation system to more recent times when it found a variety of applications to both timing and navigation. This work is intended to present the story of Loran-C in a readable and understandable way without resorting to the complicated mathematical formulation of the theory or detailed instrumentation aspects. Thus, the history, experimental and theoretical developments, political decisions, and field testing of the early equipment are described and the lessons learned can certainly be a guide for modern development of the system in all its detailed applications.

SP260-40. **Standard reference materials: selection of differential thermal analysis temperature standards through a cooperative study (SRM 758, 759, 760),** H. G. McAdie, P. D. Garn, and O. Menis, Nat. Bur. Stand. (U.S.), Spec. Publ. 260-40, 71 pages (Aug. 1972) 65 cents, SD Catalog No. C13.10:260-40.

Key words: DTA; International Confederation on Thermal Analysis; international cooperative testing; Standard Reference Materials NBS 758, 759, 760; temperature scale; thermal analysis.

The testing and evaluation program leading to the certification of 10 materials as Standard Reference Materials NBS 758, 759 and 760, for calibrating the temperature scale for thermal analysis is described. The international cooperative testing program was set up on the basis of a preliminary program initiated in 1966. Thirty-four laboratories reported to the Standards Committee of the International Confederation on Thermal Analysis. The results were obtained on a variety of apparatus under their conditions of experimentation, except that the heating rate was prescribed in the range of 4 to 10 °C per minute. The data were processed to obtain means and measures of scatter, not only in total, but separated in terms of a number of sample number of sample holder parameters. The sample holder geometry was the only parameter having a clear effect on the extrapolated onset and peak temperatures. The effects of the thermocouple position and calibration were tested, but no significant effect was found. The heating rate has only a small effect, tending to increase the spread of onset and peak temperature values from the DTA are somewhat higher than the thermodynamic equilibrium values reported in the literature. Based on the mean values from all the laboratories the standard deviation was 5 to 8 °C, which includes the bias between laboratories as well as measurement errors.

SP260-41. **Standard reference materials: use of standard light-sensitive paper for calibrating carbon arcs used in testing textiles for colorfastness to light,** L. A. Wood and P. J. Shouse, Nat. Bur. Stand. (U.S.), Spec. Publ. 260-41, 24 pages (Aug. 1972) 30 cents, SD Catalog No. C13.10:260-41.

Key words: Carbon-arcs, standardization of; color-fastness, testing of; fading tests, standardization; light-sensitive paper; paper, light-sensitive; textiles, fading of.

The use of NBS Light-Sensitive Paper and NBS Booklets of Standard Faded Strips in the standardization of carbon arcs is described. These lamps are used to determine the fading characteristics and degradation of textiles and other materials when subjected to visible and ultraviolet radiation. The light-sensitive paper is useful in calibrating the arcs in terms of NBS Standard Fading Hours (SFH) or equivalent exposure in the NBS Master Carbon-Arc Lamp.

SP260-42. **Standard reference materials: the characterization of linear polyethylene SRM 1475,** H. L. Wagner and P. H. Verdier, Editors, Nat. Bur. Stand. (U.S.), Spec. Publ. 260-42, 39 pages (Sept. 1972) 40 cents, SD Catalog No. C13.10:260-42.

Key words: Density; differential refractive index; gel permeation chromatography (GPC); light scattering; linear polyethylene; melt flow rate; molecular weight distribution; number average molecular weight; osmometry; refractive index; standard reference material; viscosity; weight average molecular weight; Z average molecular weight.

The National Bureau of Standards has issued a linear polyethylene standard reference material, SRM 1475. This material is certified for weight average molecular weight (M_w), number average molecular weight (M_n), Z average molecular weight (M_z), molecular weight distribution, limiting viscosity numbers in several solvents, melt flow rate, and density. The experimental details of the determination and certification of these properties are given in these collected papers previously published in the Journal of Research of the National Bureau of Standards.

SP260-43. **Standard reference materials: preparation and homogeneity characterization of an austenitic iron-chromium-nickel alloy,** H. Yakowitz, A. W. Ruff, and R. E. Michaelis, Nat. Bur. Stand. (U.S.), Spec. Publ. 260-43, 19 pages (Nov. 1972) 45 cents, SD Catalog No. C13.10:260-43.

Key words: Austenitic stainless steel; electron probe microanalysis; Fe-Cr-Ni alloy; homogeneity testing; metallography; stacking fault energy; Standard Reference Material.

An alloy of weight fraction 0.710 iron, 0.183 chromium and 0.107 nickel was characterized at the micrometer level of spatial resolution by means of electron probe microanalysis. This alloy, designated SRM 479, is of suitable homogeneity for use as a standard in microanalytical techniques. The coefficient of variation for each of the three elements is not more than 1.5% based on about 800 analyses involving five different specimens. There is no statistically significant variation in composition within specimens or from specimen to specimen. Electron probe microanalysis was carried out using different instrumental conditions and operators. SRM 479 is supplied as a disc about 4.6mm diameter by 1mm thick.

SP329. Supplement 1. **An index of U.S. voluntary engineering standards,** W. J. Slattery, Editor, Nat. Bur. Stand. (U.S.), Spec. Publ. 329, Suppl. 1, 459 pages (Dec. 1972) $9.00, SD Catalog No. C13.10:329.

Key words: Engineering Standards, index of; index of standards, recommended practices, specifications, test methods; Key-Word-In-Context index of voluntary standards; standards, voluntary, index of.

This supplement contains the permuted titles of more than 6,300 standards, specifications, test methods, and recommended practices published by 225 U.S. technical societies, professional organizations and trade associations. Each title can be found under all the significant key words which it contains. These key words are arranged alphabetically down the center of each page together with their surrounding context. The date of publication or last revision, the standard number and an acronym designating the standards-issuing organization appear as part of each entry.

SP348. **The science of ceramic machining and surface finishing.** Proceedings of a symposium sponsored by the American Ceramic Society, the Office of Naval Research, and the National Bureau of Standards, Nov. 2-4, 1970, held at NBS, Gaithersburg, Md., S. J. Schneider, Jr., and R. W. Rice, Editors, and C. F. Bersch, A. M. Diness, and J. B. Wachtman, Jr., Associate Editors, Nat. Bur. Stand. (U.S.), Spec. Publ. 348, 431 pages (May 1972) $5.25, SD Catalog No. C13.10:348.

Key words: Ceramic machining; ceramics; mechanical effects of machining; removal and shaping of ceramics; surface treatment.

This volume presents the proceedings of the Symposium on the Science of Ceramic Machining and Surface Finishing held at the National Bureau of Standards inGaithersburg, Md., on Nov. 2-4, 1970. The symposium was jointly sponsored by the Baltimore-Washington Section of the American Ceramic Society, the Office of Naval Research, and the National Bureau of Standards. The purpose of the conference was to survey the developing science of ceramic machining and to stimulate further progress by discussion of current problems and research programs. In addition to a panel discussion, 37 review and original research papers were presented with attention focused on four main areas: (1) Techniques and Mechanisms of Removal and Shaping (2) Surface Treatment (3) Analysis and Characterization of Machining Effects and (4) Mechanical and Other Effects of Finishing. An edited version of the floor discussion following each paper is given.

SP349. **Heavy-atom kinetic isotope effects, an indexed bibliography,** M. J. Stern and M. Wolfsberg, Nat. Bur. Stand. (U.S.), Spec. Publ. 349, 39 pages (June 1972) 45 cents, SD Catalog No. C13.10:349.

SP351. **Analytical chemistry: key to progress on national problems.** Proceedings of the 24th Annual Summer Symposium on Analytical Chemistry sponsored by *Analytical Chemistry*, ACS Division of Analytical Chemistry, and NBS Analytical Chemistry Division, and held at the National Bureau of Standards, Gaithersburg, Md., June 16-18, 1971, W. W. Meinke and J. K. Taylor, Editors, Nat. Bur. Stand. (U.S.), Spec. Publ. 351, 481 pages (Aug. 1972) $3.50, SD Catalog No. C13.10:351.

Key words: Agriculture; air pollution; analytical chemistry; biomedicine; clinical chemistry; electronics; oceanography; solid state; water pollution.

This book is the formal report of the proceedings of the 1971 Summer Symposium in Analytical Chemistry held at the National Bureau of Standards, June 16-18, 1971, and cosponsored by the Analytical Chemistry Division of NBS, *Analytical Chemistry*, and the American Chemical Society's Division of Analytical Chemistry. It contains six invited papers by subject matter experts comprehensively reviewing urgent research problems for which advanced analytical techniques need to be developed in the important areas of agriculture, air pollution, clinical chemistry and biomedicine, oceanography, solid state research and electronics, and water pollution. Summaries of related discussions by leading analytical chemists serving as panel members or in attendance at the Symposium are included. Hundreds of important analytical problems retarding progress in these impor-

491-397 O - 73 - 7

tant areas are described and extensive references are given to permit a deeper insight into the problem areas. Accordingly this volume should not only stimulate interest in important problems but should provide a valuable guide for highly relevant analytical research for some time to come.

SP354. **Dental materials research.** Proceedings of the 50th Anniversary Symposium held at the National Bureau of Standards, Gaithersburg, Md., Oct. 6-8, 1969, in Recognition of Fifty Years of Dental Research at NBS, G. Dickson and J. M. Cassel, Editors, Nat. Bur. Stand. (U.S.), Spec. Publ. 354, 238 pages (July 1972) $3.75, SD Catalog No. C13.10:354.

Key words: Adhesives; composite restorative materials; dental materials research; dental restorative materials; future dental needs; laboratory testing and clinical research; mechanical properties; metals research; specifications.

A Symposium on Dental Materials Research was held at the National Bureau of Standards, October 6-8, 1969, on the occasion of the fiftieth anniversary of the dental research program at NBS. The Symposium brought together outstanding researchers in the dental materials field from throughout the world for a comprehensive examination of the present state of research and a look at future dental needs and expectations. The program covered the broad dental materials field—from an examination of the oral environment to a consideration of future needs from the viewpoints of dental practice, dental education, dental industry, and basic science. Invited papers covered metals research, new developments in nonmetallic restorative materials, dynamic methods for determining the mechanical properties of dental materials, and problems of evaluating dental materials and making such evaluations useful to clinical dentistry through the development of specifications.

SP361. Volume 2. **Performance concept in buildings.** Opening addresses, rapporteur reviews, and discussions. Proceedings of a symposium jointly sponsored by the International Union of Testing and Research Laboratories for Materials and Structures (RILEM), the American Society for Testing and Materials (ASTM), and the International Council for Building Research Studies and Documentation (CIB), Philadelphia, Pa., May 2-5, 1972, B. E. Foster, Editor, Nat. Bur. Stand. (U.S.), Spec. Publ. 361, Vol. 2, 169 pages (Sept. 1972) $1.75, SD Catalog No. C13.10:361, Vol. 2.

Key words: Buildings; components; design procedures; experience in use; materials; performance evaluation; performance requirements; user requirements.

Volume 2 records the proceedings of the Joint RILEM-ASTM-CIB Symposium on the Performance Concept in Buildings which was held in Philadelphia on May 2-5, 1972. Volume 1 contains the 82 papers accepted for the Symposium and was published prior to the meetings. This second volume contains the opening addresses; the reports of the rapporteurs, which include a review of the papers and a general discussion in each of six areas; such discussion as was submitted in writing; a general summary of the Symposium with conclusions drawn by the closing rapporteur; and statements by representatives of the three sponsoring organizations outlining the present and probable future activity of these organizations in furthering the performance concept in buildings. The subject matter covered in the papers includes physiological, anthropometrical, psychological, sociological, and economic human requirements and methods of evaluation; physical requirements and methods of evaluation in mechanical, acoustical, thermal, dimensional stability, compatibility, fire properties, and geometry areas; operation and maintenance requirements and methods of evaluation in such areas as maintenance, repair, replacement, and versatility; techniques and problems in applying the performance concept to design; and experience gained in application of the performance concept in design, building, and building use.

SP364. **Solid state chemistry.** Proceedings of the 5th Materials Research Symposium sponsored by the Institute for Materials Research, National Bureau of Standards, Oct. 18-21, 1971, held at Gaithersburg, Md., R. S. Roth and S. J. Schneider, Jr., Editors, Nat. Bur. Stand. (U.S.), Spec. Publ. 364, 799 pages (July 1972) $7.50, SD Catalog No. C13.10:364.

Key words: Chalcogenides; crystallographic shear; electron optical lattice images; lone pair geometry; nonstoichiometry; oxides; refractory hard metals; Solid State Chemistry.

This book presents the Proceedings of the 5th Materials Research Symposium on "Solid State Chemistry" held at the National Bureau of Standards, Gaithersburg, Md., on Oct. 18-21, 1971. The symposium was sponsored by the Institute for Materials Research, NBS. The purpose of the conference was to explore the realm of new inorganic crystalline materials emphasizing crystal chemical and structural aspects, providing a forum for discussion of new research problems and techniques. A total of 56 invited and contributed papers were presented. In addition, the symposium included three unscheduled talks and an open discussion period consisting of four impromptu lectures on very current subjects dealing with nonstoichiometry. The Proceedings are divided into four main groupings, I Oxides, II Borides, Carbides, Silicides, and Related Materials, III Chalcogenides, and IV Open Discussion on Nonstoichiometry. An edited version is given of the floor discussion following each paper.

SP366. **Bibliography on atomic line shapes and shifts (1889 through March 1972),** J. R. Fuhr, W. L. Wiese, and L. J. Roszman, Nat. Bur. Stand. (U.S.), Spec. Publ. 366, 165 pages (Sept. 1972) $1.75, SD Catalog No. C13.10:366.

Key words: Atomic; instrumental broadening; line shapes; line shifts; pressure broadening; resonance broadening; Stark broadening; Van der Waals broadening.

This is the first general, annotated bibliography on atomic line shapes and shifts. It covers exhaustively the atomic spectral line broadening literature in about 1400 separate references extending from 1889 through March 1972. The bibliography contains four major parts: (1) All general interest papers are catalogued according to the broadening mechanisms (and, further, according to special topics under several of the mechanisms), and as to whether the work is a general theory, a general review, a table of profiles or parameters, a comment on existing work, a study of general experimental measurement techniques, or an experimental effort of general importance. Also included are selected papers on important applications of line broadening and on miscellaneous topics relating to atomic spectral line shapes and shifts. (2) In Part 2, all papers containing numerical data are ordered as to element, ionization stage, broadening mechanism (in the case of foreign gas broadening the perturbing species are listed), and it is indicated whether the data are experimentally or theoretically derived. (3) While in the two preceding parts of the bibliography the references are listed for brevity by identification numbers only, in Part 3 all references are listed completely by journal, authors, and title and are arranged chronologically and alphabetically within each year according to the principal authors. (4) A final section contains a list of all authors and their papers.

SP368. **Electrical engineering units and constants,** G. F. Montgomery, Nat. Bur. Stand. (U.S.), Spec. Publ. 368, 2 pages (1972) 10 cents, SD Catalog No. C13.10:368.

SP372. **Laser induced damage in optical materials: 1972.** Proceedings of a Symposium Sponsored by the American Society for Testing and Materials and by the National Bureau of Standards, June 14-15, 1972, NBS, Boulder, Colo., A. J. Glass and A. H. Guenther, Editors, Nat. Bur. Stand. (U.S.), Spec. Publ. 372, 215 pages (Oct. 1972) $1.75, SD Catalog No. C13.10:372.

Key words: IR windows and mirrors; laser damage; laser materials; self-focusing; thin films.

The fourth ASTM Symposium on Laser Induced Damage in Optical Materials was held at the National Bureau of Standards in Boulder, Colo., on June 14-15, 1972. This symposium is held as part of the activity of Subcommittee II on Lasers and Laser Materials, of the ASTM. Subcommittee II is charged with the responsibility of formulating standards for laser materials, components, and devices. The chairman of Subcommittee II is Haynes Lee of Owen-Illinois, Inc. Co-chairmen for the damage symposia are Dr. Arthur H. Guenther of the Air Force Weapons Laboratory, and Professor Alexander J. Glass, Chairman of the Department of Electrical Engineering at Wayne State University.

Approximately 125 attendees at the symposium heard 21 papers on topics relating to laser induced damage in glass, crystalline materials, nonlinear optical materials, thin film dielectric coatings, and infrared components. Particular attention was given to the process of plasma formation at dielectric surfaces, the role played by self-focusing in bulk damage in solids, damage morphology of thin film coatings, and the role of absorption in IR component failure.

The proceedings of these Symposia represent the major source of information in the field of laser induced damage in optical materials. The Symposia themselves, along with the periodic meetings of Subcommittee II, provide a unique forum for the exchange of information regarding laser materials specifications among the manufacturers and users of laser devices, components, and systems. The Symposium also serves as a mechanism of information gathering, to enable the Subcommittee to write informed and realistic specifications.

SP373. **Bibliography of temperature measurement, January 1953 to December 1969,** P. D. Freeze and L. P. Parker, Nat. Bur. Stand. (U.S.), Spec. Publ. 373, 140 pages (Nov. 1972) $2.00, SD Catalog No. C13.10:373.

NSRDS-NBS3. Section 6. **Selected tables of atomic spectra: A. Atomic energy levels—second edition; B. Multiplet tables, HI, D, T (Data derived from the analyses of optical spectra),** C. E. Moore and E. O. Hulburt, Nat. Stand. Ref. Data Ser., Nat. Bur. Stand. (U.S.), 3, Sec. 6, 36 pages (Sept. 1972) 40 cents, SD Catalog No. C13.48:3/Sec. 6.

Key words: Atomic energy levels, HI, D, T; hydrogen spectra, HI, D, T; multiplet tables, HI, D, T; spectra HI, D, T; wavelengths, hydrogen spectra HI, D, T.

The present publication is the sixth Section of a series being prepared in response to the persistent need for a current revision of two sets of tables containing data on atomic spectra as derived from analyses of optical spectra. As in the previous sections, Part A contains the atomic energy levels and Part B the multiplet tables. The spectra of hydrogen and of the isotopes deuterium and tritium are included. The form of presentation is described in detail in the text to Section 1.

NSRDS-NBS39. **Tables of molecular vibrational frequencies, consolidated Volume I,** T. Shimanouchi, Nat. Stand. Ref. Data Ser., Nat. Bur. Stand. (U.S.), 39, 164 pages (June 1972) $3.00, SD Catalog No. C13.48:39.

Key words: Fundamental frequencies; infrared spectra; polyatomic molecules; Raman spectra; vibrational frequencies.

The compilations of fundamental vibrational frequencies of molecules previously published as NSRDS-NBS6, NSRDS-NBS11, and NSRDS-NBS17 have been revised and extended to 52 additional molecules. This consolidated volume includes data on a total of 223 molecules. Selected values of the fundamental vibrational frequencies are given for each molecule, together with observed infrared and Raman spectral data and citations to the original literature. The selection of vibrational fundamentals has been based on careful studies of the spectral data and comprehensive normal-coordinate analyses. An estimate of the accuracy of the selected values is included. The tables provide a convenient source of information for those who require vibrational energy levels and related properties in molecular spectroscopy, thermodynamics, analytical chemistry, and other fields of physics and chemistry.

NSRDS-NBS41. **Crystal structure transformations in binary halides,** C. N. R. Rao and M. Natarajan, Nat. Stand Ref. Data Ser., Nat. Bur. Stand. (U.S.), 41, 53 pages (July 1972) 55 cents, SD Catalog No. C13.48:41.

Key words: Binary halides; crystal structure transformation; electronic data; phase transformation; spectroscopic data; thermodynamic data; x-ray diffraction data.

A critical survey of the data describing crystal structure transformations in binary halides is compiled. Data on thermodynamic, crystallographic, spectroscopic and electronic properties are given for each transformation. Experimental techniques used to obtain the data are named and comments on the data are included in the tables. The literature is surveyed up to 1970. References have been selected on the basis of their pertinence to the data which are cited and do not represent all the available literature.

NSRDS-NBS42. **Selected specific rates of reactions of the solvated electron in alcohols,** E. Watson, Jr., and S. Roy, Nat. Stand. Ref. Data Ser., Nat. Bur. Stand. (U.S.), 42, 22 pages (Aug. 1972) 30 cents, SD Catalog No. C13.48:42.

Key words: Alcohols; chemical kinetics; data compilation; radiation chemistry; rates; solvated electron.

Solvated electrons are generated in alcohols by radiolysis, photolysis, reaction with sodium, etc. Rates of reactions of e_s^- with solvent and solute molecules, ions, and transients, in alcohol solutions, have been compiled. Arrhenius parameters are tabulated for some reactions.

FIPS PUB 8-2. **Standard metropolitan statistical areas,** H. E. McEwen, Standards Coordinator, Nat. Bur. Stand. (U.S.), Fed. Info. Process. Stand. Publ. (FIPS Pub.) 8-2, 17 pages (1972) 30 cents, SD Catalog No. C13.52:8-2.

FIPS PUB 12-1. **Federal information processing standards index,** H. E. McEwen, Standards Coordinator, Nat. Bur. Stand. (U.S.), Fed. Info. Process. Stand. Publ. (FIPS Pub.) 12-1, 140 pages (1972) $1.25, SD Catalog No. C13.52:12-1.

Key words: American National Standards; computers, data elements and codes; data processing systems; Federal Information Processing Standards; International Organization for Standardization; management information systems; U.S. Government.

This publication provides material concerning standardization activities in the area of information processing at the Federal, National and International levels. Also included are related policy and procedural guideline documents. A list of Federal Government participants involved in the development of Federal Information Processing Standards is provided. This FIPS PUB is revised and updated annually. Supersedes NBS FIPS PUB 12.

FIPS PUB 22. **Synchronous signaling rates between data terminal and data communication equipment,** G. E. Clark, Jr., Standards Coordinator, Nat. Bur. Stand. (U.S.), Fed. Info. Process. Stand. Publ. (FIPS Pub.) 22, 4 pages (1972) 15 cents, SD Catalog No. C13.52:22.

Key words: Data communication equipment; data processing terminal equipment; data transmission (voice band); Federal Information Processing Standards; synchronous signaling rates; teleprocessing.

This publication prescribes speeds for transferring binary encoded information in synchronous serial or parallel forms between data terminal and data communication equipment employing voice band communication facilities. Speeds ranging from 75 to 9600 bits-per-second are specified.

PS55-72. **Rigid poly (vinyl chloride) (PVC) plastic siding,** L. H. Breden, Technical Standards Coordinator, Nat. Bur. Stand. (U.S.), Prod. Stand. 55-72, 11 pages (Nov. 1972) 15 cents, SD Catalog No. C13.02/2:55-72.

Key words: Building materials; flammability of outdoor siding; plastic material; poly (vinyl chloride) siding; siding, poly (vinyl chloride); weathering of plastic siding.

This Voluntary Product Standard establishes requirements and methods of test for the materials, dimensions, weight, warp, shrinkage, flammability, impact strength, weatherability, expansion, and appearance of extruded single wall siding, manufactured from rigid PVC compound. Methods of indicating compliance with this Standard are also provided.

TN379-1. **Standard time and frequency: its generation, control, and dissemination from the National Bureau of Standards Time and Frequency Division,** J. B. Milton, Nat. Bur. Stand. (U.S.), Tech. Note 379-1, 26 pages (June 1972) 35 cents, SD Catalog No. C13.46:379-1.

Key words: Clock synchronization; frequency and time dissemination; primary frequency standard; standard frequency broadcasts; time interval; time scales.

The Time and Frequency Division of the National Bureau of Standards produces the NBS time scales, AT(NBS) and UTC(NBS). These time scales are developed by utilizing the properties of the NBS frequency standard, NBSFS. The main byproduct of these time scales is the operational clock systems. These operational clock systems are used, among other things, to calibrate the clocks and secondary standards necessary for the operation of the NBS radio stations, WWV, WWVB, WWVL, and WWVH. These stations transmit UTC(NBS), and various tones, alerts, and corrections for time-of-day information.

TN467. **Activation analysis: a bibliography through 1971,** G. J. Lutz, R. J. Boreni, R. S. Maddock, and J. Wing, Editors, Nat. Bur. Stand. (U.S.), Tech. Note 467, 892 pages (Aug. 1972) $7.00, SD Catalog No. C13.46:467.

Key words: Activation analysis; bibliography; element determined; literature file; matrix analyzed; technique used.

References to papers published in the open literature which describe work using activation analysis are printed from a computer based storage and retrieval system. Published as a two-part volume, part 1 is a listing of references according to accession numbers (approximately 6200) while part 2 is composed of four appendices. Appendix I is an index for the element determined, Appendix II is an index of the matrix analyzed, Appendix III is an index of the technique used, Appendix IV is an author index. The two parts when used together, permit a literature search defined by the several indices. Supersedes NBS TN467, Parts 1 and 2 issued May 1971.

TN587. **Organic Chemistry Section: summary of activities, July 1970 to June 1971,** R. Schaffer, Editor, Nat. Bur. Stand. (U.S.), Tech. Note 587, 131 pages (Aug. 1972) $1.25, SD Catalog No. C13.46:587.

Key words: Bilirubin; cholesterol; cortisol; e.s.r.; D-mannitol; NADH; n.m.r.; purity; SRM; Standard Reference Materials; VMA.

This report of the Organic Chemistry Section of the National Bureau of Standard's Institute for Materials Research provides a summary of a year's scientific activity; as such, it covers both work that was completed and some that is still in progress. The development of Standard Reference Materials (SRM's) and their certification, and journal publications describing aspects of that work, as well as other research activities, are the output of the Section.

In the SRM category, the major subjects of this report are bilirubin, cholesterol, cortisol, D-glucose, 4-hydroxy-3-methoxy-DL-mandelic acid (VMA), D-mannitol, and the reduced form of nicotinamide adenine dinucleotide (NADH).

Studies concerning carbohydrates include synthetic work with D-psicose, n.m.r. employing internuclear double-resonance, and mass spectroscopy of 6-deoxy-1,2:3,5-di-*O*-isopropylidene-α-D-glucose, spectroscopic studies of derivatives of 6-amino-6-deoxy-D-glucose-6-^{15}N (employing mass spectrometry, Fourier-transform, ^{13}C-n.m.r. and hetero-nuclear, ^{15}N indor techniques), and *p*-bromophenylosotriazoles of inositols.

Other research utilized e.s.r. and involved periodic acid oxidation of azines, solid-state oxidation of benzenehexol on active manganese dioxide, and the formation of stable radical-anions from glyoxal bis(phenylhydrazone).

TN594-2. **Optical radiation measurements: Photometric instrumentation and research (1970 to 1971),** E. F. Zalewski, A. R. Schaefer, K. Mohan, and D. A. McSparron, Nat. Bur. Stand. (U.S.), Tech. Note 594-2, 44 pages (Sept. 1972) 50 cents, SD Catalog No. C13.46:594-2.

Key words: Instrumentation; lamp orientation; lamp power circuitry; lamp stability; photodetector amplifier; photometry.

This document was written primarily to serve two purposes. First, some of the basic instrumentation which has recently been developed for use in photometry at NBS is described. The design and application of photodetector amplifiers, lamp power circuitry, and mechanical instrumentation are discussed. Second, three photometric experiments are described: the stability testing of some flux lamps and intensity lamps and the determination of the dependence of relative intensity on orientation. These experiments and their conclusions have proven useful in pointing out areas which need further investigation and in planning the directions of future work.

TN594-3. **Optical radiation measurements: Photometric calibration procedures,** V. I. Burns and D. A. McSparron, Nat. Bur. Stand. (U.S.), Tech. Note 594-3, 35 pages (Nov. 1972) 60 cents, SD Catalog No. C13.46:594-3.

Key words: Calibration procedures; color temperatures; luminous flux; luminous intensity; photometry; uncertainty.

The National Bureau of Standards supplies calibrations of luminous intensity, luminous flux and color temperature on a routine basis. The procedures, equipment, and techniques used to perform these calibrations as of October 1972 are described. Details of the uncertainty information currently available, including estimates and procedures for determining uncertainties of the reported values, are also presented.

TN619. **Millimeter attenuation and reflection coefficient measurement system,** B. C. Yates and W. Larson, Nat. Bur. Stand. (U.S.), Tech. Note 619, 175 pages (July 1972) $1.50, SD Catalog No. C13.46:619.

Key words: Attenuation; measurement system; millimeter; reflection coefficient, VSWR.

This paper presents the details to implement a WR 15 attenuation and reflection coefficient magnitude measurement system. A discussion of precision and of systematic error is given along with equations for estimating limits of the error. Machine drawings are provided to fabricate the waveguide standards and necessary hardware not commercially available.

TN621. **Liquid-vapor equilibrium in the binary systems of He^4 and He^3 with nD_2 and nH_2,** M. J. Hiza, Nat. Bur. Stand. (U.S.), Tech. Note 621, 66 pages (July 1972) 65 cents, SD Catalog No. C13.46:621.

Key words: Binary systems; gas solubility; He^4-nD_2; He^3-nD_2; He^4-nH_2, He^3-nH_2; liquid-vapor equilibrium; nD_2 vapor pressure; nH_2 vapor pressure.

Experimental data are reported for the equilibrium liquid and vapor phase compositions of the He^4-nD_2 and He^3-nD_2 systems from 20 to 30 K and the He^4-nH_2 and He^3-nH_2 systems from 20 to 28 K. The maximum experimental pressures were 20 and 16 atm (2.0 and 1.6 MN/m^2) for the He^4 and He^3 systems, respectively. In addition, vapor pressures were measured from 20 to 34 K for nD_2 and from 20 to 30 K for nH_2.

Values of Henry's constants, enhancement factors, K-values, and heats of solution were derived from the experimental data for each system. The derived properties are compared with those derived from previous data for the He^4-nH_2, He^4-pH_2, and He^3-nH_2 systems.

TN623. **Invariance of the cross ratio applied to microwave network analysis,** R. W. Beatty, Nat. Bur. Stand. (U.S.), Tech. Note 623, 23 pages (Sept. 1972) 35 cents, C13.46:623.

TN624. **An evaluation of several cryogenic turbine flowmeters,** J. A. Brennan, R. W. Stokes, D. B. Mann, and C. H. Kneebone, Nat. Bur. Stand. (U.S.), Tech. Note 624, 90 pages (Oct. 1972) $1.00, SD Catalog No. C13.46:624.

Key words: Cryogenic; flow; liquid nitrogen; mass; mass flowmeters; measurement; turbine flowmeters; volume flowmeters.

The National Bureau of Standards (NBS) and the Compressed Gas Association (CGA) have jointly sponsored a research program on cryogenic flow measurement. A cryogenic flow research facility was constructed and has been used to evaluate cryogenic flowmeters operating on several different principles.

The operation and the accuracy of the flow facility is briefly described. The performance of the flowmeters in liquid nitrogen is described by reporting the precision and bias of the meters before and after an 80-hour stability test and by defining the existence of temperature, pressure, flow rate, subcooling, and time order (wear) dependencies.

Meters were evaluated with flow rates ranging from 20 to 210 gpm (1.3 to 13.2 l/s), pressures ranging from 32 to 112 psia (0.22 to 0.77 MN/m^2), and with temperatures ranging from 72 to 90 K.

TN700. **COMBO: A general-purpose program for searching, annotating, encoding-decoding, and reformatting data files,** R. McClenon and J. Hilsenrath, Nat. Bur. Stand. (U.S.), Tech. Note 700, 68 pages (1972) 75 cents, Stock No. 0303-0921.

Key words: Alphanumeric data files; data retrieval; editing program; file editor; FORTRAN program; general-purpose modular programming; reformatting program; report generator; searching program.

COMBO, a FORTRAN program for searching magnetic tape files, generating reports, and reformatting the file, is described and listed. The program is capable of reading separate card images from a file blocked in physical records and recognizing logical blocks marked by a fixed-field ID. Up to 99 different types of lines, each with its own format, can be recognized by examining a special code or label. The program can be instructed to search for the occurrence of each of certain character strings, using a different list for each type of line and two levels of Boolean logic. Lines can be broken into pieces, using either a fixed-field format or a single separator or flags to define the pieces, and the pieces can be rearranged, with labels or comments optionally inserted between them. Editing, in which specified strings are replaced by other strings, can also be performed. The program can accommodate a variable number of cards of each type per block. It was assembled from general-purpose subroutines of modular design and is substantially machine-independent.

TN706. **Structural performance evaluation of innovative building systems,** F. Y. Yokel and N. F. Somes, Nat. Bur. Stand. (U.S.), Tech. Note 706, 16 pages (Aug. 1972) 25 cents, Stock No. 0303-1010.

Key words: Building; connections; housing; neoprene; performance criteria; performance evaluation; performance testing; reinforced concrete; standard tests; structure, testing.

Considerable attention has recently been focused on the development of performance criteria. Performance criteria are presently used in the U.S. by the Building Research Division of the Institute for Applied Technology, National Bureau of Standards, to evaluate innovative building systems.

While building codes and design standards are usually related to specific building materials and design solutions, performance criteria are derived from user requirements and are independent of specific technological solutions.

Many attributes inherent in traditional building systems which are acceptable to the user may not be present in untried innovative systems. The performance criteria therefore address themselves to many aspects of structural performance which are not considered in present codes and design standards.

The successful application of performance criteria depends on the feasibility of evaluating compliance.

Performance can be evaluated by analysis by judgment based on past experience, or by physical simulation. Deterioration with time must be considered, and performance criteria are viewed as minimum requirements which should be met at any time during the service life of a structure. An example is presented where physical testing was used to evaluate the performance of a high-rise housing system.

TN726. **Testing and fabrication of wire-bond electrical connections—a comprehensive survey,** H. A. Schafft, Nat. Bur. Stand. (U.S.), Tech. Note 726, 140 pages (Sept. 1972) $1.25, SD Catalog No. C13.46:726.

Key words: Bonding; degradation (wire bond); discrete devices; electrical interconnection; fabrication (wire bond); failure (wire bond); hybrid circuits; integrated circuits; microelectronics; reliability; semiconductor devices; survey (wire bond); testing (wire bond); thermocompression bonding; ultrasonic bonding; wire bond.

The fabrication and testing of wire-bond electrical connections used in integrated circuits, hybrid circuits, and low-power discrete semiconductor devices are surveyed comprehensively. The survey is generally restricted to wire-bond electrical connections where the wire diameter is less than 2 mils and where the wire is bonded either by thermocompressive or ultrasonic means. Under the general heading of fabrication, the essential features of the thermocompression and ultrasonic bonding processes, the fabrication procedures, and the characteristics of the constituent materials of the wire bond pertinent to high reliability are surveyed. Also included is a review of the interaction of gold and aluminum as one of the primary failure mechanisms in wire bonds. Both new and old test methods are surveyed with emphasis on their capabilities and limitations. In particular, the following test methods are discussed: visual inspection; pull, shear, air blast, push, ultrasonic stress, centrifuge, mechanical shock, variable frequency vibration, vibration fatigue, short-duration stress pulse, temperature cycling, thermal shock, bond interface resistance, and electrical continuity tests; noise measurement; and ul-

trasonic bond monitoring. Analyses of some of the methods with regard to the stress that the test imposes on the wire bond have been made and the results are used in discussing the relevant methods.

TN733. **Methods of measurement for semiconductor materials, process control, and devices, quarterly report January 1 to March 31, 1972,** W. M. Bullis, Editor, Nat. Bur. Stand. (U.S.), Tech. Note 733, 59 pages (Sept. 1972) 60 cents, SD Catalog No. C13.46:733.

Key words: Aluminum wire; base transit time; carrier lifetime; die attachment; electrical properties; epitaxial silicon; gamma-ray detectors; germanium; gold-doped silicon; infrared response; methods of measurement; microelectronics; microwave diodes; nuclear radiation detectors; probe techniques (a-c); resistivity; ribbon wire bonding; semiconductor devices; semiconductor materials; semiconductor process control; silicon; thermal resistance; thermographic measurements; ultrasonic bonding; wire bonds.

This quarterly progress report, fifteenth of a series, describes NBS activities directed toward the development of methods of measurement for semiconductor materials, process control, and devices. Significant accomplishments during this reporting period include development of a procedure to correct for the substantial differences of transistor delay time, a device characteristic frequently used as a screen in radiation hardness assurance tests, as measured with different instruments or with the same instrument at different frequencies; association of infrared response spectra of poor quality germanium gamma-ray detectors with spectra of detectors fabricated from portions of a good crystal that had been degraded in known ways; and confirmation of the excellent quality and cosmetic appearance of ultrasonic bonds made with aluminum ribbon wire. Work is continuing on measurement of resistivity of semiconductor crystals; study of gold-doped silicon; development of the infrared response technique; evaluation of wire bonds and die attachment; and measurement of thermal properties of semiconductor devices, delay time and related carrier transport properties in junction devices, and noise properties of microwave diodes. Supplementary data concerning staff, standards committee activities, technical services, and publications are included as appendixes.

TN735. **The effects of magnetic fields on magnetic storage media used in computers,** S. B. Geller, Nat. Bur. Stand. (U.S.), Tech. Note 735, 35 pages (July 1972) 40 cents, SD Catalog No. C13.46:735.

Key words: Erasure, magnetic media; erasure, permanent magnet; erasure, shielding against; erasure, signal loss due to; magnet fields, erasure with; magnetic media, computer; magnetic media, information damage; permanent magnets; permanent magnet, erasure with; shielding.

Experiments have been performed with different types of magnets to determine their effects on the information stored on magnetic storage media. The test results that were obtained with recorded computer tapes are discussed and guidelines are suggested to computer installation managers for protecting their recorded tapes, disks and drums against unwarranted erasure by magnetic fields. The effects of other forms of energy on recorded magnetic media are briefly considered.

TN736. **Carrier lifetime measurement by the photoconductive decay method,** R. L. Mattis and A. J. Baroody, Jr., Nat. Bur. Stand. (U.S.), Tech. Note 736, 52 pages (Sept. 1972) 50 cents, SD Catalog No. C13.46:736.

Key words: Carrier lifetime; germanium; photoconductive decay; silicon.

The photoconductive decay (PCD) method of carrier lifetime measurement is discussed with emphasis on experimental and analytical work done at NBS. The relationship between photoconductive decay time τ_{PCD}, bulk decay time τ_B, and lifetime is described briefly and the PCD method is summarized. The determination of τ_B from τ_{PCD} and the influence of higher modes of recombination are discussed.

Experimental data, supported by theoretical considerations, are presented to demonstrate the dependence of τ_{PCD} on excess carrier density, the type of light source, specimen homogeneity, filter thickness, and temperature. The dependences of τ_{PCD} on excess carrier density and temperature are consequences of the statistics of the recombination process. Measurements made with chopped light excitation are shown to be less in error due to higher modes of recombination than are measurements made with pulsed light excitation. The presence of inhomogeneities is verified in two crystals. Use of a filter is also shown to reduce the influence of higher modes. An unexpected reduction in τ_{PCD} with increasing filter thickness is shown to be caused by an inhomogeneity.

Other experimental conditions are discussed as they affect the measurement of τ_{PCD}. It is shown that the light turnoff must be sufficiently fast and the series resistance sufficiently large that they do not interfere with the measurement. Equations are developed whereby the specimen current and illumination pattern can be chosen such that carrier sweep-out at the ends of the specimen and ohmic heating are avoided. The end contacts must be sufficiently ohmic that excessive contact resistance does not interfere with the measurement.

Trapping is defined and the means for identifying it are discussed briefly. The PCD method is inappropriate for determining minority carrier lifetime when trapping is present or under other circumstances when the hole and electron lifetimes are unequal.

TN737. **Interior/exterior noise levels of over-the-road trucks: report of tests,** W. A. Leasure, Jr., T. L. Quindry, D. E. Mathews, and J. M. Heinen, Nat. Bur. Stand. (U.S.), Tech. Note 737, 317 pages (Sept. 1972) $2.25, SD Catalog No. C13.46:737.

Key words: Acoustics; noise measurement; noise (sound); truck noise (exterior); truck noise (interior); trucks.

This report presents the results of interior and exterior noise measurements which were made on a representative sample of fifteen over-the-road trucks under various operational modes. In-cab measurements were made six inches from the right and left ears of the driver with windows open and closed. Simultaneous exterior measurements were made utilizing a six-microphone array. Graphic histories of A-weighted sound level versus time are presented for all test conditions and microphone locations. The National Bureau of Standards made the field measurements and tabulated the data; however, interpretation of the results is the responsibility of the Department of Transportation and the American Trucking Associations—the joint sponsors of the study. These data supplement the limited in-cab data available in the public domain and will form part of public Docket No. MC-22 Advanced Notice of Proposed Rule Making concerning vehicle interior noise levels which was issued by the Bureau of Motor Carrier Safety, Department of Transportation, in response to Federal Regulations concerning occupational noise exposure.

TN738. **Subroutine for the calculation of CODEN check characters,** D. Garvin, Nat. Bur. Stand. (U.S.), Tech. Note 738, 12 pages (Sept. 1972) 25 cents, SD Catalog No. C13.46:738.

Key words: Check characters; CODEN; computer program; journal abbreviations.

A FORTRAN subroutine is described that computes the check character for an ASTM CODEN for Journal Titles. This routine, written for input in Hollerith characters, is adaptable to other coding schemes. A listing of the routine is provided.

TN739. **A universal dropout tester for magnetic storage media,** S. B. Geller, Nat. Bur. Stand. (U.S.), Tech. Note 739, 32 pages (Sept. 1972) 35 cents, SD Catalog No. C13.46:739.

Key words: Dropouts, cassette tapes; dropouts, computer magnetic tapes; dropouts, instrumentation magnetic tapes; dropouts, measurement system; magnetic storage media; signal amplitude, dropouts.

This Technical Note describes a signal dropout detection and counting system which was designed to make measurements on 1/2 inch magnetic computer tape, magnetic instrumentation tapes and magnetic cassette tapes as required by existing and potential Federal Specifications. The calibration and operational procedures for the system are described in detail.

TN742. **United States and Canadian fabric flammability standards,** R. G. Katz, Nat. Bur. Stand. (U.S.), Tech. Note 742, 59 pages (Oct. 1972) 60 cents, SD Catalog No. C13.46:742.

Key words: Blankets; Canada; carpets; clothing; fabric flammability testing; fabrics; Flammable Fabrics Act; Hazardous Products Act; mattresses; sleepwear; standards; United States.

Current fabric flammability standards of the United States and Canada are described. The 1967 amendment to the Flammable Fabrics Act of 1953 gave impetus to basic and applied research in the United States and to the development of new test methods and standards for fabric products. Commercial Standard 191-53, the 45-degree angle test, applies to most clothing items, but a new stringent vertical test was developed for children's sleepwear. A small flame source, i.e., a standard methenamine tablet, is used to test carpets and rugs, while a smoldering cigarette is the ignition source for a mattress standard. The test methods attempt to simulate actual conditions.

In 1970, Canada amended the Hazardous Products Act of 1969 to (a) ban from sale those products already declared dangerously flammable by the United States, and (b) ban from sale some berets and sweatshirts that did not meet the 45-degree angle test. Later amendments (1971) deleted the 1970 amendments and established a basic minimum flammability standard covering all textile products for consumer use. A more stringent standard was established for children's sleepwear and bedding (excluding mattresses, mattress pads and pillows) that use the same 45-degree angle test but with a time of flame spread of 7 seconds or less.

TN744. **Disclosures on: New syntheses of perfluorostyrene and other highly fluorinated derivatives; temperature-, radiation-, and vacuum-resistant magnetic tape; conductometric titration cell; mill work positioner; process for fabricating superconducting microbridges; apparatus for displaying average wind vane or other shaft position; and document numbering machine responsive to a staple in a print area for printing in an alternate area,** D. Robbins and A. J. Englert, Editors, Nat. Bur. Stand. (U.S.), Tech. Note 744, 31 pages (Nov. 1972) 55 cents, SD Catalog No. C13.46:744.

Key words: Conductometry; decoding matrix; fluoroolefins; integrator; magnetic sensing probe; magnetic tape; microbridge; numbering machine; perfluorostyrene; shaft position encoder; staple detector; superconducting; synthesis, chemical; titration; wind vane; work positioner.

This Note describes and illustrates seven developments that are believed to embody interesting and unusual solutions to current problems in their fields.

TN746. **Estimates of the nature and extent of lead paint poisoning in the United States,** J. F. Gilsinn, Nat. Bur. Stand. (U.S.), Tech. Note 746, 163 pages (Dec. 1972) $2.00, SD Catalog No. C13.46:746.

Key words: Childhood diseases; estimation; health problems; lead; lead paint; lead paint poisoning; lead poisoning; mathematical modeling; models; urban health problems.

This report evaluates the nationwide magnitude and extent of pediatric lead poisoning resulting from the ingestion of lead-based paint. Estimates are given of the number of children who have elevated blood lead levels (40 μg or more of lead per 100 ml of whole blood) in each of 241 Standard Metropolitan Statistical Areas throughout the country. The mathematical models used to obtain these estimates are documented together with the assumptions and data upon which those models are based. Partial validation of both models and assumptions is also reported.

TN747. **Critical evaluation of data in the physical sciences—A status report on the National Standard Reference Data System, June 1972,** S. A. Rossmassler, Editor, Nat. Bur. Stand. (U.S.), Tech. Note 747, 79 pages (Nov. 1972) $1.25, SD Catalog No. C13.46:747.

Key words: Atomic and molecular data; chemical kinetics; colloid and surface properties; data systems design; information services; mechanical properties; nuclear data; standard reference data; solid state data; thermodynamic and transport properties.

This is a report on the status of the National Standard Reference Data System as of June 1972. Recent activities of the Office of Standard Reference Data are summarized and future plans are indicated. A complete list of data evaluation projects supported by the Office of Standard Reference Data during Fiscal Year 1972 is included; this list also includes projects which received financial support during an earlier fiscal year, and which are still actively involved in some aspect of data compilation and evaluation, or which are still preparing a product for publication. Progress in data processing and in information services is reviewed. The appendix includes a listing of continuing data centers in the United states and a list of publications resulting from the standard reference data program.

The following Bibliography Series are available by purchase from the National Technical Information Service (NTIS), Springfield, Va. 22151.

COM-72-10621. **Index and cumulative list of papers on radiation chemistry,** Vol. V, Nos. 1-26, Jan. through June 1972, Radiation Chemistry Data Center, Radiation Laboratory, University of Notre Dame, Jan. 1972, $6.00.

Key words: Biological systems; esr; hot atom chemistry; luminescence; photochemistry; polymers; radiation chemistry; radiation chemistry theory.

The Radiation Chemistry Data Center, as part of its operations, collects, keywords, and stores literature of fundamental radiation chemistry and several related fields. Since 1968 references to this literature have been stored in computer files. These files have been used for retrospective researches and for the Weekly List of Papers on Radiation Chemistry which has been used as a current-awareness aid by radiation chemists since 1968. This index to and cumulation of entries in the Weekly List of Papers on Radiation Chemistry for the period of January through June 1972 is intended as a guide to the recent literature and as a searching tool for those who would find a printed index valuable.

The following are outside publications by the NBS staff, as soon after issuance as practical. For completeness, earlier references not previously reported may be included from time to time. The five-digit number at the beginning of each entry is used for record keeping only and should not be used when requesting reprints or other information.

12820. Kurylo, M. J., **Absolute rate constants for the addition of O(^{3}P) atoms to propylene,** *Chem. Phys. Lett.* **14,** No. 1, 117-120 (May 1, 1972).

Key words: Hydrogen atoms; propylene; reaction rate; resonance fluorescence.

The rate of addition of oxygen (^3P) atoms to propylene has been investigated by the flash photolysis resonance fluorescence technique. Using O_2 as the atom source, the reaction was studied from 201 to 424 K. A linear least squares treatment of the Arrhenius data gave: $k=(4.17\pm0.33)\times10^{-12}\exp[-(76\pm44)/1.987T]$ in units of cm^3 molecule^{-1} sec^{-1}.

12821. Marchetti, M. A., Krauss, M., Weiss, A. W., **Symmetry-adapted pair correlations in O and O$^-$,** *Phys. Rev. A* **5,** No. 6, 2387-2390 (June 1972).

Key words: Electron affinity; O, O$^-$; pair-correlation energy; shell-correlation energy; symmetry-adapted.

A symmetry-adapted pair-correlation approximation has been used to calculate the electron affinity of the oxygen atom. The calculated electron affinity is 1.47 eV which is in reasonable agreement with experimental values. The present results add to the evidence that the energy difference between similar systems can be calculated with reasonable accuracy using symmetry-adapted pair energies.

12822. de Graaf, L. A., Rush, J. J., Flotow, H. E., Rowe, J. M., **Quasielastic thermal neutron scattering by hydrogen in α-vanadium hydride,** *J. Chem. Phys.* **56,** No. 9, 4574-4581 (May 1, 1972).

Key words: Debye-Waller factor; hydrogen diffusion, interstitial site; linewidth; momentum transfer; neutron scattering, quasielastic scattering; vanadium hydride; vibration.

The diffusion process of hydrogen in vanadium has been studied by quasielastic thermal neutron scattering. Neutron linewidths associated with diffusion broadening have been determined at 485 K for $VH_{0.198}$ and $VH_{0.570}$. These measurements cover a range of momentum transfers (Q) for elastic scattering up to 4.1 Å^{-1}. This is much larger than the momentum transfers obtained in earlier cold-neutron experiments, where no conclusive comparison was possible between data and proposed models involving diffusive jumps between octahedral and tetrahedral sites. The linewidth results for α-$VH_{0.57}$ are compared with these models and with an extension developed in the present paper. Although no complete agreement was obtained, this comparison leads to the conclusion that jumps between tetrahedral sites are predominant in the diffusion process. Differences in the linewidth behavior for $VH_{0.198}$ and $VH_{0.570}$, and the fact that the measured widths at large Q increase rapidly with Q rather than approaching an asymptotic value as predicted by the theory, are discussed. It is suggested that these effects and the large Debye-Waller factors found in the present and previous neutron experiments are connected with the relative magnitudes of diffusion relaxation time and the jump time between sites.

12823. Davis, D. D., Huie, R. E., Herron, J. T., Kurylo, M. J., Braun, W., **Absolute rate constants for the reaction of atomic oxygen with ethylene over the temperature range 232-500 K,** *J. Chem. Phys.* **56,** No. 10, 4868-4876 (May 15, 1972).

Key words: Absolute rate constants; atomic oxygen; ethylene; gas phase kinetics.

Rate constants for the reaction of atomic oxygen with ethylene were measured over a temperature range of 232-500 K using the flash photolysis-resonance fluorescence technique. The rate constant at room temperature was also determined using a flash photolysis-kinetic absorption spectroscopy system and a discharge-flow system coupled to a mass spectrometer. Within the experimental errors of the three techniques, good agreement was found for the rate constant at 298 K. The bimolecular rate constant was also found invariant to changes in both total pressure and reactant concentration. Over the temperature range of the experiments, the rate data could be f. ted by a simple Arrhenius expression of the form,

$$k=5.42\pm0.30\times10^{-12}\exp[(-1130\pm32\text{ cal mole}^{-1})/RT]\text{ cm}^3\text{ molecule}^{-1}\cdot\text{sec}^{-1}.$$

12824. Eby, R. K., Colson, J. P., **Alpha relaxation in polyethylene,** *J. Appl. Phys.* **41,** No. 11, 4313-4316 (Oct. 1970).

Key words: Annealing; density; lamella thickness; mechanical; polyethylene; relaxation; solvent; unit cell.

Data are presented to show that a previously reported correlation of the strength of the alpha relaxation in annealed solution-grown crystals of polyethylene with the inverse of lamella thickness is not unique. Nor is a previously reported dependence of relaxation temperature on lamella thickness unique. As the lamella thickness changes with annealing temperature, the unit cell dimensions, the macroscopic density, and the residual solvent content of the crystals also change. Thus, there are apparent correlations between these parameters and the relaxation strength and temperature. Since it is not obvious which, if any, of these correlations is the fundamental one with regard to the alpha relaxation, some caution must be exerted in interpreting them. As an example of this, data are discussed to suggest that there is at least one other presently unknown parameter of importance to the relaxation.

12825. Scheer, M. D., Klein, R., McKinley, J. D., **Halogens adsorbed on molybdenum: their surface lifetimes and desorption kinetics,** *Surface Sci.* **30,** No. 2, 251-262 (Apr. 1972).

Key words: Desorption kinetics; halogen surface lifetimes; molybdenum; negative surface ionization.

The surface lifetimes of fluorine, chlorine, bromine and iodine adsorbed on a molybdenum surface have been obtained from measurements of the halide ion desorption flux using the modulated molecular beam technique. Measurements were made at temperatures between 1350 and 1850 K and at surface coverages of less than 10^{10} halogen atoms cm^{-2}. The temperature-lifetime data were fitted to an Arrhenius expression from which the binding energies, $\bar{l}$, and pre-exponential factors $\bar{\tau}^0$, were obtained:

F: $\bar{l}=4.65$ eV and $\bar{\tau}^0=3\times10^{-16}$ s;
Cl: $\bar{l}=4.11$ eV and $\bar{\tau}^0=3\times10^{-16}$ s;
Br: $\bar{l}=3.70$ eV and $\bar{\tau}^0=2\times10^{-15}$ s;
I: $\bar{l}=3.15$ eV and $\bar{\tau}^0=1\times10^{-14}$ s.

It was concluded that the halogens are adsorbed as strongly bound surface compounds, MoX (where X is either F, Cl, Br, or I) from which gaseous ions and neutral atoms desorb at rates consistent with the Saha-Langmuir relationship. From that relationship and the above data, separate binding energies and pre-exponentials were calculated for ion and neutral desorption. The importance of the desorption of MoX was assessed.

12826. Reader, J., Epstein, G. L., **Analysis of the spectrum of quadruply ionized yttrium (Y v),** *J. Opt. Soc. Amer.* **62,** No. 5, 619-622 (May 1972).

Key words: Spectra; ultraviolet; wavelengths; yttrium.

The Y v spectrum has been observed in a sliding-spark discharge with the NBS 10.7-m normal-incidence vacuum spectrograph. The analysis has yielded all the levels of the $4p^45s$ configuration and nearly all levels of $4p^44d$ that can combine with the $4p^5\ ^2P$ ground term. The $4s^24p^44d+4s^24p^45s+4s4p^6$ levels have been theoretically interpreted, including configuration-interaction effects. The $4s4p^6\ ^2S_{1/2}$ level was found to have a 26% $4s^24p^44d(^1D)^2S$ character and the $4s^24p^44d(^1D)^2S_{1/2}$ level a 22% $4s4p^6\ ^2S$ character. The energy parameters determined from a least-squares fit of the observed level values are compared with Hartree-Fock calculations. The ionization energy is estimated to be 75.0 ± 0.5 eV.

12827. Barnes, J. D., Fanconi, B. M., **Raman spectroscopy, rotational isomerism, and the "rotator" phase transition in *n*-alkanes,** *J. Chem. Phys.* **56,** No. 10, 5190-5192 (May 15, 1972).

Key words: *n*-alkanes; Raman spectroscopy; rotator phase; rotational isomerism.

Raman spectra of *n*-nonadecane in the ordered and rotator phases are compared to that of the liquid phase to determine the amount of rotational isomerism in the rotator phase. It is concluded that there is little or no rotational isomerism in the rotator phase.

12828. Okabe, H., **Photodissociation of CS_2 in the vacuum ultraviolet; determination of $D_0°$(SC-S),** *J. Chem. Phys.* **56,** No. 9, 4381-4384 (May 1, 1972).

Key words: Bond dissociation energy; CS_2; CS $A\,^1\Pi$; $D_0°$(SC-S); fluorescence; photodissociation; vacuum ultraviolet.

It has been shown that a major primary photochemical process of CS_2 in the vacuum ultraviolet is the reaction,

$$CS_2 \xrightarrow{h\nu} CS\ A\,^1\Pi + S^3P_2,$$

in apparent violation of the spin conservation rule. From the threshold energy of incident photons required to produce the fluorescence, CS $A\,^1\Pi - X\,^1\Sigma$, $D_0°$(SC-S) = 4.463 ± 0.014 eV or 102.9 ± 0.32 kcal/mole has been obtained in excellent agreement with the value derived previously from the photoionization of CS_2. Other related thermochemical data are derived and are compared with those obtained by various methods. The fluorescence excitation spectrum shows peaks corresponding to Rydberg series I and II, indicating that the above reaction is mainly the result of predissociation from Rydberg states. The fluorescence efficiencies became quite small above incident photon energies corresponding to the first ionization potential of CS_2. The CS $A\,^1\Pi$ fluorescence spectrum produced by the 1236 Å line photolysis shows vibrational levels populated up to $v' = 5$. The absorption coefficient of CS_2 has been measured in the region 1200 – 1400 Å.

12829. Camus, P., Sugar, J., **Theoretical study and interpretation of the electronic configurations in TM IL II. Odd excited configurations $4f^{12}(5d+6s)6p$ and $4f^{13}7s$,** *Phys. Scr.* **4,** 263-268 (1971).

Key words: Energy levels; theory; thulium.

The calculation of the energy eigenvalues and the Lande *g* factors of the configuration $4f^{12}(5d+6s)6p$ taken together has allowed the identification of 175 odd levels with a mean error of 97 cm^{-1}. The configuration $4f^{12}5d6p$ is identified at 44 838 cm^{-1}. The eigenvectors of $f^{12}sp$ and those of $f^{12}dp$ for the matrices with *J* greater than or equal to 5 are given in the $^*J_1J_2$ coupling scheme where $^*J_1$ is an eigenvector of the real core of f^{12}. The four levels of the configuration $4f^{13}7s$ are interpreted and the value of the IP of Tm II fitted by interpolation with the neighbouring elements, which is 12.05 volts, is confirmed.

12830. Camus, P., Sugar, J., **Theoretical study and interpretation of the electronic configurations in Tm II. I. Even configurations $4f^{12}(5d+6s)^2+4f^{13}6p$,** *Phys. Scr.* **4,** 257-261 (1971).

Key words: Energy levels; theory; thulium.

The calculation of the energy eigenvalues and the Lande *g* factors of the configurations $4f^{12}(5d+6s)^2+4f^{13}6p$ taken together has led to the interpretation of 155 even levels whose energies are predicted with an rms error of 105 cm^{-1}. The configuration $4f^{12}5d^2$ is correlated with 36 experimental levels, among which is the lowest level at 30 508 cm^{-1}. Eigenvectors of the subgroup of configurations $f^{12}ds+f^{13}p$ are given in the J_1J_2 coupling scheme, which is the closest to the physical coupling.

12831. Tsang, W., **Comparative rate single-pulse shock tube studies on the thermal decomposition of cyclohexene, 2,2,3-trimethylbutane, isopropyl bromide, and ethylcyclobutane,** *Int. J. Chem. Kinet.* **II,** 311-323 (1970).

Key words: Bond energy; cyclohexane; decomposition; gas phase; isopropyl bromide; shock tube; *t*-butyl radical decyclization; 2,2,3-trimethylbutane.

A check of the data from comparative rate single-pulse shock tube experiments has been carried out through the use of a new standard reaction, the decyclization reaction of ethylcyclobutane. The rate expressions for cyclohexene and 2,2,3-trimethylbutane have been found to be

$$k(C_6H_{10} \rightarrow 1,3\text{-}C_4H_6 + C_2H_4) = 10^{15.3} \exp(-33{,}690/T)\ \text{sec}^{-1},\quad 950-1100\ \text{K}, 2-6\ \text{atm}$$

$$k(t\text{-}C_4H_9 - iC_3H_7 \rightarrow t\text{-}C_4H_9\cdot + iC_3H_7\cdot)$$

$$= 10^{16.5} \exp(-36{,}830/T)\ \text{sec}^{-1}, 1000-1100\ \text{K}, 2-6\ \text{atm}$$

in excellent agreement with previously published results. Most of the small discrepancy that does exist is apparently due to the differences between the present and earlier (decomposition of isopropyl bromide) "standard" reaction. For the latter process, the present study yields

$$k(iC_3H_7Br \rightarrow C_3H_6 + HBr)$$

$$\rightarrow 10^{13.73} \exp(-23{,}970/T)\ \text{sec}^{-1}, 800-1000\ \text{K}, 2-6\ \text{atm}$$

These results confirm the correctness of previously published comparative rate single-pulse shock tube experiments. They demonstrate once again that for the decomposition of paraffin hydrocarbons, calculated preexponential factors are at least an order of magnitude higher than the directly measured number and that the accepted value of the heat of formation of *t*-butyl radicals ΔH_{f300} ($tC_4H_9\cdot$) = 29 kJ (6.8 kcals) is at least 10 kJ too low. Finally, attention is called to recent studies on neopentane decomposition in flow and static systems which are in complete agreement with the present conclusions.

12832. Tsang, W., **Rate and mechanism of thermal decomposition of 4-methyl-1-pentyne in a single-pulse shock tube,** *Int. J. Chem. Kinet.* **II,** 23-36 (1970).

Key words: Allene; bond energy; comparative rate; gas phase; heats of formation; kinetics; molecular reaction; propynyl; pyrolysis; single pulse shock tube; 4-methylpentyne-1.

Dilute mixtures of 4-methyl-1-pentyne have been pyrolyzed in a single-pulse shock tube. The decomposition process involves bond breaking:

$$HC{\equiv}C7CH_2(i\text{-}C_3H_7) \xrightarrow{k_B} HC{\equiv}C{-}CH_2\cdot(\text{propynyl}) + i\text{-}C_3H_7.$$

as well as a molecular reaction:

$$HC{\equiv}C{-}CH_2(i\text{-}C_3H_7) \xrightarrow{k_M} C_3H_4(\text{allene}) + C_3H_6.$$

The rate parameters are:

$$k_B = 10^{15.56} \exp(-34{,}940/T)\ (\text{sec}^{-1})$$

$$k_M = 10^{13.1} \exp(-29{,}670/T)\ (\text{sec}^{-1}) \qquad 1100\ \text{K}, 1.5-5\ \text{atm}$$

The heat of formation of propynyl radical is thus ΔH_{f300} = 338 kJ mol^{-1} (80.7 kcal mol^{-1}). This leads to a propynyl resonance energy of 40 kJ mol^{-1} (9.6 kcal mol^{-1}).

12833. Ehrlich, M., **Response of thermoluminescent dosimeters to 15 MeV electrons and ^{60}Co gamma rays,** *Health Phys.* **18,** 287-289 (1970).

Key words: Absorbed dose; CaF_2:Dy; dosimeters; LiF; response; thermoluminescence; 15 MeV electrons; ^{60}Co gamma rays.

Thermoluminescence dosimeters (TLD) were mailed along with Fricke dosimeters to some of the participants in the NBS electron-

dosimetry uniformity studies, for irradiation with 15 MeV electrons in a polystyrene block. The electron-irradiated TLD and Fricke dosimeters then were returned to NBS for evaluation along with similar dosimeters exposed at NBS to ^{60}Co gamma rays. Three TLD systems were used: LiF TLD-100 plaques, LiF TLD-100 powder in gelatine capsules, and CaF_2:Dy TLD-200 plaques. For the gamma rays, absorbed dose in the TLD material was computed from exposure, and for the electrons, it was computed from the absorbed dose measured in the Fricke dosimeters. Within the limits of experimental precision and the reliability of the computations, the relative TL response per unit absorbed dose in the three systems was found to be the same for ^{60}Co gamma rays and for 15 MeV electrons.

12834. Wilson, W. K., Hebert, R. L., **Evaluation of the stability of manifold papers,** *Tappi* **55,** No. 7, 1103-1107 (July 1972).

Key words: Aging; alkalinity; burst strength; degradation; differential thermal analysis; durability; manifold papers; loads; pH; reflectance; stability; storage; tear strength; testing.

The relative stabilities of a group of seven manifold papers were determined by accelerated aging in flowing air at 90 °C and 50% relative humidity. One alkaline paper, one neutral-sized paper, and five acid papers were included. Changes during aging were noted by monitoring folding endurance, pH, tearing strength, bursting strength, load elongation, and reflectance. The alkaline paper was very stable, the neutral-sized paper somewhat less stable, and the acid papers could be ranked in stability approximately according to their pH values. The temperature at which a massive decomposition endotherm (differential thermal analysis) occurred also appeared to be a function of pH.

12835. Schaffer, R., **Occurrence, properties and preparation of naturally occurring monosaccharides (including 6-deoxy sugars),** Chapter in *The Carbohydrates. Chemistry and Biochemistry,* Second Edition, W. Pigman and D. Horton, Eds., **1A,** 69-111 (Academic Press, Inc., New York, N.Y., 1972).

12836. Young, R., Ward, J., Scire, F., **Observation of metal-vacuum-metal tunneling, field emission, and the transition region,** *Phys. Rev. Lett.* **27,** No. 14, 922-924 (Oct. 4, 1971).

Key words: Field emission; MVM tunneling; surface finish; surface physics; tunneling.

We report what we believe are the first observations of metal-vacuum-metal tunneling. A field emitter is brought close to a metal surface and the current-voltage characteristic is measured in three regions: the Fowler-Nordheim region, the intermediate region, and the metal-vacuum-metal region.

12837. Young, R. D., **Surface microtopography,** *Phys. Today* **24,** No. 11, 42-49 (Nov. 1971).

Key words: Microscope; microtopography; single-crystal surface; surface; surface finish; surface profile.

The growing field of surface science would benefit considerably from measurements of surface microtopography down to the atomic level. A brief review is presented of several instruments used to quantitatively characterize the surface microtopography of metallic surfaces. Techniques are discussed for employing the transmission electron microscope, the scanning electron microscope, the optical interference microscope and an engineering profile measuring instrument to measure surfaces suitable for surface science experiments. In addition a new noncontacting instrument, which is presently under development will be described. It is concluded that several techniques are presently available for detecting single atom steps on single-crystal surfaces.

12838. Berger, M. J., Seltzer, S. M., **Bremsstrahlung in the atmosphere,** *J. Atmos. Terr. Phys.* **34,** 85-108 (1972).

Key words: Aurora; balloon experiments; bremsstrahlung; electrons; energy spectrum; sodium iodide detectors.

Calculations are described pertaining to the emission of bremsstrahlung by electrons in the upper atmosphere and the penetration of this radiation to atmospheric depths of 3-10 g cm^{-2} where it can be measured by balloon-borne detectors. The calculations take into account the multiple scattering and slowing down of electrons, and the multiple Compton scattering and photoelectric absorption of bremsstrahlung photons. Numerical data have been generated for electron beams incident onto the atmosphere with energies between 20 keV and 2 MeV, assuming wide-area precipitation and an incident angular distribution isotropic over the downward hemisphere. The results relate the number and energy spectrum of the incident electrons to the bremsstrahlung flux spectrum at balloon heights. The interpretation of some observed bremsstrahlung flux spectra is attempted.

12839. Sugar, J., **Potential-barrier effects in photoabsorption. II. Interpretation of photoabsorption resonances in lanthanide metals at the 4*d*-electron threshold,** *Phys. Rev. B* **5,** No. 5, 1785-1792 (Mar. 1, 1972).

Key words: Lanthanides; metallic spectrum; photoabsorption.

The resonances in the photoabsorption spectra of the lanthanides near the 4*d* absorption edge are interpreted as transitions of the type $4d^{10}4f^N \rightarrow 4d^94f^{N+1}$. Calculations of the $4d^94f^{N+1}$ energy levels and relative *gf* values for these transitions are shown to be in good agreement with the observed absorption spectra. The assumption that the lanthanides occur in trivalent form (with the exception of Eu and Yb) in the metallic solid state is confirmed by these results.

12840. Srinivasan, G. R., Tweer, I., Macedo, P. B., Sarkar, A., Haller, W., **Phase separation in SiO_2-B_2O_3-Na_2O system,** *J. Non-Cryst. Solids* **6,** 221-239 (1971).

Key words: Electron microscopy; immiscible oxide; nucleation and growth; phase decomposition; phase separation; sodium-borosilicate.

Isothermal studies of the phase separation occurring in the SiO_2-$B_2O_3Na_2O$ system near the center of the miscibility gap are made at three temperatures. Early stage observations of the phase morphology indicate that phase interconnectivity is probably due to nucleation and subsequent intersecting growth of silica-rich particles. It is found also that the extent of interconnectivity is strongly dependent on the volume ratio of the coexisting phases. Evidence is also presented that the glass of present composition is in a two-phase region rather than the three-phase region previously reported. It is also shown that there is very little rotation of the tie-lines between 748 and 650 °C.

12841. Fuller, E. G., **Nuclear reaction theory and the photonuclear giant resonance,** (Proc. 5th Congress of Yugoslavian Mathematicians, Physicists and Astronomers, Skopje, Yugoslavia, Sept. 13-14, 1972), Vol. II, *Physics,* No. 5, 5-10 (Macedonian Society of Mathematicians, Physicists and Astronomers, Skopje, Yugoslavia, 1972).

Key words: Coupled-channel; eigenchannel; giant resonance; photonuclear; reaction theory.

A brief review is given of the continuum theory of nuclear reactions with particular emphasis on the eigenchannel and coupled channel approaches as applied to the photonuclear giant resonance. Comparison of the theoretical results with experimental data indicates that at best the existing theories can describe only the gross features of the giant resonance. The experimental data seem to indicate the existence of large coherence effects in the giant resonance region.

12842. Goldberg, R. N., Frank, H. S., **Liquid junction potentials and single-ion activities by computer simulation. I. The concentration cell with transference,** *J. Phys. Chem.* **76,** No. 12, 1758-1762 (1972).

Key words: Computer simulation; electrochemistry; ionic activities; liquid junction potentials; thermodynamics.

The liquid junction potentials in KCl, NaCl, and HCl concentration cells with transference have been evaluated by computer simulation, making use of Onsager flux coefficients tabulated by Miller, and of a convenient formalism for single-ion activity coefficients to make possible the representation of osmotic driving forces. Varying assumptions regarding single-ion activity coefficients lead to varying values of a computed steady-state junction potential, but these differences are canceled by corresponding differences in calculated electrode potentials, so that the computed overall cell potential remains unchanged—*i.e.*, measurement of the potential of a concentration cell with transference can give no information about single-ion activity coefficients. This expected result plus the agreement of computed cell potentials with experimental ones speaks both for the essential validity of the method and for the mutual self-consistency of the numerical values inserted for Onsager coefficients and for mean ionic activity coefficients. In contrast to the steady-state cell potential, the time rise of the calculated potential is sensitive to the choice made for the single-ion activity coefficient parameter. There would thus seem to exist a possibility for determining single-ion activities in an experiment, if the time rise of the cell potential, after the formation of the junction, could be measured on a nanosecond time scale.

12843. Currie, L. A., **On the interpretation of errors in counting experiments,** *Anal. Lett.* **4,** No. 12, 873-882 (1971).

12844. Carpenter, B. S., **Boron and uranium determination in simulated lunar glass by the nuclear track technique,** (Proc. American Nuclear Society 16th Annual Meeting, Los Angeles, Calif., June 28-July 2, 1970), *Trans. Amer. Nucl. Soc.* **13,** No. 1, 79 (1970).

Key words: Alpha particles; boron; fission; fragments; recoiling fission fragments; trace element glasses; uranium.

Recoiling fission fragments and alpha particles were used to determine sub-microgram quantities of uranium and boron in three (50, 1 and 0.02 ppm) Trace Element Glasses certified by the National Bureau of Standards. Procedures for preparing the sample, irradiating the sample in the NBS Reactor, counting and calculations of results are given.

12845. Kirstein, A. F., **Discussion of the paper "Behavior of fiber glass reinforced concrete beams" by E. G. Nawy, G. E. Neuwerth, and C. J. Phillips,** *J. Struct. Div. Proc. Amer. Soc. Civil Eng.* **98,** No. ST5, 1206-1207 (May 1972).

12846. Plummer, E. W., Bell, A. E., **Field emission energy distributions of hydrogen and deuterium on the (100) and (110) planes of tungsten,** *J. Vac. Sci. Technol.* **9,** No. 2, 583-590 (Mar.-Apr. 1972).

Key words: Energy distribution; field emission; hydrogen; tungsten; tunneling.

Total energy distributions of field emitted electrons from the tungsten (110) and (100) planes as a function of coverage by hydrogen and deuterium have been recorded utilizing a spherical deflection energy analyzer. The elastic tunneling resonance spectrum gives a plot of the "local density of states" in the adsorbate. The inelastic tunneling spectrum reveals those discrete excitation energies available in the adsorbate–substrate complex. These spectroscopic data have been used to infer the chemical nature of the binding states which have been observed in the flash desorption spectrum of hydrogen from tungsten.

12847. Gadzuk, J. W., **Tunneling from Cambridge surface states,** *J. Vac. Sci. Technol.* **9,** No. 2, 591-596 (Mar.-Apr. 1972).

12848. Marzetta, L. A., **An evaluation of the three-voltmeter method for ac power measurement,** (Proc. Conf. Digest on Precision Electromagnetic Measurement, Boulder, Colo., June 26, 1972), *IEEE Trans. Instr. Meas.*, pp. 41-42 (June 26, 1972).

12849. Lehman, D. R., **Quasielastic electron scattering from ^{3}He and ^{3}H,** *Phys. Rev. C* **3,** No. 5, 1827-1840 (May 1971).

Key words: Electron scattering; final state rescattering; helium-3; separable potential; three-body problem; tritium.

Quasielastic electron scattering from ^{3}He and ^{3}H is investigated with a model in which the two-nucleon interaction is described by a separable potential. Cross sections are given in the impulse approximation for the ejected proton and scattered electron detected in coincidence, and for detection of only the scattered electron. Both two- and three-body breakup of ^{3}He and ^{3}H are considered, with final-state interactions between the spectator nucleons included in three-body breakup. Good agreement is obtained with all the electrodisintegration data, except the ^{3}He coincidence data, for wave functions derived from separable potentials which reproduce the s-wave two-nucleon phase shifts at low and medium energies. Rescattering corrections between the spectator particles are found to be important in calculating three-body disintegration. The need for more refined and reliable coincidence data is reaffirmed.

12850. Menke, J. L., **A fast pulse-dc integrator,** *Nucl. Instrum. Methods* **64,** 61-68 (1968).

12851. Shah, J. A., Danos, M., **Study of the neutron-proton correlations in the shell model,** *Phys. Rev.* **183,** No. 4, 899-907 (July 20, 1969).

Key words: Correlations; neutrons; pairing; quartetting; shell-model; structure; wave function.

A shell-model treatment is given for the spectra of the nuclei where there are two protons and two neutrons outside a doubly closed shell. The only restriction is that like-nucleons are required to occupy the same angular momentum state. In addition to this general wave function, more restricted wave functions also are investigated, viz., the pairing wave function (as least one pair of like nucleons is coupled to zero angular momentum) which contain no n-p correlations; the quartetting wave function (two unlike nucleons are first coupled to the maximum angular momentum, then the two pairs are coupled to I, the nuclear angular momentum) which does contain n-p correlations; and a superposition of pairing and quartetting wave functions. Results for ^{44}Ti, ^{64}Zn, and ^{204}Hg are given. The ground states are reproduced quite well by the pairing wave function; it seems, however, to fail for the excited states. The overlap between the general and the quartetting wave function is quite large. Finally, results are also given for the pairing force, which has only a $T=1$ component.

12852. Casella, R. C., **Time reversal symmetry and its breaking in physics,** *Phys. Teacher* **8,** No. 3, 114-122 (Mar. 1970).

12853. Lightbody, J. W., Jr., Penner, S., **Electroexcitation of the C^{12} giant resonance,** *Phys. Rev. Lett.* **24,** No. 6, 274-276 (Feb. 9, 1970).

Key words: Electroexcitation; energy dependent potential; Goldhaber-Teller model; longitudinal; matrix elements; momentum transfer; particle-hole model; quasi-elastic model; radiation tail; transverse.

Electroexcitation of C^{12} in and above the giant resonance has been measured at several angles and incident electron energies in order to obtain transverse and longitudinal reduced matrix elements. Results are presented for a q range of from 0.35 to 0.84 fm^{-1} and for excitation of 22-37 MeV. Comparison is made with the recent calculation by de-Forest of quasielastic scattering, as well as with earlier particle-hole and liquid-drop-model calculations.

12854. Mohan, R., Danos, M., Biedenharn, L. C., **Three-fluid hydrodynamical model and the proton distribution in ^{208}Pb,** *Phys. Rev. Lett.* **23,** No. 15, 868-870 (Oct. 1969).

Key words: Electron scattering; hydrodynamic model; isospin mixing; nuclear charge distribution; nuclear structure; short range correlations.

A three-fluid hydrodynamical model for nuclei is proposed and it is shown that the observed rise in proton density near the surface of ^{208}Pb can be accounted for in this model.

12855. Wyckoff, J. M., **Integrated cross sections for ^{209}Bi(γ,$xnyp$) reactions,** *Phys. Rev.* **159,** No. 4, 953-954 (July 20, 1967).

Key words: Bismuth; gamma rays; integrated cross section; isomer; lead; linac; lithium drifted germanium; photonuclear; spallation.

Integrated cross sections for the photoproduction of $^{200-206}$Bi and $^{200-204}$Pb from ^{209}Bi have been measured. A single sample was activated during a 10-minute 137-MeV bremsstrahlung bombardment by the NBS Linac, and γ-rays from the daughter products were measured with a Ge(Li) spectrometer over a two-month period to obtain relative yields. The yield data were used along with the established (γ,2n) integrated cross section and a calculated thick-target bremsstrahlung spectrum to derive integrated cross sections as follows: ^{206}Bi(168 ± 25), ^{205}Bi(88 ± 22), ^{204}Bi(55 ± 16), ^{203}Bi(66 ± 23), ^{202}Bi(31 ± 12), ^{201}Bi(10.7 ± 5.9), ^{200}Bi(5.7 ± 3.4), ^{204}Pb(8.0 ± 2.4), ^{203}Pb(3.8 ± 1.3), ^{202}Pb(3.4 ± 1.3), ^{201}Pb(15.3 ± 8.4), and ^{200}Pb(1.62 ± .97) MeV mb. Evidence is also presented for an 11.5-h isomeric state in ^{200}Pb.

12856. Wyckoff, J. M., **Photon energy emission from spallation products produced by 3-13 GeV electrons,** *Health Phys.* **18,** 693-704 (June 1970).

Key words: Photon energy; production cross sections; spallation products; 3-13 GeV electron beam.

A calculation of the energy emitted as photons from the ensemble of spallation products produced by a 3-13.3 GeV electron beam has been made. The time range of 1 hr-50 months after irradiation is encompassed using measured production cross sections for Al, Fe, Ni and Cu, major structural materials used around high energy particle accelerators. Similar calculations have been made for Mo, In, Ta and Pb by estimating production cross sections for some of the nuclides for which measured production cross sections were not available. Additional production cross sections measured for 3, 5 and 10 GeV electrons and comparisons with published 3-30 GeV proton spallation data are used to show the general applicability of the calculated decay curves. Graphs of the instantaneous irradiation case are included as well as some illustrative results for photon energy emitted following extended irradiation periods.

12857. Praderie, F., Thomas, R. N., **On estimates of the nonradiative energy input to the solar chromosphere from the H$^-$ emission,** *Astrophys. J.* **172,** No. 2, 485-490 (Mar. 1, 1972).

Key words: H$^-$ radiative losses; non-LTE effects on mechanical heating; solar chromospheres.

The inclusion of non-LTE effects in the computation of mechanical heating in a gray atmosphere changes previous LTE estimates by a factor of $4b_{H^-}$.

12858. O'Toole, W. E., III, Keplinger, M. S., **An experimental program for automatic indexing at the National Bureau of Standards,** *Proc. American Society for Information Science, Philadelphia, Pa., Oct. 11-15, 1970,* **7,** 301-308 (American Society for Information Science, Washington, D.C., Oct. 1970).

12859. Holt, H. K., Sellin, I. A., **Time-dependent theory of Stark quenching of 2S states in hydrogen and helium,** *Phys. Rev. A* **6,** No. 1, 508-512 (July 1972).

Key words: Lifetimes; one- and two-electron 2S states; Stark quenching; time-dependent theory.

A nonperturbative time-dependent theory which gives Stark-quenching lifetimes in agreement with experiment for both one- and two-electron 2S states is presented. This theory differs from the conventional Bethe-Lamb theory of Stark quenching, but reduces to this older theory, for one electron atoms only, when a well-known sum rule is applied.

12860. Wyckoff, H. O., Rossi, H. H., **Dosimetric fundamentals and irradiation limits. 1.1. radiation quantities and units,** Chapter 1 in *Engineering Compendium on Radiation Shielding* **I,** 1-5, (Springer-Verlag, New York, N.Y., 1968).

Key words: Definitions; glossary; radiation quantities; radiation shielding; radiation units.

This is part of an introduction to a book on radiation shielding. It includes definitions of quantities and units to be used in the book.

12861. Wachtman, J. B., Jr., Capps, W., Mandel, J., **Biaxial flexure tests of ceramic substrates,** *J. Mater.* **7,** No. 2, 188-194 (1972).

Key words: Aluminum oxide; bending; brittleness; ceramics; electronics; flexural strength; fractures (materials); mechanical tests; modulus of rupture tests; substrates; surface properties.

A method for determining the strength of thin, circular disks of brittle materials utilizing an exact elastic solution for small deflections was developed and tested in an interlaboratory program. The method determines the strength in biaxial flexure by supporting the specimen on three equally spaced balls concentric with the load, which is applied to the center of the specimen by a flat piston. This allows slightly warped specimens to be tested and produces results unaffected by the edge condition of the specimen. These features make the method suitable for assessing the effect of surface condition on strength. Results on eight types of polycrystalline alumina ceramics ranging in strength from 46,000 to 96,000 psi show that a coefficient of variation of about seven percent can be achieved by testing five specimens and that different laboratories generally obtain good agreement on strength values.

12862. Hanley, H. J. M., Klein, M., **Application of the m-6-8 potential to simple gases,** *J. Phys. Chem.* **76,** No. 12, 1743-1751 (1972).

Key words: Carbon dioxide; diffusion; dispersion coefficients; methane; m-6-8 potential; nitrogen; oxygen; rare gases; thermal conductivity; thermal diffusion; viscosity.

The m-6-8 model potential function is applied to the gases argon, krypton, xenon, nitrogen, methane, and carbon dioxide and to the properties viscosity coefficient, self-diffusion coefficient, thermal conductivity coefficient, virial coefficient, and the isotopic thermal diffusion factor. The potential is shown to have a considerable advantage over previous simple analytic models in that it can satisfy two criteria: (a) it can be used to correlate a given property for all the gases studied over a wide temperature range with a single set of parameters, and (b) it can be used to correlate both transport and equilibrium properties for the monatomic gases with a single set of parameters. Reasons for the failure of polyatomic gases to satisfy (b) are suggested. A brief discussion on the relation of the potential to theory is given.

12863. Spencer, L. V., **On the accuracy of transport calculations using moments methods,** *Trans. Amer. Nucl. Soc.* **14,** No. 1, 339 (June 1971).

Key words: Biorthogonal functions; gamma rays; moments methods; neutrons; shielding; truncation errors.

Expressions are given for bounds to the truncation error of finite U_n^k polynomial representations of γ-ray and neutron spatial flux distributions. An extension to representations of a class including sums of exponentials is also noted.

12864. Leiss, J. E., **Beam loading and transient behavior in traveling wave electron linear accelerators,** Chapter in *Linear Accelerators,* P. M. Lapostolle and A. L. Septier, eds., pp. 147-172 (North-Holland Publ. Co., Amsterdam, The Netherlands, 1970).

Key words: Accelerators; beam loading; dispersive effects; linear accelerator; transients.

In the linear accelerator the transfer of energy from the accelerator to the beam, known as beam loading, can be so efficient that the behavior of the accelerator can not be even qualitatively described without consideration of beam loading. The energy of loading, and changes in the radio frequency power density at some points in the accelerating waveguides of an order of magnitude are observed.

A review of methods to calculate beam loading in the traveling wave linear accelerator is presented. Both steady state and transient conditions are examined in various approximations.

12865. Swartzendruber, L. J., Evans, B. J., **Hyperfine fields at the antimony sites in the Heusler-type ni_xMnSb alloys,** (Proc. 17th AIP Conf. on Magnetism and Magnetic Materials, Chicago, Ill., Nov. 15-18, 1971), Chapter in *Magnetism and Magnetic Materials*, C. D. Graham, Jr., and J. J. Rhyne, eds., No. 5, 539-543 (June 1972).

Key words: Alloys; hyperfine fields; Mössbauer effect; order-disorder; ^{121}Sb.

The ^{121}Sb Mössbauer effect has been utilized to study hyperfine fields in the ferromagnetic alloys Ni_xMnSb for $1 \leq x \leq 2$. For $x=2$, the crystal structure is of the Cu_2MnAl ($L2_1$) type characteristic of Heusler alloys. As x is reduced, Ni vacancies appear until, for $x=1$, the ordered Cl_b structure is obtained. Our results indicate a ^{121}Sb saturation magnetic hyperfine field of approximately $+300$ kG with a relatively small dependence on Ni concentration. It is possible to understand this result by using two assumptions: (i) the Ni atoms make only a small contribution to the conduction band and (ii) the Sb hyperfine field samples the average spin polarization of the material. The Mössbauer spectra form a sensitive probe to reveal disorder not easily observed by x-ray diffraction. A spin-echo measurement of ^{123}Sb in NiMnSb gives good agreement with the ^{121}Sb Mössbauer effect results.

12866. Swartzendruber, L. J., Bennett, L. H., Kinsman, K. R., **Crystallographic and magnetic transformations of Fe precipitates in Cu,** (Proc. 17th AIP Conf. on Magnetism and Magnetic Materials, Chicago, Ill., Nov. 15-18, 1971), Chapter in *Magnetism and Magnetic Materials*, C. D. Graham, Jr., and J. J. Rhyne, eds., No. 5, 408-412 (June 1972).

Key words: Alloys; copper; crystallography; iron; Mössbauer effect; precipitation.

The Mössbauer effect has been used to characterize the magnetic state, and hence the crystallographic form, of very small Fe-rich precipitates extracted from a Cu matrix. The precipitates form in the Cu matrix as antiferromagnetic (Néel temperature ~ 60 K) metastable fcc crystals. When this two phase matrix is deformed or the precipitates selectively isolated from the matrix, a portion of the precipitates spontaneously transform (martensitically), at least partially, to bcc Fe. By a newly developed procedure we have extracted these fcc precipitates from the matrix, collected, and mounted them for observation by Mössbauer spectroscopy. The samples observed consist of small particles of Fe, containing $\sim 0.5\%$ Cu, in the size range 0.1-0.2μm. Since the fcc and bcc crystal structures of Fe have widely different magnetic properties, the Mössbauer effect can be used to quantitatively characterize the crystallographic transformation. In the extracted precipitates conversion to bcc is essentially complete, in contrast to the only partial transformation induced by deformation. An upper limit ($< 0.3\%$) can be placed on the amount of retained antiferromagnetic phase.

12867. Sharp, K. G., Coyle, T. D., **Perfluoro(alkylsilanes). II. Trifluoro(trifluoromethyl)silane and trifluoro(pentafluoroethyl)silane,** *Inorg. Chem.* **11**, 1259-1264 (1972).

Key words: Alpha-elimination; carbenes; difluorocarbene; difluoroiodo(perfluoroalkyl)silanes; fluoroalkysilanes; fluoro(trifluoromethyl)carbene; silicon difluoride; trifluoro(pentafluoroethyl)silane; trifluoro(trifluoromethyl)silane.

The perfluoro(alkylsilanes) CF_3SiF_3 (I) and $C_2F_5SiF_3$ (II) have been prepared and characterized. Synthesis was effected by fluorination of the corresponding difluoroiodo(perfluoroalkyl)silanes, obtained by the reaction of SiF_2 with the appropriate perfluoroalkyl iodide. Both compounds are stable at room temperature. Products from thermolysis of I at *ca.* 80° or above and of II at 160° or above, as pure compounds or in the presence of added reagents, are consistent with a decomposition mechanism involving α-fluorine transfer and the intermediacy of the carbenes $:CF_2$ and cF_3CF, respectively. Basic and aqueous hydrolytic behaviors are described.

12868. McMaster, W. H., Del Grande, N. K., Mallett, J. H., Hubbell, J. H., **Compilation of x-ray cross sections,** *Sec. II, Rev. 1, University of California Radiation Laboratory Report 50174, 353 pages*, Lawrence Livermore Laboratory, Livermore, Calif., (May 1969).

Key words: Attenuation coefficient; coherent scattering; compilation; cross section; incoherent scattering; photoelectric absorption; photons; x-rays.

This report contains graphs and tables of x-ray cross sections in the range of 1 keV to 1 MeV. The total cross sections presented are the sum of computed scattering cross sections and a combination of the fit to derived experimental and theoretical photoelectric cross sections.

12869. Dikkers, R. D., Yokel, F. Y., **Strength of brick walls subject to axial compression and bending,** (Proc. 2d International Brick Masonry Conf., Stoke-on-Trent, England, Apr. 12-15, 1970), Chapter in *SIBMAC Proceedings*, H. W. H. West and K. H. Speed, eds., No. 19, 125-132 (The British Ceramic Research Association, Stoke-on-Trent, England, 1971).

Key words: Brick walls; combined loading; compressive strength; flexural strength; high bond mortar; masonry walls; moment magnifier effect; slenderness effects; structural stability.

Unreinforced brick wall panels, 4-in. thick, 4-ft wide, and 8-ft high, were tested by applying uniform transverse loads, uniform axial compressive loads, or a combination of both types of loading. Companion prisms were also tested to determine their strength in compression and flexure. Data from both the wall and prism tests were used to develop analytical procedures for predicting the strength of walls subjected to axial compression and bending.

A new analytical approach is proposed to evaluate both strength and slenderness effects in masonry walls. The application of this approach would lead to new design procedures, closely paralleling similar procedures recently introduced in the USA for other engineered materials, such as steel and reinforced concrete.

12870. Rowen, J. W., Murphey, W. M., Smith, C. N., **Assessment of material unaccounted for control criteria** (Proc. Symp. Progress in Safeguards Techniques, International Atomic Energy Agency, Vienna, Austria, 1970), Chapter in *Safeguards Techniques* **II**, 291-310 (Dec. 1970).

Key words: Inventory fluctuations; measurement errors; normalization factors; process activity; unidentified process losses.

Some of the factors that affect the usefulness of Material Unaccounted For (MUF) control criteria include process activity, measurement errors, normalization factors, time frame, inventory fluctuations and unidentified process losses.

It is important to know whether and how such criteria vary with the character of the data source and with variations in facility situations. This paper theoretically analyzes MUF criteria corresponding to three types of data sources and two situations. The two situations differ in that measurement errors are known in one but unknown in the other. Quantitative criterion expressions are developed for the six possible conditions of evaluation resulting from the three types of data sources and the two measurement situations. The statistical ex-

pressions developed are compared with each other and some available data are presented. Tentative conclusions are drawn with respect to the comparative sensitivities of the criteria resulting from the six possibilities. These conclusions will be tested in the U.S. Atomic Energy Commission's integrated safeguards experiments. These experiments which will provide data for some of the situations will involve subprocess, batch and campaign balances in which information on measurement errors will be available.

12871. Kidnay, A. J., Miller, R. C., Hiza, M. J., **Solid-vapor and liquid-vapor phase equilibria for the helium-krypton system,** *Ind. Eng. Chem. Fundam.* **10,** No. 3, 459-465 (Aug. 1971).

Key words: Cryogenic; helium-krypton; liquid-vapor; phase equilibria; solid-vapor.

A vapor-recirculation equilibrium cell was used to investigate both the solid-vapor and liquid-vapor equilibria and the three-phase curve for the system helium-krypton. Gas-phase compositions were measured above solid krypton at 100.00, 105.00, 110.00, and 115.00 K and at pressures to 120 atm (12.16 MN/m²). Both gas and liquid compositions were determined at 117.09, 120.85, 129.60, 139.56, and 150.00 K for the same range of pressures. Analysis of the gas-phase data by both the virial and modified Redlich-Kwong equations indicates that a deviation parameter of about 0.3 is necessary for the geometric-mean mixing rule for energy parameters. Comparison of the Henry's law constants for the liquid phase with the statistical model of Miller and Prausnitz indicates a somewhat larger deviation parameter.

12872. Eisenhauer, C., **Some current problems in OCD fallout shielding calculations,** *Proc. Special Sessions on Gamma-Ray Production and Transport and on Civil Defense Shielding, Winter Meeting American Nuclear Society, Chicago, Ill., Nov. 1967, A. E. Straker, ed.,* **ANS-SD-7,** (TID) 4500, pp. 143-156 (1969).

12873. Johnson, W. T. K., Dick, C. E., **Half-life measurement of several short-lived nuclear isomers,** *Nucl. Instrum. Methods* **99,** No. 2, 221-226 (1972).

Key words: Bromine; cadmium; erbium; gold; half lives; iridium; measurement; nuclear isomers; solenium; tungsten.

Bremsstrahlung produced by 3.5 MeV electrons incident on a platinum target was used to populate nuclear isomers in several nuclei through excitation of higher lying states. A shuttle was constructed to transport targets of natural isotopic abundance from an irradiation position to a measuring position. Other than a low background the activity measured was due entirely to the isomeric decay. The measured half-lives in seconds are ^{77m}Se 17.58 ± 0.12, ^{79m}Br: 4.97 ± 0.10, ^{167m}Er: 2.28 ± 0.03, ^{179m}Hf: 18.77 ± 0.07, ^{183m}W: 5.56 ± 0.25, ^{191m}Ir: 4.88 ± 0.03, and ^{197m}Au: 7.86 ± 0.04. The data are presented and the methods of analysis are discussed. The results are compared to recent literature values.

12874. Kondo, A., Brenner, F. C., **Research for a uniform quality grading system for tires. VI. Comparison of the effect of front and rear wheel drive vehicles on projected tread wear of a tire,** *Rubber Chem. Technol.* **44,** No. 4, 960-961 (Sept. 1971).

12875. Linzer, M. A., **A frequency swept injection locked nuclear induction spectrometer with signal averaging,** *Rev. Sci. Instrum.* **43,** No. 5, 723-726 (May 1972).

Key words: Frequency-sweep; injection-locking; nmr; nqr; nuclear induction; signal averaging.

A frequency sweep injection technique, suitable for signal averaging and fast passage studies, has been developed for use with a nuclear induction spectrometer.

12876. Treu, S., **A conceptual framework for the searcher-system interface,** *Proc. Workshop on Interactive Bibliographic Search: The User/Computer Interface, Palo Alto, Calif., Jan. 14-15, 1971,* D. E. Walker, ed., pp. 53-66 (AFIPS Press, Montvale, N.J., 1971).

12877. Petrescu-Prahova, I., Winogradoff, N. N., **Photoluminescence in compensated *n*-type, Si-doped gallium arsenide,** *J. Phys. Chem. Solids* **32,** 1873-1879 (1971).

Key words: Amphoteric compensation; band tailing; coulomb potential screening; gallium arsenide; photoluminescence; silicon doping.

Band tailing observed in highly doped GaAs and other semiconductors has been attributed to screened coulomb potentials. The amphoteric nature of melt-grown, Si-doped samples, limiting the free electron concentration to below $n = 5 \times 10^{18}$ cm^{-3}, permitted the unequivocal study of the band tail parameters as a function of impurity concentration at virtually constant free carrier screening over a silicon concentration range from 2.6×10^{18} to 1.2×10^{20} cm^{-3}. The photoluminescent spectra of such samples consisted of two broad bands, one of which, centered at 1.2 eV, decreased with increasing temperature and vanished at the higher temperatures where accurate analysis of the shape of the other band, centered at any energy close to the band gap, could be made. The intensity of the low energy side of the latter band was found to be exponential proportional to exp $(h\nu/E_0)$, and the dependence of E_0 on the concentration of the silicon dopant was determined. Since a change of the excitation intensity over two orders of magnitude did not change the position or shape of the band-to-band "line," it was concluded that the nature of the spectra reflects exponential density-of-states tails at the conduction band edge.

12878. Skopik, D. M., Dodge, W. R., **^{4}He$(e,d)e'^2$H angular-distribution and cross-section measurements between 36 and 50 MeV,** *Phys. Rev. C* **6,** No. 1, 43-53 (July 1972).

Key words: E-2 angular distributions; electric-quadrupole transition; identical particles; virtual photons; ^{4}He photodisintegration.

Measurements of the angular distributions in the "virtual photon" energy interval of 40 ± 1 MeV and the total cross section in the energy interval of 35.7 – 49.4 MeV of the ^{4}He$(e,d)e'^2$H reaction are presented. The data are compared with early calculations and with more recent cluster-model and dispersive calculations.

12879. Robertson, A. F., **Discussion of paper "Fire and the curtain wall" by H. L. Malhotra, United Kingdom,** (Proc. Symp. of CIB Conf. on Curtain Walls, Paris, France, Mar. 3-6, 1970), *Symp. Papers in Light Facades,* pp. 74-75 (June 1971).

12880. Caswell, R. S., **Review of measurements of absolute neutron emission rates and spectra from neutron sources,** (Proc. Amer. Nucl. Soc. National Topical Meeting on Neutron Sources and Applications, Augusta, Ga., Apr. 19-21, 1971), Chapter in *Neutron Sources and Applications, CONF-710402,* **I,** 1-53 – 1-62 (1971).

Key words: Manganous sulfate bath; neutron emission rate; neutron sources; neutron spectra; neutron spectrum measurement methods; ^{252}Cf.

The measurement of the absolute neutron emission rate of neutron sources has been reviewed with emphasis on the manganous sulfate bath method, and is found to be in good quantitative shape. In precision applications, such as ν (neutrons/fission) and certain cross section measurements, higher accuracy would, nevertheless, be desirable. Significant improvement in the accuracy of (β, n) source calibrations could be obtained by resolution of the discrepancy on the magnitude of the fast neutron loss to nuclear reactions in the manganous sulfate bath.

Recent developments in the techniques of measuring spectra of neutron sources has led to the beginning of reliable measurements in

the energy region below 1 MeV. The source spectrum measurement field is, nevertheless, in semi-quantitative state. Further intercomparisons of measurement methods are needed, and also, the resolution of a discrepancy on the neutron energy spectrum for the ^{252}Cf spontaneous fission neutron source.

12881. Jacox, M. E., Milligan, D. E., **Vibrational and electronic spectra of the O_3^- anion isolated in an argon matrix,** *J. Mol. Spectrosc.* **43,** No. 1, 148-167 (July 1972).

Key words: Charge transfer; electron attachment; infrared spectrum; matrix isolation; molecular orbitals; $O_2 + O^-$ reaction; O_3^- anion; ultraviolet spectrum.

The O_3^- anion has been stabilized in an argon matrix at 14 K in concentration sufficient for the detection of the antisymmetric stretching fundamental, ν_3, and of a band system between 5100 and 3700 Å. Both the reaction of O^- (produced by the interaction of photoelectrons with N_2O) with O_2 and the charge-transfer interaction between O_3 and K atoms have served as sources of O_3^- in these studies. Although the ν_3 absorption is slightly dependent upon the alkali metal used as the photoelectron source, the experiments suggest that the ν_3 absorption of P_3^- isolated in an argon lattice should lie very close to 800 cm^{-1}. Detailed isotopic studies support the proposed vibrational assignment and demonstrate that the valence angle of ground-state O_3^- is $110 \pm 5°$ and that the oxygen-oxygen bonds are considerably weaker than those of O_3. The nature of the observed electronic transition of O_3^- is discussed, and evidence is considered for the presence of a low-lying dissociative state.

12882. Celotta, R. J., Bennett, R. A., Hall, J. L., Siegel, M. W., Levine, J., **Molecular photodetachment spectrometry. II. The electron affinity of O_2 and the structure of O_2,** *Phys. Rev. A* **6,** No. 2, 631-642 (Aug. 1972).

Key words: Electron affinity; molecular constant; molecular oxygen; negative ions, photodetachment.

A beam of O_2^- ions, extracted from a glow discharge in N_2O, is crossed with the linearly polarized intracavity photon beam of an argon-ion laser (4880 Å). Electrons photodetached at right angles to the crossed beams are energy filtered by a hemispherical analyzer. The electron energy spectra are characteristic of photodetachment from the $v' = 0$ state of O_2^- to the $X^3\Sigma_g^-$ and $a^1\Delta_g$ state of O_2. Vibrational state analysis is facilitated by the use of isotopes. The electron affinity obtained is 0.440 ± 0.008 eV. Additionally, we have measured the relative transition probabilities as a function of final vibrational state and the angular distributions of the outgoing electrons. The relative intensities, corrected by the angular distributions, determine through Franck-Condon-factor analysis the internuclear distance for the negative ion. We find $r_e'' = 1.341 \pm 0.010$ Å and therefore $B_e'' = 1.17 \pm 0.02$ cm^{-1}.

12883. Siegel, M. W., Celotta, R. J., Hall, J. L., Levine, J., Bennett, R. A., **Molecular photodetachment spectrometry. I. The electron affinity of nitric oxide and the molecular constants of NO^-,** *Phys. Rev. A* **6,** No. 2, 607-631 (Aug. 1972).

Key words: Electron affinity; molecular constants; negative ions; nitric oxide; photodetachment.

We apply laser photodetachment and photoelectron spectrometry for the first time to the study of molecular negative ions. We describe in detail the study of the nitric oxide ion NO^-; a following paper reports results for O_2^-. We use the NO^- results to develop and illustrate in detail the principles and applications of the technique. A mass-selected NO^- beam (680 eV) is crossed with a linearly polarized monochromatic (4880−Å) argon-ion laser beam, and electrons photodetached into a $4\pi/2000$-sr solid angle perpendicular to the crossed beams are energy analyzed using a hemispherical electrostatic monochromator. The data yield a set of vertical detachment energies between vibrational states of NO^- and NO, and relative intensities for these transitions. Angular distributions about the polarization direction are studied by rotating the laser polarization while maintaining the mutually perpendicular ion-beam-laser-beam-electron-collection geometry. For each transition we measure the anisotropy parameter β, corresponding to the form $[1 + \beta P_2(\cos\theta)]$ for the angular distribution. Several arguments, including data on NO^{18-} photodetachment, are used to identify the initial and final vibrational states. Molecular rotational effects, and effects associated with the spin-orbit splitting of the final $NO(X^2\Pi)$ state are identified and included in the analysis. A Franck-Condon-factor analysis of the observed relative cross sections, parametrized by trial values of the NO^- molecular constants, is used to determine that for NO^- $\omega_e'' = 1470 \pm 200$ cm^{-1}, $r_e'' = 1.258 \pm 0.010$ Å, and $B_e'' = 1.427 \pm 0.02$ cm^{-1}. Using these constants, the measured vertical detachment energy is reduced by rotational and spin-orbit effects to the electron affinity $E_A(NO) = 24_{-5}^{+10}$ MeV.

12884. Utton, D. B., Tsang, T., **Coupled nuclear spin relaxation and internal rotations in magnesium fluosilicate hexahydrate,** *J. Chem. Phys.* **56,** No. 1, 116-119 (Jan. 1, 1972).

Key words: Internal motion; magnesium fluosilicate hexahydrate; nuclear magnetic resonance; relaxation.

Both proton and fluorine nuclear spin-lattice relaxations have been studied by the 180-90° pulse method in $MgSiF_6 \cdot 6H_2O$ at 25 and 13 MHz over the temperature range 170-350 K. Nonexponential behaviors have been observed. Both ^1H and ^{19}F relaxations may be characterized by the same pair of relaxation times, the shorter component due to the intermolecular H−F dipolar interaction. The results indicate that the SiF_6^{2-} ions are reorienting with an activation energy, $V = 31 \pm 4$ kJ/mole $= 7.5 \pm 1.0$ kcal/mole, and a frequency factor $\tau_0 = 10^{-14 \pm 1}$ sec. These values are consistent with other hydrogen-bonded fluorine compounds.

12885. Hutchinson, J. M. R., Garfinkel, S. B., **Standardization of cadmium-109 sources for γ-ray emission rate,** *Int. J. Appl. Radiat. Isotop.* **22,** 405-414 (1971).

Key words: Cadmium-109; cobalt-57; gamma-ray emission rate; iron-57; photoelectron escape; silver-109m; standardization; well crystal counting.

The standardization of ^{109}Cd sources for 88-keV γ-ray emission rate has been performed using a NaI(Tl) well crystal which gives a nearly 4π geometry. Since the low-energy portion of the 88-keV γ-ray spectrum is obscured by 22-keV X-ray pulses, the total counting rate cannot be found by merely summing the counting rates for all the channels in the distribution. A method, in which the spectrum is broken down into eight components, is used to determine the number of degraded 88-keV γ-ray pulses. The calibration is performed by summing the counting rates of the various components below an arbitrarily chosen energy of 39 keV, and adding them to the total counting rate above 39 keV. The process in which photoelectrons escape into the aluminum liner of the well is found to be responsible for most of the degraded 88-keV γ-ray pulses which fall below 39 keV. The estimated systematic error in the measurement is ± 0.9 percent.

Using ^{57}Co sources which have been accurately calibrated by coincidence counting, the 2-in. × 2-in. NaI(Tl) well crystal is shown to have a γ-ray detection efficiency of 100 percent with an uncertainty of ± 0.2 percent (after corrections have been made for well-wall γ-ray absorption and escape out of the well). The total abundance for 122- and 136-keV ^{57}Fe photons emitted per decay from ^{57}Co has been measured to be 0.963 ± 0.003.

12886. Hutchinson, J. M. R., Lantz, J. L., Mann, W. B., Mullen, P. A., Rodríguez-Pasqués, R. H., **An anti-coincidence shielded NaI(Tl) system at NBS,** *IEEE Trans. Nucl. Sci.* **NS-19,** No. 1, 117-118 (Feb. 1972).

Key words: Anti-coincidence; anti-Compton; gamma rays; low level radioactivity; multidimensional; radioactivity.

An anti-Compton, anti-coincidence shielded NaI(Tl) spectrometer is described.

12887. Rodríguez-Pasqués, R. H., **Microactivity radiochemistry,** *Proc. 2d Inter-American Conference on Radiochemistry, Mexico City, Mexico, Apr. 22-25, 1968,* pp. 278-289 (Published by Secretaría General de la Organización de Estados Americanos, Washington, D.C., 1971).

Key words: Detection limits; high sensitivity counting; low-level; low-level separations; microactivity; radiochemistry; radionuclide identification; specific activity threshold.

Microactivity is taken as synonymous of low-level radioactivity, and is defined as 1 dpm/g, or less. The refinements of technique developed to deal with these low levels have widened the field of radiochemical and nuclear chemistry research with new subjects. Two general requirements are discussed, namely high sensitivity detection, and refined chemical techniques.

The difficult problem of radionuclide identification at microactivity level is also examined.

12888. Hirshfeld, A. T., Hoppes, D. D., Mann, W. B., Schima, F. J., **Nuclear orientation of ^{82}Br in iron,** (Proc. Int. Conf. on Hyperfine Interactions in Excited Nuclei, Rehovot, Israel, Sept. 6-11, 1970), Chapter in *Hyperfine Interactions in Excited Nuclei* **1,** 335-338 (Gordon and Breach Sci. Publ., New York, London, Paris, 1971).

Key words: Beta rays; gamma rays; hyperfine interactions; isotope separator; magnetic moment; nuclear orientation; ^{82}Br.

^{82}Br was implanted in .025 mm thick iron foil, using the NBS high-resolution isotope separator. The bromine was oriented by cooling by adiabatic demagnetization and the anisotropy of the emitted beta and gamma radiation observed. For the upper 40% of the $5^- \rightarrow 4^-$ beta spectrum an asymmetry of $\pm .046 \pm .004$ was observed at a foil temperature of 35 mK. This, taken together with the observed anisotropies for seven gamma peaks, indicates an effective field of 400^{+400}_{-100} kG acting on a fraction of the bromine atoms. The sign of the ^{82}Br magnetic dipole moment is positive, assuming a positive value for the effective field.

12889. Soulen, R. J., Jr., Colwell, J. H., **The equivalence of the superconducting transition temperature of pure indium as determined by electrical resistance, magnetic susceptibility, and heat-capacity measurements,** *J. Low Temp. Phys.* **5,** No. 3, 325-333 (1971).

Key words: Carbon resistance thermometry; electrical resistance; heat capacity; indium; magnetic susceptibility; superconductivity; thermometric fixed point; transition temperature.

The superconducting transition temperature of a well-annealed polycrystalline sample of pure indium was determined by three different techniques. The heat-capacity and susceptibility transitions are approximately 1 mK wide and span the same temperature interval. The resistance transition is less than 0.2 mK wide and occurs at the center of the other transitions. By choosing the midpoint of each transition the three measurements are identical to within 0.1 mK.

12890. Cook, C. C., Allred, C. M., **An excitation system for piston attenuators,** *IEEE Trans. Instr. Meas.* **IM-20,** No. 1, 10-16 (Feb. 1971).

12891. Gimmestad, G. G., Pardoe, G. W. F., Gebbie, H. A., **The study of dimeric molecules in ammonia vapour of submillimeter wave spectroscopy,** *J. Quant. Spectrosc. Radiat. Transfer* **12,** 559-567 (1972).

Key words: Ammonia; dimers; infrared.

Absorption by true dimers can be distinguished from that attributable to transient pairs by being spectrally narrow and by having a temperature dependence characterized by a well defined binding energy. Using these criteria, the presence of dimers in ammonia gas under conditions near those of saturated vapor is deduced from the observation of narrow spectral features near 10 cm^{-1}, and a heat of dimerization of 3.6 ± 0.8 kilocalories per mole. This value, of the order of what would be expected from breaking single hydrogen bonds, is a little lower than the values found by other methods. The presence of dimers should be considered in interpreting line shape observation at high pressures.

12892. Zimmerman, J. E., **Josephson effect devices and low-frequency field sensing,** *Cryogenics* **12,** No. 1, 19-31 (Feb. 1972).

Key words: Cryogenics; Josephson effect; magnetometry; superconductivity.

Three major areas of application of the Josephson effect are recognized; absolute standards, millimetre and sub-millimetre wave sensing, and dc and low-frequency current, voltage, and magnetic field sensing. In the latter area, single junction rf-biased low-inductance loop devices in a number of different forms (junction types and loop geometries) have been developed with sensitivities of the order of $10^{-15}T(10^{-11}G)$ or $10^{-19}V$. These sensors are being used in applications as diverse as magnetocardiography and absolute noise thermometry in the millikelvin range. As amplifiers, they are characterized by demonstrated equivalent noise temperatures of less than a few millikelvin, and probably a few microkelvin (theoretical). Highly reliable thin-film loop devices in a number of different forms have been developed in several laboratories, but the more easily-made point-contact devices are probably the most widely used. Many of the characteristics of the devices can be easily interpreted with the aid of a pendulum analogue.

12893. Ruff, A. W., Jr., **Interpretation of x-ray diffraction data with regard to stacking faults in silver-tin alloys,** *J. Appl. Phys. Commun.* **43,** No. 6, 2909-2911 (June 1972).

Key words: Alloys; dislocation; stacking-fault energy; stacking-fault probability; x ray.

Several alternative interpretations of data from fcc silver-tin alloys are discussed in examining the relation between stacking-fault probability and stacking-fault energy. One important aspect concerns the true variation of dislocation density with alloy composition.

12894. Siegwarth, J. D., Radebaugh, R., **The design of optimum heat exchangers for dilution refrigerators,** *Rev. Sci. Instrum.* **43,** No. 2, 197-204 (Feb. 1972).

Key words: Cryogenics; dilution refrigerator; heat exchangers; helium-3; helium-4.

The behavior of discrete heat exchangers as a function of temperature, heat transfer area, and ^{3}He flow rate is shown for a general case by means of some machine calculated curves. From these curves, the appropriate heat exchanger size can be determined for the various steps of a discrete heat exchanger. Also, curves for the mixing chamber temperature T_m as a function of total surface area divided by flow rate for various amounts of external heat to the mixer are shown for the continuous exchanger. From these curves the optimum ^{3}He flow rate for a given heat input and exchanger size can be determined. Viscous heating has been included in the calculation of one typical coaxial tube exchanger. It is found that heating in the dilute stream has negligible effect on T_m, whereas the viscous heating in the concentrated side, though several times smaller than that in the dilute side, has considerably more effect on T_m. Based on this behavior, an improved method of "heat sinking" heat leak paths to the mixer is suggested.

12895. Mizushima, M., Evenson, K. M., Wells, J. S., **Laser magnetic resonance of the NO molecule using 78-, 79-, and 119-μm H_2O laser lines,** *Phys. Rev. A* **5,** No. 5, 2276-2287 (May 1972).

Key words: g Factor; laser magnetic resonance; NO; spin-orbit coupling constant; water vapor laser.

The magnetic resonance of the NO molecule is observed using the 78-, 79-, and 119-μm lines of the H_2O laser as the radiation source. The resonances in three cases are due to the $(^2\Pi_{1/2}J=12.5)\rightarrow(^2\Pi_{3/2}J=12.5)$, $(^2\Pi_{1/2}J=11.5)\rightarrow(^2\Pi_{3/2}J=11.5)$, and $(^2\Pi_{1/2}J=12.5)\rightarrow(^2\Pi_{3/2}J=11.5)$ transitions, respectively. Most of them are magnetic dipole transitions, but a few electric dipole transitions are also observed. It is found that the calculated g factors $g_{e2}(11.5)=g_{d2}(11.5)=-0.0064$, $g_{e1}(11.5)=g_{d1}(11.5)=0.0272$, $g_{e2}(12.5)=g_{d2}(12.5)=-0.0092$, $g_{e1}(12.5)=g_{d1}(12.5)=0.0270$, and the calculated Λ-doublet separations $f_{e2}(11.5)-f_{d2}(12.5)=243$ MHz, $f_{e1}(11.5)-f_{d1}(11.5)=4323$ MHz, are consistent with our experimental results. The hyperfine structure and the second-order effects are also in agreement with theoretical values. The average separation between the $^2\Pi_{3/2}$ and $^2\Pi_{1/2}$ states for a given J, which we call X_J, is found to be 126.4469 ± 0.0005 and 127.5786 ± 0.0005 cm^{-1} for $J=11.5$ and 12.5, respectively. The conventional spin-orbit coupling constant is found to be 123.1580 ± 0.0010 cm^{-1} when $J=12.5$ or 11.5. [The conventional spin-orbit coupling constant A_c, commonly referred to as A, is given by $A-\delta(J+1/2)^2+1/4\gamma$ in our notation.] The coupling constant μ_s for the $\vec{S}\cdot\vec{N}$ term is found to be -0.006 ± 0.002 cm^{-1}.

12896. Prydz, R., Goodwin, R. D., **Experimental melting and vapor pressures of methane,** *J. Chem. Thermodyn.* **4,** No. 1, 127-133 (Jan. 1972).

Key words: Boiling point; critical-point pressure; melting pressure; methane; triple-point constants; vapor pressure.

Thirteen melting pressures to 210 atm are represented by the Simon equation with a root mean square deviation of 0.05 atm (0.08 percent). This representation is highly sensitive to the triple point temperature, yielding 90.680 K (IPTS-1968). These pressures agree within 0.5 percent with the less precise data of one other investigator at temperatures above 93 K. One hundred and five vapor pressures from the triple point to the critical point are represented by a new, non-analytic equation with a root mean square relative deviation of 0.01 percent. The derived triple point pressure is 0.1159 atm. At the assigned critical point temperature of 190.53 K the pressure is 45.356 atm. Deviations of some of the data from other sources exceed one percent at $T<140$ K.

12897. Ledbetter, H. M., **An approximation of $\theta_{elastic}$ for cubic metals,** *J. Phys. F* **2,** No. 2, 262-269 (Mar. 1972).

Key words: Crystal properties; Debye temperature; elastic constants; velocity/elastic waves.

The Debye characteristic temperature θ has been calculated from the elastic coefficients for 24 cubic elements by an approximate method proposed previously by other workers. The approximation requires that the elastic secular equation be solved only for the three principal cubic directions. New weighting coefficients for these directions were determined by a least squares best-fit procedure, based on computationally "exact" values of θ. Comparisons with the results of previous three term approximations indicate which set of weighting coefficients gives the best approximation to θ.

12898. McDonald, D. G., Risley, A. S., Cupp, J. D., Evenson, K. M., Ashley, J. R., **Four-hundredth-order harmonic mixing of microwave and infrared laser radiation using a Josephson junction and a maser,** *Appl. Phys. Lett.* **20,** No. 8, 296-299 (Apr. 15, 1972).

Key words: Cryotemperatures; harmonic mixing; infrared detectors; Josephson junctions; laser frequency measurements; lasers; superconductivity.

For mixing in a Josephson junction at infrared frequencies, we have shown that the available power from the junction increases as the intermediate frequency is increased. Following this result an infrared receiver has been developed incorporating a 9-GHz maser preamplifier at the i.f. Using this system, the beat between the 401st harmonic of a high-quality microwave source and a 3.8-THz infrared laser has been observed. Also, for low-order mixing at 3.8 THz, a comparison of beat signals from a Josephson junction and a room-temperature mixer has been made.

12899. Ledbetter, H. M., Wayman, C. M., **The crystallography of the β-to-β'' AuCd martensitic transformation,** *Acta Met.* **20,** No. 1, 19-30 (Jan. 1972).

Key words: Crystallography; gold-cadmium alloys; martensite; phase transformations.

The crystallography of the martensitic transformation in near-equiatomic AuCd alloys is re-examined, experimentally and theoretically, from the viewpoint that the low-temperature β'' phase has either trigonal or hexagonal symmetry. The elements of the Bain strain accompanying the transformation are found to be smaller than those reported for any other metallic system. As a result, only the habit plane and the twin ratio are useful quantities for characterizing the transformation. Predictions of the present study are in accord with existing measurements of these quantities. The reported lattice correspondence is believed to be unique for the martensitic transformation of a beta phase alloy.

12900. Manning, J. R., **Impurity-correlation factors for diffusion in diamond-structure crystals,** *Phys. Rev. B* **6,** No. 4, 1344-1355 (Aug. 15, 1972).

Key words: Correlation factor; diamond structure; diffusion; impurity; jump frequency; vacancy.

The correlation equations for impurity diffusion in the diamond structure have much in common with the equations for self-diffusion in pure face-centered-cubic and diamond structures. Comparison of these equations allows the four-frequency expression for the impurity-correlation factor in the diamond structure to be calculated to the same precision as the correlation factor for self-diffusion in a pure face-centered-cubic structure. This precision is an order of magnitude better than that for any previous calculation of this impurity-correlation factor. The calculation also illustrates an effect that choice of diffusion direction can have on the form of the correlation-factor equations. In these calculations, a generalized method is developed of calculating impurity-correlation factors in terms of effective-vacancy-return probabilities U_q, including contributions from vacancies which move far away from the impurity before effectively returning to their original site. Connections between various calculational techniques are discussed. The accurate values obtained here are compared with previous calculations done by a variety of other methods. This allows an evaluation of the problems arising in various standard calculational techniques.

12901. Foote, W. J., Hunter, R. D., **Improved gearing for rotary-vane attenuators,** *Rev. Sci. Instrum.* **43,** No. 7, 1042-1043 (July 1972).

12902. Swartzendruber, L. J., Bennett, L. H., **Retained austenite developed during surface grinding of a carbon steel,** *Scr. Met.* **6,** 737-742 (Aug. 1972).

12903. Hyman, A., Perloff, A., **The crystal structure of bismuth (2:1) borate, $2Bi_2O_3\cdot B_2O_3$,** *Acta Crystallogr.* **B28,** Part 7, 2007-2011 (1972).

Key words: Bismuth; borate; x-ray crystal structure.

The crystal structure of bismuth (2:1) borate ($2Bi_2O_3\cdot B_2O_3$) was determined by single-crystal x-ray diffraction analysis. Proper classification of this compound is as an oxide-orthoborate with the formula $Bi_4O_3(BO_3)_2$. The material crystallizes in the monoclinic system, $P2_1/c$, with 4 formula units in a cell of dimensions $a=11.107$, $b=6.627$, $c=11.044$ Å and $\beta=91.04°$. Intensity data were obtained on an automated diffractometer using Nb-filtered Mo $K\alpha$ radiation ($\lambda=0.71069$ Å). Bismuth positions were established by direct phase

determining procedures and the remaining atomic positions found from a three-dimensional difference synthesis phased by the bismuth atoms. Full-matrix, least-squares, isotropic refinement of the structure yielded a residual $R = 5.1\%$ for 2098 observed reflections. The structure contains discrete planar BO_3^{3-} anions held together by coordination to bismuth atoms. Additional oxygen atoms, coordinated only to bismuth, are present. The average B – O distances is 1.38 Å. The minimum Bi – O distance found is 2.14 Å. Some of the bismuth atoms do not have a clearly delineated coordination shell.

12904. Perloff, A., **The crystal structures of hydrated calcium and ammonium monofluorophosphates: $CaPO_3F \cdot 2H_2O$ and $(NH_4)_2PO_3F \cdot H_2O$,** *Acta Crystallogr.* **B28,** Part 7, 2183-2191 (1972).

Key words: Ammonium fluorophosphate monohydrate; calcium fluorophosphate dihydrate; crystal structure; fluorophosphate ion.

With the primary intention of establishing the dimensions and configuration of the monofluorophosphate ion, the crystal structures of the calcium and ammonium salts have been determined by three-dimensional x-ray diffraction analysis. Data were measured on an automated diffractometer using Nb-filtered Mo $K\alpha$ radiation, $\lambda = 0.71069$ Å. Both structures were established by direct phase determining techniques and refined by full-matrix least-squares analysis using anisotropic thermal parameters for the nonhydrogen atoms and isotropic thermal parameters for the hydrogen atoms. All hydrogen atoms were located in difference maps and the hydrogen bonding in these structures could be unambiguously determined. The crystal data (at 25 °C) and final R values are: $CaPO_3F \cdot 2H_2O$; $P\bar{1}$, $a = 8.6497$ (7), $b = 6.4614$ (6), $c = 5.7353$ (4) Å, $\alpha = 119.003$ (7), $\beta = 110.853$ (7), $\gamma = 94.146$ (8)°, $V = 249.94$ Å^3, $Z = 2$, $\rho_c = 2.313$ g.cm^{-3}, $R = 2.0\%$ (1254 observed data). $(NH_4)_2PO_3F \cdot H_2O$; $P2_1/c$, $a = 6.3042$ (5), $b = 8.2942$ (7), $c = 12.7597$ (10) Å, $\beta = 98.415$ (8)°, $V = 660.00$ Å^3, $Z = 4$, $\rho_c = 1.530$ g.cm^{-3}, $R = 3.6\%$ (1721 observed data). The average dimensions of the PO_3F^{2-} ion are; P – F 1.585, P – O 1.506 Å, F – P – O 104.5 and O – P – O 114.0°.

12905. Cezairliyan, A., **Measurement of melting point and electrical resistivity (above 3600 K) of tungsten by a pulse heating method,** *High Temp. Sci.* **4,** No. 3, 248-252 (June 1972).

Key words: Electrical resistivity; high-speed measurements; high temperature; melting point; thermodynamics; tungsten.

A subsecond duration pulse heating method is used to measure the melting point, and electrical resistivity of tungsten above 3600 K. The results yield a value of 3695 K (on the International Practical Temperature Scale of 1968) for the melting point with an estimated inaccuracy of 15 K. Estimated inaccuracy in electrical resistivity measurements is 1%.

12906. Rubin, R. J., **Velocity autocorrelation function of a large cluster of particles in a one-dimensional crystal,** *J. Chem. Phys.* **57,** No. 1, 312-316 (July 1, 1972).

Key words: Diffusion coefficient; harmonic crystal; velocity autocorrelation function.

The velocity autocorrelation function of the center of gravity of a cluster of Q particles in a one-dimensional harmonic crystal is determined in the limit $Q \to \infty$. In this limit, the autocorrelation decreases linearly from one to zero. In the continuum limit of the lattice equations of motion the same linear form is obtained for the velocity autocorrelation function. The coefficient of self-diffusion of the cluster of Q particles equals kT, a result which is exact and independent of cluster size.

12907. Vidal, C. R., Hessel, M. M., **Heat-pipe oven for homogeneous mixtures of saturated and unsaturated vapors; application to NaLi,** *J. Appl. Phys.* **43,** No. 6, 2776-2780 (June 1972).

Key words: Heat-pipe oven; laser induced resonance fluorescence; NaLi molecule; vapor mixtures.

A heat-pipe oven has been developed to produce homogeneous mixtures of a saturated vapor with an unsaturated vapor at any arbitrary well-defined ratio. The oven is able to handle materials of widely different vapor pressures and the zone containing the homogeneous vapor mixture can be made to extend over any desired path length. With this heat-pipe oven containing sodium and lithium, the laser- and collision-induced fluorescence spectrum of the NaLi molecule has been used to study the operation of the oven. The first observation of a "propensity rule" for a polar molecule (the $\Delta J = +1$ collision-induced NaLi line is stronger than the corresponding $\Delta J = -1$ or 0 line) is reported.

12908. Paule, R. C., **Low level calibration mixtures for gaseous pollutants,** *Anal. Chem.* **44,** No. 8, 1537-1539 (July 1972).

Key words: Air pollution standards; calibration mixtures (of gases); microbubbles; microstandards; NO; SO_2.

Low level SO_2 calibration mixtures have been produced using a technique of mixing known weight SO_2 microbubbles with a diluent gas. Procedures used in the production and measurement of the microbubbles of pure pollutant and in the subsequent on-the-spot dilution of the microbubbles are described. A necessary and effective passivation procedure for the dilution cylinder is given, along with a discussion of other factors that can affect the standard.

12909. Rubin, R. J., **Span of a polymer chain,** *J. Chem. Phys.* **56,** No. 12, 5747-5757 (June 15, 1972).

Key words: Chain polymer; degenerate Dvoretzky-Erdös problem; lattice model; random walk.

The x span of a polymer chain is defined as the difference between the largest x coordinate and the smallest x coordinate of any segments in the chain. The polymer chain is represented by a nearest-neighbor lattice-model random walk in which the mean square displacement of each component of a single step is 1/3. The distribution function of the x span of an N step random walk is obtained; and the following asymptotic formulas are obtained for its first and second moments, respectively, $2(2N/3\pi)^{1/2}$ and $4 \ln 2\, N/3$. The corresponding moments of the magnitude of the x component of the end-to-end distance are $(2N/3\pi)^{1/2}$ and $N/3$. Excluded volume effects are not considered. It is noted that the problem of calculating the first moment of the x span is identical with the one-dimensional case of the Dvoretzky-Erdös problem, namely, the calculation of the average number of different lattice sites visited in an N-step random walk on a d-dimensional lattice.

12910. Jones, M. C., Palmer, D. C., Tien, C. L., **Infrared absorptivities of transition metals at room and liquid-helium temperatures,** *J. Opt. Soc. Amer.* **62,** No. 3, 353-360 (Mar. 1972).

Key words: Absorption; chromium; iron; mirror; nickel; platinum; reflection.

Experimental data are presented for the normal spectral absorptivities of the transition metals, nickel, iron, platinum, and chromium at both room and liquid-helium temperatures in the wavelength range 2.5-50 μm. The absorptivities were derived from reflectivity measurements made relative to a room-temperature vapor-deposited gold reference mirror. The absorptivity of the gold reference mirror was measured calorimetrically, by use of infrared laser sources. Investigation of various methods of sample-surface preparation resulted in the choice of a vacuum-annealing process as the final stage. The experimental results are discussed on the basis of the anomalous-skin-effect theory modified for multiple conduction bands. As predicted, the results approach a single-band model towards the longer wavelengths. Agreement between theory and experiment is considerably improved by taking into account the modification of the relaxation time due to the photon-electron-phonon in-

teraction proposed by Holstein and Gurzhi; but, particularly at helium temperatures, the calculated curve is consistently below the experimental results.

12911. Greenspan, M., **Acoustic transmission line: some impedance properties,** *J. Acoust. Soc. Amer. Letters to Editor* **52,** No. 1, Part 2, 455-457 (July 1972).

Key words: Acoustic impedance; acoustic transmission line; sound absorption.

The imaginary part of the effective density of a fluid or of a viscoelastic material is zero. The contrary notion arises from an inadequate definition of characteristic impedance. The attenuation cannot exceed 2π Np per wavelength.

12912. Smith, R. V., **Two-phase, two-component critical flow in a venturi,** *J. Basic Eng. Trans. ASME, Series D* **94,** No. 1, 147-155 (Mar. 1972).

Key words: Critical flow; droplet flow; liquid film flow; transport coefficients; two-component flow; two-phase flow; venturi flow.

This paper reports the results of an analytical and experimental investigation whose object was to test the hypothesis that the flow of the gas phase controls critical and near critical two-phase flow for cases where the gas flow is essentially in separate streams. The results substantiate the hypothesis. The analytical results also indicate that one-dimensional flow equations with reasonably accurate estimates for the droplet size and for the drag and heat transfer coefficients will adequately describe critical and near critical flow over a wide range of flow conditions.

12913. Patrician, T. J., Ledbetter, H. M., Reed, R. P., **On the apparent rotation of transformation twins in Fe-Ni martensites,** *Metallurgical Trans.* **3,** No. 4, 947-952 (Apr. 1972).

Key words: Crystal imperfections; electron diffraction crystallography; iron alloys; nickel alloys; phase transformations/solid-state; twinning.

Fe-Ni alloys containing 28 to 33 wt pct Ni have been studied by transmission electron microscopy and by selected area diffraction to elucidate the phenomenon of the apparent deviation of the twin interface from the twinning plane $\{112\}_m$. Trace analyses of the twin interfaces are reported for 35 cases. Deviations of the twin trace, as projected onto the image plane, of up to 46 deg from those expected from $\{122\}_m$ transformation twins were observed. Contrary to previous interpretations, the conclusion of this study is that the deviations are due to the uncertainty of the orientation of the foil surface with respect to the electron beam. Thus, it has not been shown explicitly that this phenomenon provides a basis either for invoking multiple lattice invariant shears or for explaining habit plane scatter.

12914. Dickens, B., Bowen, J. S., Brown, W. E., **A refinement of the crystal structure of $CaHPO_4$ (synthetic monetite),** *Acta Crystallogr.* **B28,** Part 3, 797-806 (Mar. 1972).

Key words: Calcium coordinations; calcium phosphates; hydrogen bonding; monetite single crystals; x-ray diffraction.

$CaHPO_4$, synthetic monetite, crystallizes in the triclinic unit cell $a = 6.910$ (1), $b = 6.627$ (2), $c = 6.998$ (2) Å, $\alpha = 96.34$ (2)°, $\beta = 103.82$ (2)°, $\gamma = 88.33$ (2)° at 25 °C with cell contents of $4[CaHPO_4]$. The structure has been refined in space-group $P\bar{1}$ by the method of least-squares to $R_w = 0.032$, $R = 0.031$ using 3738 observed x-ray reflections measured on a diffractometer. Corrections were made for absorption, anomalous dispersion and isotropic secondary extinction.

The structure may be considered to consist of $CaHPO_4$ chains bonded together by Ca...O bonds and three types of hydrogen bonds. One type of hydrogen bond, O(1) – H(1)...O(5), is normal but is at the short end of the normal range with O(1)...O(5) = 2.565 (1) Å; one, O(7) – H(2)...O(7'), is very short with O(7)...O(7') = 2.458 (2) Å and is across a nominal center of symmetry; and one, O(6) – H(3)...O(8) where O(6)...O(8) = 2.669 (1) Å, is in the normal range but is presumed to be statistically disordered, with hydrogen covalently bonded to half of the O(6) atoms on average. The P – O distances support the choice of these hydrogen positions. Ca(1) is coordinated to seven oxygen atoms in an approximately pentagonal bipyramid with Ca(1)...O distances ranging from 2.2951 (9) Å to 2.763 (1) Å. Ca(2) is coordinated to eight oxygen atoms with Ca(2)...O distances ranging from 2.379 (1) Å to 2.5718 (9) Å, which all indicate strong Ca...O bonding. The Ca coordinations in several calcium phosphates and related compounds are compared.

12915. Bowen, R. L., Argentar, H., **A stabilizing comonomer: I. Synthesis and confirmation of structure,** *J. Dent. Res.* **51,** No. 4, 1071-1074 (July-Aug. 1972).

Key words: Antioxidants; biomaterials; comonomers; inhibitors; polymerization; stabilizers; toxicity.

A compound (BHM) was synthesized that can stabilize monomers by inhibiting premature polymerization but that can serve as a monomer in the polymerization after the initiator system is activated. The structural formula of BHM (3,5-di-*tert*-butyl-4-hydroxybenzyl methacrylate) was confirmed by nuclear magnetic resonance analysis.

12916. Paffenbarger, G. C., **Guide to Dental Materials and Devices: a historical review,** *J. Amer. Dent. Ass.* **84,** 1333-1335 (June 1972).

Key words: Certification program; guide; list of certified dental materials; specifications; Wilmer Souder.

The Guide to Dental Materials and Devices is a biennial publication of the American Dental Association. It started in 1955 as a publication of the ADA Specifications for Dental Materials. Dr. Wilmer Souder, a physicist who was the founder and former chief of the Dental Research Section, National Bureau of Standards, originated the idea and gave the motivation for the original specification for dental materials and the subsequent Guide. The Guide is not intended to replace dental materials textbooks, but is a source of current information for dentists, assistants and dental prosthetic laboratory technicians to guide them in their selection and use of dental materials. The sixth Edition 1972-1973 will be published in May or June of this year. It is a professional book with extensive references and is prepared by a professional society for its members and their auxiliaries.

12917. Mihalas, D., Hummer, D. G., Conti, P. S., **On the N III λλ4640, 4097 lines in Of stars,** *Astrophys. J.* **175,** No. 2, Part 2, L99-L104 (July 15, 1972).

Key words: Dielectronic recombination; ionized nitrogen; Of stars; stellar atmospheres; stellar spectra.

Detailed calculations based on non-LTE plane-parallel model atmospheres show that the N III emission lines at λλ4634, 4640, 4641 observed in Of stars are produced primarily by dielectronic recombination to $3d\,^3D$ followed by the $3d$-$3p$ transition in a *compact atmosphere*. The $3p$ state in turn is drained by two-electron transitions to the $2p^2$ levels. We find that λ4640 is in emission for $T_{eff} \leq 37{,}000$ K for main-sequence objects (33,000 K for giants), while λ4097 remains strongly in absorption, in accordance with observations. The calculated equivalent widths are in substantial agreement with the observed values for those Of stars with He II λ4686 in absorption, i.e., for those objects designated by Walborn as O((*f*)).

12918. Peterson, R. L., **Pseudoresonances in the magnetophonon structure of nondegenerate semiconductors,** *Phys. Rev. Lett.* **28,** No. 7, 431-434 (Feb. 14, 1972).

Key words: Boltzmann equation; magnetophonon effect; semiconductors; transport theory.

A new oscillatory behavior of semiconductor transport properties in quantizing magnetic fields is predicted on general arguments. The "pseudoresonances" are due to the pairing off of single-LO-phonon emission and absorption processes ending at the infinite density-of-states region. An exact calculation of Ohmic longitudinal magnetoresistance shows that at "high" temperatures, the pseudoresonance amplitudes are comparable to the usual magnetophonon resonances. The pseudoresonances have probably been seen, but attributed to 2LO-phonon scattering processes.

12919. Young, R., Ward, J., Scire, F., **The topografiner: an instrument for measuring surface microtopography,** *Rev. Sci. Instrum.* **43,** No. 7, 999-1011 (July 1972).

Key words: Diffraction grating; field emission; micrometrology; profile; surface; surface instrumentation; surface metrology; topography; tunneling.

A noncontacting instrument for measuring the microtopography of metallic surfaces has been developed to the point where the feasibility of constructing a prototype instrument has been demonstrated. The resolution of the preprototype unit is 30 Å perpendicular to the surface and 4000 Å in the plane of the surface. Inherent noise in the perpendicular direction corresponds to 3 Å or one atomic layer. By using a typical field emitter with radius of 100 Å, an ultimate limit of 200 Å would be expected for the horizontal resolution. Topographic maps of an infrared diffraction grating have been measured in order to demonstrate the performance of the instrument in measuring a well characterized surface. The instrument has been shown to conform to the Fowler-Nordheim description of field emission while spaced at the usual operating distances from the surface. When moved to within 30 Å of the surface, its performance is compatible with Simmons' theory of MVM tunneling. In the MVM mode, the instrument is capable of performing a noncontacting measurement of the position of a surface to within about 3 Å. The instrument can be used in surface science experiments to study the density of single and multiple atom steps on single crystal surfaces, adsorption of gases, and processes involving electronic excitations at surfaces.

12920. Opal, C. B., Beaty, E. C., Peterson, W. K., **Tables of secondary-electron-production cross sections,** *At. Data* **4,** No. 3, 209-253 (July 1972).

Key words: Atmospheric gases; cross section measurement; noble gases; secondary electrons.

The normalized results of relative measurements of electron-production cross sections differential in angle over the 30 to 150° range and in ejected energy over the 4 to 200 eV range are tabulated. Primary electron energies from 50 to 2000 eV were used in the study of He, N_2, and O_2. The remaining gases (Ne, Ar, Kr, Xe, H_2, CH_4, NH_3, H_2O, CO, C_2H_2, NO, and CO_2) were studied under 500 eV impact. Measurements were performed in a crossed-beam apparatus with the use of a rotatable electron gun and a fixed hemispherical electrostatic energy analyzer.

12921. Dickens, B., Bowen, J. S., **Refinement of the crystal structure of $Ca(H_2PO_4)_2 \cdot H_2O$,** *Acta Crystallogr.* **B27,** Part 11, 2247-2255 (Nov. 1971).

Key words: Calcium phosphates; crystal structure; hydrated calcium phosphate; hydrogen bonding; monocalcium phosphate monohydrate; single crystal x-ray diffraction.

$Ca(H_2PO_4)_2 \cdot H_2O$ crystallizes in space group $P\bar{1}$ in the triclinic unit cell $a = 5.6261$ (5), $b = 11.889$ (2), $c = 6.4731$ (8) Å, $\alpha = 98.633$ (6), $\beta = 118.262$ (6), and $\gamma = 83.344$ (6)° at 25 °C with $Z = 2$. The structure was refined with 3401 observed reflections measured on a diffractometer to $R_w = 0.033$, $R_o = 0.069$. Corrections were made for absorption, anomalous dispersion, and isotropic secondary extinction. The structure contains $Ca(H_2PO_4)^+$ chains which form corrugated layers. Between these layers are layers of $(H_2PO_4)^-$ ions and water molecules. Hydrogen atoms have been located approximately; ideal positions for the hydrogen atoms have been calculated. The two sets of hydrogen positions differ by ~ 0.28 Å. One hydrogen bond, in which the water molecule is the donor, is apparently bifurcated. All other hydrogen atoms form normal hydrogen bonds, with each hydrogen site seemingly fully occupied. The disorder of one hydrogen atom between the centrosymmetrically related atoms O(1) and O(1') was postulated by earlier workers. The P – O and O...O distances and electron-density maps obtained here show that there is no hydrogen atom in this position.

12922. Bowen, R. L., Argentar, H., **Tertiary aromatic amine accelerators with molecular weights above 400,** *J. Dent. Res.* **51,** No. 2, 473-482 (Mar.-Apr. 1972).

Key words: Accelerators; amines; color-stable composites; crystalline amine polymerization accelerators; synthesis; toxicity.

With the proper ring substituents, tertiary aromatic amines with large substituents on the nitrogen atom can be effective accelerators in free radical polymerization. Resistance to discoloration appears to be primarily a function of the substituents on the aromatic ring of the amine, whereas the rate of polymerization is dependent on both the alkyl substituents on the ring and the groups attached to the nitrogen atom.

12923. Brauer, G. M., Huget, E. F., **Dental adhesives,** Chapter 16 in *The Chemistry of Biosurfaces,* M. L. Hair, ed., **2,** 731-800 (Marcel Dekker, New York, N.Y., 1972).

Key words: Adhesives; adhesive test methods; bioadhesives; dental adhesives; dental resins; reactivity of tooth surfaces; tooth surface treatments.

Reactions occurring at the tooth surfaces and methods for obtaining bonding of restorative resins to enamel and dentin are reviewed. The composition of the tooth structure and the physical and mechanical properties of enamel and dentin are given. Studies of the reactivity of tooth surfaces as determined from adsorption, heats of immersion and wettability measurements are discussed. The effectiveness of various surface treatments such as by etching agents, enzymes, coupling agents and surface grafting techniques are examined. The potential organic polymeric adhesive systems, including bioadhesives useful for dental applications, are summarized. Methods of testing the magnitude of the adhesive joint are described.

12924. Jefferies, J. T., Orrall, F. Q., Zirker, J. B., **The interpretation of total line intensities from optically thin gases. I. A general method,** *Solar Phys.* **22,** No. 2, 307-316 (Feb. 1972).

Key words: Optically thin line emission; radiative transfer; solar corona; spectroscopic diagnostics.

We describe a general method for inferring, from the line emission of an optically thin medium, the physical state of the gas along the column in the line of sight which is sampled by the observations. Since it is not possible to infer the distribution of the physical state parameters with position in the line of sight – any arbitrary rearrangement of material giving equivalent line emission – we seek instead to specify the state in another way. A unique specification is found in terms of the bivariate distribution function $\mu(n, T)$, describing the partitioning of the matter in the gas over the density and temperature. We show that, given sufficient observational data, it is in principle possible to determine both $\mu(n, T)$, and the chemical composition. With less complete data the acuity of the analysis is correspondingly reduced.

The method is devised for application to the astronomical case, especially for studies of the solar corona, the chromosphere-corona transition region, planetary nebulae and other optically thin sources. We illustrate the formulation for the situation encountered in the solar corona.

12925. Jefferies, J. T., Orrall, F. Q., Zirker, J. B., **The interpretation of total line intensities from optically thin gases. II. The coronal forbidden lines,** *Solar Phys.* **22,** No. 2, 317-326 (Feb. 1972).

Key words: Optically thin line emission; radiative transfer; solar corona; spectroscopic diagnostics.

We discuss the application of a general diagnostic procedure, developed in the preceding paper of this series, to the inference of the physical state of coronal condensations from a knowledge of their forbidden line emission. We consider the limitations set on such an analysis by inadequacies in existing data and indicate the additional observations in the infrared and ultraviolet, as well as the visible, which will be needed for development of the full power of the diagnostic method.

12926. Jefferies, J. T., Orrall, F. Q., Zirker, J. B., **The interpretation of total line intensities from optically thin gases. III. Application to coronal forbidden line spectra,** *Solar Phys.* **22,** No. 2, 327-343 (Feb. 1972).

Key words: Optically thin line emission; radiative transfer; solar corona; spectroscopic diagnostics.

The diagnostic method developed in the two preceding papers of this series is applied to coronal forbidden line intensity data obtained at eclipses in 1952, 1961, 1965, 1966, and 1970. The application of the method is limited by the nature of the data but allows a first inference of the relationship between electron density and temperature in the condensations observed at these eclipses, and of the distribution of tions—effectively 10^6 to 2.4×10^6 *K*. We determine the relative abundance of nickel to iron in the corona, finding a value in agreement with latest photospheric determinations and with a similar (factor of two) uncertainty. We are also able to set lower limits to the abundance of iron with respect to hydrogen, again finding values consistent with recent photospheric determinations.

12927. Lightbody, J. W., Jr., **Electron scattering from one- and two-phonon vibrational states,** *Phys. Lett.* **38B,** No. 7, 475-479 (Apr. 3, 1972).

Key words: Admixture; anharmonicities; branching ratios; electron scattering; phonons; reorientation effect.

Admixtures of one- and two-phonon states are required to fit (e, e′) form factors for the lowest two 2^+ states in several even-even vibrational nuclei. These anharmonic wave functions correctly reproduce radiative branching ratios and excited state quadrupole moments.

12928. Neuhausen, R., Lightbody, J. W., Jr., Fivozinsky, S. P., Penner, S., **Elastic electron scattering from Zn isotopes,** *Phys. Rev. C* **5,** No. 1, 124-128 (Jan. 1972).

Key words: Electron scattering; nuclear radii; nuclear sizes; zinc nuclei.

Elastic electron scattering from the stable even-even Zn isotopes was measured in the region of the first diffraction minimum ($0.3 \leq q \leq 1.1$ fm^{-1}). The cross-section ratios for each pair of isotopes were used to determine the change in the rms radius. The rms radius follows an $A^{1/3}$ law between ^{64}Zn and ^{66}Zn and between ^{68}Zn and ^{70}Zn; whereas, between ^{66}Zn and ^{68}Zn the rms radius decreases significantly.

12929. Bergstrom, J. C., Crannell, H., Kline, F. J., O'Brien, J. T., Lightbody, J. W., Jr., Fivozinsky, S. P., **Electroexcitation of the giant resonance of ^{13}C,** *Phys. Rev. C* **4,** No. 5, 1514-1532 (Nov. 1971).

Key words: Continuum spectra; efficiencies; fine structure; giant resonance; isospin splitting; pygmy; pygmy resonance; radiative tails; resonance weak coupling; ^{12}C, ^{13}C.

The giant resonance of ^{13}C has been investigated by means of inelastic electron scattering. The incident energies and scattering angles employed were 77.0 MeV (75°), 106.0 MeV (75°), 55.4 MeV (145.7°), and 81.0 MeV (145.7°). The data show a distinct splitting of the resonance into two large peaks near 20.5 and 24.5 MeV. Some fine structure is observed which correlates well with the position of excitations calculated by Easlea. Considerable strength is observed in the region of 14-MeV excitation which may correspond to the "pygmy" resonance seen in the photonuclear work of Cook. Data were also taken consecutively on ^{12}C. The form factors for ^{12}C and ^{13}C are compared. The presence of the extra neutron in ^{13}C results in a major restructuring of the giant-resonance strength. The possibility of an isotopic splitting in the ^{13}C giant resonance is discussed.

12930. Pruitt, J. S., **Electron beam current monitoring system II,** *Nucl. Instrum. Methods* **100,** 433-443 (1972).

Key words: Beam; calibration electron; Faraday-cup; ferrite; monitor.

A reliable method for absolute calibration of a ferrite electron beam current monitor with a pulse generator has been developed and tested. The absolute accuracy of pulser calibrations and Faraday cup calibrations of the National Bureau of Standards ferrite monitor has been compared by using them both to determine the Faraday cup error. These independent determinations differ by a maximum of 0.11% and an average of 0.03% at six different energies in the 20-120 MeV range, using beam currents between 0.6 and 25 μA. Variation of the Faraday cup error with energy is shown to compare favorably with the predictions of other authors, and the good agreement is used to argue that the influence of beam microstructure on the ferrite calibration is less than 0.1%.

12931. Becker, D. A., **Trace analysis for platinum in glasses by neutron activation,** *Anal. Chim. Acta* **61,** 1-6 (1972).

Key words: Glasses; neutron activation analysis; radiochemical separations; spontaneous deposition; trace analysis.

Trace amounts of platinum were determined in eight glasses. These glasses had been prepared under special conditions, and information on both the surface and interior platinum was desired. Previous microscopic examination of the glass samples had identified platinum on the surface of at least four of the samples. The platinum was analyzed using the nuclear reaction $^{198}\mathrm{Pt}(n,\gamma)^{199}\mathrm{Pt}\xrightarrow{\beta}{}^{199}\mathrm{Au}$. The ^{199}Au product has a 3.15 day $T_{1/2}$ and $E\gamma$ of 158 and 208 keV. Samples were irradiated in the NBSR for 2 hours at 1.3×10^{13} n. cm^{-2} sec^{-1}. After irradiation, the glasses were etched with aqua regia for the determination of surface platinum, and then dissolved in HF and $HClO_4$ for the determination of interior platinum. The radioactive ^{199}Au was separated from the matrix by spontaneous deposition on metallic zinc. Experimental sensitivites of 0.02 μg platinum were obtained.

12932. Pringle, W. C., Jr., **Microwave spectrum, vibration-rotation interaction, and ring puckering vibration in silacyclobutane and silacyclobutane-1,1-d_2,** *J. Chem. Phys.* **54,** No. 12, 4979-4988 (June 15, 1971).

Key words: Dipole moment; molecular structure; ring puckering vibration; rotational spectrum; silacyclobutane; vibrational potential functions; vibration-rotation interaction.

The microwave spectrum of the molecules silacyclobutane and silacyclobutane-1, 1-d_2 has been observed between 8 and 55 GHz and the first four vibrational states assigned. The ground state rotational constants of the former molecule are 8815.75, 6289.00, and 4245.32 MHz. The first two inversionlike intervals of the ring puckering mode were determined to be 75.75 and 7790 MHz in the normal isotopic species; the corresponding intervals in the deuterated species are 43.06 and 4430 MHz. The effect of these frequencies on the determination of the potential energy for the ring puckering vibration was investigated. The ring configuration was shown to be significantly puckered in the ground state. The *a* component of the dipole moment was found to be nearly constant in the four vibrational states of the

normal molecule, $\mu_a = 0.4396$ D, while the out-of-plane transition moment between inversion doublets dropped rapidly as the inversion levels approached the top of the barrier.

12933. Peterson, R. L., **Longitudinal magnetoresistance in polar semiconductors: a displaced-Maxwellian analysis,** *Phys. Rev. B* **5,** No. 10, 3994-4000 (May 15, 1972).

Key words: InSb; magnetophonon; magnetoresistance; semiconductors; transport theory.

The displaced-Maxwellian distribution function is used to study longitudinal magnetoresistance in polar semiconductors, when several carrier scattering mechanisms are simultaneously active. Although both the $B = 0$ and the quantum-limit expressions for the resistance are largely the same as those obtained from the Boltzmann equation, numerical calculations show that the displaced Maxwellian is unable to account for longitudinal magnetoresistance minima often observed in the magnetophonon structure of polar materials. In the hot-electron regime, the displaced Maxwellian can give maxima or minima, depending upon lattice temperature and type of scattering mechanisms.

12934. Wiese, W. L., Kelleher, D. E., Paquette, D. R., **Detailed study of the Stark broadening of Balmer lines in a high-density plasma,** *Phys. Rev. A* **6,** No. 3, 1132-1153 (Sept. 1972).

Key words: Asymmetries; hydrogen lines; line profiles; shifts; stabilized arc; Stark broadening.

The Stark-broadened profiles of the Balmer lines H_α, H_β, H_γ, and H_δ have been measured in a high-current, wall-stabilized arc operated in hydrogen. Temperatures and electron densities have been determined with a plasma model assuming partial local thermodynamic equilibrium (LTE), after a detailed plasma analysis revealed small deviations from complete LTE. The temperatures have been determined from line-to-continuum intensity ratios using H_β and continuum points in the near uv, and the electron densities were derived from absolute intensity measurements. The investigations cover the range of electron densities between 1.5×10^{16} and 10^{17} cm^{-3} and temperatures between 0.9×10^4 and 1.4×10^4 K. Extensive comparisons with recent Stark-broadening theories and other experiments have been undertaken with the following principal results: The most pronounced differences between this experiment and theory occur in and near the line centers, where the measured profiles show systematically less structure than the calculations predict. Comparisons of the calculated and precisely measured ratios between the 1/2, 1/4, and 1/8 widths within *each* line show that the recent theories are internally consistent within 6% for H_β and H_γ, whereas for H_α inconsistencies of order 25% occur. Similar inconsistencies, somewhat larger respectively, are found for the theoretical values of the half-width ratios between *different* Balmer lines. For the most important line H_β, the measured half-widths agree within 7% with the calculated values. The total experimental error in this comparison, which originates predominantly in the electron-density measurement, is estimated not to exceed 6%. Very reproducible asymmetries and red shifts are observed for H_β and H_γ. Somewhat smaller red shifts are also obtained for H_α. The shifts are approximately linear functions of the electron density. Comparisons with other experimental data show appreciable scatter between the various results. We estimate that for the most-often-studied line H_β the uncertainties in the theoretical Stark widths are of the order of (5-7)% for the range of our experiment.

12935. Moore, G. A., **Automatic methods for analysis of microstructures,** (American Society for Testing and Materials Symp. on Stereology and Quantitative Metallography, Atlantic City, N.J., June 28, 1971), *Amer. Soc. Test. Mater. Spec. Tech. Publ.* **504,** pp. 59-80 (July 1972).

Key words: Aggregates; anisotropy; automation; computers; mechanical properties; microscopes; microstructure; particle distribution; phase mapping; quality control; scanning; television systems; variability; variance (statistics).

From the viewpoint of materials engineering and quality control the significant aspects of the microstructure of a material as a whole constitute a gestalt which controls mechanical behavior. This gestalt can be specified by six sterologically valid parameters measuring phase percentage, size and spacing of particles, variability among portions of the material, general anisotropy, and degree of patternness. Raster scanning devices of either the mechanical or television type are intrinsically capable of easily measuring these six parameters. Provision for each is available in at least one of the present television scanners. Minor changes are desirable to provide this common set of measurements with all instruments and to improve accuracy.

In contrast, microarchitectural processes which identify, measure, and selectively count individual object sections require massive programming effort and are inefficient and time consuming in present computers. Selective specimen preparation and human designation of objects are preferable to machine identification. Some proposals for more efficient and more human-like machines are mentioned. Materials engineers should try to avoid these difficult processes whenever feasible.

12936. Curl, R. F., Jr., Evenson, K. M., Wells, J. S., **Laser magnetic resonance spectrum of NO_2 at 337 μm and 311 μm,** *J. Chem. Phys.* **56,** No. 10, 5143-5151 (May 15, 1972).

Key words: HCN laser; laser magnetic resonance; NO_2; spectroscopy.

The Zeeman components of several rotational transitions of nitrogen dioxide have been observed in absorption using the 311 and 337 μm lines of an HCN laser as a source. The Zeeman components of four rotational transitions (two at 311 μm and two at 337 μm) have been assigned. Two components of the g tensor have been determined from the spectrum by least square fitting. The anisotropic component $(aa)_g^{(S)}$, obtained as -0.010, agrees well with that predicted from theory, but the isotropic component $(0)_g^{(S)}$, obtained as 2.013, does not agree satisfactorily with theoretical prediction or with solid phase measurements both of which give 1.9997. The rotational frequencies of the four transitions have also been obtained.

12937. Billingsley, F. P., II, Krauss, M., **Coupled multiconfigurational self-consistent-field method for atomic dipole polarizabilities. I. Theory and application to carbon,** *Phys. Rev. A* **6,** No. 3, 855-865 (Sept. 1972).

Key words: Carbon (^1D); carbon (^1P); carbon (^3S); multiconfiguration; static dipole polarizability; variation method.

A method for calculating static dipole polarizabilities of atoms within a multiconfigurational self-consistent-field (SCF) framework is presented. The method involves the direct solution of the multiconfigurational SCF equations of an atom in the presence of a perturbing field which is simulated by a charged particle. The use of a multiconfigurational framework allows this technique to be applied straightforwardly to any given state of both degenerate and nondegenerate atoms, and also allows the explicit introduction of correlation effects. Sample calculations are reported for the static dipole polarizabilities of the carbon atom in its ^1S, ^1D, and ^3P states with partial inclusion of correlation. The results are compared with those obtained from many-body perturbation theory, and other techniques. In addition, a prescription for specifying a sufficiently flexible set of polarization basis functions is described.

12938. Jacox, M. E., Milligan, D. E., **Spectrum and structure of the O_3^- and O_4^- anions isolated in an argon matrix,** *Chem. Phys. Lett.* **14,** No. 4, 518-521 (June 15, 1972).

Key words: Charge transfer; infrared spectrum; isotopic substitution; matrix isolation; $O^- + O_2$ reaction; O_3^- anion; O_4^- anion; structure; ultraviolet spectrum.

An absorption which appears near 800 cm^{-1} upon reaction of O^- with O_2 in an argon matrix has been assigned as ν_3 of O_3^-, with a valence angle of $110 \pm 5°$, and an absorption near 1000 cm^{-1} can be assigned to *trans*-O_4^-

12939. Franklin, A. D., **Defect equilibria in alkaline earth fluorides containing rare earth ions,** *Tech. Rep.* **AFML-TR-72-31,** 48 pages (Air Force Materials Laboratory, Air Force Systems Command, Wright-Patterson Air Force Base, Ohio, Mar. 1972).

Key words: Anelastic relaxation; CaF_2; density; dielectric relaxation; EPR; equilibria; point defects; rare-earth doping.

The point defects present in GdF_3-doped CaF_2, with concentrations ranging from 0.01 to 0.46 mole percent GdF_3, have been studied using measurements of density, EPR, and dielectric and anelastic relaxation as a function of concentration and of annealing temperature in an He + HF atmosphere in the range 500 to 1100 °C. The density measurements showed no dependence upon annealing. The unit cell contents increased in mass with increasing GdF_3 concentration more rapidly than expected on the basis of substitutional Gd^{3+} and interstitial F^- ions, and suggest the incorporation of an HF molecule with each GdF_3 unit. The role previously suggested for cation vacancies in the annealing behavior appears untenable in light of these density results. The reorientation kinetics of the pair formed by association of the mobile interstitial F^- ion with the immobile Gd^{3+} ion were studied using EPR line-broadening and dielectric relaxation measurements, and some anelastic relaxation measurements were made as well. The EPR line-broadening and dielectric relaxation data could be fitted very well with the same model, in which reorientation takes place in a mode dominated by nearest-neighbor jumps of the interstitial F^- ion. This jump frequency is given by $3.1 \times 10^{12} \exp(-0.38 \text{ ev/kT}) \text{ s}^{-1}$. Additional relaxation modes appear in both the dielectric and anelastic spectra, and at least 2 and perhaps 3 centers are involved, as yet unidentified.

12940. Richmond, J. C., Kneissl, G. J., **Procedures for the precise determination of thermal radiation properties,** *Tech. Rep.* **AFML-TR-70-121,** 104 pages (Air Force Materials Laboratory, Air Force Systems Command, Wright-Patterson Air Force Base, Ohio, Oct. 1970).

Key words: Emittance; graphite; iridium; laser-source integrating sphere; reflectance; shallow cavity emittance; surface characterization; thoria; tungsten.

The broad objective of this program, which has continued for several years, is to develop equipment and procedures for measuring the important thermal radiation properties of materials, particularly those used in aircraft, missiles, and space vehicles, at temperatures up to the melting points of the most refractory materials. During the period covered by this report the specific objectives were to complete development of the laser-source integrating sphere reflectometer, and to prepare emittance standards for use at temperatures above 1400 K (2000 °F). The laser-source integrating sphere reflectometer consisted of (1) a helium-neon laser as a source, capable of operation at 0.6328, 1.15, and 3.39 μm; (2) a 35 cm (14 in.) diameter sphere coated with barium sulphate or sodium chloride; (3) a lead sulfide detector; and (4) a radio-frequency generator for heating the sample by induction. A spike filter, transmitting at the laser-wavelength, placed in front of the detector, reflected or absorbed most of the background radiation from the hot sample, and a chopped incident beam together with synchronous amplification of the signal from the detector was used to eliminate the effect of the remaining background radiation. The integrating sphere could be evacuated, or used with an atmosphere of purified helium. An error analysis showed that the measured absolute reflectance is measured with a bias of less than one percent of the measured value. Data are presented on the directional-hemispherical reflectance [$\rho(12°;2\pi)$] at temperatures in the range of 1300 to 2500 K of well characterized samples of thoria, iridium, two lots of graphite and two lots of tungsten. Precision of measurement on the order of 0.0005 in reflectance units, expressed as the standard deviation of six replicate measurements, was attained. Samples of one lot of tungsten and one lot of graphite were supplied by Arthur D. Little, Inc., from the same lots as those for which thermal conductivity data are reported in AFML-TR-69-2. Data are also presented for the normal total emittance of alumina, thoria, magnesia, zirconia, graphite, iridium and two lots of tungsten, obtained by the shallow cavity technique and modifications thereof, at temperatures in the range of 1400 to 2500 K (about 2000 to 4000 °F).

12941. Mountain, R. D., **Temperature dependence of depolarized scattered light near the critical point,** (Proc. of the Colloquium on Light Scattering by Fluids, Paris, France, July 15-17, 1971), *J. Phys.* **33,** Supplement 2-3, C1-265–C1-268 (Feb.-Mar. 1972).

Key words: Correlation length; critical opalescence; critical phenomena; depolarized scattering; light scattering; Ornstein-Zernike correlation function.

The double scattering formalism of Frish and McKenna is used to investigate the temperature dependence of the depolarized scattering in the vicinity of the critical point of a one component fluid composed of spherical molecules. The terms involving two particle correlations are estimated using the Ornstein-Zernike correlation function. The ratio of the intensity of the *H-H* to *V-V* scattering is found to diverge as $k\xi \ln(1/k\xi)$. The possibility of using depolarized scattering as a probe of three and four particle correlations near the critical point is discussed.

12942. McNesby, J. R., Braun, W., Ball, J., **Vacuum ultraviolet techniques in photochemistry,** Chapter 11 in *Creation and Detection of Excited State,* A. A. Lamola, ed., **1,** 503-586 (Marcel Dekker, Inc., New York, N.Y., 1971).

Key words: Actinometry; experimental; light sources; photochemistry; vacuum ultraviolet; window materials.

Vacuum ultraviolet techniques in photochemistry are reviewed from the standpoint of light sources (both continuously operated and pulsed), window materials, actinometry and chemical applications. Emphasis is given to modern physical techniques.

12943. Leasure, W. A., Jr., **Considerations in the development of measurement procedures for the regulation and monitoring of noise pollution,** (Proc. 2d Urban Technology Conf. and Technical Display, San Francisco, Calif., July 24-26, 1972), *AIAA Paper No.* **72-622,** pp. 1-10 (American Institute of Aeronautics, New York, N.Y., 1972).

Key words: Acoustics; noise measurement; noise pollution; noise regulations; noise (sound).

A noise standard or regulation should be based on accurate, reliable and relevant measurements. In this paper, an outline is given of some of the basic considerations in developing measurement systems which are required in order to effectively regulate or monitor noise pollution or to assess the alternative strategies for noise abatement and control. The importance of these considerations is reinforced through a discussion of the questions addressed during the design of a test procedure and measurement methodology for a specific program in the area of motor vehicle noise.

12944. Wood, L. A., Bullman, G. W., **Creep and other tensile properties of rubber crosslinked by dicumyl peroxide,** *J. Polym. Sci.*: Part A-2, **10,** 43-50 (Jan. 1972).

Key words: Creep; modulus; rubber, natural; tensile properties; tensile strength; ultimate elongation.

Natural rubber crosslinked by dicumyl peroxide in amounts up to 25 parts per hundred of rubber (phr) showed a maximum in tensile strength near 1 phr, followed by a steep decrease to a minimum near 5 phr. The ultimate elongation decreased from 870% at 0.5 phr to

about 10% above 10 phr. The modulus increased linearly with increase of crosslinking. The creep rate decreased from 5.6% per decade at 0.5 phr to zero at 5 phr and higher values. Crystallization, with a resultant abrupt increase in creep, was noted in specimens held in the stretched condition for more than one day. Between 5 and 25 phr this system (when crystallization is avoided) appears to function as an ideal elastic network and can be recommended for studies of rubber elasticity since no variation of modulus with time is observed.

12945. Miller, A., McLaughlin, W. L., Lynggard, B., **A scanning spectrophotometer for reading thin-film dosimeters,** *Dan. At. Energy Comm. Risö Rep. No.* **M-1525,** pp. 1-21 (Aug. 1972).

Key words; Dose distribution; dosimetry; electron beams; microdensitometry; spectropho tometry; thin films.

It is possible to convert a conventional spectrophotometer into a versatile scanning spectrophotometer, without great difficulty or expense. The improved instrument can be tailored to perform many electro-optical tasks by the appropriate arrangement of modular components. In this work, basic optical components (light sources, monochromator, and sample chamber) of a conventional spectrophotometer were used on an optical bench. Specially designed accessories could be added to these components in order to measure at given wavelengths (from 200 to 800 nm) spatial variation (down to less than 10 μm) of optical transmission or reflection quantities in thin-film dosimeters, over a wide dynamic range. For high-speed data acquisition, analogue-to-digital conversion could be programmed to give tabular or graphical absorbed dose readings from calibrated film as a function of optical or spatial variables.

12946. Beatty, R. W., **Efficiencies of microwave 2-ports from reflection coefficient measurements,** *IEEE Trans. Microwave Theory Tech.* **MTT-20,** No. 5, 343-344 (May 1972).

Key words: Efficiency of two-port; measurement of 2-port efficiency; microwave measurements.

It is well-known that one can determine the efficiency of a microwave 2-port by measuring the reflection coefficient Γ_1 at the input port when the output port is terminated by a sliding short circuit. The locus of Γ_1 is a circle whose radius equals the efficiency η_{2m} for energy entering port 2 when port 1 is terminated in a nonreflecting load. Similarly η_{1m} is the radius of the Γ_2 circle when port 1 is terminated in a sliding short circuit.

This note describes a procedure for obtaining, from the same measured data, new reflection coefficients Γ_{1N} and Γ_{2N}, whose circular loci have radii R_{1N} and R_{2N} which give the efficiencies of the 2-port when connected to an arbitrary load of reflection coefficient Γ_L.

Thus the Γ_1 or Γ_2 data may be used to obtain the efficiency of the 2-port when terminated in any arbitrary load. The method is potentially more accurate than the 3-point method since errors can be reduced by drawing a circle through many measured points.

12947. Arthur, M. G., **A precision HF-noise power measurement system,** *ISA Trans.* **10,** No. 3, 264-268 (1971).

Key words: Measurement system; noise comparator; noise measurement; noise standards.

This paper describes a precision HF noise power measurement system used at the National Bureau of Standards. It includes reference standard noise generators operating at approximately 77 and 373 K and an instrument for comparing the noise power of a noise source against the reference standards. The comparison instrument is a sum-and-difference correlation radiometer. Both the standards and the comparison instrument operate at 3, 30, and 60 MHz, and can be used with noise sources having source impedances of 50 ohms, unbalanced. Measurement uncertainty is typically less than 1% for sources with noise temperatures from 75 to 30,000 K.

12948. Fong, J. T., Simmons, J. A., **A non-equilibrium thermodynamic theory of simple materials based on a single-integral entropic functional,** (Proc. Int. Symp. on Foundations of Plasticity, Warsaw, Poland, Aug. 1972), *Arch. Mech. Stos.* **24,** No. 3, 363-372 (1972).

Key words: Anisotropy; continuum mechanics; entaxy; entropy; irreversibility; non-equilibrium state; nonlinear theory; plasticity; thermodynamics; viscoelasticity; yielding.

Based on the notion of a single-integral entropic functional as first introduced by Bernstein, Kearsley, and Zapas for a class of simple fluids in 1964, we present a non-equilibrium, irreversible thermodynamic theory of simple materials with fading memory within the general framework of Coleman's thermodynamic theory. Our theory is then modified, in a heuristic approach, to include "plasticity" by identifying the single-integral entropic functional with Bridgman's notion of "generalized entropy" for plastic deformations.

12949. Karp, S. S., Matteson, T. T., Maltese, M. D., **A search and rescue simulation model (SARSIM),** *Proc. Tokyo 1971 AICA Symp. on Simulation of Complex Systems, Tokyo, Japan, Sept. 3-7, 1971,* pp. I-4/1–I-4/8 (The Society of Analog Technique of Japan, Tokyo, Japan, Sept. 1971).

12950. Geltman, S., **Applications of pseudo-state expansions,** (Proc. VII Int. Conf. on the Physics of Electronic and Atomic Collisions, Amsterdam, July 26, 1971), Chapter in *Physics of Electronic and Atomic Collisions,* T. R. Gover and F. J. de Heer, eds. pp. 216-231 (North-Holland Publ. Co., Amsterdam, The Netherlands, 1972).

Key words: Close coupling; electron-atom scattering; polarizabilities; pseudo-states; Sturmians.

The various types of pseudo-state expansions which have been applied to the scattering of a charged particle by atoms are discussed. Of the applications so far made, greater success has been achieved in the case of low energy electron-hydrogen scattering than for high-energy proton-hydrogen scattering.

12951. Coyne, J. J., Meshkov, S., **High-energy total cross sections and symmetry relations,** *Phys. Rev. D* **6,** No. 1, 399-402 (July 1, 1972).

Key words: Barger-Rubin; Johnson-Treiman; SU(3), SU(6); symmetry; total cross sections.

Recent Serpukhov measurements of meson-baryon total cross sections allow comparisons with the Johnson-Treiman and Barger-Rubin relations. For 25-55-GeV/c incident meson momenta, the Johnson-Treiman relation, $1/2\Delta(Kp) = \Delta(\pi p)$, is well satisfied. The less restrictive Barger-Rubin relation holds for most of the Serpukhov points. Linear extrapolation of Serpukhov fits for $\Delta(Kp)$ and $\Delta(\pi p)$ to high momenta leads to the prediction of large violations of the Johnson-Treiman relations.

12952. Hockey, B. J., **Observations by transmission electron microscopy on the subsurface damage produced in aluminum oxide by mechanical polishing and grinding,** (Proc. British Ceramic Society Meeting, Textural Studies of Ceramics, London, England, Dec. 16-17, 1970), Paper No. 6 in *Textural Studies of Ceramics, Proceedings No.* **20,** pp. 95-115 (British Ceramic Society, Shelton, Stoke-on-Trent, Great Britain, June 1972).

Key words; Aluminum oxide; dislocations; mechanical polishing and grinding; microtwins; transmission electron microscopy.

Transmission electron microscopy was used to examine the near-surface regions of Al_2O_3 crystals which were: (1) polished with 0.25 μm diamond, (2) polished with 0.3 μm alumina powder, or (3) ground with a diamond-impregnated wheel.

Near-surface regions of diamond-polished polycrystalline and (0001) single-crystal sections contained a relatively uniform high den-

sity of dislocations generally in the form of half-loops and closely associated with surface scratches. Similar subsurface damage, but to a lesser extent, was found in alumina-polished polycrystalline specimens. In both cases, depth of subsurface damage was estimated to be 1-2 μm.

Observations on diamond-ground polycrystalline specimens at a depth of 2-4 μm below the original surfaces (necessitated by the residual stresses and irregular topography) revealed penetrating arrays of dislocations and/or microtwins (basal and rhombohedral), depending on the orientation of the grain. Large numbers of basal twins, in particular, were found in diamond-ground $(0\bar{1}12)$ specimens, while a (0001) section contained only non-basal dislocations. Maximum depth of damage produced by grinding was estimated to be $\approx 20\,\mu$m.

The effect of briefly (1-4 hrs) annealing diamond-polished specimens at temperatures between 700 and 1500 °C was also investigated. Dislocation activity (and stress relief) was apparent after annealing at 900 °C and led to the development of large dislocation networks at 1200 °C. Annealing at 1500 °C, however, resulted in thermal etching and the elimination of nearly all subsurface damage.

12953. Hellwig, H.; Bell, H. E., Kartaschoff, P., Bergquist, J. C., **Frequency stability of methane-stabilized He-Ne lasers,** *J. Appl. Phys.* **43,** No. 2, 450-452 (Feb. 1972).

Key words: Frequency stability; He-Ne laser; laser stabilization; length standard; methane frequency standard; saturated absorption; time standard.

Free-running laser stabilities of 1.5×10^{-11} for the millisecond region and methane-locked stabilities of 10^{-13} for 10-sec averaging time are achieved with a minimum of shock and vibration isolation in an ordinary laboratory environment. Superior stability performance is obtained with dc excitation as compared to rf excitation. The experimental setup is described in some detail.

12954. Kamper, R. A., Simmonds, M. B., **Broadband superconducting quantum magnetometer,** *Appl. Phys. Lett.* **20,** No. 8, 270-272 (Apr. 15, 1972).

Key words: Magnetometer; microwaves; quantum interference; superconductivity.

We describe the design, operation, and performance of a superconducting quantum interference device (SQUID) which operates at a frequency of 9 GHz. It is sensitive to variations of magnetic field in a frequency band from 0 to 1 GHz.

12955. Grimes, D. N., **Optical autocorrelator with special application to MTF measurement,** *Appl. Opt.* **11,** No. 4, 914-918 (Apr. 1972).

Key words: Autocorrelation; interferometry; lens testing; modulation transfer function; optics; physical optics; Sagnac interferometer.

An optical autocorrelator is described which is based on a modified Sagnac two-mirror interferometer that operates in the zero-fringe mode. The real-time radiant flux output is the square of the autocorrelation of the aperture function. In a particular application, when the aperture function is the pupil function of a lens under test, the autocorrelator output is the MTF of the lens. The system is not limited in focal length; aperture size is limited only by the sizes of the beam splitters and mirrors. Experimental results are given with comparison data for both infinite-conjugate MTF and the autocorrelation of an annular aperture. Methods of adapting the system for measurement of the phase of the transfer function and for finite conjugate testing are also described.

12956. Hils, D., McCusker, M. V., Kleinpoppen, H., Smith, S. J., **Differential and direct differential elastic scattering cross sections for electrons and potassium atoms,** *Phys. Rev. Lett.* **29,** No. 7, 398-401 (Aug. 14, 1972).

Key words: Cross sections; elastic scattering; spin polarization.

In a modulated crossed-beam experiment we have elastically scattered unpolarized electrons of 3.3 eV energy from spin-polarized K atoms. A measurement of the polarization of the scattered electron yields $|f(\theta)|^2/\sigma(\theta)$. Our measured values of $|f|^2/\sigma(\theta)$ show a significant angular shift relative to the theoretical curve in forward-angle scattering ($\theta = 20 - 40°$). This shift is not apparent in measurements of the differential scattering cross section $\sigma(\theta)$ over the same angular range, which, however, do show a significant angular shift in the range $\theta = 50 - 120°$.

12957. Kartaschoff, P., Barnes, J. A., **Standard time and frequency generation,** *Proc. IEEE* **60,** No. 5, 493-501 (May 1972).

Key words: Accuracy; basic standards; frequency; frequency metrology; stability; standards; time scales.

The basic properties of atomic primary frequency standards are reviewed. A continuously running frequency source combined with counting, storage, and display devices results in a clock. Time scales are obtained by setting clocks with respect to a convenient origin. The accuracy of a primary frequency standard is a combined theoretical and experimental assessment of the uncertainties of all known possible sources of bias from the idealized definition. Recommended standard measures for the stability are the spectral density of fractional frequency fluctuations (frequency domain) and the two-sample no-dead time Allan variance (time domain). The operation of atomic frequency standards is based on various methods of particle interrogation to observe the transitions, particle confinement to obtain sufficient interaction time, and particle preparation to obtain the desired energy level populations. Passive resonator and active oscillator (maser) modes of operation are discussed; the former has some fundamental advantages.

A review of the state of the art and current practice shows that cesium beam resonator standards have the best documented accuracy capability (5×10^{-13}) and, in their commercial versions, are presently the best available clocks.

There are three concepts related to time: time interval, date, and synchronization. In order to assign dates to events, time scales have to be established. The steadily growing need for a very precise and uniform time scale has resulted in a new internationally coordinated time scale, IAT.

Frequency metrology will have increasing impact on both length and voltage metrology in the near future.

12958. Wells, J. S., Evenson, K. M., Day, G. W., Halford, D., **Role of infrared frequency synthesis in metrology,** *Proc. IEEE* **60,** No. 5, 621-623 (May 1972).

Key words: Frequency metrology; frequency of lasers; infrared frequency synthesis; laser frequency stabilization; methane-stabilized He-Ne laser; speed of light.

Infrared frequency synthesis (IFS) techniques are briefly surveyed, and some important results are summarized. The recent measurement of the frequency of the methane-stabilized He-Ne laser is significant due to the accurate measurement of the methane wavelength and its fundamental role in metrology. The possibilities of an improved value for the speed of light and of additional applications for frequency measurements at various levels of accuracy are discussed.

12959. Allan, D. W., **Time transfer using near-synchronous reception of optical pulsar signals,** *Proc. IEEE* **60,** No. 5, 625-627 (May 1972).

Key words: Accurate time dissemination; optical pulsars; precision timing; simultaneous reception; synchronization; time transfer.

The concept of time transfer between two geographically separated locations by using nearly simultaneous reception times from a common transmission has been used very fruitfully, e.g., the TV line-10 time transfer system and Loran-C. Some germane aspects of the concept are discussed and use of a signal from the optical pulsar NP0532 as the common transmitter is considered.

Theoretical considerations suggest that time could be transferred using this mode to an accuracy of about 2 μs and with global coverage. Some data were made available from Lawrence Radiation Laboratory giving the dates of pulsar events received at their observatory and also at the Harvard Observatory. A precision of about 13 μs was inferred from the data analysis.

This optical pulsar time transfer system seems to be feasible and worthy of further consideration because of the high accuracy and precision (a few microseconds for both) potentially achievable. For this potential, the development costs appear to be favorably competitive.

12960. Halford, D., Hellwig, H., Wells, J. S., **Progress and feasibility for a unified standard for frequency, time, and length,** *Proc. IEEE* **60,** No. 5, 623-625 (May 1972).

12961. Penn, R. W., **Volume changes accompanying the extension of rubber,** *Trans. Soc. Rheol.* **14,** No. 4, 509-517 (1970).

12962. Artru, M-C., Kaufman, V., **Analysis of the spectrum of triply-ionized magnesium (Mg IV),** *J. Opt. Soc. Amer.* **62,** No. 8, 949-957 (Aug. 1972).

12963. Ivey, D. L., Keese, C. J., Neill, A. H., Jr., Brenner, C., **Interaction of vehicle and road surface,** *Highw. Res. Rec., Anti-Skid Program Management and Related Papers, 22 Reports,* No. 376, 40-53 (1971).

12964. Powell, C. J., **Internal x-ray photoemission in aluminum: Excitation of electrons from the valence bands,** *Solid State Commun.* **10,** No. 12, 1161-1164 (June 15, 1972).

12965. McDaniel, C. L., **Phase relations in the CaO-Pt system in air,** *J. Amer. Ceram. Soc. Discussions and Notes* **55,** No. 8, 426-427 (Aug. 1972).

12966. Franklin, A. D., **Statistical thermodynamics of point defects in crystals,** Chapter 1 in *Point Defects in Solids,* J. Crawford and L. Slifken, eds., **1,** 1-101 (Plenum Press, Inc., New York, N.Y., 1972).

12967. Sullivan, D. B., **Low temperature voltage divider and null detector,** *Rev. Sci. Instrum.* **43,** No. 3, 499-505 (Mar. 1972).

12968. Meijer, P. H. E., **Specific heat and susceptibility in chromium methylammonium alum above the critical temperature,** *Phys. Rev. B* **6,** No. 1, 214-222 (July 1, 1972).

12969. Krauss, M., Neumann, D., **Energy curves of CO_2^-,** *Chem. Phys. Lett.* **14,** No. 1, 26-28 (May 1, 1972).

12970. Linzer, M., Brown, R. L., **Line parameters of absorption and dispersion Lorentzian curves under conditions of combined modulation and saturation distortion,** *J. Magn. Resonance* **7,** 335-358 (1972).

12971. Brown, R. L., **Use of fiber optics in the study of chemiluminescent reactions,** *Rev. Sci. Instrum.* **43,** No. 5, 756-758 (May 1972).

12972. Mangum, B. W., Utton, D. B., **NMR of ^{14}N in cerous magnesium nitrate hydrate,** *Physica* **60,** No. 1, 63-72 (1972).

12973. Allan, D. W., Blair, B. E., Davis, D. D., Machlan, H. E., **Precision and accuracy of remote synchronization via network television broadcasts, Loran-C, and portable clocks,** *Metrologia* **8,** No. 2, 64-72 (Apr. 1972).

12974. Clark, A. F., Deason, V. A., Powell, R. L., **Characterization of high purity metals by the eddy current decay method,** *Cryogenics* **12,** No. 1, 35-39 (Feb. 1972).

12975. Sparks, L. L., Powell, R. L., **Methods for assessing homogeneity and interchangeability of thermocouple wires,** *Cryogenics* **12,** No. 1, 40-43 (Feb. 1972).

Key words: Cryogenics; dipping; evaluation; heterogeneity; liquid helium; liquid nitrogen; low temperature; Seebeck effect; temperature measurement; thermoelectric properties.

Chemical and physical imperfections and inhomogeneities in thermocouple wire cause spurious voltages whenever these imperfections are subjected to temperature gradients. Thermocouple wires from different spools (or even from widely separated lengths on the same spool) usually exhibit significant differences in their thermoelectric properties. For accurate thermometry it is important to know the range of spurious voltages to be expected from a specific material. Simple laboratory methods are described for determining the effects of short-range inhomogeneities or long-range variations. Examples of results from tests are discussed in order to point out both the usefulness and the limitations of the methods.

12976. Jackson, A. D., Maximon, L. C., **Integrals of products of Bessel functions,** *SIAM J. Math. Anal.* **3,** No. 3, 446-460 (Aug. 1972).

12977. McKinney, J. E., Penn, R. W., **Composite dilatometer for measuring density of liquids and solids,** *Rev. Sci. Instrum.* **43,** No. 8, 1211-1213 (Aug. 1972).

Key words: Compressibility; density; dilatometer; pressure; specific volume; temperature; thermal expansion.

A composite dilatometer for measuring densities of liquids and solids over wide ranges of temperature and pressure is described. The dilatometer has a glass capillary and a mechanically removable seal at the base to facilitate loading. The seal is leakproof, and constant volume is maintained with successive loadings.

12978. Kelly, G. E., Sengers, J. V., **Kinetic theory of droplet growth in nucleation,** *J. Chem. Phys.* **57,** No. 4, 1441-1458 (Aug. 15, 1972).

Key words: Droplet growth; inverse Knudsen number expansion; kinetic theory; nearly-free molecular regime; nucleation.

A kinetic theory is presented for the mass flux to a liquid droplet surrounded by its pure vapor. When the mass flux Γ is expanded in terms of a parameter α which is the ratio of the droplet size to the mean free path (inverse Knudsen number), one obtains a series of the form $\Gamma = \Gamma^{(0)} + \Gamma^{(1)}\alpha + \Gamma^{(2)}\alpha^2 \ln\alpha + \ldots$ The coefficients of the first three terms of this expansion are derived by solving the Boltzmann equation using a modified Knudsen number iteration procedure. It is shown that the coefficients are determined by integrals associated with sequences of successive collisions among a number of vapor molecules and the droplet. These collision integrals bear a close similarity to the collision integrals derived earlier from the *generalized* Boltzmann equation for the density dependence of the transport properties of gases.

12979. Waxman, M., Hastings, J. R., **Proposed experiment to determine the effect of pressure on the emf of thermocouples,** *J. Appl. Phys.* **43,** No. 6, 2629-2632 (June 1972).

Key words: emf, thermocouple, effect of pressure on; hot-junction temperature, nonlinear evaluation of; hot-junction temperature, pressurized furnace; indirect temperature measurements; nonlinear data analysis, pressurized emf of thermocouples; pressure, effect on emf of thermocouples; simulated experiment,

pressurized emf of thermocouples; temperature, measurement at high pressure; thermocouples, effect of pressure on emf of.

A new experimental procedure to determine the effect of pressure on the emf-vs-temperature behavior of thermocouples has been conceived and tested with simulated data on a computer. An important advantage of this procedure is that the temperature of the hot junction can be accurately evaluated without the necessity of measuring it directly. Instead, the emf of the pressurized thermocouple is expressed parametrically as an appropriate function of several variables: (i) a measurable property related to the hot-junction temperature, such as the electric power to the pressurized furnace; (ii) the cold-junction temperature; and (iii) a reference temperature, such as 100 °C, at which the pressure effect is known. By variation of the experimental conditions, a set of overdetermined equations is obtained from which the parameters can be evaluated, and thus the emf-vs-temperature relationship of the pressurized thermocouple can be determined. Our experience with simulated data indicates that for the temperature range from 100 to 1200 °C and for pressures to about 7 GN/m^2 (70 kbar), the procedure should not introduce a temperature error greater than the error associated with the measurements of the emf, power, and cold-junction temperature.

12980. MacDonald, R. A., **Cauchy relations for second- and third-order elastic constants,** *Phys. Rev. B* **5,** No. 10, 4139-4143 (May 15, 1972).

Key words: Cauchy relations; central force interaction; cubic crystals; second- and third-order elastic constants; stress-free equilibrium; third-neighbor model.

The results of an earlier paper on the relation between elastic constants and second- and third-order force constants in face-centered-cubic and body-centered-cubic lattices appeared to conflict with the Cauchy relations $C_{12}=C_{44}$, $C_{112}=C_{166}$, $C_{123}=C_{456}=C_{144}$ obtained by Cousins. We show here that no conflict exists when we ensure that the lattice is in stress-free equilibrium, a necessary condition for Cauchy relations to hold. However, for the case of nearest- and next-nearest-neighbor central-force interactions previously considered, we obtain only special cases of these Cauchy relations. We extend our earlier work to include further neighbors and find that the Cauchy relations are obtained when third neighbors contribute to the elastic constants.

12981. Cassidy, E. C., **Pulsed laser Kerr system polarimeter for electro-optical fringe pattern measurement of transient electrical parameters,** *Rev. Sci. Instrum.* **43,** No. 6, 886-893 (June 1972).

Key words: Electric fields; electrical measurements; electro-optics; high-speed photography; high-speed techniques; high-voltage techniques; Kerr effect; laser application; optical techniques; pulse techniques.

Novel electro-optical fringe pattern methods are developed for measurement of transient high voltages and electric fields. Several techniques employing the Kerr effect, a pulsed laser source, and high-speed photographic recording equipment are described. Typical fringe pattern results are compared with conventional resistive divider measurements.

12982. Hellwig, H., Bell, H. E., **Experimental results with atomic hydrogen storage beam systems,** *Proc. 26th Annual Symp. on Frequency Control, Atlantic City, N.J., June 6-8, 1972,* pp. 242-247 (Electronic Industries Association, Washington, D.C., June 6-8, 1972).

Key words: Atomic hydrogen beam; atomic hydrogen generation; dispersion; frequency stability; frequency standard; hydrogen atom detection; hydrogen flux calibration; hydrogen maser; relaxation measurements; spin exchange.

Two atomic hydrogen storage beam devices are described, one based on the detection of hydrogen atoms, the other on the detection of changes in the microwave signal due to the hydrogen resonance. Electron bombardment ionization is used for the detection of atomic hydrogen. Efficiencies of up to 10^{-3} are measured using a method which is based on the study of pulse decay at maser oscillation threshold. Quantitative measurements of the atomic hydrogen beam intensity as a function of source pressure and RF discharge power are given. The overall efficiency of the atomic hydrogen detection in the hydrogen storage beam device is estimated at 10^{-7}. Ways to increase the efficiency are indicated.

A frequency standard is described in which a quartz crystal oscillator is locked to the hydrogen hyperfine transition using the dispersion of this resonance. The hydrogen storage beam apparatus closely resembles a hydrogen maser with a low-Q cavity below oscillation threshold. Cavity pulling can be reduced to a point where environmental temperature fluctuations limit the stability mainly via the second-order Doppler effect. Locking to the dispersion feature of the resonance eliminates the need for frequency modulation in order to find line-center. The stability of the frequency standard was measured against crystal oscillators and cesium beam frequency standards; stabilities of 4×10^{-13} were recorded for sampling times of 30 seconds and of 3 hours.

12983. Mangum, B. W., Thornton, D. D., **Magnetic phase diagrams of $GdVO_4$ and $GdAsO_4$,** (Proc. 17th AIP Conf. on Magnetism and Magnetic Materials, Chicago, Ill., Nov. 16-19, 1971), Chapter in *Magnetism and Magnetic Materials,* C. D. Graham, Jr., and J. J. Rhyne, eds., No. 5, 311-315 (1972).

Key words: $GdAsO_4$; $GdVO_4$; Heisenberg antiferromagnets; low temperatures; magnetizations.

$GdAsO_4$ and $GdVO_4$ are Heisenberg antiferromagnets with relatively large anisotropy fields, about half of which is dipolar in origin. The ratios of the anisotropy to the exchange fields for the salts, based on the molecular field theory and using the published values of the interaction constants, indicate that both salts should have spin-flop phases. We have measured the magnetization and its derivative of $GdVO_4$ and $GdAsO_4$ as a function of applied magnetic field for various temperatures below T_N and derived their magnetic phase diagrams. $GdVO_4$ ($T_N=2.50$ K) is a textbook type example of a system having a spin-flop phase with $T_3=1.37$ K. The critical field for the transition from the antiferromagnetic to the spin-flop phase is 10.5 kG and that for the transition from the spin-flop to the ferromagnetic (or saturated paramagnetic) phase is 21.8 kG. $GdAsO_4$ ($T_N=1.26$ K) does not have a simple spin-flop phase but undergoes transitions to two intermediate phases before undergoing a transition to the ferromagnetic (or saturated paramagnetic) phase. The critical point for $GdAsO_4$ is $T_c=0.47$ K and the critical fields are: $B_{c1}=6.1$ kG, $B_{c2}=6.4$ kG, and $B_{c3}\simeq 9$ kG.

12984. Rubin, L. G., Powell, R. L., Anderson, A. C., **Conference Report—The Fifth Symposium on temperature,** *Cryogenics* **11,** No. 6, 489-493 (Dec. 1971).

Key words: Temperature scales; thermocouples; thermometry.

The review briefly describes the talks on thermocouples and temperature scales. The article mentions the authors, their affiliations, and brief synopses of the more significant talks.

12985. Weiss, A. W., **Calculations of the $2sns\ ^1S$ and $2p3p\ ^{3,1}P$ levels of Be I,** *Phys. Rev. A* **6,** No. 4, 1261-1266 (Oct. 1972).

Key words: Atomic spectra; lifetimes; oscillator strengths; wavelengths.

Large scale configuration-interaction calculations are carried out on the $2sns\ ^1S$ series of Be I in an attempt to account for the anomalous behavior of the measured f values for the 3455-Å line, which had been identified as the $2s2p\ ^1P-2p^2\ ^1S$ transition. The calculations indicate that the series is very nearly purely Rydberg in character and that $2p^2\ ^1S$ is not embedded in the series between $6s$ and $7s$, as

had been previously assigned. Additional variational calculations on the $2snp$ and $2p3p$ levels indicate that a reidentification of the 3455-Å line with the $2s3p\ ^1P-2p3p\ ^1P$ transition is consistent with both lifetime and wavelength measurements. These calculations also predict lines at 2148 and 4528 Å, which have recently been found in beam-foil spectra.

12986. Allan, D. W., Machlan, H. E., Marshall, J., **Time transfer using nearly simultaneous reception times of a common transmission,** *Proc. 26th Annual Symp. on Frequency Control, Atlantic City, N. J., June 6-8, 1972*, pp. 309-316 (Electronic Industries Association, Washington, D.C., June 6-8, 1972).

12987. Smith, J. C., Kermish, G. A., Fenstermaker, C. A., **Separation of filler particles from the matrix in a particulate-loaded composite subjected to tensile stress,** (Proc. ACS Symp. on Recent Advances in Adhesion, Washington, D.C., Sept. 13-15, 1971), *J. Adhes.* **4,** No. 2, 109-122 (1972).

Key words: Adhesion; composite materials; epoxy polymer; silane coupling agents; stress-strain properties.

Simultaneous measurements of tensile stress, longitudinal strain, and transverse strain were obtained on particulate-filled composites. The matrix was a flexible epoxy polymer. Small glass spheres were used as filler in various volume ratios up to 0.35. The spheres were pretreated as follows: clean, coated with a parting agent, coated with either of two silane coupling agents. The volume-expansion behaviors of these four systems of composites showed differences attributed to matrix-filler separation and subsequent vacuole formation. Stress-strain behaviors were especially sensitive to this dewetting process. These two types of data, obtained simultaneously and considered together, thus provide valuable information about interface adhesion.

12988. Schooley, J. F., Soulen, R. J., Jr., **Thermometric fixed points using superconductivity,** *Advan. Cryog. Eng.* **17,** 192-198 (1972).

Key words: Calibration techniques; cryogenic temperature scale; OSRM; pure elements; superconductivity; thermometric fixed points.

Superconductive transitions in lead, indium, aluminum, zinc, and cadmium samples have been found to be both narrow and reproducible, suggesting their use as calibrating fixed points on the cryogenic temperature scale. Devices based on these measurements have been constructed. These results and their use in cryogenic thermometry are discussed.

12989. Mangum, B. W., Utton, D. B., **Low-temperature transitions in tetramethylammonium manganese chloride,** *Phys. Rev. B* **6,** No. 7, 2790-2795 (Oct. 1, 1972).

Key words: Cooperative transition; magnetic susceptibility; NMR; TMC.

We have measured the proton nuclear magnetic resonance of tetramethylammonium manganese chloride, a linear chain antiferromagnet, in the temperature region 0.4-300 K. In addition, its ac magnetic susceptibility was measured in applied fields of 0 to 22 kG in the temperature range 0.3-4.2 K. When measured along the crystallographic c axis, the zero-field susceptibility had an anomaly at 0.84 K. When the external field was applied perpendicularly to the c axis below 0.8 K, a critical field of 11.5 kG was observed in dM/dB. The proton NMR did not indicate any *cooperative transition* to a magnetically ordered state of the Mn^{2+} spins. It did indicate, however, a gradual diminution of fluctuations in the crystallographic ab plane until a nonrandom order had been established between chains below approximately 0.8 K. We find that the tetramethylammonium groups cease all rotations below 39 K. In the region of 40 to 50 K, the tetramethylammonium groups not only undergo some hindered rotations, but their orientation is different from the published room-temperature x-ray diffraction results. Above 50 K only a single narrow NMR line is observed and, consequently, no additional information on the crystal structure could be obtained.

12990. Colwell, J. H., Mangum, B. W., **The heat capacity of $TmAsO_4$ near its Jahn-Teller transition; evidence of a low-lying excited state,** *Solid State Commun.* **11,** 83-87 (1972).

Key words: Heat capacity; Jahn-Teller effect; molecular field approximation; Schottky anomaly; thulium arsenate; $TmAsO_4$.

We have measured the heat capacity of $TmAsO_4$ between 2 and 12 K and have established that there is a singlet state at approximately 20 K (14 cm^{-1}) above the ground state doublet. The heat capacity is accounted for on the basis of models which, in addition to the contribution from the low-lying singlet state, use the molecular field model to approximate the heat capacity arising from the Jahn-Teller splitting of the ground state doublet.

12991. Branscomb, L. M., **A metric America—and the paper industry,** *Tappi* **55,** No. 8, 1227-1230 (Aug. 1972).

12992. Tate, E. L., **NBS and the field service libraries of the Department of Commerce and the Interior Department,** *Proc. U.S. Department of Interior, Sixth Annual Library Workshop, Vancouver, Wash., Sept. 27-Oct. 1, 1971*, pp. 65-68 (U.S. Department of Interior, Office of Library Services, Washington, D.C., 1972).

12993. Pfrang, E. O., Yokel, F. Y., **Evaluation of innovative structural systems with respect to creep buckling,** *Proc. RILEM Int. Symp. on Experimental Analysis of Instability Problems on Reduced and Full-Scale Models, Buenos Aires, Argentina, Sept. 13-18, 1971*, **3,** 229-255 (1971).

Key words: Buckling; columns; creep; creep buckling; full-scale testing; load capacity; performance criteria; performance evaluation; performance testing; structural analysis; structural testing.

A major effort is now underway in the United States to introduce industrialized housing systems. This effort was initiated by the Department of Housing and Urban Development and is known as Operation Breakthrough. As a part of this effort, performance criteria were developed which make it possible to evaluate the structural adequacy of innovative systems. The criteria, analysis, and testing with respect to creep buckling are discussed. A case history is presented of the evaluation of the structural adequacy with respect to creep buckling of an innovative reinforced concrete system. The system was evaluated by full-scale testing and by analysis. An analytical approach was developed to predict the adequacy of reinforced concrete structural systems with respect to creep buckling.

12994. Semmelroth, C. C., **Adjustment of the Munsell-value and W*-scales to uniform lightness steps for various background reflectances,** *Appl. Opt.* **10,** No. 1, 14-18 (Jan. 1971).

12995. Ritter, J. J., Coyle, T. D., Bellama, J. M., **Reactions of tetrachlorodiborane (4) with fluoroolefins,** *J. Organometal Chem.* **42,** 25-31 (1972).

Key words: Boron; boron subhalides; fluoroolefins; halides; haloolefin; organoboron compounds; tetrachlorodiborane (4); tetrafluorodiborane (4).

Tetrachlorodiborane (4) reacts with trifluoroethylene to give dichloro-2,2-difluorovinylborane and both isomers of dichloro-2-chloro-2-fluorovinylborane. These compounds can be converted to the corresponding difluoro (halovinyl) boranes by treatment with SbF_3. Reaction of B_2Cl_4 with vinyl fluoride gives 1,1,2-tris (dichloroboryl) ethane. A facile halogen exchange with B_2Cl_4 was observed for a number of fluoroolefins, including vinyl fluoride, 1,1-difluoroethylene, 2-fluoropropene, and 3,3,3-trifluoropropene. No reaction was observed with 2,3,3,3-tetrafluoropropene.

12996. Rebbert, R. E., Lias, S. G., Ausloos, P., **Vacuum ultraviolet photolysis of methane. Reaction of methylene,** *Chem. Phys. Lett.* **12,** No. 2, 323-326 (Dec. 15, 1971).

Key words: Deactivation; insertion reaction; lifetime; methane; methylene; photolysis; quantum yields.

Methylene radicals formed in the photolysis of methane (123.6 and 104.8–106.7 nm) insert into the C–H bond of methane to produce ethane molecules whose lifetime is independent of the energy of the photon. Deactivation of ethane by collision with methane is stepwise, and the lifetime of the insertion product is shorter than reported in previous CH_2CO photolysis studies.

12997. deWit, R., **The relation between continuous and discrete disclinations,** (Proc. Int. Symp. on Foundations of Plasticity, Warsaw, Poland, Aug. 30-Sept. 2, 1972), *Arch. Mech.* **24,** No. 3, 499-510 (Wolters-Noordhoff Publ. Co., 1972).

Key words: Continuous; continuum; defect; disclination; discrete; dislocation; distortion; Green's function; incompatibility; plasticity; strain; Volterra.

A recent paper of Mura introduces plastic and elastic distortions to describe a theory of disclinations. Our objection to this approach is that the "elastic distortion" is not a state quantity when disclinations are present. Mura's "plastic distortion" for a line singularity is examined in the light of our theory and found to represent a dislocation wall terminating inside the body on a dislocation loop. Mura's "plastic rotation" is found to represent a dislocation wall terminating on a disclination. The sum of these two gives the "disclination" loop. Explicit expressions are derived for the elastic strain and bend-twist in both the discrete and continuous cases, which show that, contrary to the "elastic distortion," they are indeed state quantities.

12998. Forman, R. A., Brower, W. S., Jr., Parker, H. S., **Phonons and the green exciton series in cuprous oxide, Cu_2O,** *Phys. Lett.* **36A,** No. 5, 395-396 (Sept. 27, 1971).

Key words: Copper oxide; cuprous oxide; excitons; forbidden bandgap; phonons.

Examination of the optical absorption edge spectra of samples of melt-grown cuprous oxide enables identification of features of the green exciton series overlying the yellow series. Identification of the green series $n=1$ line allows new interpretations of various features seen earlier by other workers.

12999. Sieck, L. W., Hellner, L., Gorden, R., Jr., **Kinetic mass spectrometric determination of the absolute rate coefficient for the reaction NH_3^+ ($v=0$) + $NH_3 \rightarrow NH_4^+ + NH_2$ at thermal kinetic energies,** *Chem. Phys. Lett.* **10,** No. 5, 502-503 (Sept. 1, 1971).

Key words: Ammonia; mass spectrometry; photoionization; rate constants; thermal energy; vibrational energy.

The absolute thermal rate coefficient for the reaction $NH_3^+ + NH_3 \rightarrow NH_4^+ + NH_2$ has been determined experimentally for the first time for NH_3^+ ($v=0$) reactant ions. An increase in E_{rib} results in a decrease in the rate coefficient for proton transfer.

13000. Ausloos, P., **Far ultraviolet photolysis of alkanes,** *Mol. Photochem.* **4,** No. 1, 39-55 (1972).

Key words: Energy partitioning; energy transfer; excited states; fluorescence; photoionization; photolysis; quantum yields.

The effect of wavelength on the primary photophysical and photochemical processes is reviewed. Quantum yields of the photoionization and of the photochemical decomposition of selected alkanes are presented. The modes of dissociation of neutral electronically excited alkanes are related to information derived from high resolution gas phase absorption spectra and from liquid phase fluorescence measurements. The effect of phase on the primary decomposition mechanism and on energy transfer processes is examined in the light of recent findings. New experimental information on the energy partitioning among fragments produced in the primary dissociation of CH_4 and C_3H_8 is presented.

13001. Mandel, J., **The statistical validation of tests,** *Mater. Res. Stand.* **12,** No. 9, 8-13,62 (Sept. 1972).

Key words: Experimental error; measurement; statistical control; statistical design; test methods.

Basic to the evaluation of test methods is an understanding of the behavior of measurements, and particularly of the disturbances caused by random and systematic experimental errors. The concept of statistical control is discussed in terms of measuring processes. Finally, the role of statistical models and designs is illustrated by an example dealing with certain physical characteristics of a blood expander.

13002: Sieck, L. W., Ausloos, P., **Ion-molecule reaction chains in isobutene,** *J. Chem. Phys.* **56,** No. 2, 1010-1011 (Jan. 15, 1972).

Key words: Ion-molecule reactions; isobutene; photoionization; polymerization; radiolysis.

The vapor phase ionic-chain reaction occurring in isobutene and propylene have been investigated both in the NBS high pressure photoionization mass spectrometer and in the closed systems photolysis. We have determined for the first time that the formation of stable dimer ions $(C_4H_8)_2^+$ in isobutene competes effectively with formation of $C_4H_9^+$. Dimeric ions are also observed in propylene. These dimeric ions are found to transfer H_2 to isobutene and propylene to yield isobutane and propane, respectively. The failure of other investigators to observe these sequences is discussed.

13003. Sieck, L. W., Searles, S. K., **High-pressure photoionization mass spectrometry. II. A study of thermal H^- (H^0) and H_2^- (H_2^0) transfer reactions occurring in alkane-olefin mixtures,** *J. Amer. Chem. Soc.* **92,** 10, 2937-2943 (May 20, 1970).

Key words: Alkanes; ion-molecule reactions; mass spectrometry; photoionization; rate coefficient; vapor phase.

Following photoionization of the C_nH_{2n} (olefin) or RH_2 (alkane or cycloalkane) component in RH_2-C_nH_{2n} mixtures with either 1236-Å (10.0 eV) or 1165-Å (10.6 eV) radiation, the following two classes of reactions have been investigated: (I) $C_nH_{2n}^+ + RH_2 \rightarrow C_nH_{2n+1} + RH^+$ (H^- transfer) or $C_nH_{2n+2} + R^+$ (H_2^- transfer); (II) $RH_2^+ + C_nH_{2n} \rightarrow C_nH_{2n+1} + RH^+$ (H transfer) or $C_nH_{2n+2} + R^+$ (H_2 transfer). Although these processes have been subjected to considerable scrutiny, the relative rate constants $k(H^-)/k(H_2^-)$ or $k(H^0)/k(H_2^0)$ found previously by kinetic mass spectrometry for any given reaction pair have always been considerably higher than those derived from photoionization and radiolysis experiments conducted in static systems. However, the values derived in our instrument, which reflect the interactions of ions at thermal energy, are in excellent agreement with the relative transfer efficiencies and other rate parameters derived from static experiments and suggest that kinetic and/or internal energy effects may have been important in previous experiments carried out in mass spectrometers. Rate constants and relative transfer efficiencies found for a number of reaction pairs are reported, and the nature of the collision complex is discussed.

13004. McBee, C. L., Kruger, J., **Nature of passive films on iron-chromium alloys,** *Electrochim. Acta* **17,** 1337-1341 (Oct. 1972).

Key words: Amorphous; diffraction; Fe-Cr; lattice parameter; 1 N H_2SO_4; oxide; passive; spinel.

Fe-Cr foils of a range of Cr content were anodically polarized in 1 N H_2SO_4 for passive film growth. The resulting oxide films were then studied while still in contact with the metal substrate with transmission electron diffraction at 100 kV.

Comparisons were made between the diffraction results for the Fe-Cr foils and previous diffraction studies for Fe foils. The diffraction patterns obtained revealed that as Cr content increased the oxide films were generally less able to sustain an epitaxial relationship with the substrates. The lower Cr foils had oxide patterns that could be fitted to a spinel structure; the lattice parameter in these cases increased with increasing Cr content. The highest Cr-content alloy, Fe-24% Cr, did not show any oxide pattern. It is concluded that the films tend to become amorphous as the Cr content of the alloy is increased.

13005. Sindt, C. F., Ludtke, P. R., **Characteristics of slush and boiling methane and methane mixtures,** *Proc. XIIIth Int. Congress of the International Institute of Refrigeration, Washington, D.C., Aug. 27-Sept. 3, 1971*, pp. 1-6 (Int. Inst. of Refrigeration, Paris, France, 1971).

Key words: Binary mixtures; cryogenic mixtures; liquefied natural gas; methane; slush methane; slush natural gas.

Liquefied natural gas (LNG) and methane are in contention as fuels for high performance aircraft, rocket engines, and motor vehicles. They have the advantages, over kerosene and gasoline, of higher specific heat of combustion and cleaner combustion, and they are six times more dense than liquid hydrogen. Some of the applications for either methane or LNG would benefit from the increased heat capacity and the increased density of mixtures of liquid and solid such as slush. Because of these potential advantages, the characteristics of slush and boiling methane and binary mixtures of methane and other natural gas constituents were investigated. Subcooled liquid or slush would also serve to reduce or eliminate fuel losses that would accompany reduction in fuel tank pressure as the aircraft gains altitude.

The scope of the program was the characterization of slush prepared from pure methane and binary mixtures of methane with nitrogen, ethane, and propane, and the investigations of the boiling characteristics of these mixtures.

13006. Grabner, L., Forman, R. A., Wong, E. Y., **Spectroscopy of Cr^{3+} in $CsCr(SO_4)_2 \cdot 12H_2O/D_2O$, a β-alum,** *Phys. Rev. B* **6,** No. 3, 797-801 (Aug. 1, 1972).

Key words: α-, β-, γ-alums; crystal field splitting; disorder; energy transfer; inequivalent sites.

The trigonal-field splitting of $^2\bar{E}$ into $\bar{E}$ and $2\bar{A}$ states is found to be $\bar{E}-2\bar{A}=-120$ cm^{-1} by identifying $2\bar{A}$. The no-phonon lines of deuterated samples are isotope shifted 6 cm^{-1} to the red. The following generalizations suffice to relate the spectra of the Cr-alums: (i) They are due to $^4A_2 \rightarrow \bar{E}, 2\bar{A}(^2E)$ transitions. The splitting of ^2E is large for the β-alums, small for the α-alums. (ii) Sulfate-group disorder, found in all α-alums, complicates their spectra by adding inequivalent Cr^{3+} sites.

13007. Frederikse, H. P. R., Hosler, W. R., **Excitons in solid and liquid thallous chloride,** *Solid State Commun.* **9,** No. 10, 709-712 (1971).

Key words: Excitons; liquid state; thallous chloride.

The absorption edge of thallous chloride has been measured below and above melting point. In the crystal this edge represents the low energy tail of a strongly absorbing Wannier exciton. The similarity between the shape and temperature dependence of this absorption in the solid and in the liquid states suggests that Wannier-like excitons exist also in liquid thallous chloride.

13008. Grabner, L., **Exciton emission and donor-acceptor association in thallium bromide,** *Phys. Rev. B* **4,** No. 4, 1335-1339 (Aug. 15, 1971).

Key words: Donor-acceptor pairs; excitons; thallium bromide.

Free- and bound-exciton emission with longitudinal optical (LO) phonon cooperation is reported in undoped TlBr. The binding energies of the bound excitons with respect to the free exciton are 4 and 7 MeV, respectively. A photocurrent peak at the energy of the free exciton at 4 K is interpreted as due to an Auger process at the bound-exciton complexes. Extrinsic photocurrent is reported. The temperature dependence of its excitation spectrum is anomalous from the point of view of the conventional Riehl-Schön recombination model and is shown to be consistent with a model involving donor-acceptor pairs.

13009. Forman, R. A., **Order-disorder transition in lithium imide, Li_2NH,** *J. Chem. Phys. Letters to Editor* **55,** No. 4, 1987-1988 (Aug. 15, 1971).

Key words: Dipole ordering; DTA; NMR; order-disorder; phase transition; thermal analysis.

On the basis of differential thermal analysis results and previous NMR studies, we believe we have discovered an order-disorder transition, possibly of the λ-type, of NH^{2-} dipoles in the cubic antifluorite compound lithium imide, Li_2NH.

13010. Franzen, D. L., **CW gas breakdown in argon using 10.6-μm laser radiation,** *Appl. Phys. Lett.* **21,** No. 2, 62-64 (July 15, 1972).

Key words: Gas breakdown; plasma.

A very intense gas breakdown spark has been extended to a continuous arc in argon using a focused cw CO_2 laser. To achieve cw breakdown, the focal volume of a mirror focusing a high-power CO_2 laser was preionized by a single pulse from a CO_2 TEA laser. The electron density created by the pulsed laser is sufficient to start the cw plasma. This letter reports accurate measurements of pulsed thresholds as well as preionized cw thresholds for breakdown in argon. Also, a study of the time development of the cw plasma is presented.

13011. Hedges, R. E. M., Drummond, D. L., Gallagher, A., **Extreme-wing line broadening and Cs-inert-gas potentials,** *Phys. Rev. A* **6,** No. 4, 1519-1544 (Oct. 1972).

Key words: Cesium; inert gas; line broadening; molecules.

The emission profiles of the cesium resonance lines broadened by collisions with inert gases have been measured from about 50-1000 cm^{-1} from line center. The emission is observed from optically excited Cs in a cell whose temperature is varied from about 300-800 K. By measuring the wing intensity relative to the entire line intensity from optically thin Cs, the profiles can be related to theoretical models without knowledge of the cesium density. The quasistatic theory of line broadening, extended to include the distribution of perturber positions about the Cs, is used to analyze the data. The observed temperature dependence of the emission profiles is associated with the temperature dependence of the perturber distribution in the Cs-inert-gas adiabatic potential. The quasistatic spectrum depends on the difference between excited- and ground-state adiabatic potentials, so each potential is thereby separately determined from the data. The $X\Sigma$, $A\Pi$, and $B\Sigma$ potentials for the 3.5–5-Å region are given.

13012. Kitching, P., Moss, G. A., Olsen, W. C., Roberts, W. J., Alder, J. C., Dollhopf, W., Kossler, W. J., Perdrisat, C. F., Lehman, D. R., Priest, J. R., **Reactions (p,pd) and $(p,2p)$ on helium-3 at 590 MeV,** *Phys. Rev. C* **6,** No. 3, 769-772 (Sept. 1972).

Key words: Confidence cross sections; ^{3}He(pd) vertex; plane wave impulse approximations; quasi-free scattering; separable potentials; three-body problem.

The reaction ^{3}He(p,pd) has been studied for recoil momenta of the spectator proton up to 230 MeV/c. The cross section of ^{3}He$(p,2p)$ was measured up to 100 MeV/c. The results are interpreted in terms of the plane-wave impulse approximation and the form factors for ^{3}He $\rightarrow dp$ and ^{3}He$\rightarrow p(pn)$ are compared with a calculation of the ^{3}He wave function in which the two-nucleon interaction is described by a separable potential which reproduces the low-energy properties of the two-nucleon system.

13013. Markus, W., **A constant volume valve,** *Rev. Sci. Instrum. Notes* **43,** No. 1, 158-159 (Jan. 1972).

13014. Cohen, M. I., Young, K. F., Chang, T-T., Brower, W. S., Jr., **Phase transitions in $CsPbCl_3$,** *J. Appl. Phys.* **42,** No. 13, 5267-5272 (Dec. 1971).

Key words: $CsPbCl_3$; EPR of Gd^{3+}; phase transitions.

Measurements of dielectric properties, pyroelectricity, and the electron paramagnetic resonance spectrum of Gd^{3+} as a function of temperature have been used to examine the phase transitions in $CsPbCl_3$. The results indicate the presence of five phase transitions and the loss of a center of symmetry at 194 K. The results together with the apparent order of the transitions, and published data, enable the Landau criterion to be used so that the point group of each phase may be identified. A reasonable choice of space group is also made.

13015. Forman, R. A., Brower, W. S., Jr., **Optical spectra of thallium-doped ammonium chloride,** *J. Lumin.* **4,** No. 2, 98-104 (Sept. 1971).

Key words: Ammonium chloride; luminescence, optical absorption; optical spectra; thallium ion.

The low temperature optical spectra associated with the thallium ion in doped samples of ammonium chloride have been investigated. Absorption, photoluminescence and luminescence excitation spectra are presented for this CsCl-structure (cubic) phosphor.

13016. Feldman, A., Horowitz, D., Waxler, R. M., **Relative importance of electrostriction and the Kerr effect to self-focusing in optical glasses,** *Appl. Phys. Lett.* **21,** No. 6, 260-262 (Sept. 15, 1972).

Key words: Damage threshold; electrostriction; Kerr-effect; laser damage in glasses; optical glasses; self-focusing.

The damage threshold for three optical glasses was found to be higher for circularly polarized radiation than for linear polarization, using 26-nsec pulses from a Nd:glass laser. The damage was assumed to result from self-focusing. The fractional contribution of electrostriction to the total nonlinear index n_2 is estimated to be 0.8 ± 0.2 for borosilicate crown glass, 1.15 ± 0.35 for fused silica, and 0.4 ± 0.1 for dense flint glass, assuming the Kerr effect to be the only other self-focusing mechanism. The data are consistent with present concepts of glass structure. The high damage threshold in fused silica is attributed to its relatively small Kerr effect.

13017. Forman, R. A., Hosler, W. R., Blunt, R. F., **The bandgap of cadmium fluoride,** *Solid State Commun.* **10,** No. 1, 19-24 (1972).

Key words: Bandgap; band structure; cadmium fluoride excitons; optical absorption; reflectivity; semiconductor.

Measurements of optical absorption and reflection at and below room temperature have been used to indicate that cadmium fluoride is a direct allowed bandgap material. In absorption an Urbach-type edge is observed, with the extrapolations from various temperatures intersecting to indicate an excitonic bandedge of ~ 7.6 eV in agreement with the reflectivity data. The absorption data are in accord with the thermal behavior expected for an allowed excitonic transition.

13018. Mandel, J., **Principal components, analysis of variance and data structure,** *Statist. Neerlandica,* pp. 119-129 (Aug. 1972).

Key words: Analysis of variance; data structure; principal components; two-factor data.

The relation between principal components and analysis of variance is examined. It is shown that the model underlying the extended analysis of variance developed by GOLLOB and MANDEL is useful also as a model for principal component analysis. The elucidation of structure of two-factor data using the new analysis of variance model is illustrated by an example taken from thermodynamics.

13019. Kraft, R., **Analyticity and reflectivity for first order systems of elliptic type in two independent variables,** *J. Math. Anal. Appl.* **29,** No. 1, 1-17 (Jan. 1970).

13020. Rockett, J. A., **Fire research and safety center and the fire marshal,** *Fire J.* **64,** No. 6, 50-53 (Nov. 1970).

13021. Dillon, T. A., Stephenson, J. C., **Multiquantum vibrational-energy exchange,** *Phys. Rev. A* **6,** No. 4, 1460-1468 (Oct. 1972).

Key words: Born; CO; collisions; exchange; multiquantum.

A theory for exchange of vibrational quanta between molecules is formulated which does not rely on the Born expansion of the S matrix. A transformation is derived which diagonalizes the vibrational operators responsible for exchange. The scattering operator is then expanded in a series of rotational tensor operators which permits evaluation of S-matrix elements to all orders. This formulation shows that multiquantum processes, both rotational and vibrational, play an important role when transition moments are large. Numerical calculations for vibrational exchange rates of carbon monoxide are compared with results of the first Born approximation from which they differ significantly. The dependence of the cross section on vibrational-energy defect is much less drastic than that of the Born approximation. The present calculations indicate that cross sections for the exchange of more than one vibrational quantum are substantial, in marked contrast to the Born approximation where they are forbidden. The size of these multiquantum cross sections indicates that they can play an important role in the detailed kinetic modeling of CO lasers.

13022. Harman, G. G., Leedy, K. O., **An experimental model of the microelectronic ultrasonic wire bonding mechanism,** *Proc. 10th Annual IEEE Reliability Physics Symposium, Las Vegas, Nevada, Apr. 5-7, 1972,* pp. 49-56 (1972).

13023. Bennett, H. S., Stoneham, A. M., **Effects of random fields on radiative decay of color centers,** *Phys. Rev. B* **6,** No. 8, 3086-3090 (Oct. 15, 1972).

13024. Baker, L. C. W., Baker, V. S., Wasfi, S. H., Candela, G. A., Kahn, A. H., **Isomorphous heteropoly complexes containing various pairs of paramagnetic atoms. Exchange-coupled differing spins with absence of long-range magnetic interactions. A new class of paramagnetic behavior. Theoretical treatment. Novel geometrical isomerism,** *J. Amer. Chem. Soc.* **94,** No. 1 , 5499-5501 (July 26, 1972).

Key words: CO; exchange coupling; Fe; heteropoly complexes; Keggin structures; magnetic spins; magnetic susceptibility; paired spins; tungsto-heteropoly complexes.

Coupled pairs of differing magnetic ions in tungsto-heteropoly complexes have been studied by magnetic susceptibility over the temperature range 2 to 300 K. The two substitutional sites are surrounded by oxygen ions in octahedral and tetrahedral coordinations with one oxygen ion in common. The ions studied were Co^{2+}, Co^{3+}, and Fe^{3+}, in a total of five combinations on the two sites, offering a unique set of symmetries and ions for examining super-exchange effects. The susceptibility has been analyzed according to the spin Hamiltonian

$$\mathcal{H} = \beta(g_1\mathbf{S}_1 + g_2\mathbf{S}_2) \cdot \mathbf{H} - J\mathbf{S}_1 \cdot \mathbf{S}_2;$$

fitted values of J range from -6 to -70 K depending on the combinations of ions. The experimental agreement with the spin Hamiltonian for all cases studied is satisfactory for this unique system.

13025. Linsky, J. L., Mount, G. H., **On the validity of a generalized Kirchhoff's Law for a nonisothermal scattering and absorptive medium,** *Icarus* **17,** 193-197 (1972).

Key words: Emissivity; Kirchhoff's Law; lunar surfaces; planetary atmospheres; reflectivity.

The relationship of directional hemispherical reflectivity to emissivity is investigated for a nonisothermal medium with isotropic coherent scattering and absorption. Departures from a generalized Kirchhoff's Law occur due to the long range nature of the scattering process. Such departures occur in lunar thermal emission at microwave but not at infrared frequencies.

13026. Trombka, J. I., Eller, E., Oswald, G. A., Berger, M. J., Seltzer, S. M., **^{252}Cf neutron induced radiative capture gamma rays for high energy detector calibration,** (Proc. Amer. Nucl. Soc. Nation,al Topical Meeting on Neutron Sources and Applications, Augusta, Ga., April 19-21, 1971), Chapter in *Neutron Sources and Applications,* **CONF-710402,** III, III- 3—III- 7 (National Technical Information Service, Springfield, Va. 22151, 1971).

Key words: California; gamma rays; neutrons; radiative capture; response functions; sodium iodide detector.

High energy gamma ray sources produced by prompt neutron radiative capture were developed in order to study the variation of pulse height, the shape of pulse height distribution, and resolution as a function of energy for scintillation detectors. The system as described below has also been used to calibrate the gamma ray spectrometers which will be flown aboard Apollo 15 and 16.

Spectral distribution of gamma rays in the 3 to 12 MeV energy region using a 3 in. × 3 in. NaI(Tl) detector have been studied for a number of nuclear species such as: Nickel with lines at 8.999 and 8.533 MeV; Mercury—5.967, 4.842, 4.740, and 3.289 MeV; and Hydrogen—2.223 MeV. The neutron excitation of these samples was carried out by placing these samples in a neutron moderator near a ^{252}Cf source (~ 2 μg).

Methods for inferring photon spectra from the pulse height spectra have been developed and are to be used to interpret the gamma ray measurements carried out during the Apollo 15 and 16 flights. Detailed knowledge of the response of the flight detectors as a function of energy is required to perform the analysis. In the energy region above 3 MeV, it is extremely difficult to obtain response functions for truly monoenergetic gamma rays. Therefore the following approach has been taken: Monte Carlo calculations have been carried out to determine the nature of these response functions in the 3 to 12 MeV region. These spectra have been compared with the experimentally determined spectra obtained using the ^{252}Cf system described above. These comparisons form a basis for predicting the shape of the pulse height spectrum for gamma rays of any energy in this range.

13027. Cowan, D. O., Candela, G. A., Kaufman, F., **The organic solid state. V. Symmetry distortions in ferrocenium compounds,** *J. Amer. Chem. Soc.* **93,** No. 16, 3889-3893 (Aug. 11, 1971).

Key words: Biferrocene; electron resonance; susceptibility; symmetry changes.

The magnetic susceptibilities of biferrocene [Fe(II)Fe(III)] picrate (**1**) and biferrocene [Fe(III)Fe(III)] difluoroborate (**2**) were determined from 2 to 300 K. The experimental curves for the effective magnetic moment (μ_{eff}) are compared with theoretical curves based on a model involving molecular distortion from axial symmetry. For compound **1**, in the temperature range 77-300 K, the best-fit temperature-independent distortion factor (δ = 1000 cm^{-1}/ferrocenium unit) is large when compared to previously observed distortions. The deviation from the theoretical μ_{eff} curve for this compound is small. For compound **2** in the temperature range 77-300 K the best-fit temperature-independent distortion factor is 750 cm^{-1}/ferrocenium unit; while in the temperature range 2-4 K the distortion factor is considerably smaller (δ = 1 0 cm^{-1}/ferrocenium unit). The electron spin resonance spectra of compounds **1** and **2** were measured at 77 and 298 K. The observed g values were used to calculate the effective magnetic moments and the distortion factors for compounds **1** and **2**. These values are in good agreement with those obtained from the magnetic susceptibility measurements. The observed low-temperature collapse of the g_x, g_y signal and the appearance of a new g_z signal (compound **2**) are consistent with a large reduction in the distortion parameter at low temperature.

13028. Waclawski, B. J., Plummer, E. W., **Photoemission observation of a surface state of tungsten,** *Phys. Rev. Lett.* **29,** No. 12, 783-786 (Sept. 1972).

Key words: Adsorption; energy distribution; photoemission; surface states.

Photoelectron energy distributions from clean, polycrystalline tungsten reveal a surface-sensitive peak about 0.4 eV below the Fermi energy. This peak, which is identified as a surface state, rapidly decays during gas adsorption, and concomitant growth of a new peak at ~ 2.5 eV below the Fermi energy is observed. Over the energy range of the surface-state peak, the strength of surface-state emission relative to bulk emission decreases with increasing photon energy. These results quantitatively substantiate existing field-emission data and qualitatively agree with model photoemission calculations.

13029. Steiner, B., **Photodetachment: Cross sections and electron affinities,** Chapter 7 in *Case Studies in Atomic Collision Physics,* E. W. McDaniel and M. R. C. McDowell, Eds., **2,** 485-545 (North-Holland Publ. Co., Amsterdam, The Netherlands, 1972).

Key words: Atomic; crossed beam; cross section; electron affinitive; molecular; photodetachment.

The status of negative ion photodetachment cross section determination is reviewed, both theory and experiment. A selected table of best values is derived. Threshold behavior is examined separately. Crossed beam experimental techniques are described in detail. Finally, the status of atomic and molecular electron affinity determinations is reviewed and an extensive table of preferred values is compiled.

13030. Nargolwalla, S. S., **Application of neutron generators to activation analysis,** (Proc. Second Oak Ridge Conf. on the Use of Small Accelerators for Teaching and Research, Oak Ridge, Tenn., Mar. 23-25, 1970), *USAEC Rept. Conf.* **700322,** 185-204 (Oct. 1970).

Key words: Accuracy; activation analysis; element; generator; micro; precision; reactor; selectivity; semimicro; sensitivity.

Neutron activation analysis has gained wide acceptance in recent years as a very sensitive and specific method for the qualitative and quantitative determination of most of the elements in the periodic table. Until very recently, however, activation analysis was limited to the use of thermal neutrons generated in a nuclear reactor. Today, the development of low-cost neutron generators has considerably added to the scope of the technique, and made it available to most well-equipped analytical laboratories. This review summarizes some of the key developments in neutron generator technology which have had a significant bearing in the acceptance of neutron generators for the precise and accurate determination of a large number of elements at the semimicro and macro levels of concentration.

Recent advances in the design and utilization of experimental hardware such as sample-placement devices, experimental designs and special long-lived neutron producing targets are discussed. Descriptions of some investigations pertaining to the evaluation of systematic errors in activation analysis with neutron generators are presented, and various aspects of analytical significance related to the use of this type of radiation source are emphasized. In this regard, advantages offered by the neutron generator for the analysis of light elements are given. Research in the area of cross section measurements and their implications in light of the practical sample due to degradation of the nominal 14.7 MeV neutrons is described. Typical

sensitivities obtainable with present-day neutron outputs from neutron generators are critically examined and anomalies between expected theoretical sensitivities and experimental sample response in high energy neutrons are discussed.

Pertinent applications of neutron generator activation analysis techniques in the areas of metallurgy, biochemistry, mineralogy and standard materials are described. Special attention is drawn to the introduction of this technique to the solution of industrial quality control problems. A brief treatment of the on-line analytical capabilities of neutron generators, particularly of the sealed-tube type is given. In this connection, efforts made toward the computerization of analytical procedures and data reduction are emphasized. In conclusion, the contribution of this analytical technique in terms of sensitivity, specificity, accuracy and precision, and possible future developments of the fast neutron facility are discussed.

13031. Baker, L. C. W., Baker, V. E. S., Wasfi, S. H., Candela, G. A., Kahn, A. H., **Exchange interactions between pairs of differing magnetic spins in heteropoly complexes,** *J. Chem. Phys.* **56,** No. 10, 4917-4923 (May 15, 1972).

Key words: Co; Fe; heteropoly complexes; Keggin structures; magnetic spins; magnetic susceptibility; paired spins; tungsto-heteropoly complexes.

Coupled pairs of differing magnetic spins in tungsto-heteropoly complexes have been investigated by studying the magnetic susceptibility over the temperature range 2-300 K. The two sites of the magnetic ions are surrounded by oxygen ions in octahedral and tetrahedral coordinations with one oxygen ion in common. The ions studied were Co^{2+}, Co^{3+}, and Fe^{3+} in a total of six combinations on the two sites, offering a unique set of symmetries and ions for examining super-exchange effects. A closed form for the susceptibility has been obtained on assuming the spin Hamiltonian

$$\mathcal{H} = \beta(g_1\mathbf{S}_1 + g_2\mathbf{S}_2)\,\mathbf{H} - J\mathbf{S}_1 \cdot \mathbf{S}_2,$$

allowing for the possibility of $g_1 \neq g_2$, $S_1 \neq S_2$. Fitted values of J/k range from -6 to -70 K depending on the combination of ions. The experimental agreement with the spin Hamiltonian for all cases studied is satisfactory for this system.

13032. McAlister, A. J., Cuthill, J. R., Dobbyn, R. C., Williams, M. L., Watson, R. E., **Soft-x-ray studies of ferromagnetic and paramagnetic iron,** *Phys. Rev. Lett.* **29,** No. 3, 179-182 (July 17, 1972).

Key words: Band ferromagnetism; Fe; magnetic transition; M spectrum; soft-x-ray.

The soft-x-ray $M_{2,3}$ emission spectrum of Fe has been measured below (560 °C, $T/T_c = 0.8$) and above (840 °C, $T/T_c = 1.07$) the Curie point, and has revealed motion of distinct structural features within the d bands on passing through T_c. The results, taken with earlier photoemission data on Fe and Ni, are in excellent numerical agreement with, while in no sense providing verification of, the band ferromagnetism description of Stoner, Wohlfarth, and Slater for these metals.

13033. Reno, R. C., Swartzendruber, L. J., **Time-differential perturbed angular correlations on ^{57}Fe in Cu-Ni alloys: Mössbauer doublets explained,** *Phys. Rev. Lett.* **29,** No. 11, 712-715 (Sept. 11, 1972).

Key words: Cu-Ni-Fe alloys; hyperfine fields; Mössbauer effect; perturbed angular correlation.

It is shown that when hyperfine interactions at ^{57}Fe nuclei are studied by both Mössbauer effect and time-differential perturbed angular correlations, information is obtained which is unavailable from either technique alone. In particular, previous ambiguities in the interpretation of ^{57}Fe Mössbauer spectra of Cu-Ni alloys are removed: The Mössbauer doublet is shown to be primarily due to a distribution of electric field gradients acting on the ^{57}Fe nuclei.

13034. Nahman, N. S., Holt, D. R., **Transient analysis of coaxial cables using the skin effect approximation $A + B\sqrt{s}$** *IEEE Trans. Circuit Theory CT-19,* No. 5, 443-451 (Sept. 1972).

Key words: Analysis; cables; coaxial; skin effect; time-domain; transient; transmission.

The purpose of this paper is to demonstrate the utility of the function $A + B\sqrt{s}$ for approximating the coaxial line series impedance (skin effect) in applications to transient analysis. The time domain response expansions of Holt are modified in terms of two adjustable parameters which replace the physical parameters R and K. The modified expansions are truncated to yield condensed expressions useful for analysis and design. Two types of terminations are considered: 1) nonreflective, terminated in the characteristic impedance $Z_0(s)$, and 2) doubly reflective, sending and receiving ends each terminated in the nominal characteristic impedance $R_0 = \lim_{s\to\infty} Z_0(s) = \sqrt{L/C}$. Experimental data are presented on the frequency and time domain insertion responses of three commercial cables: RG 5B/U – 68.6 m (225 ft), RG 21/U – 96.8 m (317 ft), and RG 58A/U – 137 m (450 ft). Theoretical and experimental time domain responses for the sending- and receiving-end voltages are compared over the time interval from the order of 10 ns to that of 10 μs. It is demonstrated that the parameters A and B can be adjusted to provide functions of time which closely approximate the actual time domain response over different intervals.

**Publications with prices and SD Catalog numbers indicated may be purchased directly from the Superintendent of Documents, U.S. Government Printing Office, Washington, D.C. 20402 (foreign: one-fourth additional). NBS nonperiodical series are also available from the National Technical Information Service (NTIS). Springfield, Va., 22151. Reprints from outside journals and the NBS Journal of Research may often be obtained directly from the authors by title only.*

U. S. GOVERNMENT PRINTING OFFICE : 1973 O - 491-397

UNIVERSITY MICROFILMS INC
ATTN SERIALS SECTION
300 NORTH ZEEB RD
ANN ARBOR MI 48106

UNITED STATES
GOVERNMENT PRINTING OFFICE
PUBLIC DOCUMENTS DEPARTMENT
WASHINGTON, D.C. 20402

OFFICIAL BUSINESS
PENALTY FOR PRIVATE USE, $300

U.S. DEPARTMENT OF COMMERCE
POSTAGE AND FEES PAID
375

U.S.MAIL

JOURNAL OF RESEARCH of the National Bureau of Standards
A. Physics and Chemistry

Vol. 77A, No. 2 Mar.–Apr. 1973

Contents

Page

An adiabatic solution calorimeter and measurements of a standard reaction for solution calorimetry. E. J. Prosen and Marthada V. Kilday. 179

The enthalpy of solution of low quartz (α-quartz) in aqueous hydrofluoric acid. Marthada V. Kilday and Edward J. Prosen. 205

Enthalpies of solution of BeO(c) in HF(aq) and in HCl(aq). M. V. Kilday, E. J. Prosen, and D. D. Wagman. 217

The enthalpies of formation of BeO(c) and BeF_2(c). Vivian B. Parker. 227

Vapor pressure and heat of sublimation of tungsten. E. R. Plante and A. B. Sessoms. 237

Gas phase far ultraviolet photolysis and radiolysis of vinyl chloride. P. Ausloos, R. E. Rebbert, and M. H. J. Wijnen. 243

Pulse radiolysis of methane. R. E. Rebbert, S. G. Lias, and P. Ausloos. 249

Relation of vitron theory to 2-layer-liquid immiscibility in binary silicate and borate glass melts. Leroy W. Tilton. 259

Publications of the National Bureau of Standards. 273

Library of Congress Catalog Card Number: 62-37059

For sale by the Superintendent of Documents, U.S. Government Printing Office, Washington, D.C. 20402. (Order by SD Catalog No. C 13.22/sec.A:77/2). Subscription price: $17.00 a year; $4.25 additional for foreign mailing.

UNITED STATES GOVERNMENT PRINTING OFFICE, WASHINGTON : 1973